COMPUTATIONAL MODELLING OF THERMAL-HYDROLOGICAL-MECHANICAL PROCESSES IN GEOLOGICAL MEDIA

by

Thanh Son Nguyen

May, 1995

Civil Engineering and Applied Mechanics

McGill University, Montreal, Quebec, H3A 2K6

A thesis submitted to the Faculty of Graduate Studies and Research in partial fulfillment of the requirements for the degree of Doctor of Philosophy

ISBN 0-612-08139-7

Modelling of Thermo-Hydro-Mechanical Processes in Geological Media

A ma mère et à la mémoire de mon père.

Abstract

There are a number of engineering situations where fluid-saturated geological media can be subjected to thermal effects. These include the disposal of heat- emitting nuclear fuel wastes in saturated geological formations, extraction of energy resources such as oil and natural gas by steam injection and the recovery of geothermal energy by ground source heat exchangers. The objective of this thesis is to study the coupled thermal-hydrological-mechanical (T-H-M) response of fractured geological media by the computational implementation of mathematical models. From the generalization of Biot's classical theory of consolidation of a saturated porous elastic medium to include thermal effects, we first derived the equations governing coupled T-H-M processes in saturated geological media. In order to obtain numerical solutions for the governing equations, the finite element method was used. A finite element computer code, FRACON (FRActured media CONsolidation) , was developed in order to simulate plane strain and axisymmetric problems. Eight-noded isoparametric elements were developed to represent the intact regions of the geological medium, while special joint elements were developed to simulate discrete joints. The intact regions of the geological medium was assumed to exhibit linear elasticbehaviour. The joints between intact regions were modelled by constitutive relationships which reproduced both linear elastic and nonlinear elasto-plastic responses. The elasto-plastic stress-strain relationship of the joint was formulated by appeal to classical theories of interface plasticity. The elasto-plastic model for joint behaviour thus formulated is capable of reproducing many of the fundamental features of mechanical behaviour associated with naturally occuring joints, such as dilation under shear and strain softening due to surface asperity degradation. Furthermore, the thesis presents a physically-based

hydraulic model of the joint that permits the inclusion of the effects of shear dilation and gouge production on the permeability of the joint.

The development of the FRACON code followed an extensive procedure of code verification via analytical solutions and intercode comparison. A unique set of benchmark problems was proposed in order to perform code verification for coupled T-H-M .

The FRACON code was used to interpret certain laboratory and field experiments, including the following:

- coupled T-H-M laboratory experiment on a block of cementitious material
- lab experiments on joint shear behaviour under constant normal stress and constant normal stiffness conditions
- coupled shear-flow laboratory experiment on a joint
- Field experiments of fluid injection in a horizontal fracture in a granitic rock mass

Lastly, the FRACON code was used to simulate the coupled T-H-M response of a rock mass to radiogenic heat from nuclear fuel wastes buried in the rock formation . The coupled H-M response of this rock mass to a future glaciation scenario was also simulated. It was shown that the mechanical/hydraulic regimes of the rock mass could be significantly changed by the above two factors. The importance of the consideration of T-H-M processes in the overall scheme of safety assessment of sites targeted for nuclear fuel waste repositories is supported by the findings of this thesis.

Résumé

Les effets thermiques dans les formations géologiques saturées sont importants dans certains projets, comme par exemple: l'évacuation en profondeur des déchets de combustibles irradiés dans les formations géologiques saturées, l'extraction des ressources naturelles comme le pétrole et le gaz naturel par la méthode d'injection de vapeur, et l'exploitation de l'énergie géothermique. L'objectif de cette recherche est d'étudier par l'implémentation numérique de modèles mathématiques, le phénomène de couplage thermique-hydrologique-mécanique (T-H-M) dans les milieux géologiques fracturés. Pour inclure les effets thermiques, nous avons effectué la généralisation de la théorie de consolidation des milieux poro-élastiques saturés de Biot , et ainsi obtenu les équations différentielles décrivant le phénomène de couplage T-H-M de ces milieux. Pour obtenir les solutions numériques de ces équations, nous avons utilisé la méthode des éléments finis. Un logiciel en éléments finis, FRACON (FRActured media CONsolidation), a été développé pour simuler les problèmes axisymmétriques et en déformation plane. Des éléments isoparamétriques à huit noeuds ont été développés pour simuler la partie intacte du milieu géologique, et des élements spéciaux ont été développés pour simuler les joints. Le comportement de la partie intacte est considéré linéaire élastique alors que les joints peuvent avoir un comportement élastique ou élasto-plastique. La relation contrainte-déformation de ces joints a été formulée à partir des théories classiques de la plasticité des interfaces. Le modèle élasto-plastique ainsi formulé peut prédire plusieurs traits fondamentaux du comportement mécanique des joints rocheux naturels, comme la dilatation due au cisaillement, et le radoucissement dû à l'endommagement des aspérités. De plus, nous avons développé un modèle hydraulique du joint qui permet de simuler l'influence, sur la perméabilité, de la dilation et de la formation des débris causées par le cisaillement.

Le logiciel FRACON a été soumis à une vérification intensive par comparaison aux solutions analytiques et par comparaison des résultats avec d'autres logiciels. Un ensemble de problèmes de référence a ainsi été proposé pour permettre la vérification de logiciels semblables au logiciel FRACON.

Le logiciel FRACON a été utilisé pour interpréter de nombreuses expériences en laboratoire et in-situ:

- Une expérience en laboratoire du couplage T-H-M sur un bloc de roche artificielle
- des expériences en laboratoire sur le comportement au cisaillement des joints rocheux, à contrainte normale et rigidité normale constantes
- une expérience en laboratoire du couplage mécanique-hydraulique d'un joint rocheux
- des expériences in-situ d'injection de fluide dans une fracture horizontale dans une masse rocheuse granitique.

En dernier lieu, le logiciel FRACON a été utilisé pour simuler l'effet de la chaleur produite par les déchets de combustibles nucléaires sur le comportement T-H-M d'une formation géologique contenant ces déchets. L'effet d'une future période glaciaire a aussi été étudié. Nous avons trouvé que le régime hydro-mécanique de la masse rocheuse peut être profondément modifié par ces deux facteurs. Nous recommandons de considérer le phénomène de couplage T-H-M dans l'évaluation de la sûreté des sites potentiels pour l'évacuation de déchets radioactifs.

Acknowledgements

Many individuals are responsible for making this research work possible. It is a pleasure to acknowledge their contribution:

My thesis supervisor, Professor A.P.S. Selvadurai is deeply thanked for his guidance, careful review and encouragement. From the close interaction we had, many new ideas and improvement to this work has resulted. The completion of this thesis would not be possible without him.

I sincerely thank my employer, the Atomic Energy Control Board, for its financial support and for allowing me time to pursue further knowledge. In particular, I sincerely thank Mr. M. Duncan, Mr. G. Jack and Mrs C. Maloney, who gave approval for the financial and time committment required for this project.

My Section Head at the Atomic Energy Control Board, Mr. K. Bragg, is particularly responsible for encouraging me to undertake this research work. His moral support, and his patience and comprehension during the last months of preparing this thesis deserve my deep gratitude.

I sincerely thank my colleague at the Atomic Energy Control Board, Mr. P. Flavelle for his constructive comments on the publications resulting from the research performed during my doctoral studies. Mr. D. Metcalfe, Mr. V. Poliscuk, Dr. D. Bottomley, Dr. J. Wallach, and Dr. S. Lei, also from the AECB, are also sincerely thanked for the peer review they provided on these publications.

The laboratory personnel at Carleton University, Mr. K.K. Kouloufakos, Mr. P. Carnaffan, Mr. R. Weidelich are also sincerely thanked for performing the laboratory experiment on the block of cementitious material.

I am also indebted to my co-participants in the International DECOVALEX project. Many new ideas and concepts came from the DECOVALEX workshops during the last three years of operation of this project. I am grateful in particular to Professor O. Stephansson, of the Royal Institute of Technology , Stockholm, for the peer review he provided on the paper we submitted to a special issue of the International Journal of Rock Mechanics and Mining Sciences. I also thank Dr. J. Rutqvist, from the same institution, who provided the experimental data for the borehole injection tests. Dr. J. Noorishad, from the Lawrence Berkeley Laboratory, is also specially thanked for the many interesting discussions we had on T-H-M codes, rock joint behaviour and also Iranian culture and history.

En dernier lieu mais non pas le moindre, je voudrais sincèrement remercier mon épouse Phuong et notre fille Stéphanie pour leur patience et compréhension. Au cours de ces derniers mois je crains bien que mes devoirs de père de famille ne soient un peu négligés.

Table of Content

List of Main Symbols

Latin symbols

[B] : the matrix relating strain to nodal displacements in the finite element method

c: joint asperity degradation coefficient due to shearing

c' : cohesion component of shear strength in the Morh-Coulomb criterion

c_f : gouge production factor due to shearing of joint

c_v : coefficient of consolidation

C: the specific heat of the bulk medium

C_{aw}, C_w, C_a : the compressibilities of, respectively, the air/water mixture, water and air in an unsaturated porous medium

[CP] : "coupling matrix" between pore pressure and displacements in the finite element formulation of the equations of thermal consolidation

[CM] : "Mass matrix" resulting from the formulation of the equations of heat transfer and pore fluid flow

d_{ij}^e : elastic components of a joint stiffness matrix

d_{ij}^{ep} : elasto-plastic components of a joint stiffness matrix

du_i^e: the elastic components of the relative displacement at the surface of a joint

du_i^p: the plastic components of the relative displacement at the surface of a joint

[D] : matrix relating stress to strain in the finite element method

D_n : the normal component of the stress-strain matrix for joint elements

D_s : the shear component of the stress-strain matrix for joint elements

D_{sn} and D_{ns}: off-diagonal components of the stress-strain matrix for joint elements

e_{ij} : components of small strain tensor

e'_{ij} : components of small strain tensor due to effective stress

$\bar{e}_{ij}$: components of small strain tensor due to pore fluid pressure

e_h: the hydraulic aperture of a joint

e_m : the mechanical aperture of a joint

E: Young's modulus

f : proportionality factor relating the hydraulic and mechanical apertures of a joint

F: yield criterion in the theory of plasticity

F_i : component of the volumetric body force vector.

FH_I : the outward heat flux through the boundary B at node I in the finite element formulation of the heat flow equation

FQ_I : the heat generation rate at node I in the finite element formulation of the heat flow equation

$\{F_b\}$ and $\{F_a\}$: respectively the vectors representing the body force, and the force applied at the boundary B in the finite element formulation of the equilibrium equation

g_i: component of the acceleration due to gravity

G : one of the two Lamé's constants

JCS : joint compressive strength in Barton/Bandis joint strength criterion

JRC: joint roughness coefficient in Barton/Bandis joint strength criterion

K_f : bulk modulus of the fluid

K_D : the bulk modulus of the solid matrix

K_s: the bulk modulus of the solid grains

K_{ij} : components of the hydraulic conductivity tensor

[K] : the "stiffness matrix" resulting from the finite element formulation of the equation of equilibrium

[K'] : the "stiffness matrix" for the joint element in the joint local x'-y' coordinate system

[KM] : the "heat flow resistance matrix" resulting from the finite element formulation of the equation of heat transfer

[KP] : the "flow resistance matrix" resulting from the finite element formulation of the equation of pore fluid flow

k_{ij}: component of the intrinsic permeability tensor

k_{ni} : the normal stiffness of a joint at zero normal stress

k_n : joint elastic normal stiffness

m : empirical coefficient of the Hoek and Brown's criterion for rock mass failure

M : the number of moles in the ideal gas law

n : the porosity of the medium

$\overline{N_K}(x_i)$ and $N_J(x_i)$: interpolation functions (or shape functions) used in the finite element formulation of the governing equations.

p : the pore fluid pressure

p_K : pore fluid pressure at node K

p_{abs} : the absolute pressure in a fluid

p_{atm} : the atmospheric pressure

{p} : vector of nodal pressures resulting from the finite element formulation of the governing equations

q_i^c : the rate of heat flow by conduction in the ith direction [W/m^2]

q_i^{conv} : the rate of heat flow by convection in the ith direction [W/m^2]

Q : plastic potential function in the theory of plasticity

R : the universal gas constant used in ideal gas law

R and r: rebound value (m) from the Schmidt hammer test performed respectively on a clean, dry unweathered joint surface and on a wet joint surface. The value of JCS can be correlated to R and r.

s: empirical coefficient of the Hoek and brown's criterion for rock mass failure

Sr : degree of saturation

T : temperature

T_K : temperature at node K

T* : normalized time used in the theory of isothermal consolidation

{T} : vector of nodal temperatures resulting from the finite element formulation of the governing equations

[Tr] : Coordinate transformation matrix used for joint elements

u: displacement of the solid matrix in the x-direction

u_i : component of the displacement vector in the solid matrix in the ith direction

u_{iJ} : component of the displacement vector in the solid matrix in the ith direction at node J

u_r ,u_z,u_θ : the displacement components in respectively the radial, axial and hoop directions for axisymmetric problems

u : relative displacement of the joint surfaces in the shear direction

u_{peak}: relative displacement of the joint surfaces in the shear direction corresponding to the peak shear stress

v : displacement of the solid matrix in the y-direction

v: relative displacement of the joint surfaces in the normal direction

v_m : maximum closure of a joint in compression

V, V_v, V_w and V_a : respectively the total volume, volume of voids, volume of water and volume of air in an unsaturated porous medium

V_f: volume of fluid in a porous medium (equal to V_v , the volume of voids for a saturated medium)

V_{if}, V_{is} : the components of the velocities, respectively of the fluid and the solid, in the ith

direction

W_P : the plastic work produced by the shear stress in a joint

Greek symbols

α : Biot's coefficient of consolidation given by the equation:

$$\alpha = 1 - \frac{K_D}{K_S}$$

α^* : joint asperity angle

α^*_0: initial value of joint asperity angle

β : the coefficient of volumetric thermal expansion of the porous medium

β_f : the coefficient of volumetric thermal expansion of the fluid

β_s : the coefficient of volumetric thermal expansion of the solid material

$d\lambda$: a scalar multiplier used in the theory of plasticity

$\{\delta\}$: vector of nodal displacements of the solid matrix resulting from the finite element formulation of the governing equations

δ_{ij} : Kronecker delta function (=1 if i=j; = 0 otherwise).

ε_v : the volumetric strain

ϕ : friction angle

ϕ_b : angle of pure friction resistance of clean (unweathered) planar surfaces

γ : a value between 0 and 1 used in finite difference time marching schemes

κ_{ij} : component of the thermal conductivity tensor of the bulk medium

λ : one of the two Lamé's constants

μ: the viscosity of the fluid

ν : Poisson's ratio

ρ : the density of the bulk medium [kg/m^3]

ρ_f : the density of the fluid [M/L^3]

σ : normal stress across a rock joint

σ_v : total stress in the vertical direction in a rock mass

σ_{ha} : average total stress in the horizontal direction in a rock mass of the Canadian Shield

σ_{he}: higher bound of the total stress in the horizontal direction in a rock mass of the Canadian Shield

σ_c: the uniaxial compressive strength of intact samples of the rock mass, used in the Hoek and Brown failure criterion

σ_{ij} : component of the total stress tensor

σ'_{ij} : component of the effective stress tensor

σ'_{1f} : the effective major principal stress at failure in the Hoek and Brown failure criterion

σ'_3 : the effective minor principal stress in the Hoek and Brown failure criterion

τ : shear stress in a joint

τ_{peak} : peak shear stress in a joint

(ξ,η) : local coordinate system for isoparametric elements

List of Figures

List of publications resulting from the work performed for this thesis

1. T.S. Nguyen and A.P.S. Selvadurai, ' A Model for Coupled Mechanical and Hydraulic Behaviour of a Rock Joint', International Journal of Numerical and Analytical Methods in Geomechanics (in press).

2. T.S. Nguyen and A.P.S. Selvadurai, 'Coupled Thermal-Hydrological-Mechanical Processes in Sparsely Fractured Rock', Special Issue on Coupled T-H-M processes, International Journal of Rock Mechanics and Mining Sciences (in press).

3. T.S. Nguyen and A.P.S. Selvadurai, 'An Elasto-Plastic Model for Mechanical and Hydraulic Behaviour of Rock Joints', Int. Workshop on hydro-thermo mechanics of eng. clay barriers and geological barriers, 1995, Montreal (in press).

4. A.P.S. Selvadurai and T.S. Nguyen, 'A parametric Study of the Effects of Coupled Thermal-Hydrological-Mechanical Processes on a Nuclear Fuel waste repository', Int. Workshop on hydro-thermo mechanics of eng. clay barriers and geological barriers, 1995, Montreal (in press).

5. A.P.S. Selvadurai and T.S. Nguyen, 'Computational Modelling of Isothermal Consolidation of Fractured Porous Media', Computers and Geotechnics , **17** (1), 1995, 39-73.

6. A.P.S. Selvadurai and T.S. Nguyen, 'Coupled Thermal-Hydrological-Mechanical

Processes in Geological Media', 1994, Proc. of the Int. Conf. on Comp. Meth. in Struct. and Geot. Eng., University of Hong Kong, 1994.

7. T.S. Nguyen and A.P.S. Selvadurai, ' Modelling of thermal consolidation of sparsely fractured rock in the context of nuclear waste management', 'Recent developments in poroelasticity', Winter annual meeting of ASME, Chicago, 1994.

8. T.S. Nguyen and A.P.S. Selvadurai, ' Thermo-poroelastic response of a fractured geological medium', 8th International Conference of the International Association for Computer Methods and Advances in Geomechanics, Morgantown, West Virginia, 1994.

9. T.S. Nguyen, V. Poliscuk and A.P.S. Selvadurai, ' Effects of Glaciation on a Nuclear Fuel waste Repository', Canadian Geotechnical Conference, Saskatoon, 1993.

10. A.P.S. Selvadurai and T.S. Nguyen, ' Finite Element Modelling of Consolidation of Fractured Porous Media', Canadian Geotechnical Conference, Saskatoon, 1993.

CHAPTER 1

INTRODUCTION AND LITERATURE REVIEW

1.1 The multiphase nature of geomaterials

Geomaterials such as soil and rock are basically porous multiphase materials. The solid phase of a geomaterial consists of an assemblage of mineral particles. For a rock, the solid particles are cemented while for a soil, such as sand, silt or clay, the strength of the solid assemblage is mainly due to the frictional resistance at the contact points and interlocking between the particles. The solid assemblage, also called the solid matrix or solid skeleton, is pervaded by discontinuities such as pores, cracks and microcracks. These discontinuities, which we shall simply refer to as pores, can be filled with one or several types of pore material. The pore material could be a fluid in a liquid state, such as water or oil, a fluid in a gaseous state, such as air or natural gas, or a solid such as ice. In soil and rock mechanics terminology, a geomaterial is said to be saturated when its pores are filled exclusively with a liquid (usually water), and unsaturated when the pores contain both a liquid and a gas (usually air). During thermal, hydraulic and mechanical loading of a porous geomaterial, the various components of the multiphase geomaterial respond individually and also interact with one another. It is this mutual interaction between the various phases of the geomaterial that makes its behaviour distinct from the behaviour of single phase materials.

1.2 Theory of isothermal consolidation

The earliest recognition of the importance of the multiphase nature of geomaterials is generally attributed to Terzaghi (1923). In the development of the "theory of effective stress", Terzaghi postulated that when a saturated geomaterial is subjected to an external loading, this loading is partly carried by the solid skeleton and partly by the pore fluid. The ability of the pore fluid to share the external loading is an important development in the understanding of the mechanical behaviour of geomaterials. The second important development is the influence of the multiphase nature of the geomaterial on its time-dependent response to the external loading. This second aspect is clearly demonstrated by Terzaghi (1923) in the development of the classical theory of "soil consolidation". Terzaghi postulated that when a low permeability soil such as clay is subjected to an external loading, this load is initially carried by the pore fluid rather than the solid skeleton. Consequently, the pore fluid pressures immediately increase after the application of the external loading. As time progresses, flow of the pore fluid takes place from regions of high pore pressures to regions of lower pressures. This pore fluid redistribution results in a gradual pore pressure dissipation accompanied by a gradual transfer of the external loading to the solid skeleton. The gradual increase in the stresses within the solid skeleton resulting from that load transfer leads to a change in the geometrical configuration of the solid assemblage and a reduction in the pore volume which manifest in the form of consolidation of the soil.

The original developments of Terzaghi (1923) were restricted to the one-dimensional behaviour of a saturated soil, where the elastic soil skeleton is assumed to be isotropic and both the pore fluid and the solid particles are assumed to be incompressible. Biot (1941, 1955, 1956) extended these concepts to include in particular three-dimensional effects,

finite compressibility of pore fluid and solid particles and anisotropic behaviour of the soil skeleton. In the theories proposed by Terzaghi (1923) and Biot (1941, 1955, 1956), temperatures are assumed constant and consequently thermal effects are ignored. In this thesis we will use the term "theory of isothermal consolidation" to refer to the theories proposed by Terzaghi (1923) and Biot (1941, 1955, 1956), although the term "theory of poroelasticity" is also commonly encountered in the scientific literature.

The literature on the theory of isothermal consolidation is quite extensive and no attempt will be made to cover all historical and recent developments. The review by Schiffman et al. (1969), Christian (1977), Schiffman (1984), and the texts by Lewis and Schrefler (1987) and Selvadurai (1995-a) contain exhaustive information on the fundamental aspects of the theory and recent development in analytical and computational aspects. The solution techniques could be divided into two main categories: mathematical methods and numerical methods. Mathematical methods are concerned with the development of exact analytical procedures for the solution of the governing equations of isothermal consolidation, usually with simple geometries of the geomaterial domain and with various types of boundary conditions. Analytical solutions for cases when the geomaterial domain is subjected to a traction (distributed load) at a boundary are given by McNamee and Gibson (1960), Schiffman and Fungaroli (1965), Gibson, Schiffman and Pu (1968). In addition to these traction boundary value problems, mixed boundary value problems involving structures with varying degrees of flexibility (from infinitely flexible to infinitely rigid) either embedded in or in contact with the geological medium have been examined by Agbezuge and Deresiewicz(1974), Chiarella and Booker (1975), Gaszynski and Szefer (1978), Selvadurai and Yue(1994), Yue and Selvadurai (1994, 1995) and Lan and Selvadurai (1995). The use of purely mathematical methods for the development of analytical solutions for problems in isothermal consolidation represents difficult exercises in particular due to

the time-dependency associated with the response of the geological medium. For this reason and in view of the interest in the application of the theory of isothermal consolidation to practical problems, attention has been focussed mainly on numerical methods, such as the finite element method and the boundary integral equation methods. These numerical methods allow the development of approximate solutions even for complex geometries, boundary conditions and material behaviours. The finite element method has been the most widely used in engineering applications. The earliest application of the finite element method for the study of isothermal consolidation problems is due to Sandhu and Wilson (1969). These studies were followed by the work of many investigators including Christian and Boehmer (1970), Hwang et al. (1971), Ghaboussi and Wilson (1973), Small et al. (1976), and Selvadurai and Karpurapu (1989). Applications of boundary integral equations to problems in isothermal consolidation are given by Cheng and Liggett (1984-a and b), Cheng and Predeleanu (1987) and in the text by Brebbia (1984).

1.3 Coupled thermal-mechanical-hydrological processes in geological media. Extension of the classical theory of consolidation to include thermal effects

The primary focus of this thesis is the examination of the influence of thermal phenomena on the behaviour of saturated porous geomaterials. The influence of heating of geological media have important consequences or applications in a variety of problems associated with oil and gas recovery by steam injection techniques, geothermal energy extraction from underground reservoirs, and in the development of methodologies for the underground disposal of heat emitting nuclear fuel wastes. For example in the recovery of oil and gas

resources, reservoir production is stimulated by the injection of water and/or hot steam into wells drilled into the resource bearing formation. The hydraulic/thermal cracking of the rock formation induced by this injection increases the permeability of the rock formation and increases the flow rates of oil and gas to the recovery wells. In order to design the layout of the network of the injection and recovery wells, it is necessary to gain an understanding of the non-isothermal consolidation behaviour of the resource bearing formation (see for example Noorishad and Tsang, 1987; Huang et al, 1990). In the context of geothermal energy extraction, the removal of hot water from the geological formation can result in land subsidence. The use of the theory of isothermal consolidation can result in inaccurate estimates of this subsidence (Lewis and Schrefler, 1987). Cool water is usually reinjected into the geothermal reservoir to minimize the above subsidence and to minimize environmental pollution associated with the high salinity of the recovered water. The reinjected water is much colder than the rock formation of the geothermal reservoir. In order to determine the optimum reinjection rate, considerations of thermal effects need to be included in the theoretical formulation and computational modelling of the problem (Borsetto et al., 1981).

A further example of the importance of thermal effects in the behaviour of geomaterials is encountered in the disposal of heat emitting nuclear fuel wastes (NFW) in deep geological formations. Since the wastes will generate heat for hundreds to thousands of years, the structural stability of the geological formation and the groundwater movement within the formation can be influenced by the thermal pulse associated with the stored wastes. The groundwater movement in particular can have a significant influence on the rates of radionuclides migration. It is anticipated that the waste containers will fail in the future by gradual corrosion or accidental breaching. Contaminants from the wastes will then migrate through the groundwater system and will eventually reach the ground surface (Atomic

Energy of Canada Ltd, 1994-a). Due to the multiphase nature of geomaterials, the thermal (T), mechanical (M) and hydrological (H) processes taking place in the geological formation around a NFW repository are mutually dependent. The coupling of these processes could be interpreted within the theoretical framework of the theories of consolidation previously described, with the additional consideration of thermal effects. However, until now, safety assessments of potential NFW repositories have been performed without taking into account the full coupling between these processes. The importance of coupled T-H-M processes in NFW disposal was widely recognized less than a decade ago (Tsang, 1987; de Marsily, 1987). Some scientists (e.g. de Marsily, 1987) suggest that the disposal of NFW in geological formations should be delayed until the phenomenon of coupled thermal (T) -mechanical (M) - hydrological (H) processes in geomaterials is adequately understood. However, research activities in theoretical, experimental and computational aspects of coupled T-H-M processes have started to increase only recently (Pusch, 1990; SKI, 1993; Peano, 1995).

The primary motive of this thesis stems largely from the recognition of the importance of coupled thermal(T)-hydrological(H)-mechanical(M) phenomena in geological media to the safe disposal of heat emitting nuclear fuel wastes. The thesis will focus on these phenomena as they relate to the study of both intact and fractured geological media that could be encountered in a repository setting. However, the modelling methodology proposed in the thesis, based on an extension of Biot's (1941, 1955, 1956) theory of consolidation to include thermal effects, is believed to be readily adaptable to other engineering endeavours.

So far, we have presented the general theoretical background for the methodology proposed in this thesis. In the remaining sections of this chapter, we will review the

problems which are specific to the study of coupled T-H-M processes in sparsely fractured rock masses around typical NFW repositories.

1.4 The Canadian Concept for the Disposal of Nuclear Fuel Wastes

Many countries, including Canada, Sweden, France, the USA, Italy, Belgium, Finland, Switzerland, Germany, etc. which utilize nuclear energy for electricity production are investigating methodologies for the permanent disposal of the nuclear fuel wastes produced by their reactors. The disposal concept which is most likely to be implemented and being extensively studied by these countries consists of burying the wastes in repositories located in deep geological formations composed of such materials as granite, salt or clay. A typical concept for NFW disposal in dense crystalline rocks, the Canadian concept, is described in more detail in this section.

In Canada, Atomic Energy of Canada Ltd (AECL) is studying a concept where the heat emitting wastes will be emplaced in rooms in the Canadian Shield (Figure 1.1). The granitic rock formations of the Canadian Shield have an estimated age of more than 500 million years and geologists generally agree that these formations have remained relatively stable during the last hundreds of millions of years under a variety of geological and geochemical processes. According to the current conceptual design proposed by AECL (1994-a), a repository (figure 1.2) consisting of a series of disposal rooms would be excavated at a depth of 500 to 1000 m in a granitic rock formation of the Canadian Shield. The preferred emplacement method being proposed by AECL involves the in-floor emplacement option, where three rows of boreholes would be drilled along the length of each room (figure 1.2) . Corrosion resistant containers containing the wastes would be

emplaced in the boreholes. A buffer material, consisting of a mixture of sand and bentonite would be packed around the containers in the boreholes; after all boreholes have been filled, the disposal room would be filled with a backfill material consisting of a mixture of clay and crushed granite. When such a repository is completely filled and sealed, it is generally recognized that groundwater is the primary agent that could transport contaminants from the wastes to the surface . The fluxes of the water borne migration of contaminants would be minimized by several barriers. By virtue of their low dissolution rates, the waste forms themselves will constitute the first barrier. The waste containers if properly designed should be structurally stable, and have a very slow rate of corrosion. Owing to their low hydraulic conductivities and high chemical sorption potential, the buffer and backfill will minimize the rates of contaminant migration through them. The combined attenuation effects of this multiple barrier system should be such that the time required for the contaminants to reach the surface will reduce the radioactivity and concentration of these contaminants to levels harmless to humans and the environment.

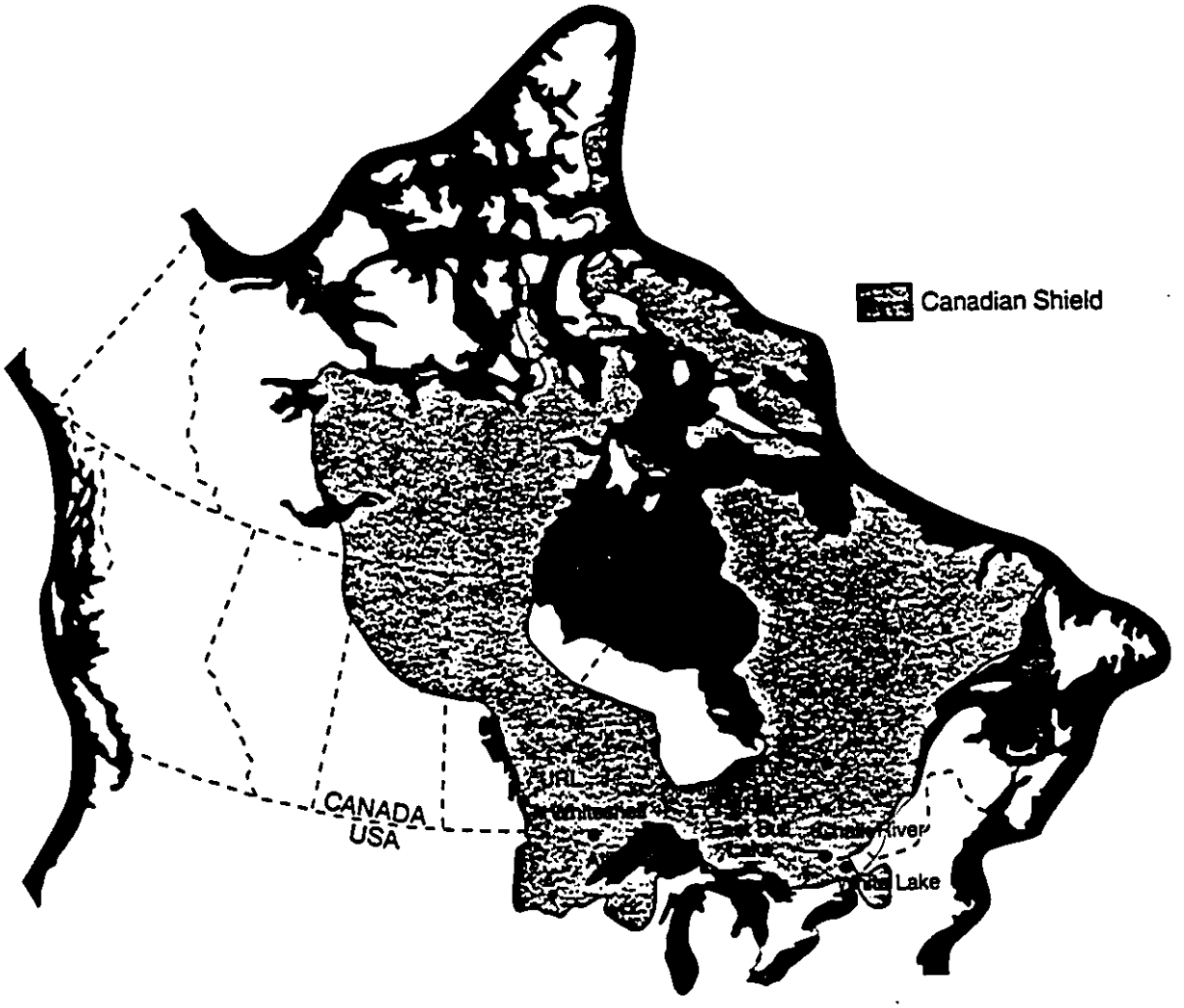

Figure 1.1 The Canadian Shield (from AECL, 1994-a)

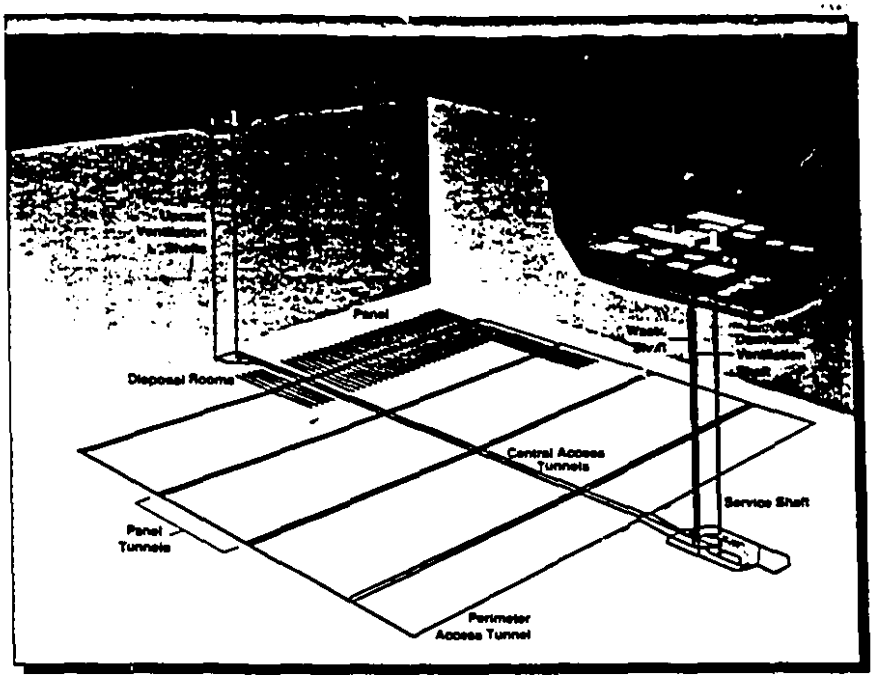

Cutaway view of repository

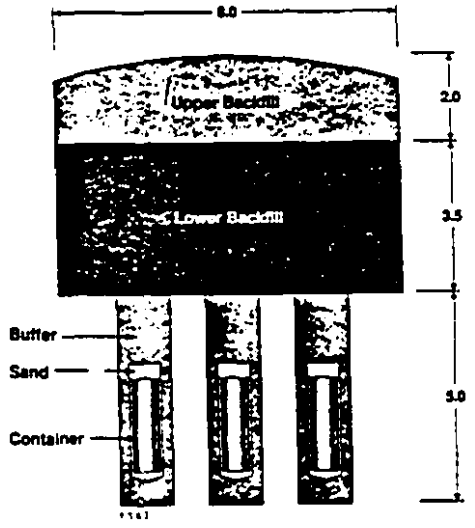

Cross-section through a room

Figure 1.2 The conceptual design for a NFW repository (From AECL, 1994-a)

According to the current conceptual design of AECL for such a NFW repository, the geological barrier is probably the most effective one (AECL, 1994-a). In this research, we will focus our attention on aspects of thermal, hydrological and mechanical processes relevant to the natural geological barrier. Aspects related to the T-H-M behaviour of the engineered geological barriers (i.e. the buffer and the backfill) are also the subject of extensive research and will not be discussed in this thesis (see e.g. Pusch, 1990). The performance of the natural geological barrier ultimately depends on its groundwater regime. To minimize the groundwater flow rates, a desirable characteristic of the host rock formation for NFW disposal would be the scarcity of joints. Conceptually, the geological formation would consist mostly of relatively intact rock with the possible presence of discrete fracture zones. In the relatively intact rock, water moves mainly in a network of pores and microcracks and also sparsely distributed joints. This relatively intact rock is also referred to as "sparsely fractured rock" (AECL, 1994-a). Fracture zones, on the other hand, are planar structures consisting of highly fractured and damaged rock. They are the most hydraulically conductive features of the rock mass. Their dimensions (length, thickness) can vary with the geological processes that were responsible for the creation of the fracture zones. Their length could be of the order of hundreds to thousands of metres and their thickness could be of the order of metres or tens of metres. In order to achieve optimal isolation, the wastes should be emplaced remote from these fracture zones. The initial groundwater regime would be disturbed by several factors and events: excavation of the rooms would be the first disturbance; the thermal pulse generated by the heat emitting wastes is the second factor; future geological events such as glaciation would also be potentially important factors adversely affecting the performance of the geological barrier. To study the effects of these disturbances on the host rock, it is necessary to examine the mutual interaction between several processes. These are identified as hydrological (H), mechanical (M), chemical (C) and thermal (T) processes (Tsang, 1987). In the present

work, we only consider the influence of three processes: Hydrological, Mechanical and Thermal.

1.5 Literature review of coupled thermal-mechanical-hydrological processes in dense sparsely fractured rock masses in the context of nuclear fuel waste disposal

Recent experimental and theoretical studies give some insight into possible effects of T-M-H coupling (interaction) on the behaviour of dense sparsely fractured rock masses that could serve as a geological medium for a nuclear fuel waste repository. Given the three T, M, H processes , Tsang (1987) considered the following four coupling combinations:

(i) Hydrological(H) - Mechanical (M) coupling

When external loads (such as the weight of a glacier) are applied to a rock mass, a new state of stress would be established, resulting in opening or closing of the cracks, microcracks, joints and fracture zones. These processes can lead to either an increase or a decrease in the hydraulic conductivity of the rock mass. When the state of stress corresponds to failure conditions, the formations of new joints could also occur resulting in an increase of the bulk permeability of the rock mass. One of the above effects was observed at the Stripa mine in Sweden, where a drift was excavated in granite (Case and Kelsall, 1987). A zone of compressive stress of 2.5 m thickness was formed adjacent to the walls and this alteration in the stress state resulted in a decrease in the hydraulic conductivity of the rock from 1×10^{-8} to 3.5×10^{-9} cm/s.

In the early stages of the application of an external load, an increase in porewater pressure will occur due to the low permeability of the rock mass. This results in a decrease in the effective stresses, which, according to the principle of effective stress, influences the mechanical response and possibly the structural integrity of the rock mass.

As discussed previously, M-H coupling could be treated with either Terzaghi's or Biot's theory of consolidation. These theories have been applied to soils with considerable success. In our opinion, in order to apply these theories with confidence to sparsely fractured rocks, in the context of NFW disposal, further theoretical and experimental developments are needed .

(ii) Hydrological (H) - Thermal (T) coupling

In the context of NFW disposal, heat is transferred from the wastes to the surrounding geological media by the processes of conduction and convection. The convective component is due to the bulk movement of the groundwater, and is directly proportional to the water velocity. Since this velocity is expected to be small , the convection component and thus the H -> T coupling is often omitted from the formulations of computational models. We will further discuss the relative importance of convective heat transport in chapter 2 and in appendix A.

There are, however, indications that the T -> H coupling component should not be neglected. Heat transfer influences flow by two basic effects: buoyancy and thermal expansion. Rae et al (1983) conducted finite element modelling of T<->H coupling in a cylindrical block of clay, 5.5 m in height, 6 m in diameter, with an embedded 100 W heater placed along the axis. The solid matrix is assumed to be rigid; thus mechanical effects are

ignored. Rae et al. (1983) observed that:

- At early times, thermal expansion of the pore water is the dominant cause of porewater flow resulting in radially diverging flow from the heat source.

- At later times, buoyancy effects are dominant; water flow in this stage is governed by the difference in density between the heated water and cooler water away from the source. Hot water rises away from the heat source, experiences cooling, reverses the flow direction and descends to lower regions of the clay block; this results in closed-loop streamlines referred to as convection cells which form in the vicinity of the heat source. The velocities and pore pressures during this stage are much smaller than those observed during the early stage .

- At a transition stage between the above two stages, the pressures and velocities decrease constantly.

Although the work of Rae et al. (1983) refers to a clay, the above processes can also occur in other porous media such as unfractured rock. Hickox and Watts (1980) performed numerical analyses of coupled T-H effects in a rigid porous medium around a cylindrical heat source with a decay in the rate of heat emission. The results obtained by Hickox and Watts (1980) are qualitatively similar to those obtained by Rae et al.(1983).

(iii) Thermal - Mechanical coupling

In general, mechanical processes directly influence heat transfer processes by changing the length of the heat transport paths. Since the displacement field in the porous medium is expected to be small compared to the original dimensions of the system, this direct

influence is negligible. Thus, the M -> T coupling could be neglected.

The T -> M coupling is one process that has been examined quite extensively in the literature in geomechanics, in particular in the context of NFW disposal. For example, in nuclear fuel waste disposal schemes, the heat generated by the wastes will perturb the ambient temperature distribution in the rock mass surrounding a repository. This will result in thermally induced stresses and deformations in the rock mass possibly leading to the disturbance of existing joints, or the formation of new joints. Extensive modelling work has been carried on the above subject (see for example AECL, 1994-b). With a proper spacing of the waste containers and the emplacement rooms, it was shown that thermally induced jointing of the rock formation could be minimized. It is noted that in the research conducted by AECL (1994-b), porewater pressures are omitted. The rock is treated as a single phase medium and the fundamental effective stress approach as mentioned in (i) was not utilized.

(iv) Fully coupled T-M-H processes

The fully coupled T-H-M analysis integrates the influences of all processes. It is the most complex combination, where both experimental and theoretical developments are needed. Existing mathematical models for fully coupled T-H-M processes are discussed in section 1.7 . Experiments to investigate coupled T-H-M processes are very rare. The Heater Test (Schneefuss et al., 1988) is an in-situ experiment performed at Grimsel, Switzerland in order to investigate full T-H-M coupling. Two heaters were directly placed in holes vertically drilled from the floor of a test drift located at a depth of 550 m in a granitic rock formation. The power output was controlled in such a way that maximum temperatures in

the system would not exceed 90 °C. Schneefuss et al. (1988) reported the results from the activation of one of the two heaters. After one year, a temperature of 55 °C was obtained in the rock, at a distance of 0.5 m from the heater; this decreases to 40, 20, and 10 °C (ambient) at 1, 2.8 and 8.5 m respectively from the heat source. At 0.5 m from the source, pore pressure increased by 1 MPa very rapidly (within 1 or 2 months) but reverted to ambient conditions after about one year. The same behaviour was observed at 1 m, but the increase was smaller (0.4 MPa). Radial stresses increased by 10 MPa at 0.5 m, 8 MPa at 1m, and 6 MPa at 2 m from the source. Deformations were very small , and only slightly higher than the resolution of the instruments. The permeability of the rock mass did not seem to be affected by thermal effects and remained essentially constant throughout the duration of the experiment.

1.6 Literature review on joint behaviour and joint elements

Discontinuities in rock masses, which shall be referred to as "joints" in this work, constitute planes of weakness in the rock mass from the point of view of its mechanical behaviour. From the point of view of hydraulic behaviour, joints are more conductive than the surrounding intact rock. Joints have critical importance in NFW disposal, since they are the preferred paths for contaminant transport. Under external loads, sliding along the joints is likely to occur. Due to the presence of asperities at the joint surfaces, dilation usually accompanies the shearing process, leading to an initial increase in the joint aperture and permeability. The asperities of the joint walls have finite strength and are gradually destroyed during the shearing process. Gouge material is produced by the damage of the asperities and the accumulation of the gouge material can result in the reduction of flow in

the joint in the latter stages of the shearing process. The very limited number of experiments (Bandis et al., 1985; Makurat et al., 1990; Benjelloun, 1991) which investigate the effects of shear on joint permeability show that the rate of increase of the permeability slows down as shearing proceeds and in later stages, the permeability could decrease as a result of gouge production .

Fundamental research work on joints has mainly focussed on their mechanical behaviour. Patton (1966) proposed a bilinear strength criterion for rock joints. Following Patton's (1966) work, other shear strength criteria were suggested, including the studies by Ladanyi and Archambault (1970), Jaeger (1971), Barton and Choubey (1977) and Bandis et al. (1981). Barton and Choubey (1977), and Bandis et al. (1981) introduce the empirical coefficients JRC (Joint Roughness Coefficient) and JCS (Joint Compressive Strength) in their strength criterion. These empirical coefficients are easily determined either from laboratory tests or from in-situ tests and they are a measure of the roughness of the joint surface (JRC) and the strength of the asperities (JCS). Empirical relations are proposed by these authors in order to include scale-dependency of JRC and JCS. The strength criteria proposed by the above authors delineate the state of stress that separates pre-sliding and post-sliding behaviours of the joints. In order to predict the stress-strain behaviour of joints in both stages, numerous constitutive relationships have been proposed. These relationships could be categorized into two main classes. The incremental relationships (see e.g. Goodman and Dubois, 1972; Goodman, 1976; Heuze, 1979; Heuze and Barbour, 1982 ; Leichnitz, 1985 ; Barton et al., 1985; Boulon and Nova, 1990; Benjelloun, 1991) consist of piecewise linear relationship between the increment of stress and the increment of strain. These relationships are usually developed from direct shear tests under constant normal stress. The use of incremental relationships under different load paths is not straightforward and is described for example by Archambault et al. (1990), Amadei and

Saeb (1990), Skinas et al. (1990), Boulon and Nova (1990), and Benjelloun (1991). The second category of constitutive relationships are the elasto-plastic relationships, derived from the theory of plasticity. The models which fall into this class assume that prior to sliding, the deformations are elastic (recoverable). Post-sliding behaviour is characterized by plastic (irrecoverable) deformations. The state of stress that separates elastic from plastic behaviour is defined by appeal to a yield criterion. Numerous elasto-plastic models exist in the literature. These include the formulations given by Ghaboussi et al. (1973), Roberds and Einstein (1978); Hsu Yun (1979), Pande and Xiong (1982), Desai and Fishman (1987) and Plesha (1987). Reference to further recent work is also given by Selvadurai and Boulon (1995). The elasto-plastic approach has a particular appeal since different load paths and directions could be accommodated. Among the above models, the one proposed by Plesha (1987) is particularly attractive due to its simplicity and its ability to capture certain fundamental aspects of the mechanical behaviour of real joints, such as dilation under shear and strain softening (decrease in shear stress in the plastic stage) due to surface asperity degradation.

For predicting the hydraulic behaviour of rock joints, the parallel plate model, developed from the application of the Navier-Stokes equation for laminar incompressible flow between two parallel smooth plates, is employed. This procedure is widely used to calculate the effective permeability k of a fracture (see e.g. Benjelloun, 1991). The permeability of the joint is thus expressed as a function of its effective opening to fluid flow, called the hydraulic aperture. Since natural fractures are quite dissimilar to ideal parallel plates, the hydraulic aperture of the fracture is not equal to its mechanical aperture. Empirical relationships between the mechanical and hydraulic apertures were proposed by Barton (1982), Elliot et al. (1985), Witherspoon et al. (1979), Benjelloun (1991) and Boulon et al. (1993). The effect of gouge production on the permeability of the joint,

however, is not accounted for in these relationships.

All of the above constitutive relationships for joints can be implemented into finite element codes, using special joint elements. Since the pioneering work of Goodman et al. (1968), joint elements for mechanical processes have been developed by numerous researchers. Gens et al. (1995) classify these joint elements into three categories:

- Link elements which essentially consist of pairs of springs in the normal and shear direction connecting opposing nodes (e.g. Anderson and Dopp,1966; Ngo and Scordelis, 1967; Frank et al., 1982; Ahmad and Bangash, 1987). These link elements do not have any physical dimension.

- Special joint elements of finite length and small but finite thickness (e.g. Zienkiewicz et al., 1970; Ghaboussi et al., 1973; Pande and Sharma, 1979; Desai et al., 1984; Griffiths, 1985; Schweiger et al., 1990).

- Special joint elements with finite length but zero thickness (Goodman et al., 1968; Tardieu and Pouyet, 1974; Carol and Alonso, 1983; Beer, 1985).

For the last two types of elements, Ghaboussi et al. (1973) and Wilson (1977) advocate the use of relative displacement as independent degrees of freedom, in order to avoid ill-conditioning of the element stiffness matrix. This situation occurs when large numerical values are encountered in the off-diagonal terms of the stiffness matrix resulting in loss of accuracy in the final solution. Pande and Sharma (1979) showed that the problem of ill-conditioning could be avoided with a smaller aspect ratio (ratio of length to thickness) of the joint element and the limiting ratio depends on the accuracy of the computer and on the

nature of the problem being solved.

Limited investigations have been conducted to determine the performance of joint elements which include coupled T-H-M processes. Noorishad et al. (1984) developed the two-dimensional (2-D) finite element code ROCMAS to analyze coupled T-H-M processes in fractured rock masses. Discrete joints are represented by the four-noded zero-thickness element formulation proposed by Goodman et al. (1968) for mechanical and thermal processes while for flow processes, the joints are represented by a two-noded line element. Guvanasen and Chan (1991, 1995) developed a three-dimensional (3-D) finite element code, MOTIF, which has features very similar to the ROCMAS code. The joint element in the MOTIF code is a 3-D version of the formulation given in the ROCMAS code. For mechanical and thermal processes, it is an 8-noded hexahedron, while for flow processes, it is a four-noded plane element. Huyakorn and Pinder (1983) showed the formulation of a special joint element for two-dimensional analysis of coupled flow and mechanical processes. This is a thin, four-noded element characterized by a length L and a thickness b. At all four nodes, the degrees of freedom are displacements and pore fluid pressure. Huyakorn and Pinder (1983) did not provide any numerical results on the actual performance of this element.

1.7 Computational models for coupled T-H-M processes in geological media

Computational codes for the simulation of coupled T-H-M processes in geological media are scarce. All the codes found in the literature use the finite element method to solve the governing equations. The governing equations solved by these computer codes are

formulated from a generalization of Terzaghi's or Biot's theory of consolidation to include thermal effects. Most of these codes are more suitable for the analysis of soil behaviour, since Terzaghi's (as opposed to Biot's) principle of effective stress theory is adopted (as discussed later in chapter 2) and no joints are included. To our knowledge, only three codes appear to be suitable for the analysis of coupled T-H-M processes in fractured rock and could be used for the safety assessments of NFW disposal systems. These are the ROCMAS code (Noorishad et al., 1984), the MOTIF code (Guvanasen and Chan, 1991, 1995) and the FRACON code developed during this study.

Aboustit et al. (1985) developed a 2-D finite element code for thermo-elastic consolidation of porous media. Ohnishi et al. (1987) also developed a 2-D code for elastic porous media : the code was later extended to include 3-D effects (Ohnishi et al., 1990). Lewis and Schrefler (1987) developed the finite element code PLASCON to simulate non-isothermal consolidation of poro-elastic and poro-elastoplastic media. The code was verified against Booker and Savvidou's (1985) analytical solution for consolidation induced by a cylindrical heat source. Britto et al. (1989), Seneviratne et al. (1994), and a research group at ISMES in Bergamo, Italy (see e.g. Hueckel et al., 1987) developed finite element codes similar to PLASCON, in order to study thermal elasto-plastic consolidation in clays. One or all of the following two types of elements are formulated in the above codes: an isoparametric eight-noded element, where all degrees of freedom are calculated at all nodes and an isoparametric element where displacements are calculated at all nodes and pore pressure and temperature are obtained only at the corner nodes. Aboustit et al. (1985) found that the first type of element is more prone to spatial oscillations in the pore pressure, especially at early times. The above codes do not have joint elements and thus discrete discontinuities in rock masses cannot be included. In addition, all of the above codes except the PLASCON code, use Terzaghi's effective stress principle, which has limited

applicability for the study of hard rocks (see e.g. Rice and Cleary (1976) and chapter 2 of this thesis).

To our knowledge, at the present time, the only codes that can be used to simulate coupled T-H-M processes in fractured hard rock are the ROCMAS and MOTIF codes, and the FRACON code developed in this study. The ROCMAS code is a 2-D finite element code that has both solid elements in order to represent unfractured rock and joint elements to represent discontinuities in the rock mass. The MOTIF code is a 3-D finite element code that also has solid and joint elements. The governing equations in ROCMAS and MOTIF are based on a generalization of Biot's theory of consolidation to include thermal effects. The MOTIF and ROCMAS codes use incrementally linear relationships to simulate the joint mechanical behaviour based on, respectively, the models by Barton et al. (1985) and Goodman (1976). Both codes used the parallel plate model for the joint hydraulic behaviour. The solid element in the ROCMAS code is a four-noded quadrilateral elements and in the MOTIF code, it is an eight-noded hexahedron. All degrees of freedom are calculated at all nodes of the solid element in both codes. As previously mentioned, the joint element in both codes are a zero-thickness type of element. Since the nodal topology of the element is defined differently for flow and and for mechanical processes, the ROCMAS and MOTIF codes necessitate the definition of two meshes: one for analyzing the thermal and mechanical effects and another one for the analysis of pore fluid flow.

Invoking certain simplifying assumptions, Booker and Savvidou (1985) provided analytical solutions for the coupled T-H-M equations. A volumetric heat source with a constant power output embedded in an infinite porous medium was examined. The simplifying assumptions are:

- The heat source has the same properties as the host porous medium;
- The porous medium is homogeneous, isotropic and fully saturated.
- The solid skeleton is linearly elastic and obeys Hooke's law;
- The pore fluid and the solid material forming the solid skeleton are incompressible
- The hydraulic conductivity is constant

Due to the limiting assumptions of Booker and Savvidou's (1985) solution, complex boundary conditions and nonlinearities which are prevalent in most practical problems cannot be modelled. The development of numerical methods is therefore a justifiable alternative. Nevertheless, analytical solutions (such as those given by Booker and Savvidou (1985)) are invaluable in providing benchmarks for verifying the accuracy of numerical schemes.

1.8 Objectives and scope of this research

It is clear from the above literature review that coupled T-M-H processes in porous, sparsely fractured geological media, such as granitic rock, are still in an early stage of both theoretical and experimental development. Specifically, attention should be focussed on the following aspects of the modelling and computational developments:

i) The development of a mathematical model should go hand in hand with its verification and validation. In the context of NFW disposal, verification is the process by which the accuracy of the computational model is established. Verification could include such activities as comparison with analytical solutions for simple geometries and boundary conditions and comparison with other computational models that solve the same governing

equations. Validation on the other hand consists of comparing the predictions of the model with experimental observations derived from either laboratory tests or in-situ experiments. The progress in code development for T-M-H coupled processes has been hindered by both the lack of available analytical solutions to achieve verification, and the lack of experimental data to conduct validation exercises. This fact has been widely recognized (Cook, 1987; Witherspoon, 1987) . An international project, DECOVALEX (SKI, 1993), has recently been initiated, with the objective of developing fundamental models, performing code verification and validation exercises, and designing experiments to further perform validation exercises to refine the fundamental models. Test cases are defined in the DECOVALEX project to allow the participants to develop models, make predictions, compare such predictions with results of others, with analytical solutions and with experimental data.

ii) The design of laboratory or in-situ experiments and the interpretation of the results are problematic without mathematical models capable of simulating the experiments.

iii) Although the theories of isothermal consolidation developed by Terzaghi and Biot have been widely and successfully used to predict the consolidation behaviour of soils, more studies are needed in order to extend the theories to sparsely jointed rocks, especially when temperature effects are included. In contrast to soils, the solid grains in rocks are cemented. Furthermore, rock formations, in contrast to soil masses, are characterized by the presence of discrete joints.

iv) In order to handle complex geometries and boundary conditions effectively and realistically, it is necessary to develop numerical methods, such as finite element methods or boundary integral element methods. The finite element method has the greater appeal to

engineers and is widely used in engineering applications. As discussed previously, with thermal consolidation problems, numerical difficulties could be experienced with the finite element method.

v) Joints are planes of weakness in a rock mass and their existence could have a dominant effect on the overall rock mass behaviour. Although individual joints have been the subject of much research, both from the mechanical or hydraulic perspectives, their coupled T-H-M behaviour is still not well understood.

The primary objective of this research is to further our understanding of coupled T-M-H processes in sparsely fractured hard rock by focussing attention on the aspects highlighted by the above points i) to v) . The secondary objective is to assess the implications of this coupling on the performance of a hypothetical NFW repository built in a representative geological formation. In order to achieve these objectives, our methodology would be to develop a mathematical model based on Biot's theory of consolidation, with extension to non-isothermal cases and with the incorporation of joints or discontinuities. The development of this model would go hand in hand with laboratory experiments performed at Carleton University (see Selvadurai, 1994) and by the general scientific community interested in problems of the same nature.

The research plan of this thesis is as follows:

i) Formulate the general governing equations of thermal consolidation of a poroelastic medium with a clear definition and discussion of the assumptions used in such a formulation. This will be the focus of Chapter 2.

ii) Develop a finite element code to numerically solve the coupled T-H-M equations obtained in i). Solid elements are formulated to account for the behaviour of intact rock and joint elements are formulated to account for the behaviour of joints. The finite element formulation is outlined in chapter 3.

iii) Perform verification of the code against a set of analytical solutions developed by Booker and Savvidou (1985) and others. These verification problems could constitute a useful set of benchmark problems for others who are engaged in code development. Verification is discussed in Chapter 4.

iv) Simulate a laboratory experiment, performed at Carleton University (Selvadurai, 1994), for coupled T-H-M processes on an intact cementitious material. The description of the experiment and its numerical simulation with the FRACON code is discussed in chapter 5.

v) Introduce nonlinear constitutive relationships for joints. Plesha's (1987) elasto-plastic model, with asperity degradation was adopted and extended to include hydraulic behaviour. The formulation of the extended Plesha's model is given in chapter 6.

vi) Using the joint model developed in v), simulate both laboratory and field experiments in jointed rocks performed by other researchers. These simulations are discussed in chapter 7.

vii) Simulate coupled T-M-H behaviour of a typical NFW repository. Simulate effects of a glaciation scenario on the response of such a repository. The above applications to NFW disposal are described in chapter 8.

In Chapter 9, we provide conclusion and recommendations for future work.

1.9 Statement of originality

1. To our knowledge, this is the first time a computer code has been developed for the examination of coupled T-H-M processes in intact and fractured rock with a systematic degree of code verification and validation. The governing equations are derived and expressed as far as possible in terms of fundamental physical parameters (as opposed to empirical coefficients). The derivation is shown step by step with all the fundamental principles and the underlying assumptions are clearly defined. The set of problems with analytical solutions is unique and could constitute benchmark test problems for other developers of computational schemes.

2. The joint model incorporated into the FRACON code makes it distinctly different from similar codes, such as MOTIF and ROCMAS, since it is capable of reproducing elasto-plastic behaviour with strain softening and accommodating via plausible constitutive assumptions the effect of gouge production on flow behaviour of rock joints. To our knowledge, this is the first time that the influence of gouge production on the hydraulic behaviour of joints is incorporated in a joint model . Several improvements in the joint mechanical model has also been brought to the original model proposed by Plesha (1987); this includes the derivation of the model parameters from the JRC and JCS coefficients, scale effects and the effects of normal stress on shear stress and shear dilatancy.

3. The joint element formulated is a six noded thin element where displacements are obtained at all six nodes and pore fluid pressure and temperature are obtained only at the

corner nodes. We believe that problems of spatial oscillations could be avoided with this type of element. To our knowledge, this is the first time such an element is formulated for coupled T-H-M processes.

4. The T-H-M experiment in an intact cementitious material as well as its mathematical simulation are considered to be unique. The author participated in the design of the experiment, and provided input during the construction and performance of the experiment.

5. This is the first time that the simulation of coupled T-M-H processes in the rock mass around a NFW repository is attempted in order to assess the implications on the safety performance of the repository.

CHAPTER 2

GOVERNING EQUATIONS OF THERMAL CONSOLIDATION

Biot's theory of consolidation can be generalized to include thermal effects (see e.g. Borsetto et al., 1981; Bear and Corapcioglu, 1981; Booker and Savvidou, 1985 and Lewis and Schrefler, 1987) . The parameters that enter into these equations, as well as the particular forms of the governing equations tend to differ from author to author, depending on the fundamental assumptions invoked in the derivation and the objectives of the range of applications. In this section, attention is devoted to a clear definition of the basic principles and assumptions required for the formulation of the equations governing non-isothermal consolidation which will be adopted in the development of the FRACON code.

In developing the equations governing quasi-static non-isothermal consolidation, the fundamental assumption is that the porous medium could be idealized as a continuum. Although this idealization is a priori accepted in fluid or solid mechanics, for the mechanics of porous media it requires some justifications as discussed in section 2.1. Having adopted the continum assumption, the basic principles of continuum mechanics (namely conservation of energy, mass and momentum) could then be invoked. These basic principles are universally applicable, irrespective of the nature of the medium being considered. Furthermore, in order to arrive at a well posed set of equations (i.e. a set of equations in which the number of unknowns equals the number of equations), it is

necessary to make additional assumptions which pertain to constitutive responses governing mechanical effects and transfer/transport processes; these include the following:

1. The law governing the flow of the pore fluid through the solid skeleton (Darcy's law)
2. Stress-strain relationship for solid matrix(constitutive laws)
3. A principle governing the interaction between the fluid and the solid (effective stress principle)
4. Heat transport mechanisms and in particular Fourier's law of heat conduction.

Unless otherwise stated, a Cartesian tensor notation will be used, with Einstein's summation convention applied on repeated indices. In addition, in most parts of this thesis, the sign convention for the normal stresses and the pore fluid pressure will be regarded as positive for tension fields. We will clearly indicate the situations when this sign convention is reversed.

2.1 The continuum representation of a porous medium

If one point of a porous medium is arbitrarily considered, that point could be located either in the pore fluid or in the solid matrix. In the mechanics of porous media, we will see in the following sections that one needs to define properties such as porosity and permeability, which are characteristic properties of both phases. For example, porosity is defined as the ratio of the volume of the pores over a given total volume of the porous medium. If the arbitrarily chosen point is located in the solid phase, then the porosity is zero; if it lies in a pore, then the porosity at this point is one. In the same manner, the permeability at the point being considered would be zero if the point lies on a solid particle and it would be infinite if

the points lies in a pore. Thus, if one considers the microscopic scale of a porous medium, i.e. the scale of each individual pore and each individual solid grain, the application of the laws of continuum mechanics is problematic, since such properties as permeability and porosity would be discontinuous functions. In order to overcome the above difficulty, the laws of continum mechanics are expressed on a larger scale, called the macroscopic scale, with the consideration of a REV (Representative Elementary Volume). Although the concept of a REV was implicitly adopted by many investigators, including Darcy (1856) and Terzaghi (1923), the concept was only later formalized by Hubbert (1940) and precisely defined by Bear (1972). A REV is a finite volume in a porous medium that contains a number of pores and of solid grains and that surrounds a point mathematically defined in that medium. The mean properties and also the mean parameters in the REV are assigned to the mathematical point. For example consider the temperature parameter. The volume average of temperature of the pore fluid contained in all the pores of the REV is calculated. This average temperature is then assigned to the mathematical point surrounded by the REV and it is called the pore fluid temperature at that point. Similarly, the volume average temperature of all the solid particles in the REV is calculated. This average temperature is assigned to the same mathematical point, and is called the temperature of the solid at this point. With the introduction of the REV, a property such as porosity is easily defined. The porosity at a point in space is simply the ratio of the volume of pores over the volume of solids in the REV containing the point. The REV should be large enough to contain a sufficient number of pores and solid grains so that the mean value of a given property or parameter has a statistical significance. On the other hand, the REV should be sufficiently small so that the variations of these properties and parameters from one domain to the next may be approximated by continuous functions so that the use of infinitesimal calculus is still appropriate.

The concept of a REV is adopted in the remainder of this thesis. Thus, when we refer to a certain property or parameter at a point, this property or parameter is more precisely the volume average of the same property or parameter of the REV surrounding that point.

2.2 Generalized Darcy's law governing fluid flow

Darcy's (1856) law describes with reasonable accuracy the process of flow of fluids in most geological materials (Freeze and Cherry, 1979). For water flow in soils, the law has been applied routinely (see e.g. Cedergren, 1967). In rocks, the law has been successfully applied in the mining industry to predict groundwater inflows into mines (see e.g. Franklin and Dusseault, 1989) and in the petroleum industry to predict reservoirs yield (see e.g. Huang et al., 1990). In the context of NFW disposal in geological formations, the applicability of Darcy's law is also a key feature. For example, in order to predict the transient water inflow in the main shaft after its excavation at the Underground Research Laboratory, in Whiteshell, Manitoba (Canada), flow in both sparsely fractured rocks and fracture zones were assumed to obey Darcy's law. The predicted results compare reasonably well with the actual inflow rates (AECL, 1994-c).

In most routine geotechnical applications, the pore fluid is water at a constant temperature and the original form of Darcy's law is assumed to be appropriate. Where either thermal effects are important, or in instances where the pore fluid is not water, the original form of Darcy's law has to be recast in a form which takes into account the characteristics of the permeating fluid (Huyakorn and Pinder, 1983) , i.e. :

$$V_{if} - V_{is} = \frac{k_{ij}}{n\,\mu}\left(\frac{\partial p}{\partial x_j} + \rho_f g_j\right) \qquad (2.1)$$

The parameters of the above equations are defined as follows (with typical SI units given between square brackets):

V_{if}, V_{is} are, respectively, the velocities of the fluid and the solid [m/s]

ρ_f : is the density of the fluid [kg/m^3]

μ: is the viscosity of the fluid [kg/m/s]

k_{ij}: is the intrinsic permeability tensor [m^2]

n : is the porosity of the medium [dimensionless]

g_i: is the ith component corresponding to the acceleration due to gravity [m/s^2]

A generalization of Darcy's law as in equation (2.1) is essential when one deals with fluids other than water. The hydraulic conductivity K_{ij} (generally referred to as the permeability in most geotechnical applications) is defined by the following expression that includes a component which is independent of the fluid (k_{ij}), and a fluid-dependent component characterized by its viscosity and density, i.e. :

$$K_{ij} = \frac{\rho_f g}{\mu} k_{ij} \qquad (2.2)$$

The viscosity and density of most fluids are generally temperature-dependent. When thermal effects are considered, appropriate experimentally derived temperature-dependent functions should be used for these two properties.

2.3 The generalized principle of effective stress and stress-strain relationships

The application of external loads results in the development of a total stress field σ_{ij}. In an idealized representation of a porous continuum, using the concept of a REV, it is assumed that every point of the medium is representative of both the solid and the fluid phases in the REV surrounding that point. Thus at every point in the continuum, the total stress σ_{ij} could be decomposed into one component borne by the fluid and another component called effective stress. The above principle of effective stress was first postulated by Terzaghi (1923). In Terzaghi's (1923) effective stress principle, both the pore fluid and the material composing the solid skeleton are assumed to be incompressible. Biot (1941) later extended Terzaghi's concept to include finite compressibilities of the fluid and the solid material. However, the compressibility coefficients of these two materials are not explicitly expressed in Biot's formulation but are incorporated into empirical coefficients which also depend on the elastic properties of the solid skeleton. Zienkiewicz et al. (1977) proposed an alternative form of Biot's principle of effective stress where all equations are expressed in terms of fundamental physical parameters. In the following derivations, we adopt the alternative form of the principle of effective stress proposed by Zienkiewicz et al. (1977).

The fluid is assumed to be incapable of resisting any shear, thus the stress component borne by the fluid is a scalar and is referred to as the hydrostatic fluid pressure or simply the fluid pressure or pore pressure. The total stress can be expressed in terms of the fluid pressure and the effective stress as follows:

$$\sigma_{ij} = \sigma'_{ij} + \delta_{ij} p \qquad (2.3)$$

where σ_{ij} is the total stress tensor, σ'_{ij} is the effective stress tensor , p is the pore pressure and δ_{ij} is Kronecker's delta function (=1 if i = j; = 0 if i ≠ j).

The total stress field will result in deformations of the porous solid skeleton and the pore fluid. For small deformations in the solid skeleton, the strains in the solid skeleton are represented by the small strain tensor e_{ij}, defined as:

$$e_{ij} = \frac{1}{2}\left(\frac{\partial u_i}{\partial x_j} + \frac{\partial u_j}{\partial x_i}\right) \tag{2.4}$$

where u_i are the displacement components of the solid skeleton.

The above strain could be divided into two parts: those associated with the actions of p and σ'_{ij} :

i) Since p is hydrostatic, it induces only a volumetric deformation of the solid grains :

$$\bar{e}_{kk} = \frac{p}{K_s} \tag{2.5}$$

or in term of individual components:

$$\bar{e}_{ij} = \delta_{ij}\frac{p}{3K_s} \tag{2.6}$$

where K_s is the bulk modulus of the solid material.

ii) The action of σ'_{ij} result in strain components e'_{ij}.

The total strain is the sum of the above strains:

$$e_{ij} = \bar{e}_{ij} + e'_{ij} \tag{2.7}$$

In the principle of effective stress proposed by Terzaghi (1923), due to the assumption of incompressibility of the solid grains, K_s is infinitely large and consequently, the first component of the strain tensor is neglected. Thus the deformational behaviour and failure conditions of the solid matrix is only dependent on the effective stress. This assumption is

generally valid for saturated soils, but as we shall illustrate later, might be inaccurate for cemented materials such as rocks.

Next we consider the stress-strain relationship between σ'_{ij} and e'_{ij}. The study of these constitutive relationships is the subject of much ongoing research (see e.g. Desai and Siriwardane, 1984; Chen and Baladi, 1985). These relationships describe the drained behaviour of the geological material, i.e. under conditions of zero or constant pore pressure. The simplest linearized constitutive relationship is Hooke's law for isotropic elasticity. Linear elastic behaviour serves as a useful first approximation for the study of intact hard rocks which are subjected to stress states below the failure level (see e.g. Franklin and Dusseault, 1989; Pande et al., 1990) . For simplicity, we will use Hooke's law in this thesis, although extensions to other constitutive relationships applicable to anelastic media could be accommodated. Considering the combined effects of stresses and thermally induced deformations, Hooke's law could be written as:

$$\sigma'_{ij} = 2G\, e'_{ij} + \left(\lambda\, e'_{kk} - \beta\, K_D T\right)\delta_{ij} \qquad (2.8)$$

In equation (2.8) G and λ are Lamé's constants; β is the coefficient of volumetric thermal expansion of the drained material; K_D is the bulk modulus of the drained material; T is temperature measured from a reference state.

Lamé's constants (λ and G) and the bulk modulus (K_D) are related to the more familiar Young's modulus (E) and Poisson's ratio (ν) by the following relations:

$$G = \frac{E}{2(1+\nu)}$$

$$\lambda = \frac{\nu E}{(1+\nu)(1-2\nu)} \qquad (2.9)$$

$$K_D = \lambda + \frac{2}{3}G = \frac{E}{3(1-2\nu)}$$

Upon substituting (2.7) and (2.8) into (2.3) and performing some algebraic manipulations , the total stress- total strain relationships can be written in the form:

$$\sigma_{ij} = 2G\, e_{ij} + (\lambda\, e_{kk} - \beta\, K_D T)\delta_{ij} + \alpha p \delta_{ij} \qquad (2.10)$$

where :

$$\alpha = 1 - \frac{K_D}{K_S} \qquad (2.11)$$

It is noted that the coefficient α enters into Biot's (1941) equations of consolidation as a single phenomenological parameter. In Terzaghi's (1923) equations of consolidation, α is always equal to one. It can be verified that, when one neglects the first part of the strain tensor in (2.7), one would obtain a value of α equal to unity in (2.11). Examining equation (2.11), a value of α equal to one corresponds to the case when the solid grain material is considered incompressible with respect to the matrix (i.e. $K_s >> K_D$, as implicitly assumed

by Terzaghi (1923)). This is true for soils. For rocks, this introduces inaccuracies: consider for example the typical properties of intact granite from the Canadian Shield (AECL, 1994-b):

$E = 30 \times 10^9$ Pa

$\nu = 0.25$

$K_s = 5 \times 10^{10}$ Pa (for quartz and most minerals)

From (2.9), $K_D = 2 \times 10^{10}$ Pa and thus $\alpha = 0.6$.

2.4 Equation of energy conservation

The general equations of energy conservation for a porous medium is derived by considering the solid phase and the fluid phase individually (Hassanizadeh and Gray, 1979; Bear and Corapcioglu, 1981). One thus obtains two equations of energy conservation: one for the pore fluid and one for the solid phase. Each of these equations states that the rate of heat inflow into a control volume of either pore fluid or solid material will be balanced by the increase in the internal energy in the control volume. The components of heat flow usually considered are :

i) heat conduction

ii) heat convection

iii) heat exchange between the two phases

Bear and Corapcioglu (1981) have shown that at a given point of the porous medium, the heat exchange between the solid and fluid phases is very rapid compared to other transport

processes and thus a state of thermal equilibrium could be assumed to exist between the two phases, i.e. at every point of the geological medium, the temperature in the pore fluid and the temperature in the solid phase are equal. By adopting the assumption of thermal equilibrium, the two general equations of energy conservation in a geological medium are reduced to one equation that is applicable to the bulk medium, i.e. the fluid/solid mixture. The above equation of energy conservation for the bulk medium contains two components of heat flow: heat conduction and heat convection.

Heat conduction is the transfer of heat by the activation of solid and fluid particles, without their bulk movement. The rate of heat flow by conduction is governed by Fourier's law, which states that the rate of heat flow is proportional to the temperature gradient:

$$q_i^c = - \kappa_{ij} \frac{\partial T}{\partial x_j} \tag{2.12}$$

where:

q_i^c is the heat flux by conduction in the ith direction [W/m^2]

T is temperature [^{o}C]

κ_{ij} is the thermal conductivity tensor [W/m/^{o}C]

Heat convection on the other hand is due to the bulk movement of the fluid and solid particles. In a poroelastic medium, the movement of the solid particles is negligible as compared to the movement of the fluid particles; thus it is the fluid flow which is mainly responsible for the convective heat transfer. The rate of heat transfer by convection is proportional to the rate of fluid flow. It can be shown that for geological media with low permeability, such as granitic rock masses, heat convection is negligible when compared

with heat conduction (Booker and Savvidou, 1985; Aboustit et al., 1985; Seneviratne et al., 1994; see also Appendix A for further justification).

In this work we assume that heat conduction is the main mode of heat transfer, and that Fourier's law is applicable. The equation governing conservation of energy is reduced to the following simplified form:

$$\boxed{\frac{\partial}{\partial x_i}\left(\kappa_{ij}\frac{\partial T}{\partial x_j}\right) + q = \rho C\frac{\partial T}{\partial t}} \qquad (2.13)$$

where:

κ_{ij} is the thermal conductivity tensor of the bulk medium [W/m/°C]

ρ is the density of the bulk medium [kg/m^3]

C is the specific heat of the bulk medium [J/kg/°C]

q is a volumetric rate of heat generation [W/m^3]

2.5 Equation of equilibrium

We assume that the velocities and acceleration terms associated with the movements in the solid and fluid phases are such that the inertia terms can be neglected. For a continuum, the equation of quasi-static equilibrium is:

$$\frac{\partial \sigma_{ij}}{\partial x_j} + F_i = 0 \qquad (2.14)$$

where F_i is the volumetric body force vector.

Substituting the constitutive equation (2.10) into (2.14), we obtain :

$$2G\frac{\partial e_{ij}}{\partial x_j} + \lambda\frac{\partial e_{jj}}{\partial x_i} + \alpha\frac{\partial p}{\partial x_i} - \beta K_D\frac{\partial T}{\partial x_i} + F_i = 0 \qquad (2.15)$$

Substituting the strain-displacement relation (2.4) into (2.15), we obtain:

$$\boxed{G\frac{\partial^2 u_i}{\partial x_j \partial x_j} + (G+\lambda)\frac{\partial^2 u_j}{\partial x_i \partial x_j} + \alpha\frac{\partial p}{\partial x_i} - \beta K_D\frac{\partial T}{\partial x_i} + F_i = 0} \qquad (2.16)$$

2.6 Equation of fluid mass conservation

For an elemental volume V of the medium, the net flux of fluid mass through the boundary of the volume is equal to the rate of fluid mass accumulation, i.e.

$$-\frac{\partial}{\partial x_i}\left(\rho_f n(V_{if} - V_{is})\right) = \frac{\partial}{\partial t}(n\rho_f) \qquad (2.17)$$

where n is the porosity of the medium and V_{if}, V_{is} are , respectively, the velocities of the pore fluid and the solid.

The right hand side of (2.17) could be expanded as:

$$\frac{\partial}{\partial t}(n\rho_f) = n\frac{\partial \rho_f}{\partial t} + \rho_f\frac{\partial n}{\partial t} \qquad (2.18)$$

Since a change in p and T will result in a change in volume, ρ_f is a function of p and T. Thus for variations dp and dT, the variation in ρ_f would be:

$$d\rho_f = -\rho_f\left(\frac{dp}{K_f} + \beta_f dT\right) \tag{2.19}$$

where K_f and β_f are respectively the bulk modulus and the coefficient of volumetric thermal expansion of the fluid.

The porosity n is a function of p, T and the effective stress σ'_{ij}. In order to establish the relationship between these quantities, we follow the methodology of Bishop (1973). We examine the variation in volume of an elemental volume V of the medium, under the combined action of a total stress increment $d\sigma_{ij}$ and a temperature increment dT. The total stress increment could be further divided into an effective stress increment $d\sigma'_{ij}$ and a pore fluid pressure increment dp.

i) The change in volume of the solids due to dp is:

$$dV_s = \frac{(1-n)Vdp}{K_s} \tag{2.20}$$

The total change in volume due to dp is:

$$dV = \frac{Vdp}{K_s} \tag{2.21}$$

where K_s is the bulk modulus of the solid material.

ii) According to a theorem adopted by Bruggeman et al. (1939) and later demonstrated to be valid by Biot (1955), the area of solid in any plane of area A intersecting the element is (1-n)A. The average increment of effective stress in that plane acting on the solid is thus $d\sigma'_{ij}/(1-n)$. The change in volume of the solids due to $d\sigma'_{ij}$ is :

$$dV_s = V\frac{d\sigma'_{kk}}{3K_s} \tag{2.22}$$

The total volume change due to $d\sigma'_{ij}$ is:

$$dV = V\frac{d\sigma'_{kk}}{3K_D} \tag{2.23}$$

iii) The volume change of the solids due to dT is:

$$dV_s = (1-n)V\beta_s dT \tag{2.24}$$

where β_s is the coefficient of volumetric thermal expansion of the solid material. The total volume change due to dT is:

$$dV = V\beta dT \tag{2.25}$$

The change in pore volume, dV_f, is the difference between the sum of all the dV (equations 2.21, 2.23 and 2.25) and the sum of the dV_s (equations 2.20, 2.22 and 2.24). After simplification, we obtain:

$$dV_f = V\left(n\frac{dp}{K_s} + \left(\frac{1}{K_D} - \frac{1}{K_s}\right)\frac{d\sigma'_{kk}}{3} + (\beta - (1-n)\,\beta_s)dT\right) \tag{2.26}$$

By definition:

$$dn = n\frac{dp}{K_s} + \left(\frac{1}{K_D} - \frac{1}{K_s}\right)\frac{d\sigma'_{kk}}{3} + (\beta - (1-n)\,\beta_s)dT \tag{2.27}$$

From equations (2.3) and (2.10), one has:

$$d\sigma'_{kk} = 3K_D(de_{kk} - dp/K_s - \beta dT) \tag{2.28}$$

Thus:

$$dn = \frac{(n-\alpha)dp}{K_s} + \alpha de_{kk} + ((1-\alpha)\beta - (1-n)\,\beta_s)dT \tag{2.29}$$

Using (2.19) and (2.29), equation (2.18) becomes:

$$\frac{\partial}{\partial t}(n\rho_f) = \rho_f\left[-\left(\frac{n}{K_f} - \frac{n}{K_s} + \frac{\alpha}{K_s}\right)\frac{\partial p}{\partial t} + \alpha\frac{\partial e_{kk}}{\partial t} + ((1-\alpha)\beta - (1-n)\,\beta_s - n\beta_f)\frac{\partial T}{\partial t}\right] \tag{2.30}$$

Assuming that:

$$\frac{\partial}{\partial x_i}(\rho_f n(V_{if} - V_{is})) = \rho_f\frac{\partial(n(V_{if} - V_{is}))}{\partial x_i} \tag{2.31}$$

equations (2.1) and (2.2) can be used to express the equation of fluid mass conservation

(2.17) in the following form:

$$\boxed{\begin{aligned}&\frac{\partial}{\partial x_i}\left(\frac{k_{ij}}{\mu}\left(\frac{\partial p}{\partial x_j}+\rho_f g_j\right)\right)-\left(\frac{n}{K_f}-\frac{n}{K_s}+\frac{\alpha}{K_s}\right)\frac{\partial p}{\partial t}+\\&\alpha\frac{\partial}{\partial t}\left(\frac{\partial u_i}{\partial x_i}\right)+\left((1-\alpha)\beta-(1-n)\beta_s-n\beta_f\right)\frac{\partial T}{\partial t}=0\end{aligned}} \qquad (2.32)$$

Equations (2.13), (2.16) and (2.32) form the set of governing differential equations for thermal elastic consolidation of porous media. The primary unknowns are the displacement field u_i, the pore fluid pressure p and the temperature T.

CHAPTER 3

FINITE ELEMENT FORMULATION OF THERMAL CONSOLIDATION

In this chapter, we use the Galerkin's technique to develop the finite element approximations of the equations governing consolidation under non-isothermal conditions. Under plane strain and axisymmetric conditions, only two (instead of three) spatial coordinates need be considered. We will develop two types of elements to analyze plane strain and axisymmetric problems: eight-noded isoparametric elements to represent unfractured porous media, and special six-noded interface elements to represent discontinuities.

The governing equations are as follows:

$$\frac{\partial}{\partial x_i}\left(\kappa_{ij}\frac{\partial T}{\partial x_j}\right) + q = \rho C\frac{\partial T}{\partial t} \tag{3.1a}$$

$$G\frac{\partial^2 u_i}{\partial x_j \partial x_j} + (G+\lambda)\frac{\partial^2 u_j}{\partial x_i \partial x_j} + \alpha\frac{\partial p}{\partial x_i} - \beta K_D\frac{\partial T}{\partial x_i} + F_i = 0 \tag{3.1b}$$

$$\frac{\partial}{\partial x_i}\left(\frac{k_{ij}}{\mu}\left(\frac{\partial p}{\partial x_j} + \rho_f g_j\right)\right) - c_e\frac{\partial p}{\partial t} + \alpha\frac{\partial}{\partial t}\left(\frac{\partial u_i}{\partial x_i}\right) + \beta_e\frac{\partial T}{\partial t} = 0 \tag{3.1c}$$

where:

$$c_e = n\left(\frac{1}{K_f} - \frac{1}{K_s}\right) + \frac{\alpha}{K_s} \tag{3.2a}$$

$$\beta_e = (1-\alpha)\beta - (1-n)\beta_s - n\beta_f \tag{3.2b}$$

The governing equations are applicable to the general three-dimensional case. Under plane strain conditions, the governing equations (3.1 a, b and c) maintain the same form, with the indices i and j taking values of 1 to 2. For axisymmetric conditions, the governing equations have to be transformed into cylindrical coordinates. First, we will perform the finite element formulation of the plane strain case. The axisymmetric case will be discussed in a subsequent section of this chapter.

3.1 The Galerkin method

The Galerkin (1915) method is widely used in the finite element formulation of groundwater problem (see e.g. Pinder and Gray, 1977; Huyakorn and Pinder, 1983). The Galerkin method is a special case of the general method of weighted residuals. Basically, the objective of these methods is to obtain an approximate solution to partial differential equations of the form:

$$L\upsilon - f = 0 \qquad x_j \in R \tag{3.3}$$

Where $\upsilon = \upsilon(x_j)$ is the unknown solution, which is a function of the coordinates x_j; R is the bounded domain where the equation is defined; L is an operator; $f = f(x_j)$ is a known function of x_j.

Consider n discrete points (nodes) of the domain R where at each point I, υ would assume the value υ_I. It is assumed that for any other point of R, of coordinates x_j, υ could be approximated by the the following function:

$$\hat{u} = \sum_{I=1}^{n} N_I \upsilon_I \tag{3.4}$$

Where $N_I = N_I(x_j)$ are some chosen functions of the coordinates x_j (usually polynomials), called interpolation or shape functions.

Since $\hat{u} = \hat{u}(x_j)$ is not the true solution, replacing the value of υ by $\hat{u}$ in (3.3) results in a residual R_e given by:

$$R_e = L\hat{u} - f \neq 0 \qquad x_j \in R \tag{3.5}$$

The method of weighted residuals consists of minimizing the error between the true solution υ and the approximate solution $\hat{u}$ by reducing the residual R_e to zero, in an average sense. The nodal values υ_I are calculated by solving the constraint equation that results from setting the average residual to zero:

$$\int_R w_I (L\hat{u} - f)\, dR = 0 \quad , \text{for } I=1,\ldots,n \tag{3.6}$$

where w_I are weighting functions which are functions of the coordinates x_j. In the Galerkin

method the weighting functions w_I are selected to be the same as the interpolation functions N_I. When all nodal values υ_I are obtained, by solving equation (3.6), the approximate value $\hat{u}$ could be obtained for any other point of R by making use of equation (3.4).

3.2 Finite element formulation of governing equation for plane strain conditions

Consider the governing equations of thermal consolidation (3.1 a, b, and c) in a domain R with boundary B. Using Galerkin's method, these equations can be transformed into matrix equations where the unknowns will be temperature, displacement and pore pressure at the nodal points. Following Galerkin's procedure briefly described above, let us consider n discrete points(nodes) of R where the temperature and fluid pressure are T_K and p_K (K=1,..., n), and N nodes of R where u_{iJ} (i = 1, 2; J=1,...., N) are the displacements at some time t. The fluid pressure and the displacement vector for any point of coordinates x_j in the domain R are approximated by the following relations :

$$T = T(x_j,t) = \overline{N_K}\, T_K \tag{3.7}$$

$$p = p(x_j,t) = \overline{N_K}\, p_K \tag{3.8}$$

$$u_i = u_i(x_j,t) = N_J\, u_{iJ} \tag{3.9}$$

where $\overline{N_K}$ (x_j) and N_J (x_j) are interpolation functions (or shape functions): K=1,....,n and J=1,....N; u_{iJ} is the displacement of the solid skeleton at node J in the ith direction.

In the above equations, the indices in capital letters (such as K and J) refer to nodal values,

while the indices in small letters (such as i, j) refer to coordinate directions. In the above equations, the summation convention applies to the repeated nodal indices K and J (over n and N respectively) as well as to the coordinate indices (over a value of 2). This summation convention holds true for the remainder of this chapter.

3.2.1 Galerkin formulation of the heat conduction equation

Substituting the equation of heat conduction (3.1a) into the weighted residual equation (3.6) yields:

$$\int_R \overline{N}_I \left[\frac{\partial}{\partial x_i} \left(\kappa_{ij} \frac{\partial T}{\partial x_j} \right) + q - \rho C \frac{\partial T}{\partial t} \right] dR = 0 \qquad (3.10)$$

where I = 1,.....,n.

According to Green's theorem :

$$\int_R f \frac{\partial g}{\partial x_i} dR = -\int_R g \frac{\partial f}{\partial x_i} dR + \int_B f g n_i dB \qquad (3.11)$$

where f, g are functions of x_i and t in R, and n_i is the unit normal vector to the boundary B.

Applying Green's theorem to (3.10) :

$$\int_B \overline{N}_I \kappa_{ij} \frac{\partial T}{\partial x_j} n_i dB - \int_R \frac{\partial \overline{N}_I}{\partial x_i} \kappa_{ij} \frac{\partial T}{\partial x_j} dR + \int_R q \overline{N}_I dR - \int_R \rho C \overline{N}_I \frac{\partial T}{\partial t} dR = 0 \qquad (3.12)$$

Substituting the approximation equation (3.7) into the above, one obtains:

$$\int_R \frac{\partial \overline{N_I}}{\partial x_i} \kappa_{ij} \frac{\partial \overline{N_K}}{\partial x_j} T_K dR + \int_R \rho C \overline{N_I}\, \overline{N_K} \frac{\partial T_K}{\partial t} dR = \int_B \overline{N_I} \kappa_{ij} \frac{\partial T}{\partial x_j} n_i dB + \int_R q \overline{N_I} dR \tag{3.13}$$

The above equation could be expressed in matrix form as :

$$\boxed{[KH]\{T\} + \rho C[CM]\left\{\frac{dT}{dt}\right\} = \{FH\} + \{FQ\}} \tag{3.14}$$

where:

$$KH_{IK} = \int_R \frac{\partial \overline{N_I}}{\partial x_i} \kappa_{ij} \frac{\partial \overline{N_K}}{\partial x_j} dR \tag{3.15}$$

$$CM_{IK} = \int_R \overline{N_I}\, \overline{N_K} dR \tag{3.16}$$

FH_I is, by definition, the outward heat flux through the boundary B at node I and is given by the expression:

$$FH_I = \int_B \overline{N_I} \kappa_{ij} \frac{\partial T}{\partial x_j} n_i dB \tag{3.17}$$

and FQ_I is the heat generation rate at node I: i.e.

$$FQ_I = \int_R \overline{N_I} q dR \tag{3.18}$$

3.2.2 Galerkin formulation for the equilibrium equation

Substituting the equation of equilibrium (3.1.b) into the weighted residual equation (3.6) gives:

$$\int_R N_I \left[G \frac{\partial^2 u_i}{\partial x_j \partial x_j} + (G+\lambda) \frac{\partial^2 u_j}{\partial x_i \partial x_j} + \alpha \frac{\partial p}{\partial x_i} - \beta K_D \frac{\partial T}{\partial x_i} + F_i \right] dR = 0 \tag{3.19}$$

where I=1.....N

After application of Green's theorem, equation (3.19) becomes:

$$\int_B N_I G \left(\frac{\partial u_i}{\partial x_j} + \frac{\partial u_j}{\partial x_i} \right) n_j \, dB - \int_R G \left(\frac{\partial u_i}{\partial x_j} + \frac{\partial u_j}{\partial x_i} \right) \frac{\partial N_I}{\partial x_j} dR +$$

$$+ \int_B N_I \left(\lambda \frac{\partial u_j}{\partial x_j} + \alpha p - \beta K_D T \right) n_i \, dB - \int_R \left(\lambda \frac{\partial u_j}{\partial x_j} + \alpha p - \beta K_D T \right) \frac{\partial N_I}{\partial x_i} dR + \tag{3.20}$$

$$\int_R N_I F_i \, dR = 0$$

Substituting the approximation equations (3.7)-(3.9) into the above, one obtains:

$$\int_R \left[G \frac{\partial N_I}{\partial x_j}\left(\frac{\partial N_J}{\partial x_j}u_{iJ} + \frac{\partial N_J}{\partial x_i}u_{jJ}\right) + \lambda \frac{\partial N_I}{\partial x_i}\frac{\partial N_J}{\partial x_j}u_{jJ} \right] dR + \int_R \alpha \frac{\partial N_I}{\partial x_i}\overline{N_K}p_K dR = \int_R N_I F_i \, dR + \int_B N_I \sigma_{ij} n_j \, dB + \int_R \beta K_D \frac{\partial N_I}{\partial x_i}\overline{N_K}T_K dR \tag{3.21}$$

where, from (2.10):

$$\sigma_{ij} = G\left(\frac{\partial u_i}{\partial x_j} + \frac{\partial u_j}{\partial x_i}\right) + \left(\lambda \frac{\partial u_k}{\partial x_k} + \alpha p - \beta K_D T\right)\delta_{ij} \tag{3.22}$$

Equation (3.21) can be written in matrix form as:

$$\boxed{[K]\{\delta\} + \alpha[CP]\{p\} = \{F_b\} + \{F_s\} + \beta K_D[CP]\{T\}} \tag{3.23}$$

where:

$\{p\}$ and $\{\delta\}$ are the vectors of nodal pressure and nodal displacements:

$$\{p\} = \begin{Bmatrix} p_1 \\ \cdot \\ \cdot \\ p_K \\ \cdot \\ \cdot \\ p_n \end{Bmatrix} \quad \text{and} \quad \{\delta\} = \begin{Bmatrix} \begin{Bmatrix} u_{11} \\ u_{21} \end{Bmatrix} \\ \cdot \\ \cdot \\ \begin{Bmatrix} u_{1J} \\ u_{2J} \end{Bmatrix} \\ \cdot \\ \cdot \\ \begin{Bmatrix} u_{1N} \\ u_{2N} \end{Bmatrix} \end{Bmatrix} \tag{3.24}$$

$\{F_b\}$ and $\{F_a\}$ are respectively the vectors representing the body force, and the force applied at the boundary B whose components are respectively given by the first and the second term of the right hand side of equation (3.21).

The components of the "coupling" matrix [CP] are given by the following equation:

$$CP_{IK} = \int_R \frac{\partial N_I}{\partial x_i} \overline{N_K} dR \tag{3.25}$$

Also, [K] is the well-known "stiffness matrix" of linear static problems. It is generally written in the following form:

$$[K] = \int_R [B]^T [D][B] dR \tag{3.26}$$

[D] is the stress-strain matrix. For linear elastic, isotropic materials, [D] depends on two constants: E and ν (or G and λ). [B] is the matrix relating strain to nodal displacements which depends on the shape functions N_I. Both matrices depend on the dimensionality of the problem and on the assumed stress conditions when the problem is simplified into a two-dimensional situation (plane strain, plane stress or axisymmetric). Explicit forms of [D] and [B] will be given in subsequent sections for plane strain and axisymmetric cases.

3.2.3 Galerkin formulation for the fluid mass conservation equation

Substituting the fluid mass conservation equation (3.1.c) into the weighted residual equation (3.6), one obtains:

$$\int_R \overline{N_I}\left[\frac{\partial}{\partial x_i}\left[\frac{k_{ij}}{\mu}\left(\frac{\partial p}{\partial x_j} + \rho_f g_j\right)\right] - c_e \frac{\partial p}{\partial t} + \beta_e \frac{\partial T}{\partial t} + \alpha \frac{\partial}{\partial t}\left(\frac{\partial u_i}{\partial x_i}\right)\right] dR = 0 \tag{3.27}$$

Applying Green's theorem to (3.27), one obtains:

$$\begin{aligned} &\int_B \overline{N_I} \frac{k_{ij}}{\mu}\left(\frac{\partial p}{\partial x_j} + \rho_f g_j\right) n_i \, dB - \int_R \frac{\partial \overline{N_I}}{\partial x_i} \frac{k_{ij}}{\mu}\left(\frac{\partial p}{\partial x_j} + \rho_f g_j\right) dR + \\ &\int_R \overline{N_I}\left[-c_e \frac{\partial p}{\partial t} + \beta_e \frac{\partial T}{\partial t} + \alpha \frac{\partial}{\partial t}\left(\frac{\partial u_i}{\partial x_i}\right)\right] dR = 0 \end{aligned} \tag{3.28}$$

Substituting (3.7) -(3.9) into the above equation, one obtains:

$$-\int_R \frac{\partial \overline{N_I}}{\partial x_i}\frac{k_{ij}}{\mu}\frac{\partial \overline{N_K}}{\partial x_j}p_K\,dR - c_e\int_R \overline{N_I}\;\overline{N_K}\frac{dp_K}{dt}\,dR + \alpha\int_R \overline{N_I}\frac{\partial N_J}{\partial x_i}\frac{du_{iJ}}{dt}\,dR=$$
$$-\int_B \overline{N_I}\frac{k_{ij}}{\mu}\left(\frac{\partial p}{\partial x_j}+\rho_f g_j\right)n_i\,dB + \int_R \frac{\partial \overline{N_I}}{\partial x_i}\frac{\kappa_{ij}}{\mu}\rho_f g_j\,dR - \beta_e\int_R \overline{N_I}\;\overline{N_K}\frac{dT_K}{dt}\,dR \qquad (3.29)$$

The equation (3.29) can be written in matrix form as:

$$\boxed{-[KP]\{p\} - c_e[CM]\left\{\frac{dp}{dt}\right\} + \alpha[CP]^T\left\{\frac{d\delta}{dt}\right\} = \{F_Q\} + \{F_g\} - \beta_e[CM]\left\{\frac{dT}{dt}\right\}} \qquad (3.30)$$

where:

$$KP_{IK} = \int_R \frac{\partial \overline{N_I}}{\partial x_i}\frac{k_{ij}}{\mu}\frac{\partial \overline{N_K}}{\partial x_j}\,dR \qquad (3.31)$$

$[CP]^T$ is the transpose of [CP] defined previously (3.25).

[CM] is defined in equation (3.16).

$\{F_Q\}$ is the inward fluid flux through the boundary B and is defined by the first term of the right hand sid of equation (3.29); $\{F_g\}$ is the gravity driven fluid flux defined by the second term of the right hand side of equation (3.29).

The matrix equations (3.14), (3.23) and (3.30) are the finite element approximations for the governing equations of isothermal consolidation (3.1.a- 3.1.c).

3.2.4 Finite element discretization

Following standard finite element procedures, the domain R is divided into N_e subdomains E called finite elements. Each element has n nodes for displacements calculations and N nodes for pore pressure and temperature calculations. All elements are joined together at these nodes (figure 3.1).

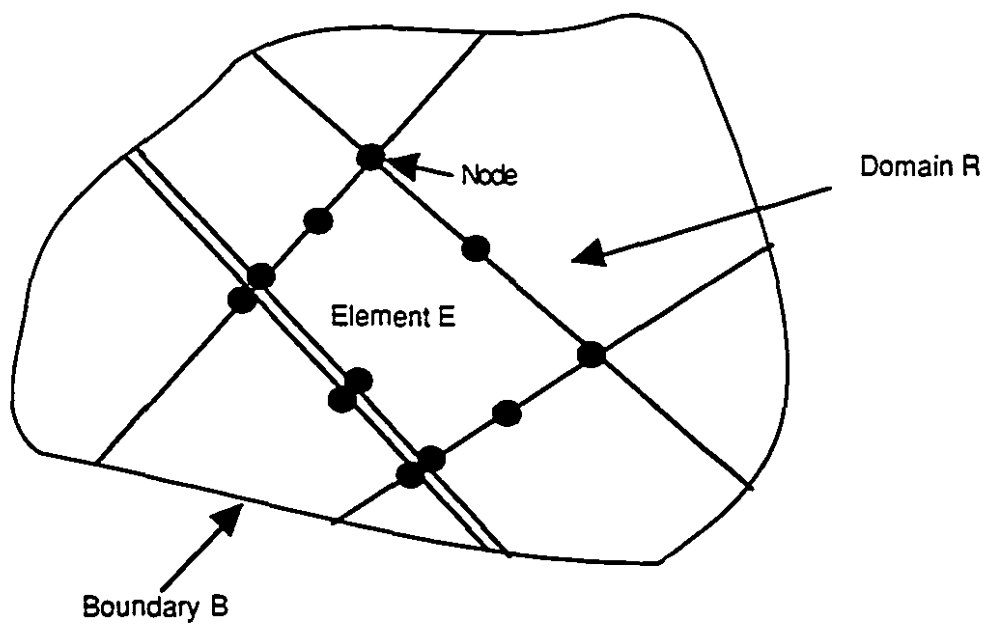

Figure 3.1 Finite element discretization of domain R

The shape functions in equations (3.7) to (3.9) are defined only at the level of each individual elements. The choice of the particular form of these shape functions should assure continuity of the pressure p, temperature T and displacement u_i at the common boundaries between elements. The previous matrix equations (3.14), (3.23), (3.30) are written for each element. The global equation for the whole domain R is obtained by summations of all the matrix equations written at an elemental level:

$$\sum_{ie=1}^{N_e} \left([KH]_{ie}\{T\} + \rho C[CM]_{ie}\left\{\frac{dT}{dt}\right\}\right) = \{FH\} + \{FQ\} \tag{3.32}$$

$$\sum_{ie=1}^{N_e} \left([K]_{ie}\{\delta\} + \alpha[CP]_{ie}\{p\}\right) = \{F_b\} + \{F_a\} + \sum_{ie=1}^{N_e} \beta K_D[CP]_{ie}\{T\} \tag{3.33}$$

$$\sum_{ie=1}^{N_e} \left\{-[KP]_{ie}\{p\} - c_e[CM]_{ie}\left\{\frac{dp}{dt}\right\} + \alpha[CP]_{ie}^T\left\{\frac{d\delta}{dt}\right\}\right\} =$$

$$\{F_Q\} + \{F_g\} - \sum_{ie=1}^{N_e} \beta_e[CM]_{ie}\left\{\frac{dT}{dt}\right\} \tag{3.34}$$

Each of the elemental matrices in the above equations are obtained by integration over the domain enclosed by the individual element. For example, the components of the element matrix $[KP]_{ie}$ are given by:

$$KP_{IK} = \int_E \frac{\partial \overline{N_I}}{\partial x_i} \frac{k_{ij}}{\mu} \frac{\partial \overline{N_K}}{\partial x_j} dE \tag{3.35}$$

Two types of elements will now be developed: a mixed 8-noded/4-noded solid element for the porous medium and a mixed 6-noded/4-noded joint element to handle discontinuities in the porous medium.

3.2.5 Solid isoparametric element

The type of elements we use for the porous medium is a mixed 8 noded-4 noded isoparametic element used by several researchers (eg Aboustit et al., 1985; Smith and Griffiths, 1988; Selvadurai and Karparapu, 1989). The displacements are calculated at the 8 nodes of this element, while fluid pressure is calculated only at the 4 corner nodes (see figure 3.2). Aboustit et al. (1985) have shown that spatial oscillations in the solution obtained for the pore pressure could be avoided with this type of element as opposed to the 8-noded element type where all degrees of freedom are calculated at all nodes. The physical explanation for this type of oscillations is as follows. Fluid pressure has the same dimension as stress. Strain is directly related to stress via the [D] matrix. Since strain is expressed in terms of spatial derivatives of displacements, the polynomials used as interpolation functions for fluid pressure should consequently be one order lower than the ones used for displacements. Nguyen (1991) has also found that the regular 8-noded isoparametric element could lead to significant spatial oscillations of the pore pressure field.

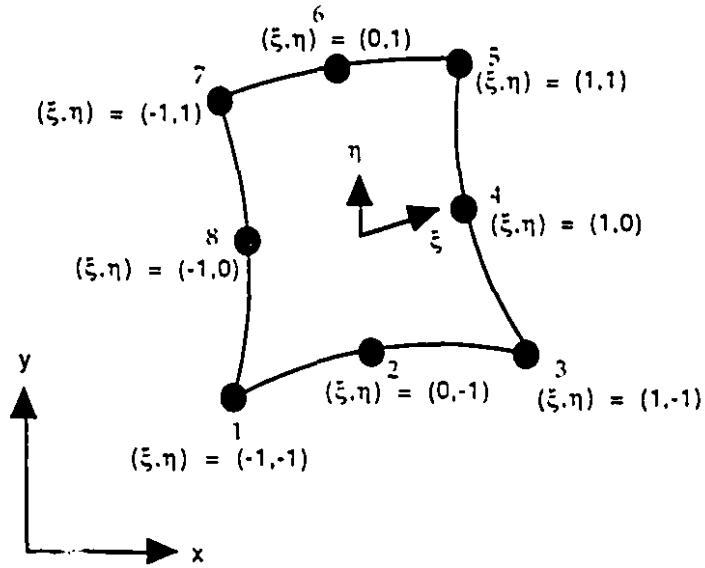

Figure 3.2 Eight-noded isoparametric elements

The interpolation functions in (3.7) to (3.9) are defined in the local coordinate system (ξ,η) as:

$$N_1 = \frac{(1-\xi)(1-\eta)}{4}$$

$$N_2 = \frac{(1+\xi)(1-\eta)}{4} \qquad (3.36.a)$$

$$N_3 = \frac{(1+\xi)(1+\eta)}{4}$$

$$N_4 = \frac{(1-\xi)(1+\eta)}{4}$$

and:

$$N_1 = \frac{-(1-\xi)(1-\eta)(1+\xi+\eta)}{4}$$

$$N_2 = \frac{(1-\xi^2)(1-\eta)}{2}$$

$$N_3 = \frac{(1+\xi)(1-\eta)(-1+\xi-\eta)}{4}$$

$$N_4 = \frac{(1-\eta^2)(1+\xi)}{2} \qquad (3.36.b)$$

$$N_5 = \frac{(1+\xi)(1+\eta)(-1+\xi+\eta)}{4}$$

$$N_6 = \frac{(1-\xi^2)(1+\eta)}{2}$$

$$N_7 = \frac{(1-\xi)(1+\eta)(-1-\xi+\eta)}{4}$$

$$N_8 = \frac{(1-\eta^2)(1-\xi)}{2}$$

Temperature, pore pressure and displacements within the elements are related to the nodal values as:

$$T = \overline{N_1}\, T_1 + \overline{N_2}\, T_3 + \overline{N_3}\, T_5 + \overline{N_4}\, T_7$$

$$p = \overline{N_1}\, p_1 + \overline{N_2}\, p_3 + \overline{N_3}\, p_5 + \overline{N_4}\, p_7 \qquad (3.37)$$

$$u_i = \sum_{j=1}^{8} N_j u_{ij}$$

The global and local cordinates are related by:

$$x_1 = x(\xi,\eta) = N_I(\xi,\eta)x_I \quad \text{and} \quad x_2 = y(\xi,\eta) = N_I(\xi,\eta)y_I \tag{3.38}$$

where I =1.....8 and summation is applied to repeated indices.

With the explicit definitions of all the shape functions given by equations (3.36), all the element matrices in equations (3.32) to (3.34) can be obtained by integration over the elements. For example, the element stiffness matrix is given by:

$$\int_E [B]^T [D][B]dxdy = \int_{-1}^{1}\int_{-1}^{1} [B]^T [D][B]\,\det[J]\,d\xi d\eta \tag{3.39}$$

where [J] is the Jacobian defined as:

$$[J] = \begin{bmatrix} \frac{\partial x}{\partial \xi} & \frac{\partial y}{\partial \xi} \\ \frac{\partial x}{\partial \eta} & \frac{\partial y}{\partial \eta} \end{bmatrix} \tag{3.40}$$

For plane strain problems, the strain-displacement matrix is given by (see e.g. Smith and Griffiths, 1988):

$$[B] = \begin{bmatrix} \frac{\partial N_1}{\partial x_1} & 0 & \cdots & \frac{\partial N_8}{\partial x_1} & 0 \\ 0 & \frac{\partial N_1}{\partial x_2} & \cdots & 0 & \frac{\partial N_8}{\partial x_2} \\ \frac{\partial N_1}{\partial x_2} & \frac{\partial N_1}{\partial x_1} & \cdots & \frac{\partial N_8}{\partial x_2} & \frac{\partial N_8}{\partial x_1} \end{bmatrix} \qquad (3.41)$$

For plane strain conditions, the stress-strain matrix is given by (see e.g. Smith and Griffiths, 1988):

$$[D] = \frac{E^*}{1-\nu^{*2}} \begin{bmatrix} 1 & \nu^* & 0 \\ \nu^* & 1 & 0 \\ 0 & 0 & \frac{1-\nu^*}{2} \end{bmatrix} \qquad (3.42)$$

where:

$$E^* = \frac{E}{(1-\nu^2)} \qquad (3.43)$$

$$\nu^* = \frac{\nu}{(1-\nu)} \tag{3.44}$$

The integrations in equation (3.39) are performed numerically using Gaussian quadrature techniques (see e.g. Smith and Griffiths, 1988).

The components of the strain tensor defined in equation (2.4) are related to the nodal displacements for each element as:

$$\begin{Bmatrix} e_{11} \\ e_{22} \\ 2e_{12} \end{Bmatrix} = [B] \begin{Bmatrix} u_1 \\ v_1 \\ \cdot \\ \cdot \\ \cdot \\ \cdot \\ u_8 \\ v_8 \end{Bmatrix} \tag{3.45}$$

where for convenience of notation, u_J is the displacement of the solid matrix in the $x=x_1$ direction at node J and v_J is the displacement of the solid matrix in the $y=x_2$ direction at node J.

The total stress-total strain relationship (cf. equation 2.10) becomes in matrix form:

$$\begin{Bmatrix}\sigma_{11}\\ \sigma_{22}\\ \sigma_{12}\end{Bmatrix} = [D]\begin{Bmatrix}e_{11}\\ e_{22}\\ 2e_{12}\end{Bmatrix} - \beta K_D\begin{Bmatrix}T\\ T\\ 0\end{Bmatrix} + \alpha\begin{Bmatrix}p\\ p\\ 0\end{Bmatrix} \tag{3.46}$$

3.2.6 Joint Element

Huyakorn and Pinder (1983) showed the formulation of a special joint element for the analysis of the isothermal consolidation of fractured porous media. This element has four nodes, and is characterized by its length L and thickness b. This element falls into the category of "thin element" as formulated by several investigators (e.g. Zienkiewicz et al., 1970; Ghaboussi et al., 1973; Pande and Sharma, 1979; Desai et al., 1984; Griffiths, 1985; Schweiger et al., 1990). The same interpolation functions are used for displacements and fluid pressure. Although no numerical example was presented by Huyakorn and Pinder (1983), it is likely that this type of element could lead to numerical instabilities, for the same rationale indicated previously for the 8-noded isoparametric element.

Considering the above, we developed a joint element with 6 nodes (figure 3.3). The displacements are calculated at all six nodes while the fluid pressure is calculated only at the corner nodes. The element is categorized as a straight "thin element" with thickness b, and length L. The local coordinate system is defined in term of the global ones as:

$$\begin{Bmatrix} x' \\ y' \end{Bmatrix} = \begin{Bmatrix} x_1 \\ y_1 \end{Bmatrix} + \begin{bmatrix} \cos\psi & \sin\psi \\ -\sin\psi & \cos\psi \end{bmatrix} \begin{Bmatrix} x \\ y \end{Bmatrix} \tag{3.47}$$

where ψ is the angle between x' and x and (x_1, y_1) are the coordinates of node 1.

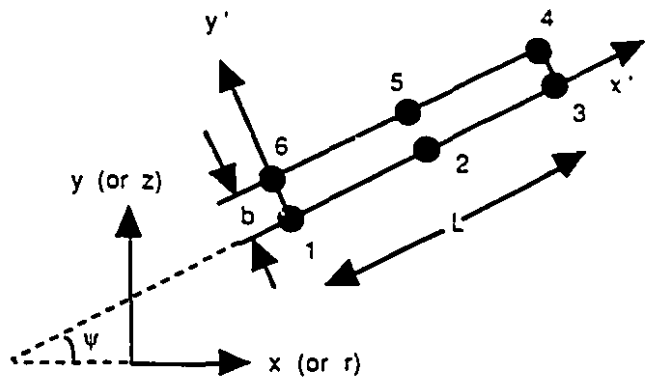

Figure 3.3 Joint element

The displacements along the bottom edge (1-2-3) and along the top edge (6-5-4) are interpolated with respected to the nodal displacements as:

$$\begin{aligned} u'_{bot} &= N_1 u'_1 + N_2 u'_2 + N_3 u'_3 \\ v'_{bot} &= N_1 v'_1 + N_2 v'_2 + N_3 v'_3 \\ u'_{top} &= N_1 u'_6 + N_2 u'_5 + N_3 u'_4 \\ v'_{top} &= N_1 v'_6 + N_2 v'_5 + N_3 v'_4 \end{aligned} \tag{3.48}$$

and the interpolation functions are defined as:

$$N_1(x') = 2x'^2/L^2 - 3x'/L + 1$$
$$N_2(x') = -4x'^2/L^2 + 4x'/L \qquad (3.49)$$
$$N_3(x') = 2x'^2/L^2 - x'/L$$

u′ and v′ are the displacement along x′ and y′ respectively. It could be seen that they are assumed to vary as a quadratic function of x′.

The strain components could be expressed in term of displacements as:

$$e_{x'x'} = \frac{\partial u'_{bot}}{\partial x'}$$
$$e_{y'y'} = \frac{v'_{top} - v'_{bot}}{b} \qquad (3.50)$$
$$2e_{x'y'} = \frac{u'_{top} - u'_{bot}}{b} + \frac{\partial v'_{bot}}{\partial x'}$$

Substituting (3.48) into (3.50), one obtains:

$$\begin{Bmatrix} e_{x'x'} \\ e_{y'y'} \\ 2e_{x'y'} \end{Bmatrix} = [B] \begin{Bmatrix} u_1' \\ v_1' \\ \cdot \\ \cdot \\ \cdot \\ \cdot \\ u_6' \\ v_6' \end{Bmatrix} \tag{3.51}$$

In eq. (3.51). [B] is the stress-displacement matrix (dimension 3x12) whose entries contain expressions of N_1 and their derivatives with respect to x′. For plane strain conditions:

$$[B] = \begin{bmatrix} \frac{\partial N_1}{\partial x'} & 0 & \frac{\partial N_2}{\partial x'} & 0 & \frac{\partial N_3}{\partial x'} & 0 & 0 & 0 & 0 & 0 & 0 & 0 \\ 0 & -\frac{N_1}{b} & 0 & -\frac{N_2}{b} & 0 & -\frac{N_3}{b} & 0 & \frac{N_3}{b} & 0 & \frac{N_2}{b} & 0 & \frac{N_1}{b} \\ -\frac{N_1}{b} & \frac{\partial N_1}{\partial x'} & -\frac{N_2}{b} & \frac{\partial N_2}{\partial x'} & -\frac{N_3}{b} & \frac{\partial N_3}{\partial x'} & \frac{N_3}{b} & 0 & \frac{N_2}{b} & 0 & \frac{N_1}{b} & 0 \end{bmatrix} \tag{3.52}$$

The stiffness matrix for the joint element would now be given in the x´-y´ coordinate system by:

$$[K'] = b\int_0^L [B]^T[D][B]\,dx' \tag{3.53}$$

where [D] is the stress-strain matrix. For plane strain conditions, [D] would take the following form:

$$[D] = \begin{bmatrix} D_{x'x'} & 0 & 0 \\ 0 & D_n & D_{ns} \\ 0 & D_{sn} & D_s \end{bmatrix} \tag{3.54}$$

Where $D_n = D_{y'y'}$ is the normal component of the stress-strain matrix: $D_s = D_{x'y'}$ is the shear component of [D] . D_{sn} and D_{ns} are equal to zero for linear elastic behaviour; they become different from zero when dilatancy of the joint due to shear is introduced (cf. chapter 6).

The components of the [K´] matrix were analytically derived. In order to obtain the stiffness matrix [K] in the global coordinate system, one needs to perform the following transformation:

$$[K] = [Tr]\,.[K']\,.\,\text{Transpose}[Tr] \tag{3.55}$$

with:

$$[Tr] = \begin{bmatrix} [A] & & & & \\ & [A] & & 0 & \\ & & [A] & & \\ & & & [A] & \\ & 0 & & & [A] \end{bmatrix} \qquad (3.56)$$

$$[A] = \begin{bmatrix} \cos\psi & \sin\psi \\ -\sin\psi & \cos\psi \end{bmatrix} \qquad (3.57)$$

In order to derive the remaining matrices in equations (3.32), (3.33) and (3.34) for the joint element, the interpolation functions for the fluid pressure have to be defined. The fluid pressure and the temperature inside the element are expressed in terms of the corner nodes' pressure and temperature as:

$$\begin{aligned} p(x',y') &= \overline{N_1}p_1 + \overline{N_2}p_3 + \overline{N_3}p_4 + \overline{N_4}p_6 \\ T(x',y') &= \overline{N_1}T_1 + \overline{N_2}T_3 + \overline{N_3}T_4 + \overline{N_4}T_6 \end{aligned} \qquad (3.58)$$

Where the interpolation functions are defined as:

$$\begin{aligned} \overline{N_1} &= 1 - \frac{x'}{L} - \frac{y'}{b} + \frac{x'y'}{bL} \\ \overline{N_2} &= \frac{x'}{L} - \frac{x'y'}{bL} \\ \overline{N_3} &= \frac{x'y'}{bL} \\ \overline{N_4} &= \frac{y'}{b} - \frac{x'y'}{bL} \end{aligned} \qquad (3.59)$$

The above interpolation functions are linear functions of x´ and y´.

The expressions for all the matrices in (3.32), (3.33) and (3.34) can now be easily derived.

For instance:

$$[CP]^T = \int_{x'=0}^{L} \int_{y'=0}^{b} \alpha \begin{Bmatrix} N_1 \\ N_2 \\ N_3 \\ N_4 \end{Bmatrix} \left\{ \frac{dN_1}{dx'} \cdot -\frac{N_1}{b} \cdot \frac{dN_2}{dx'} \cdot -\frac{N_2}{b} \cdot \frac{dN_3}{dx'} \cdot -\frac{N_3}{b} \cdot 0 \cdot \frac{N_3}{b} \cdot 0 \cdot \frac{N_2}{b} \cdot 0 \cdot \frac{N_1}{b} \right\} dx'dy' [T] \tag{3.60}$$

Where [T] is the Coordinate transformation matrix previously defined.

All the integration for the joint element matrices are performed analytically.

3.3 Axisymmetric conditions

In order to obtain the equations governing axisymmetric problems of thermal consolidation, equations (3.1 a), (3.1 b) and (3.1 c) have to be rewritten in the cylindrical coordinates (r, θ, z) defined by the following transformation rule (figure 3.4):

$$\begin{aligned} x &= r\cos\theta \\ y &= r\sin\theta \\ z &= z \end{aligned} \tag{3.61}$$

By using the chain rule and performing differentiation of the equation (3.61), one can prove the following results:

$$\frac{\partial}{\partial x} == \cos\theta \frac{\partial}{\partial r} - \frac{\sin\theta}{r} \frac{\partial}{\partial \theta}$$
$$\frac{\partial}{\partial y} == \sin\theta \frac{\partial}{\partial r} + \frac{\cos\theta}{r} \frac{\partial}{\partial \theta} \qquad (3.62)$$

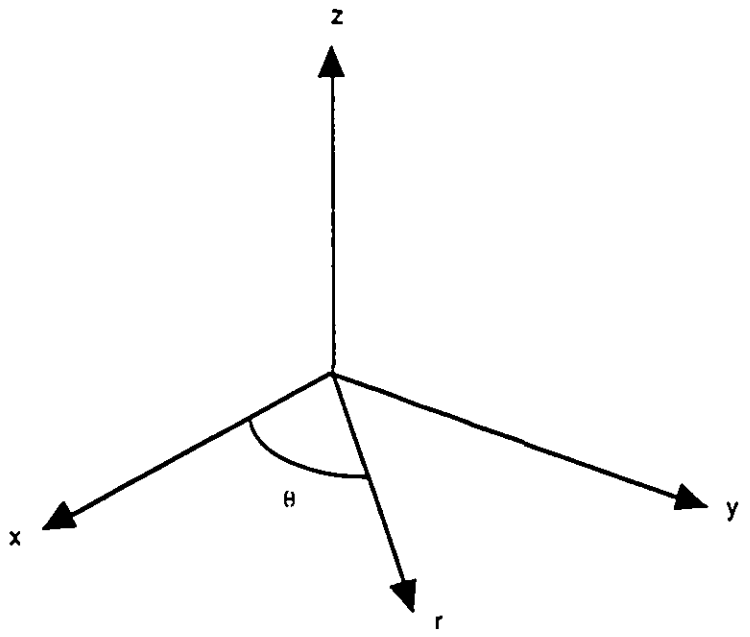

Figure 3.4 Cylindrical coordinates

The axisymmetric condition requires the following:

$$\frac{\partial T}{\partial \theta} = 0$$

$$\frac{\partial p}{\partial \theta} = 0$$

$$\frac{\partial u_r}{\partial \theta} = \frac{\partial u_z}{\partial \theta} = 0 \qquad (3.63)$$

$$u_\theta = 0$$

where $u_r = u_1$ and $u_z = u_2$ are the displacement components in the r and z directions, respectively; and u_θ is the displacement in the direction perpendicular to the r-z plane.

Applying the differentiation rule (3.62) to equations (3.1 a) to (3.1 c) and invoking the axisymmetric conditions defined by equation (3.63), we obtain the following governing equations for axisymmetric conditions:

$$\frac{\partial}{\partial x_i}\left(\kappa_{ij}\frac{\partial T}{\partial x_j}\right) + \frac{1}{x_1}\left(\kappa_{11}\frac{\partial T}{\partial x_1}\right) + q - \rho C\frac{\partial T}{\partial t} = 0 \qquad (3.64\ a)$$

$$\frac{G}{x_1}\frac{\partial}{\partial x_j}\left(x_1\frac{\partial u_i}{\partial x_j}\right) + (G+\lambda)\frac{\partial \varepsilon_v}{\partial t} - \frac{G}{x_1^2}\delta_{i1}u_1 + \alpha\frac{\partial p}{\partial x_i} - \beta K_D\frac{\partial T}{\partial x_i} + F_i = 0 \qquad (3.64\ b)$$

$$\frac{\partial}{\partial x_i}\left(\frac{k_{ij}}{\mu}\left[\frac{\partial p}{\partial x_j} + \rho_f g_j\right]\right) + \frac{1}{x_1}\left(\frac{k_{11}}{\mu}\left[\frac{\partial p}{\partial x_1} + \rho_f g_1\right]\right) - c_e\frac{\partial p}{\partial t} + \alpha\frac{\partial \varepsilon_v}{\partial t} + \beta_e\frac{\partial T}{\partial t} = 0 \qquad (3.64\ c)$$

where :

i, j vary from 1 to 2 with $x_1=r$, $x_2=z$, $u_1 = u_r$ and $u_2 = u_z$

ε_v is the volumetric strain given by:

$$\varepsilon_v = \frac{\partial u_i}{\partial x_i} + \frac{u_1}{x_1} \tag{3.65}$$

The Galerkin finite element procedure was applied to equations (3.64 a) to (3.64 c), to obtain the matrix equations equivalent to (3.32) to (3.34). The only differences between the plane strain and axisymmetric cases are as follow.

The integrals that define the elemental matrices in equations (3.32) to (3.34) are performed for the plane strain case with:

$dE = dxdy$

For the axisymmetric case:

$dE = rdrdz$

The matrices [B] and [D] for the plane strain cases are defined previously. For the axisymmetric case, an additional component of strain in the hoop direction (direction perpendicular to the r-z plane) exists:

$$\varepsilon_{\theta\theta} = \frac{u_1}{x_1} \tag{3.66}$$

The strain-displacement matrix now relates the strain components to the nodal displacements according to the following relation:

$$\begin{Bmatrix} e_{rr} \\ e_{zz} \\ 2e_{rz} \\ e_{\theta\theta} \end{Bmatrix} = [B] \begin{Bmatrix} u_{r1} \\ u_{z1} \\ . \\ u_{rI} \\ u_{zI} \\ . \\ u_{rN} \\ u_{zN} \end{Bmatrix} \tag{3.67}$$

where I=1,...N, with N=8 for eight-noded isoparametric elements and N=6 for joint elements. u_{rI} and u_{zI} are the displacements of the solid skeleton at node I in the r and z directions, respectively.

For eight-noded isoparametric elements:

$$[B] = \begin{bmatrix} \frac{\partial N_1}{\partial x_1} & 0 & . & . & . & . & \frac{\partial N_8}{\partial x_1} & 0 \\ 0 & \frac{\partial N_1}{\partial x_2} & . & . & . & . & 0 & \frac{\partial N_8}{\partial x_2} \\ \frac{\partial N_1}{\partial x_2} & \frac{\partial N_1}{\partial x_1} & . & . & . & . & \frac{\partial N_8}{\partial x_2} & \frac{\partial N_8}{\partial x_1} \\ \frac{N_1}{x_1} & 0 & . & . & . & . & \frac{N_8}{x_1} & 0 \end{bmatrix} \tag{3.68}$$

$$[D] = \frac{E(1-\nu)}{(1+\nu)(1-2\nu)} \begin{bmatrix} 1 & \frac{\nu}{1-\nu} & 0 & \frac{\nu}{1-\nu} \\ \frac{\nu}{1-\nu} & 1 & 0 & \frac{\nu}{1-\nu} \\ 0 & 0 & \frac{1-2\nu}{2(1-\nu)} & 0 \\ \frac{\nu}{1-\nu} & \frac{\nu}{1-\nu} & 0 & 1 \end{bmatrix} \tag{3.69}$$

For joint elements:

[B] =

$$\begin{bmatrix} \frac{\partial N_1}{\partial x'} & 0 & \frac{\partial N_2}{\partial x'} & 0 & \frac{\partial N_3}{\partial x'} & 0 & 0 & 0 & 0 & 0 & 0 & 0 \\ 0 & -\frac{N_1}{b} & 0 & -\frac{N_2}{b} & 0 & -\frac{N_3}{b} & 0 & \frac{N_3}{b} & 0 & \frac{N_2}{b} & 0 & \frac{N_1}{b} \\ -\frac{N_1}{b} & \frac{\partial N_1}{\partial x'} & -\frac{N_2}{b} & \frac{\partial N_2}{\partial x'} & -\frac{N_3}{b} & \frac{\partial N_3}{\partial x'} & \frac{N_3}{b} & 0 & \frac{N_2}{b} & 0 & \frac{N_1}{b} & 0 \\ \frac{N_1\cos\psi}{2r} & \frac{-N_1\sin\psi}{2r} & \frac{N_2\cos\psi}{2r} & \frac{-N_2\sin\psi}{2r} & \frac{N_3\cos\psi}{2r} & \frac{-N_3\sin\psi}{2r} & \frac{N_3\cos\psi}{2r} & \frac{-N_3\sin\psi}{2r} & \frac{N_2\cos\psi}{2r} & \frac{-N_2\sin\psi}{2r} & \frac{N_1\cos\psi}{2r} & \frac{-N_1\sin\psi}{2r} \end{bmatrix}$$

(3.70)

with r= r(node 1) + x´cosψ (see figure 3.3 where r replaces x and z replaces y in the global coordinate system for axisymmetric cases)

and:

$$[D] = \begin{bmatrix} D_{x'x'} & 0 & 0 & 0 \\ 0 & D_n & D_{ns} & 0 \\ 0 & D_{sn} & D_s & 0 \\ 0 & 0 & 0 & D_{\theta\theta} \end{bmatrix} \qquad (3.71)$$

3.4 Time marching scheme and stability

In order to handle nonlinearities, encountered in the elasto-plastic joint model to be introduced in chapter 6, we differentiate the matrix equation of equilibrium (3.33) with respect to time t in order to obtain an incremental formulation of this equation. This procedure is widely used by others (see e.g. Zienkiewicz et al., 1977; Lewis and Schrefler, 1987)

The system of matrix equations (3.32) to (3.34) to be solved now becomes:

$$\sum_{ie=1}^{N_e} \left([KH]_{ie}\{T\} + \rho C [CM]_{ie}\left\{\frac{dT}{dt}\right\}\right) = \{FH\} + \{FQ\} \tag{3.72}$$

$$\sum_{ie=1}^{N_e} \left([K]_{ie}\{\frac{d\delta}{dt}\} + \alpha [CP]_{ie}\{\frac{dp}{dt}\}\right) = \{\frac{dF_h}{dt}\} + \{\frac{dF_a}{dt}\} + \sum_{ie=1}^{N_e} \beta K_D [CP]_{ie}\left\{\frac{dT}{dt}\right\} \tag{3.73}$$

$$\sum_{ie=1}^{N_e} \left(-[KP]_{ie}\{p\} - c_e [CM]_{ie}\left\{\frac{dp}{dt}\right\} + \alpha [CP]^T_{ie}\left\{\frac{d\delta}{dt}\right\}\right) =$$
$$\{F_Q\} + \{F_g\} - \sum_{ie=1}^{N_e} \beta_e [CM]_{ie}\left\{\frac{dT}{dt}\right\} \tag{3.74}$$

For nonlinear problems, the matrices in the above equations are tangential matrices that relate increments of response ($d\delta$, dp, dT) to increments of external loads (e.g. dF_a). These matrices are dependent on the current state (δ,p,T) of the system.

Let us use the following finite difference scheme for time discretization:

$$X^{\gamma} = (1-\gamma)X^{0} + \gamma X^{1} \tag{3.75}$$

$$\frac{dX}{dt} = \frac{X^{1} - X^{0}}{\Delta t} \tag{3.76}$$

where Δt is a time increment, X^0, X^1, X^γ are the value of a quantity X at times t, t+ Δt and t+γDt respectively; γ is a value between 0 and 1. When γ=0 , the finite difference scheme is called fully explicit; when γ=1, it is called fully implicit; when γ=0.5, it is called the Crank-Nicholson scheme.

Applying the finite difference scheme (equations 3.75 and 3.76) for dp/dt, dδ/dt, dT/dt and p in equations (3.72), (3.73) and (3.74), one obtains the following global matrix equation:

$$[\gamma[KH] + \rho C[CM]]\{T\}^{1} = \{FH\}^{\gamma} + \{FQ\}^{\gamma} + [(\gamma-1)[KH] + \rho C/\Delta t[CM]]\{T\}^{0}$$

$$\begin{bmatrix} [K] & \alpha[CP] \\ \alpha[CP]^{T} & -\gamma\Delta t[KP] - c_e[CM] \end{bmatrix} \begin{Bmatrix} \{\delta\}^{1} \\ \{p\}^{1} \end{Bmatrix} =$$

$$\begin{bmatrix} [K] & \alpha[CP] \\ \alpha[CP]^{T} & (1-\gamma)\Delta t[KP] - c_e[CM] \end{bmatrix} \begin{Bmatrix} \{\delta\}^{0} \\ \{p\}^{0} \end{Bmatrix} + \tag{3.77}$$

$$\begin{Bmatrix} \{F_a\}^{1} - \{F_a\}^{0} + \{F_b\}^{1} - \{F_b\}^{0} \\ \{F_Q\}^{\gamma}\Delta t + \{F_g\}^{\gamma}\Delta t \end{Bmatrix} + \begin{bmatrix} \beta K_D[CP] & [0] \\ [0] & -\beta_e[CM] \end{bmatrix} \begin{Bmatrix} \{T\}^{1} - \{T\}^{0} \\ \{T\}^{1} - \{T\}^{0} \end{Bmatrix}$$

When $\{T\}^0$, $\{\delta\}^0$ and $\{p\}^0$ are known, the solution of equation (3.77) will give $\{T\}^1$, $\{\delta\}^1$ and $\{p\}^1$. Booker and Small (1975) and Lewis and Schrefler (1987) have shown that for $\gamma \geq 1/2$, the finite difference scheme given by equation (3.75) and (3.76) as applied to problems of consolidation is unconditionnally stable in time (no oscillations of the solution with the time variable would be found). For eight-noded isoparametric elements where all degrees of freedom are calculated at all eight nodes, Aboustit et al. (1985) have shown that spatial oscillation in the pore pressure field (especially at early times) could be avoided for some problems when γ is closer to one (γ=0.875 in the example given by Aboustit et al., 1985). Intuitively, when the pore pressure p varies very rapidly, a value of γ equal or close to one is preferable, since p^{γ} at an intermediate time $t = t^0+\gamma\Delta t$ is closer to p^1 than p^0. As will be shown in the next chapter, this is particularly true for thermal consolidation problems where the thermally induced pore pressure varies rapidly with time. We experienced very little spatial or temporal oscillations in the numerical results for the verification problems shown in the next chapter, when values of γ close to 1 (typically 0.875 or 1) were chosen.

The finite element formulation described in this chapter has been implemented in a FORTRAN code , FRACON (FRActured medium CONsolidation). In order to verify the code the results derived from the computational model are compared with a series of benchmark problems, which are primarily analytical solutions. The results of these verification activities are discussed in chapter 4.

CHAPTER 4

VERIFICATION OF THE FINITE ELEMENT CODE FRACON

Verification of a computer code is the process by which one assures that the code gives adequate numerical solutions to the governing equations. Verification could include such activities as comparison of the code results with analytical solutions or intercode comparison (i.e. comparison with the results of other codes which solve the same equations). For isothermal cases, analytical solutions for one-dimensional consolidation are available from Terzaghi (1923), for two-dimensional plane strain or axisymmetric consolidation from McNamee and Gibson (1960). Booker and Savvidou (1985) derived the analytical solutions for the non-isothermal consolidation problem related to a volumetric heat source embedded in a saturated porous medium. In this chapter we will perform verification of the FRACON code by comparison with both analytical solutions and with other codes.

In all problems simulated in this chapter and in the remainder of this thesis, gradual mesh size and time step refinements are used until the further refinements do not result in significant changes in the numerical solutions. Only the results from the "converged' mesh size and time step are shown in all the examples. More details on this procedure are

discussed by Selvadurai and Nguyen (1995).

4.1 One-dimensional isothermal consolidation

Terzaghi (1923) provided an analytical solution for the problem of the one-dimensional consolidation of a soil column of thickness H, with an impermeable base, subjected to a total stress p_0 which has a time variation in the form of a Heaviside step function. The finite element mesh and the boundary conditions for this problem are shown in figure 4.1.

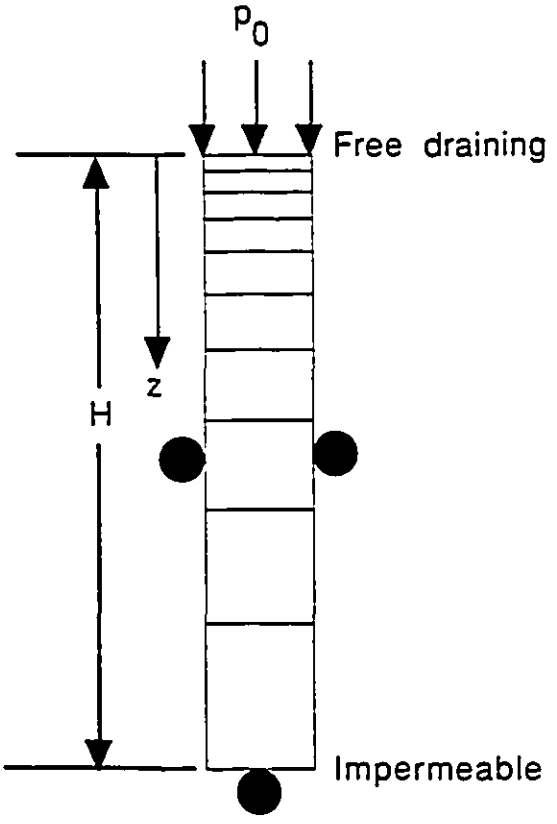

Figure 4.1 Finite element mesh for one-dimensional isothermal consolidation

The following elastic properties are used in the finite element analysis:

$E = 35 \times 10^9$ Pa

$\nu = 0.2$

For an isotropic medium, all the off-diagonal coefficients of the hydraulic conductivity tensors are equal to zero, and all diagonal terms are equal. The following value is used:

$K_{xx} = K_{yy} = K_{zz} = K = 10^{-11}$ m/s

The load at the surface is assumed to be : $p_0 = -30 \times 10^6$ Pa; and the thickness H is: H=5000 m

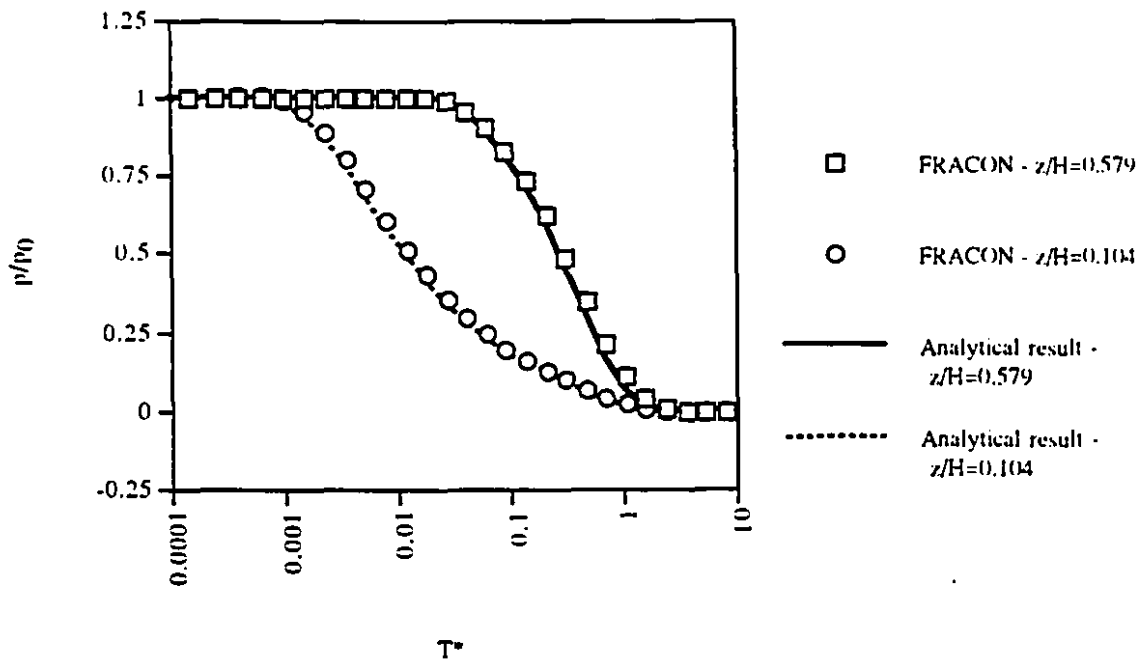

Figure 4.2 Pore pressure evolution at different depths

Figure 4.2 shows that the finite element results for the pore pressure variations with time agree well with the analytical results. The variations of normalized pore pressure p/p_0 with normalized time T* at two different depths are shown in figure 4.2. The normalized time is defined by:

$$T^* = \frac{c_v t}{H^2} \qquad (4.1)$$

and c_v is the coefficient of consolidation, that is related to the hydraulic conductivity K and the elastic constants by the relationship:

$$c_v = \frac{KE(1-\nu)}{\rho_f g(1-2\nu)(1+\nu)} \qquad (4.2)$$

where g is the acceleration of gravity and ρ_f is the density of the pore fluid.

In figure 4.3, the normalized surface settlement:

$$\frac{Gw}{p_0 H}$$

(where G is the shear modulus and w is the absolute settlement) is shown as a function of time. The agreement between the finite element and the analytical solutions is excellent.

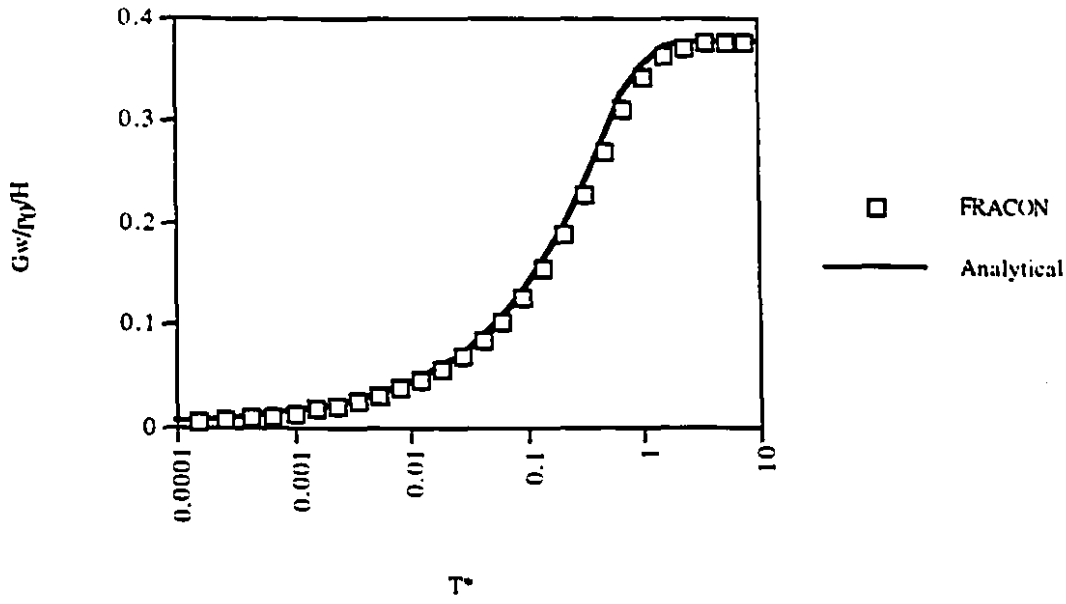

Figure 4.3 Vertical settlement of the surface

The above results of the FRACON code were obtained with a value of the integration constant γ=0.875. Figure 4.4 shows that with γ=0.5 some oscillations in the computed pore pressures occur at low values of T* (T*<0.001). For large values of T*, the finite element analysis compare very well with the analytical solution. For lower values of γ (0 or 0.2), the solution is unstable.

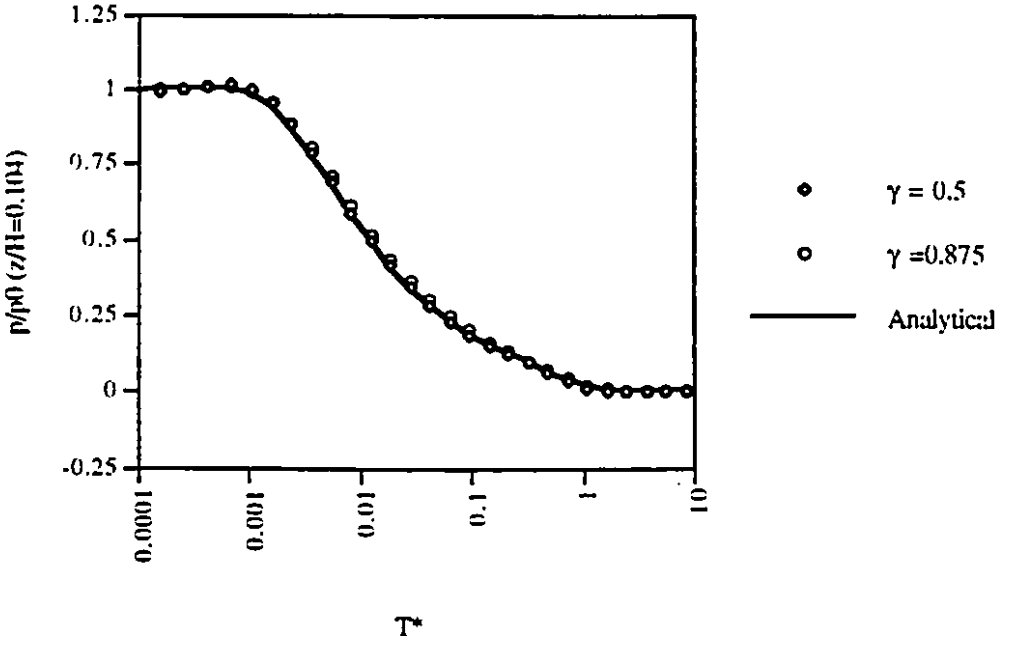

Figure 4.4 Effect of integration constant γ

4.2 Isothermal consolidation of a semi-infinite medium under plane strain and axisymmetric conditions

McNamee and Gibson (1960) developed analytical solutions for the axisymmetric and plane strain problems related to isothermal consolidation of a half-space subject to a pressure p_0 at the free surface. For plane strain conditions, the loaded area is a strip of width 2a, while for axisymmetric conditions, the loaded area is a circular region of diameter 2a (see figure 4.5). McNamee and Gibson (1960) developed integral expressions for the displacements, stresses and pore pressure. These infinite integrals can be numerically evaluated by using a suitable quadrature scheme. Simplifications can be made for the expression of the pore pressure when the Poisson's ratio is zero: i.e.

$$p(X.Z.T^*)/p_0 = \int_0^\infty K(X.\xi)e^{-\xi Z}\left\{\operatorname{erf}(\xi T^{*1/2}) + \operatorname{erf}\left(\frac{Z}{2T^{*1/2}} - \xi T^{*1/2}\right)\right\}d\xi \qquad (4.3)$$

where:

X=x/a (r/a for axisymmetric case), Z=z/a and :

$$T^* = \frac{\bar{c}\,t}{a^2} \text{ with } \bar{c} = \frac{2KG}{\rho_f g} \qquad (4.4)$$

$$K(X.\xi) = \begin{cases} \frac{2}{\pi\xi}\cos(X\xi)\sin\xi & \text{for plane strain} \\ J_0(X\xi)J_1(\xi) & \text{for axisymmetry} \end{cases} \qquad (4.5)$$

erf is the error function, defined by:

$$\operatorname{erf}(x) = \frac{2}{\sqrt{\pi}}\int_0^x e^{-\varepsilon^2}d\varepsilon$$

J_0 and J_1 are Bessel functions of the first kind of order 0 and 1 respectively.

The finite element mesh and the boundary conditions for this problem are shown in figure 4.5. The following input data are used:

a = 5869 m

$p_0 = -30\text{x}10^6$ Pa

$E=35\text{x}10^9$ Pa

$\nu = 0$

K (hydraulic conductivity for isotropic medium)=$5\text{x}10^{-11}$ m/s

The numerical and analytical results are compared in figure 4.6.a and in figure 4.6.b, respectively, for plane strain and axisymmetric conditions. In the numerical computation, a value of γ=0.875 was used. The agreement is quite good, considering that in the finite element analysis, artificial boundaries at finite distances from the loaded area have to be imposed. The FRACON code tends to overpredict the values of pore pressure with the boundary conditions shown in figure 4.5. Typically, at the peak of the pore pressure vs. time curve, the numerical value for the pore pressure is 3% higher than the true value obtained with the analytical solution; at late times (T^* =10), the boundary effects become more important, and the overprediction in the numerical result reaches a value of 30%. A second analysis, with a zero pore pressure condition specified at the right hand side boundary, was performed with the FRACON code. That resulted in an underprediction of the results by the finite element method, with typical absolute values of the underprediction similar to the former case. For both plane strain and axisymmetric conditions, the Mandel-Cryer effect (i.e. the development of a "peak" in the time-dependent response of the pore pressure) is manifested at all nodes being considered. The above phenomenon was mathematically demonstrated by Mandel (1950, 1953) for a brick-shaped body uniaxially loaded under plane strain conditions; and Cryer (1963) for a sphere subjected to a uniform pressure at its surface with free-draining conditions at this surface. The Mandel-Cryer effect has also been experimentally observed (Gibson et al., 1963; Verruijt, 1965). For the example of the uniformly loaded sphere, the Mandel-Cryer effect can be physically explained as follows (Cryer, 1963). At early times in the consolidation process, almost all of the volume change occurs near the surface where drainage occurs. Thus, the region near the surface will tend to contract, resulting in squeezing of the central regions. Consequently, the total radial stress in the central regions will increase. As there is little volume change in the central regions, the effective stress must remain constant and thus the

pore pressure must rise.

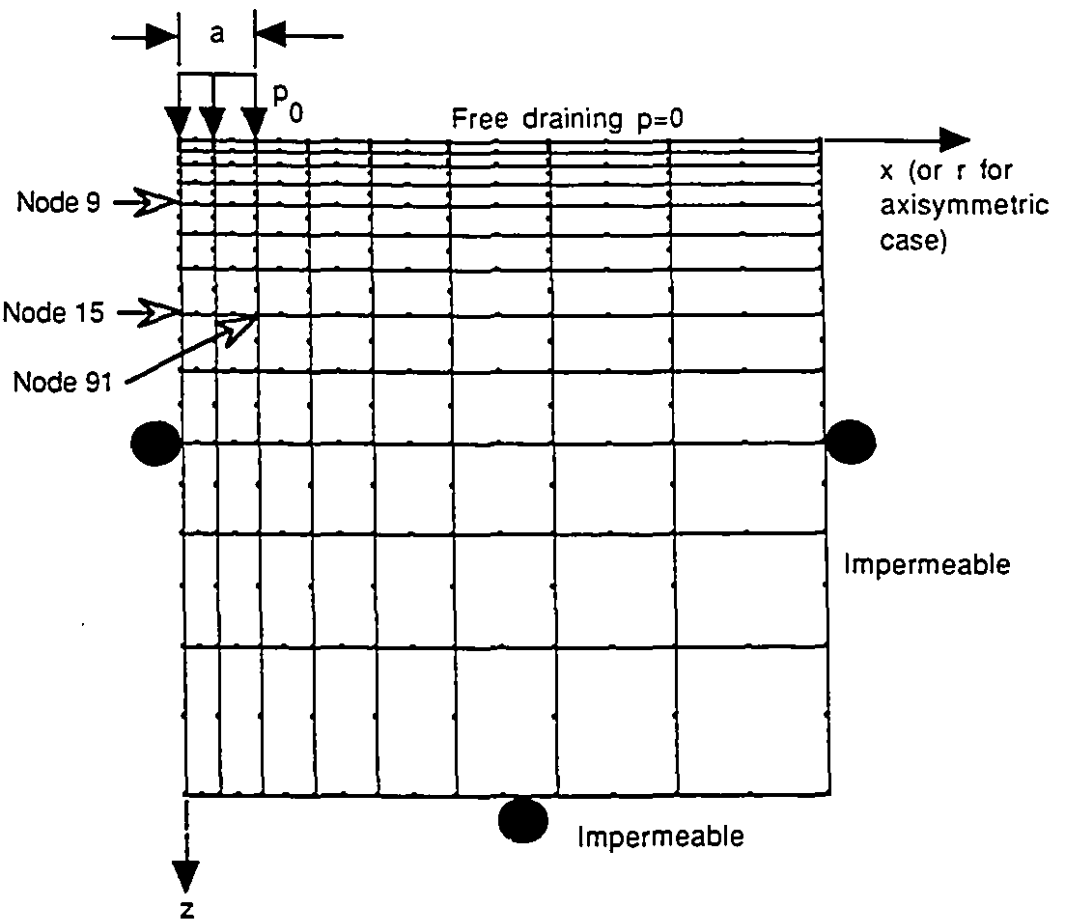

Finite element mesh dimension 50000 mx50000 m

Node 9 : x=0 z=45071
Node 15: x=0 z=36776
Node 91: x=5869 z=36776

Figure 4.5 Finite element mesh for consolidation of a half-space under plane strain or axisymmetric conditions

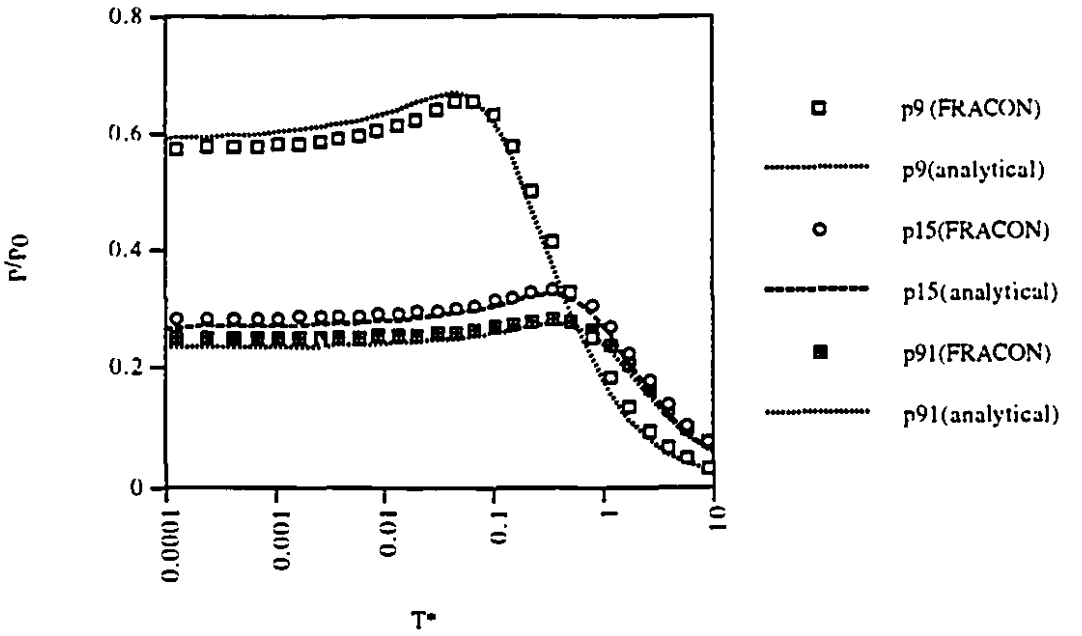

a)Plane strain

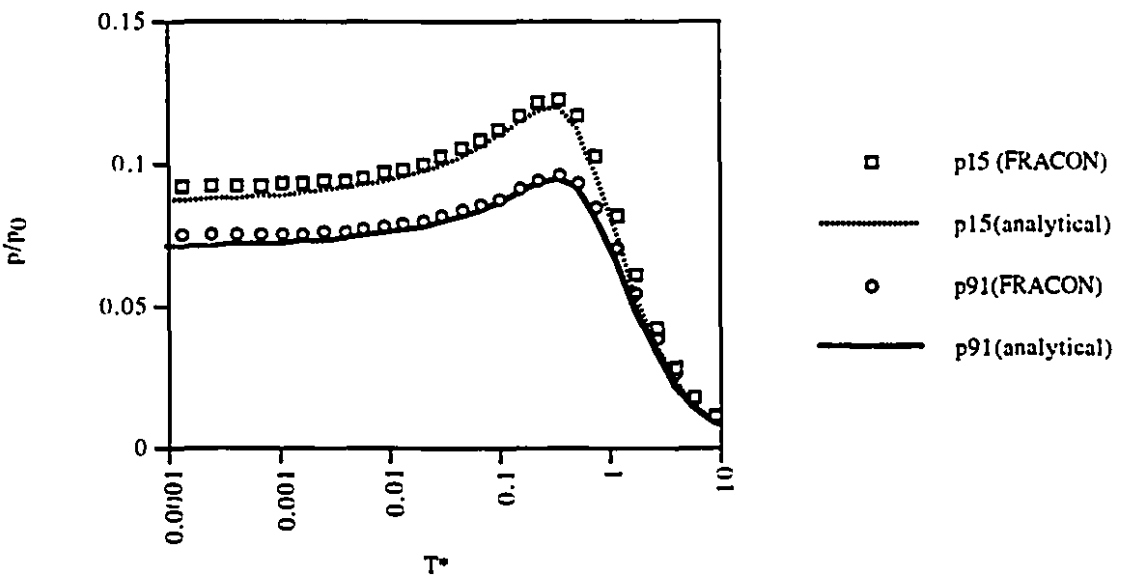

b)axisymmetric

Figure 4.6 Plane strain and axisymmetric isothermal consolidation

The integration in equation (4.3) is performed numerically using the symbolic manipulation code MATHEMATICA (Wolfram Research Inc, 1993, V.2.2). For the axisymmetric case, the numerical integration did not converge for node 9, due to the proximity of this node to the loaded area. Thus the results for that node is not shown in figure 4.6.b.

4.3 Thermally induced consolidation of an infinite medium with an embedded cylindrical heat source

Booker and Savvidou (1985) examined the problem of thermally induced consolidation of an infinite homogeneous saturated poroelastic medium due to an embedded volumetric heat source V of constant intensity q (figure 4.7).

The integral expressions for the temperature and pore pressure are:

$$T(x,y,z,t) = \int_V \frac{q}{4\pi\kappa R}\operatorname{erfc}\left(\frac{R}{2\sqrt{\frac{\kappa}{\rho C}t}}\right)dx_s dy_s dz_s \qquad (4.6)$$

$$-p(x,y,z,t) = \int_V \frac{\Phi}{1-\rho C c_v/\kappa}\frac{q}{4\pi\kappa R}\left\{\operatorname{erfc}\left(\frac{R}{2\sqrt{\frac{\kappa}{\rho C}t}}\right) - \operatorname{erfc}\left(\frac{R}{2\sqrt{c_v t}}\right)\right\}dx_s dy_s dz_s \qquad (4.7)$$

where:

$$\Phi = \{(1-n)\beta_s + n\beta_f\}(\lambda+2G) - \beta(\lambda+2\frac{G}{3}) \tag{4.8}$$

$$c_v = \frac{K(\lambda+2G)}{\rho_f g} \tag{4.9}$$

$$R=((x-x_s)^2 + (y-y_s)^2 + (z-z_s)^2)^{1/2} \tag{4.10}$$

x_s, y_s, z_s are the coordinates of a point inside the volume V (see figure 4.7)

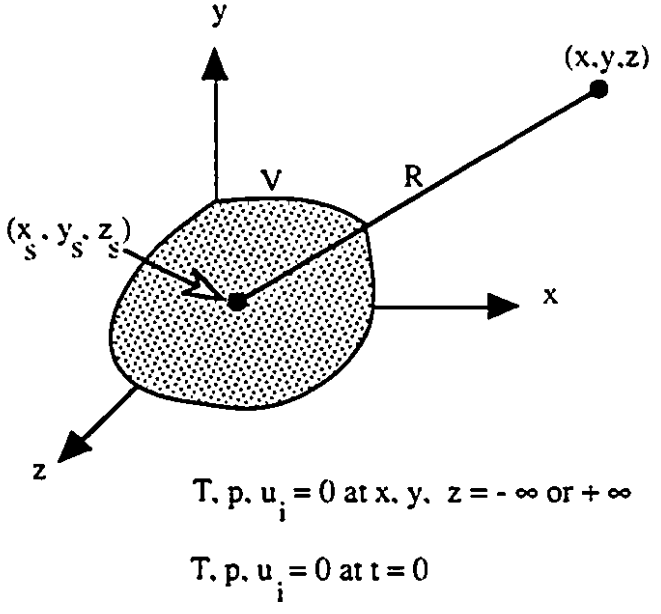

Figure 4.7 Thermally induced consolidation of poroelastic medium - Booker and Savvidou's (1985) problem

Booker and Savvidou's solutions, equations (4.6) and (4.7), are used to obtain analytical results in this section and sections 4.4 and 4.5. In this section, we consider a cylindrical heat source. The same problem has been simulated by Lewis and Schrefler (1987) with the finite element code PLASCON, using an unspecified system of units. For purposes of comparison, we use here input data identical to those specified by Lewis and Schrefler (1987) with the assumption that this data has consistent units:

radius of cylindical source: 0.3

height of cylindical source: 2

q= 1768.39

E=6000

$\nu = 0.4$

K (hydraulic conductivity for isotropic medium) = 0.4×10^{-5}

κ (thermal conductivity for isotropic medium) = 1.02857

ρC=40

n (porosity) = 0.5

β (volumetric thermal expansion coefficient of the solid matrix) = 0.9×10^{-6}

β_s (volumetric thermal expansion coefficient of the solid grain material)= 0.9×10^{-6}

β_f (volumetric thermal expansion coefficient of the pore fluid)= 0.63×10^{-5}

The finite element mesh used for this problem along with the boundary conditions are shown in figure 4.8. Axisymmetric conditions are specified. The results for the temperature and pore pressure at three different nodes are shown in figure 4.9. The results from the

FRACON code compare well with the analytical results. It could be seen that at all points, the pore pressure increases due to thermal expansion of the pore fluid, and then gradually dissipates as the medium is allowed to consolidate.

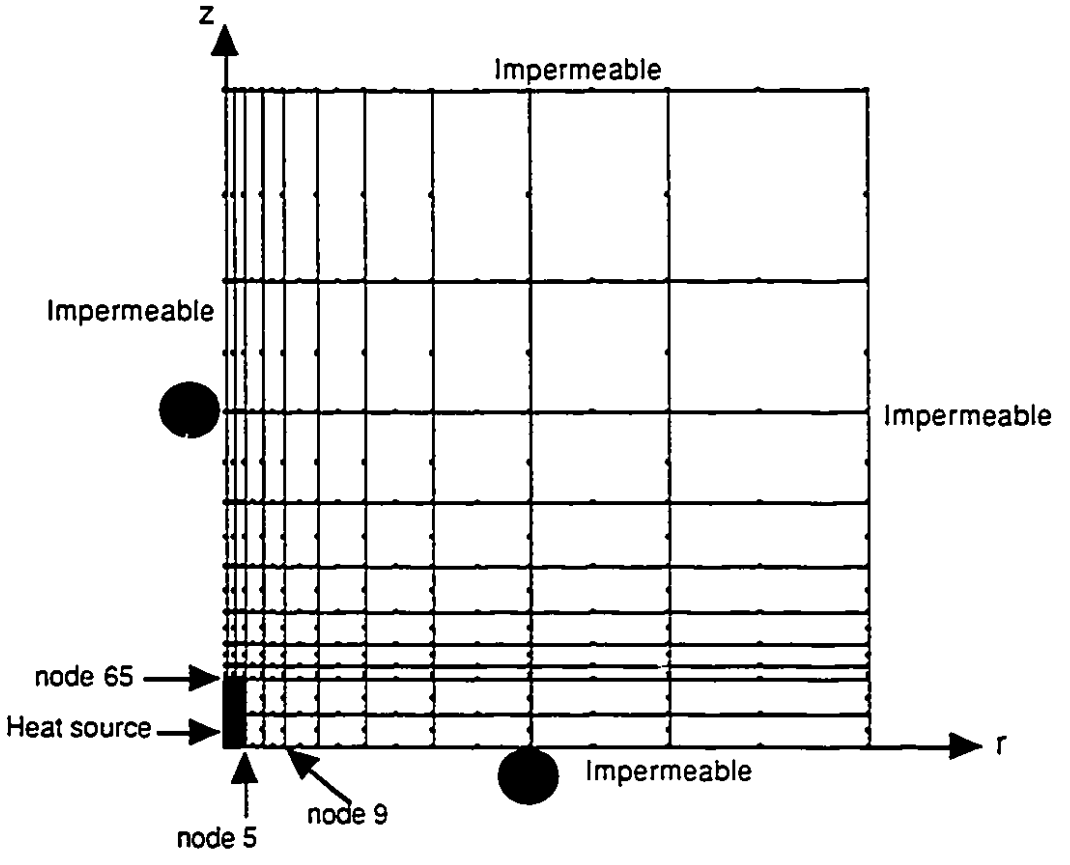

Node 5: x=0.3 z=0
Node 9: x=0.914 z=0
Node 65: x=0 z=1.

Figure 4.8 Consolidation of an infinite medium around a cylindrical heat source

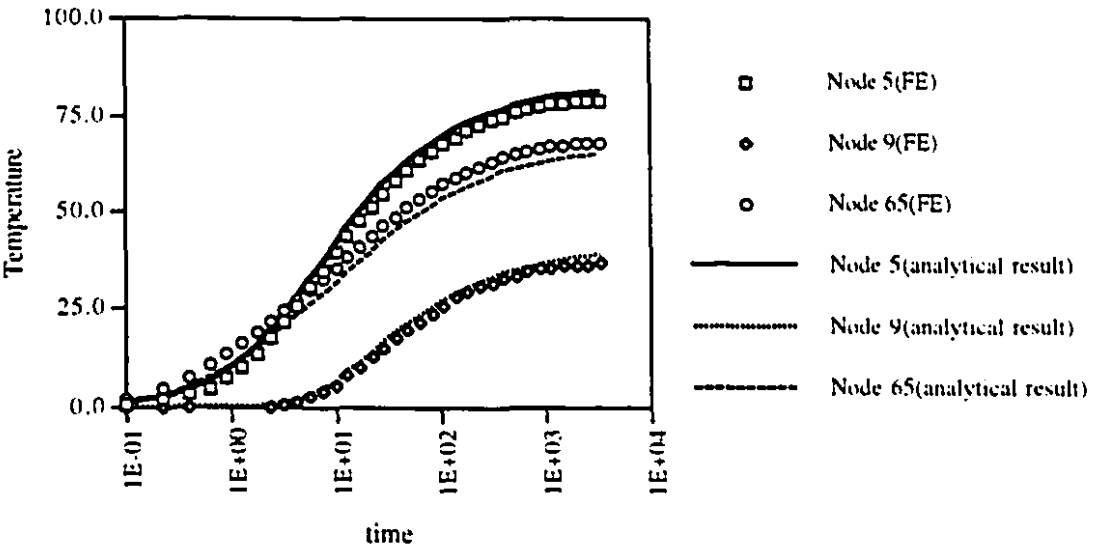

a) Temperature

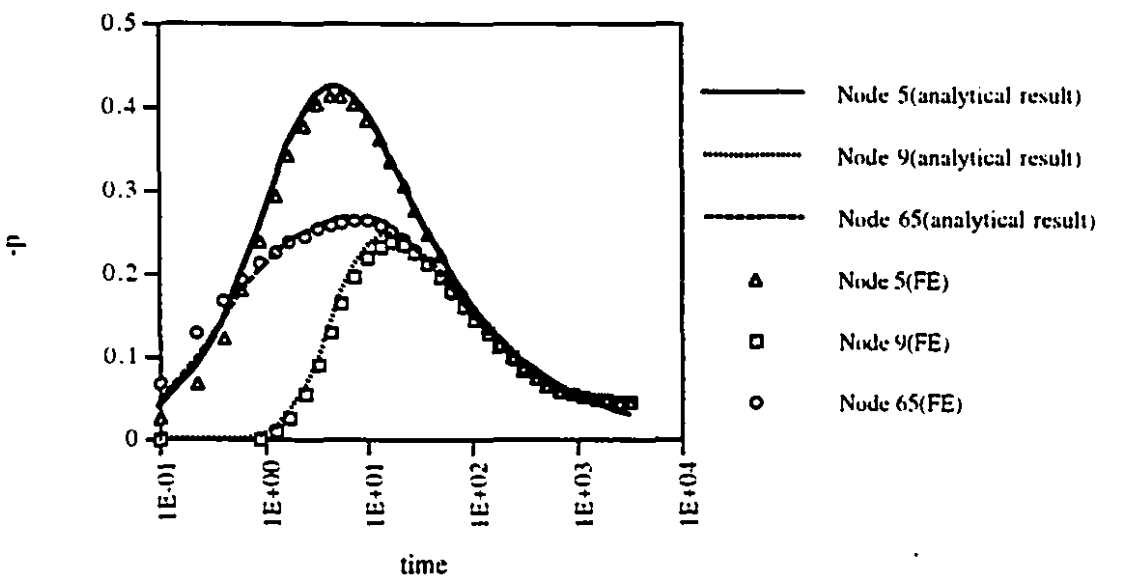

b) Pore pressure

Figure 4.9 Cylindrical heat source - Variation with time of temperature and pore pressure at different locations

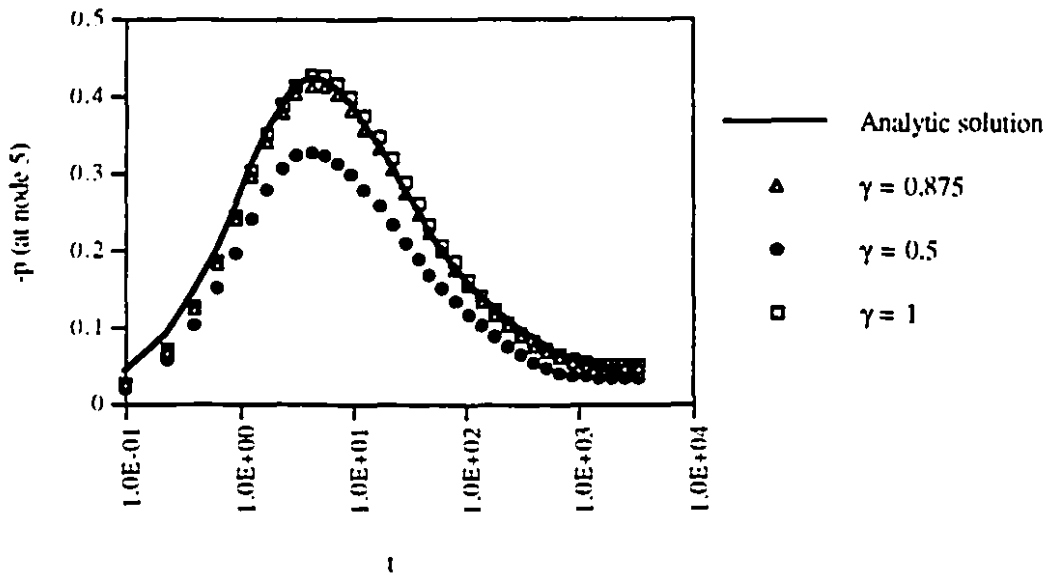

Figure 4.10 Cylindrical heat source - Effects of integration constant γ

The numerical results shown in figure 4.9 were obtained with the FRACON code using an integration constant γ=0.875. Figure 4.10 shows that values closer to 1.0 give a more accurate numerical result. The Crank-Nicholson scheme, with γ=0.5 significantly underestimates the pore pressure increase. The above result shows that, in contrast to the associated isothermal problem (cf. section 4.1), thermally induced pore pressure varies much more rapidly with time. Consequently, it is recommended that a value of γ=1 be utilized in performing the time integration schemes for most thermal consolidation problems. This value of γ is utilized in the remainder of the problems considered in this thesis.

4.4 Consolidation of an infinite medium with an embedded line heat source

We consider here the thermal consolidation problem for a line source of 1 m length emitting heat at a rate of q = 40 W/m. The schematic description of the physical problem is illustrated in figure 4.11. The finite element mesh and the boundary conditions are also shown in figure 4.11. Plane strain conditions are assumed in the finite element analysis. The line source runs through node 1 shown in figure 4.11. The following properties, typical of a cementitious material used in an experiment performed at Carleton University (Selvadurai, 1994; cf. Chapter 4), were used in the analysis:

$n = 0.001$

$E = 27$ GPa

$\nu = 0.24$

$K = 1 \times 10^{-12}$ m/s

$\kappa = 0.563$ J/m/s/°C

$\rho C = 2 \times 10^{6}$ J/m^3/°C

$\beta_s = \beta = 0.2 \times 10^{-4}$ °C^{-1}

$\beta_f = 0.4 \times 10^{-3}$ °C^{-1}

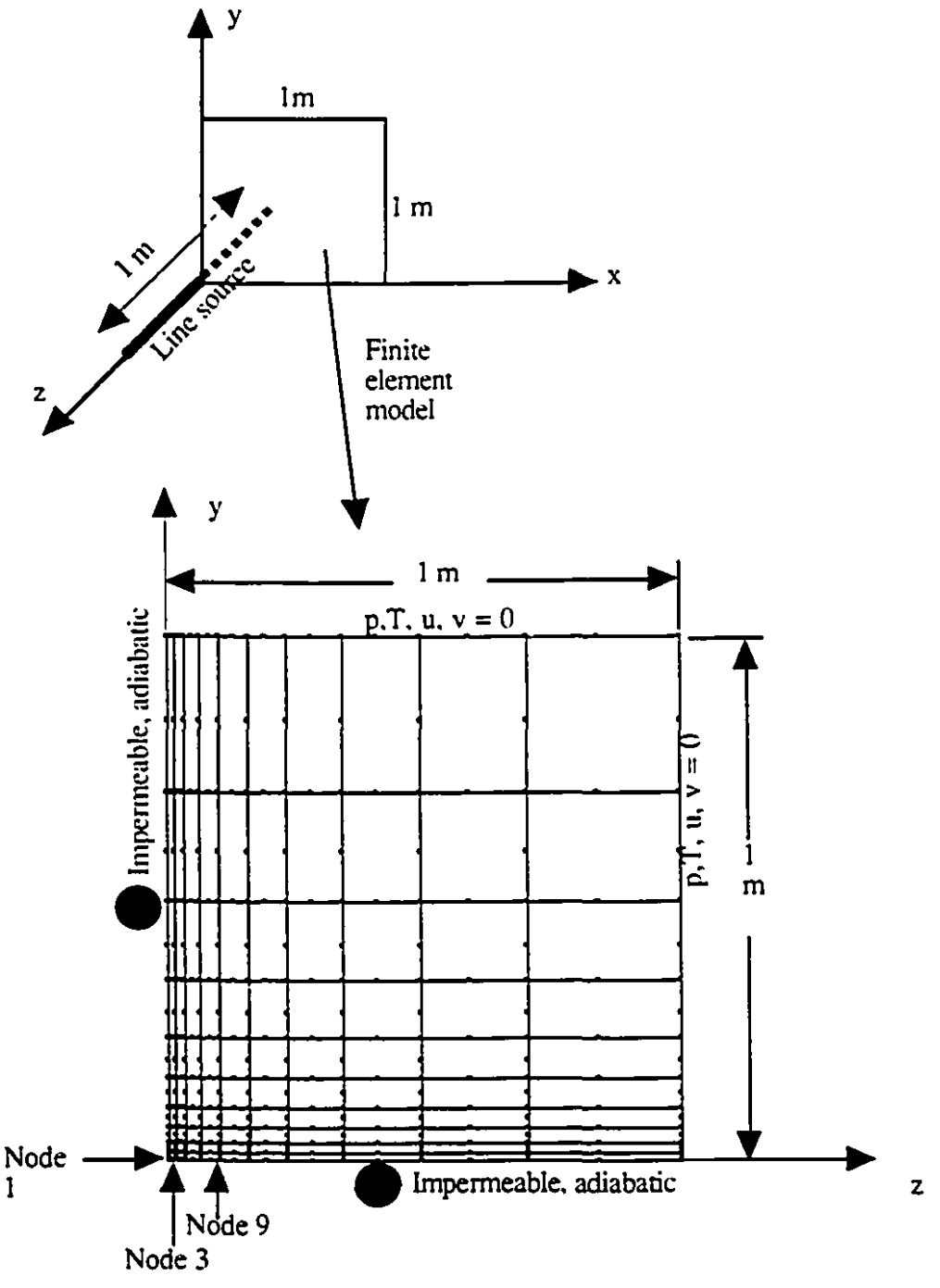

Node 3: x=0.014213 m y=0
Node 9: x=0.1 m y=0

Figure 4.11 Consolidation around a line heat source

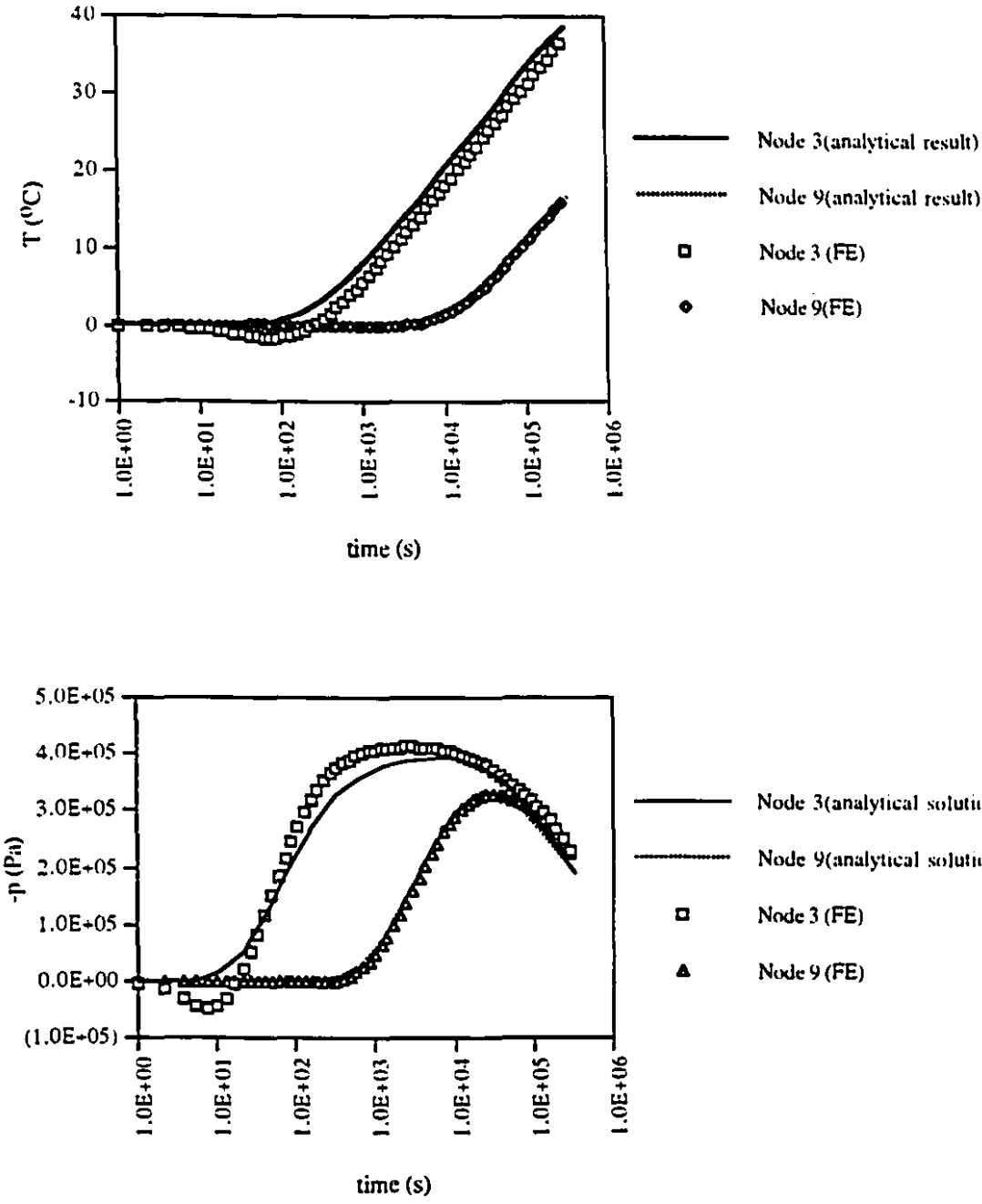

Figure 4.12 Line heat source- Variation of temperature and pore pressure with time

The temperature and pore pressure at nodes 3 and 9 are shown in figure 4.12. Except for some early time (t<100 s) oscillations for both temperature and pore pressure close to the heat source (node 3, at a distance of 0.014213 m from the source), there is reasonable agreement between the numerical and analytical results.

4.5 Consolidation of an infinite medium with a discoidal heat source

The same type of porous material as in section 4.4 is considered. The heat source now has the shape of a disc, with a heat output q= 1000 W/m^2. The schematic description of the physical problem is illustrated in figure 4.13. The finite element mesh and the boundary conditions are also shown in figure 4.13. Axisymmetric conditions are imposed in the finite element analysis. The disc-shaped heat source is centered at node 1 (figure 4.13): it has a radius of 0.0339 m, extending from node 1 to node 5.

As shown in figure 4.13, the agreement between numerical and analytical results for temperature and pore pressure is satisfactory. Close to the source (node 5) the temperature is underpredicted by the FRACON code; the pore pressure is underpredicted at early times but the peak and post-peak values for the pressure are overpredicted. The above results for node 5 suggest that, when accurate numerical results are required near the heat source, a more refined mesh discretization will be needed.

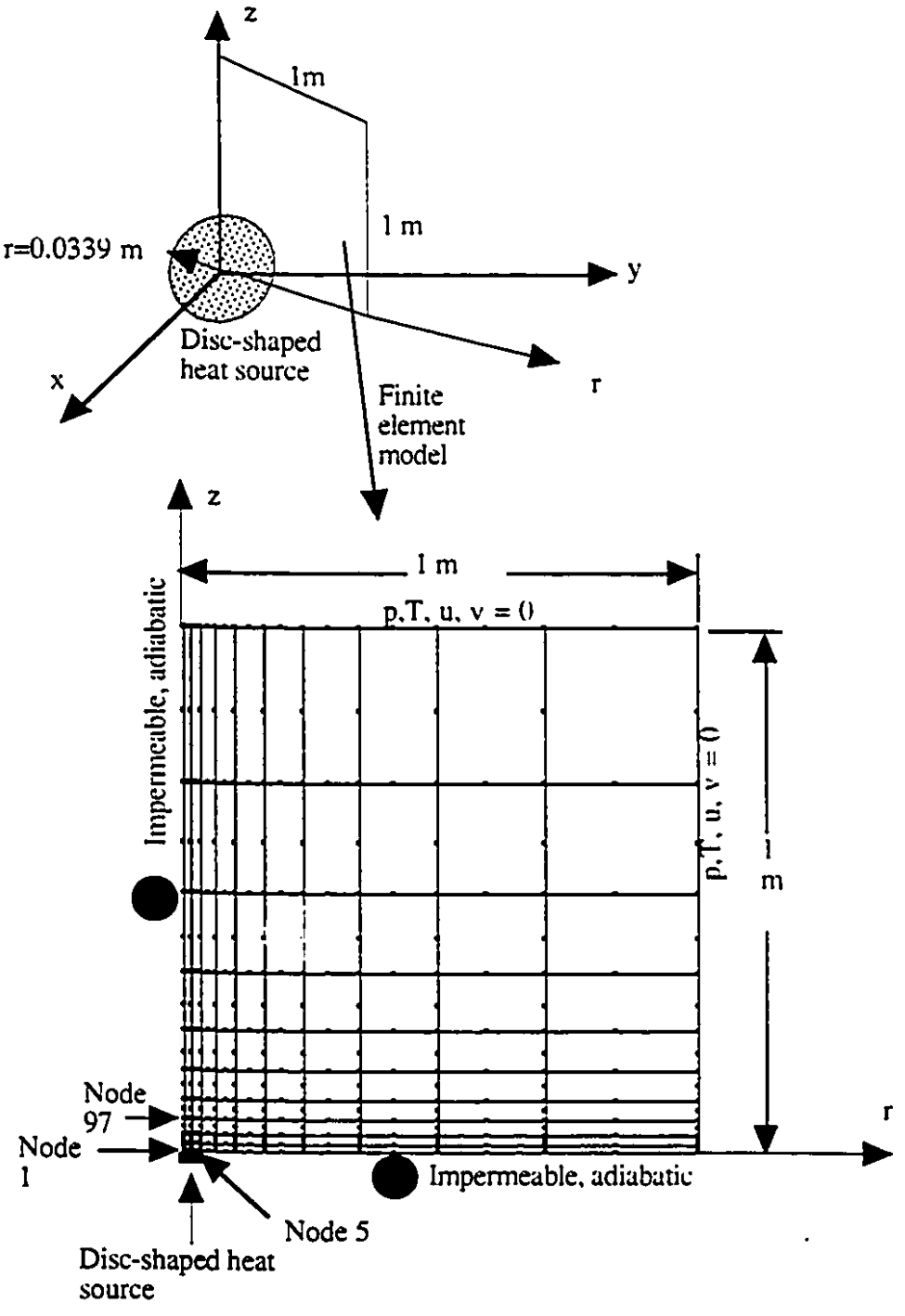

Node 5 r=0.0339 m ; z=0
Node 97 r=0 ; z= 0.06163 m

Figure 4.13 Consolidation around a disc-shaped heat source

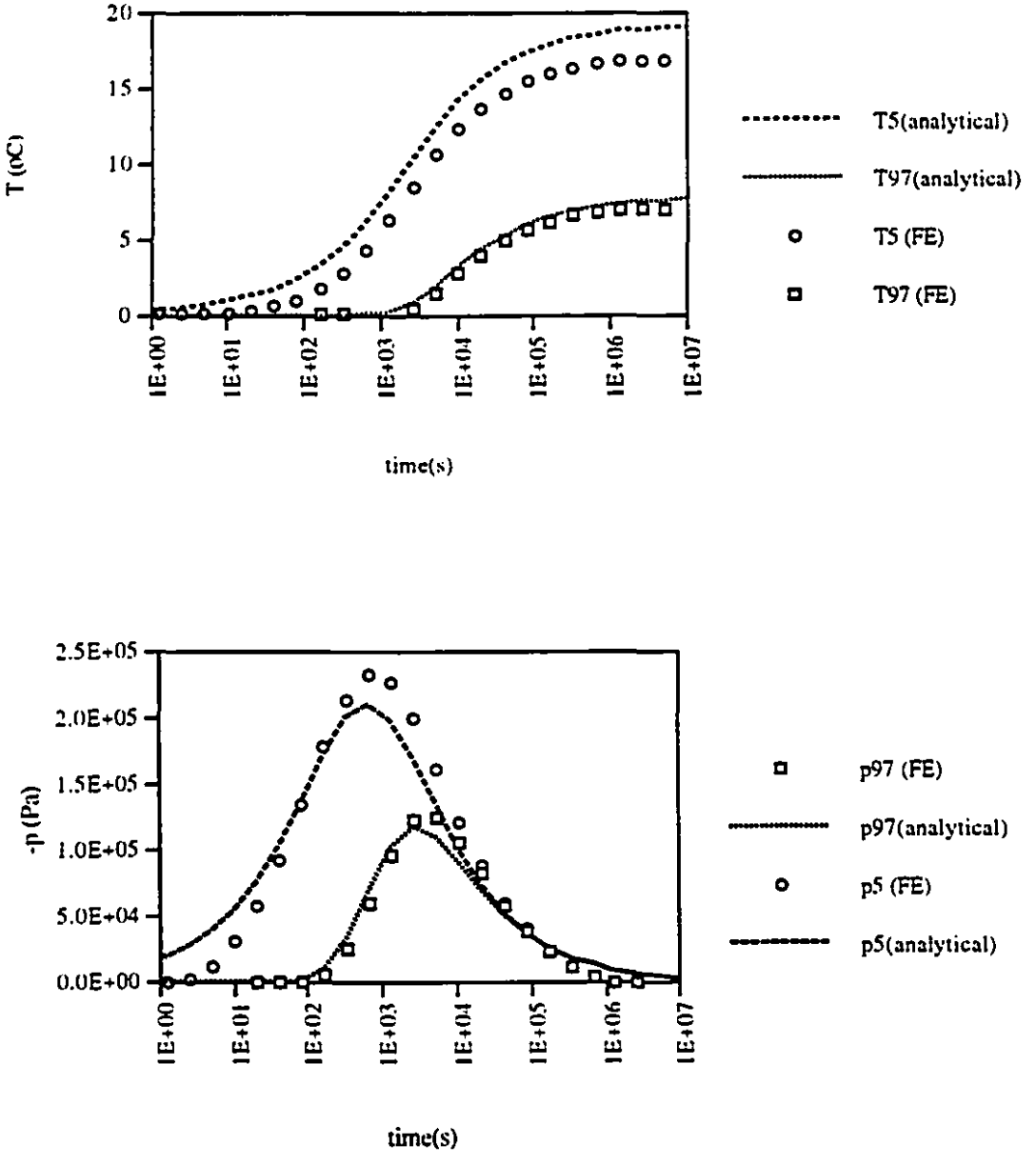

Figure 4.14 Discoidal heat source- Temperature and pore pressure evolution

4.6 Non-isothermal consolidation of a soil column

We perform here an intercode comparison for the problem of the non-isothermal consolidation of a soil column which is subjected to the combined action of a Heaviside or step function of heating and loading at its surface. To our knowledge, there is no recorded analytical solution for this problem. The problem was simulated by Lewis and Schrefler (1987) using the finite element code PLASCON and is analyzed here with the FRACON code. The finite element mesh and the boundary conditions used for the FRACON analysis are shown in figure 4.15. The mesh size and the initial time step used in the FRACON analysis is comparable to those used by Lewis and Schrefler (1987). Plane strain conditions are imposed. The surface of the soil column is submitted at time t=0 to a surface pressure p_0 and a temperature increase dT. Both loads will remain unchanged in value for time t>0.

The input data for the analysis with FRACON are the same as the ones used by Lewis and Schrefler (1987), and are in unspecified units:

$p_0 = -1$

$dT = 50$

$E=6000$

$\nu = 0.4$

$K = 0.4 \times 10^{-5}$

$\kappa = 1.02857$

$\rho C=40$

$n = 0.5$

$n = 0.5$

$\beta_s = \beta = 0.9 \times 10^{-6}$

$\beta_l = 0$

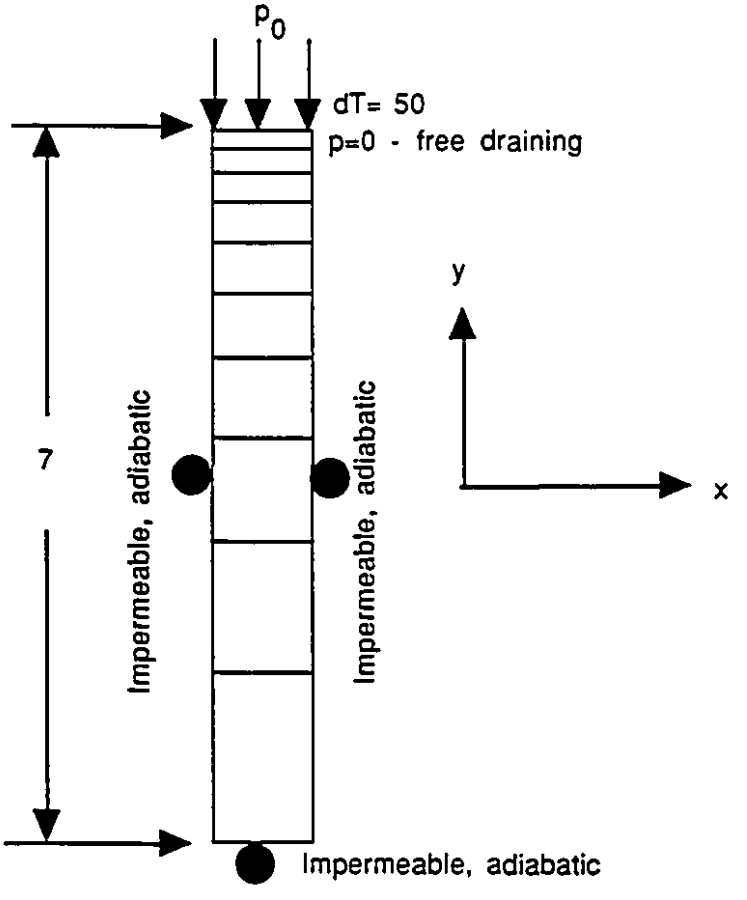

Figure 4.15 Non-isothermal consolidation of a soil column

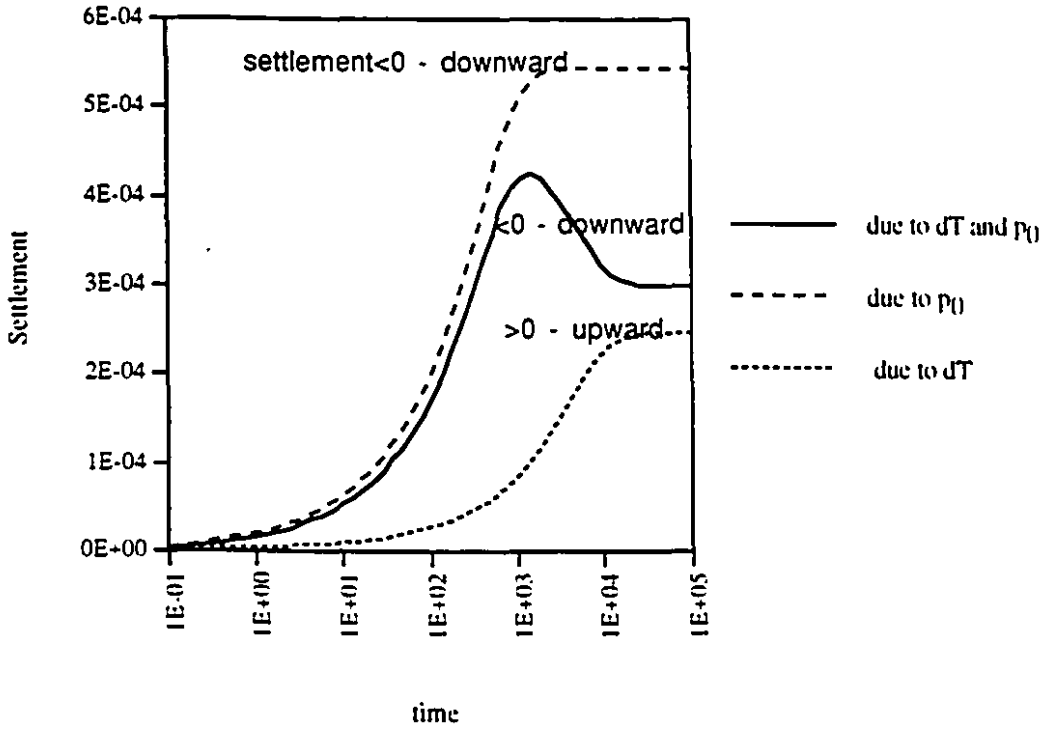

a) Results from FRACON

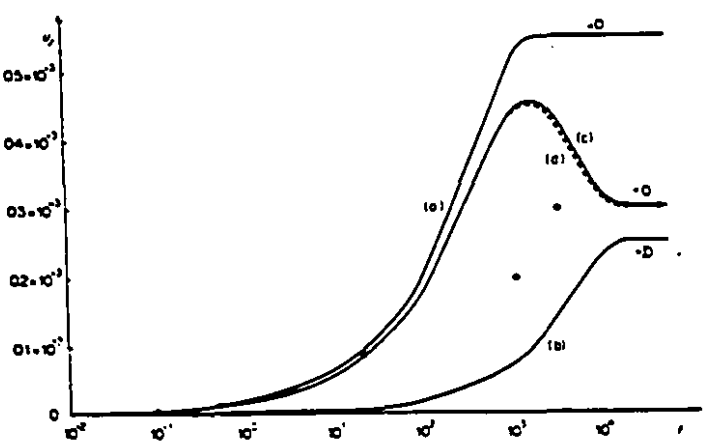

b) Results from PLASCON (Lewis and Schrefler, 1987)

Figure 4.16 Non-isothermal consolidation of a soil column - Surface settlement

The variation of the surface settlement with time is shown in figure 4.16. A visual comparison between figure 4.15 and a similar curve from Lewis and Schrefler, 1987 (fig. 7.6, curve c) shows excellent agreement between the FRACON and PLASCON results. The peak of the settement curve is due to the non-isothermal, elastic nature of the problem. The temperature increase dT tends to expand the soil column and create upward movement of the surface, while the applied pressure p_0 has the opposite effect. The settlement of the surface (middle curve) is the sum of the individual displacement caused by p_0 (upper curve) and dT (lower curve). The transient surface settlement due to p_0 reaches a steady state value sooner than the transient upward displacement due to dT, resulting in the observed peak. The upward movement due to the temperature still takes place after the peak is attained, resulting in rebounding of the surface. The final steady-state settlement is reached when both the thermally and mechanically induced displacements are at steady-state.

The exact value of the steady-state settlement and stresses for the above problem can be obtained analytically by writing Hooke's law (cf. equation 2.8) and imposing the following conditions:

$e_{xx}=e_{11}=0$

$e_{zz}=e_{33}=0$

$\sigma'_{yy}=\sigma'_{22}=p_0=-1$

One obtains the following expressions:

$$\Delta = H\left(\frac{p_0(1+\nu)(1-2\nu)}{E(1-\nu)} + \frac{\beta(1+\nu)\delta T}{3(1-\nu)}\right)$$

$$\sigma'_{xx} = \sigma'_{zz} = \frac{\nu p_0 - E\frac{\beta}{3}\delta T}{1-\nu} \qquad (4.11)$$

where H is the height of the soil column and Δ is the surface settlement.

One then obtains the following almost perfect agreement between the exact and numerical results:

Δ = 0.2995x10^{-3} (FRACON) vs. 0.2994x10^{-3} (exact)

$\sigma'_{xx} = \sigma'_{zz}$ = -0.8167 (FRACON) vs -0.8167 (exact)

4.7 Constant pressure test in a joint

A method for determining the permeability of a joint in a rock mass involves the injection of water into a borehole intersecting the plane of the joint. These tests are described in detail in chapter 7. Let us consider a horizontal joint in a rock mass. The type of injection test called " the constant pressure test" consists of sealing a section of the borehole at the elevation of the joint, and injecting water in the sealed section. Once a certain value of the pressure is reached, this value is maintained constant. The flow rate is then measured. The flow transient is a function of the constant pressure in the sealed borehole section, and of the permeability of the joint and its normal stiffness. Assuming that the joint is axially symmetric around the borehole (see figure 4.17) and that the joint behaves in a linear elastic manner, one can obtain an analytical solution to the problem in the following

manner.

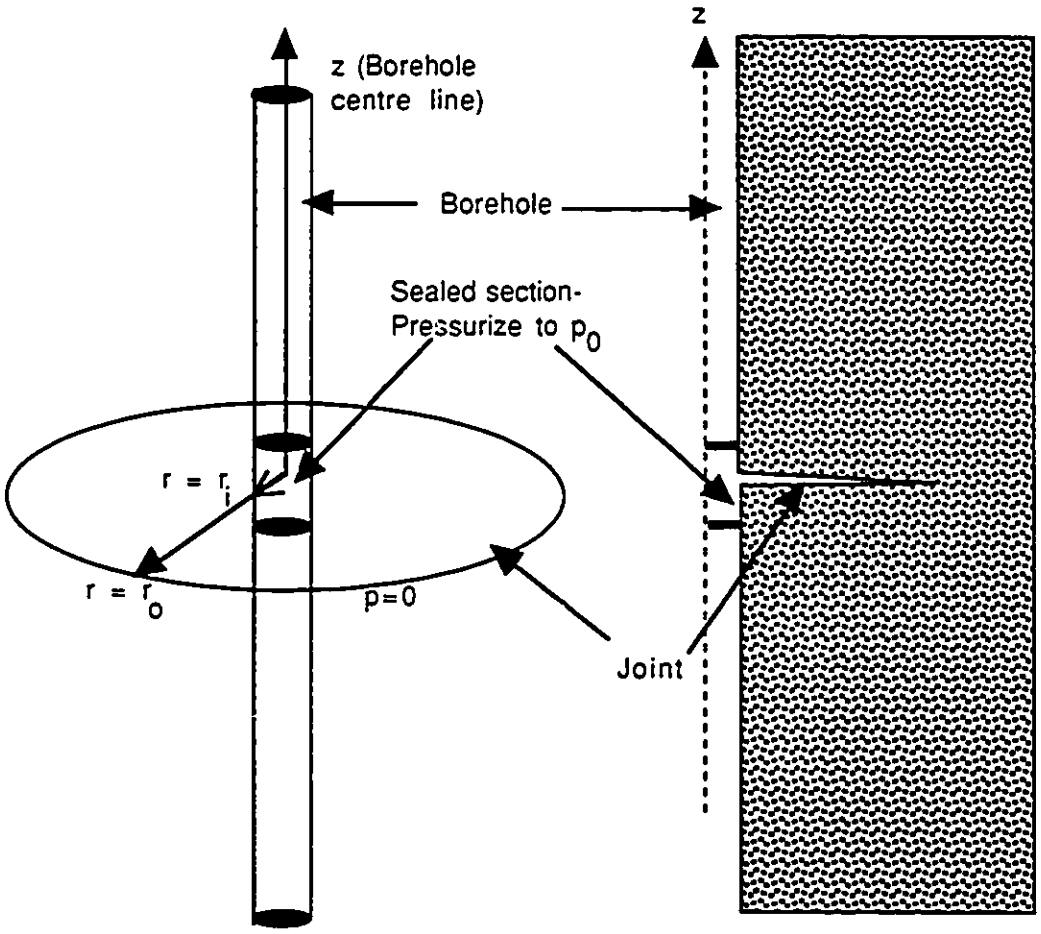

Figure 4. 17 Schematics of borehole injection test

Assuming that flow takes place only radially along the joint, and neglecting the compressibility of both the water and the solid grains, the equation of fluid mass

conservation under axisymmetric isothermal conditions (3.64 c) for the horizontal fracture becomes:

$$\frac{\partial}{\partial r}\left(\frac{k}{\mu}\left[\frac{\partial p}{\partial r}\right]\right)+\frac{1}{r}\left(\frac{k}{\mu}\left[\frac{\partial p}{\partial r}\right]\right)+\frac{\partial \varepsilon_v}{\partial t}=0 \qquad (4.12)$$

where k is the permeability of the fracture in the radial direction.

We further assume that displacement in the joint takes place only in the normal direction. Then:

$$\varepsilon_v = e_{zz} = p/D_n \qquad (4.13)$$

where D_n is the normal stiffness of the joint (cf. equation 3.71).

Substituting (4.13) into (4.12), one obtains the following uncoupled equation for pressure transient in the joint:

$$\frac{\partial}{\partial r}\left(\frac{k}{\mu}\left[\frac{\partial p}{\partial r}\right]\right)+\frac{1}{r}\left(\frac{k}{\mu}\left[\frac{\partial p}{\partial r}\right]\right)+\frac{1}{D_n}\frac{\partial p}{\partial t}=0 \qquad (4.14)$$

Equation (4.14) has the form of a classical diffusion equation. For the following boundary and initial conditions:

$$p=p_0 \text{ at } r=r_i \text{ and } p=0 \text{ at } r=r_o \quad \text{for } t>0 \; ; \; p(r)=0 \text{ at } t=0 \qquad (4.15)$$

the solution of equation (4.14) is available in standard textbooks (see e.g. Crank, 1975; Chapter 5). In equation (4.15), r_i is the radius of the borehole, r_o is the radius of the joint

and p_0 is the constant pressure maintained in the sealed section of the borehole (see figure 4.16).

The above problem was simulated with the FRACON code. The finite element mesh with the boundary conditions is shown in figure 4.18. The following properties of the joint are used:

$D_n = 10^6$ Pa

$k = 2.4 \times 10^{-11}$ m^2

$r_i = 0.028$ m

joint aperture $b = 3 \times 10^{-6}$ m

$r_o = 2$m

$p_0 = -7.5$ MPa

The fluid pressure and the vertical displacement at different radii in the joint are shown in figures 4.19 and 4.20. Good agreement between the finite element results and the analytical solutions could be observed. The fluid flow from the sealed borehole section into the fracture is shown in figure 4.21. Again the agreement between numerical and analytical values is good.

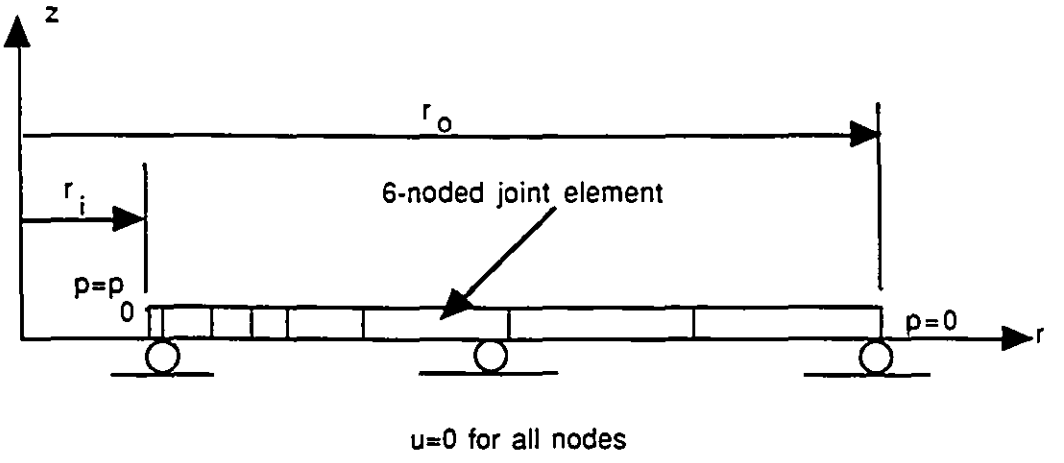

Figure 4.18 Finite element mesh for borehole injection test

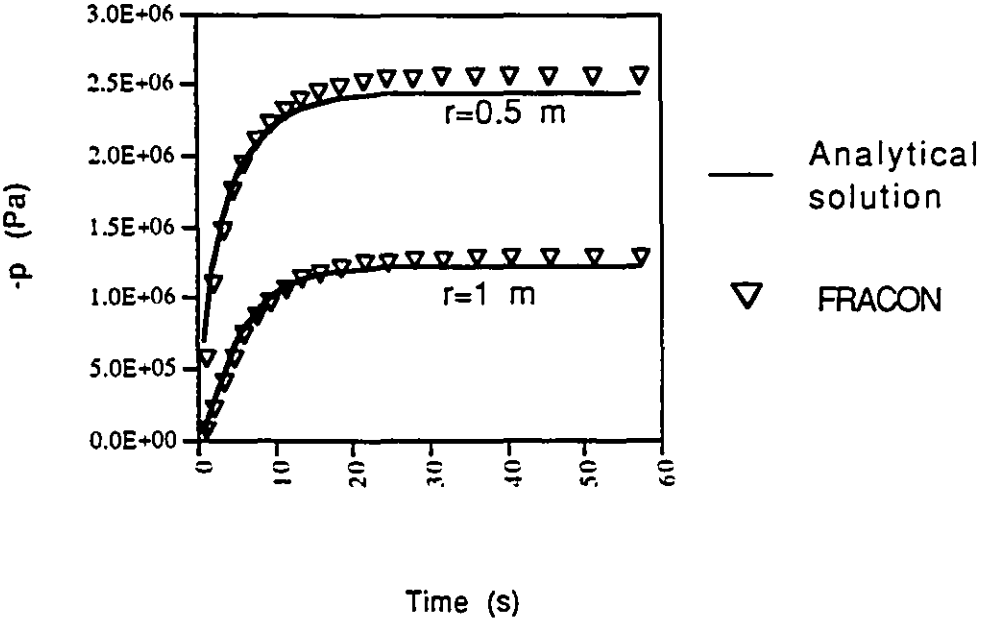

Figure 4.19 Pore pressure evolution in the joint

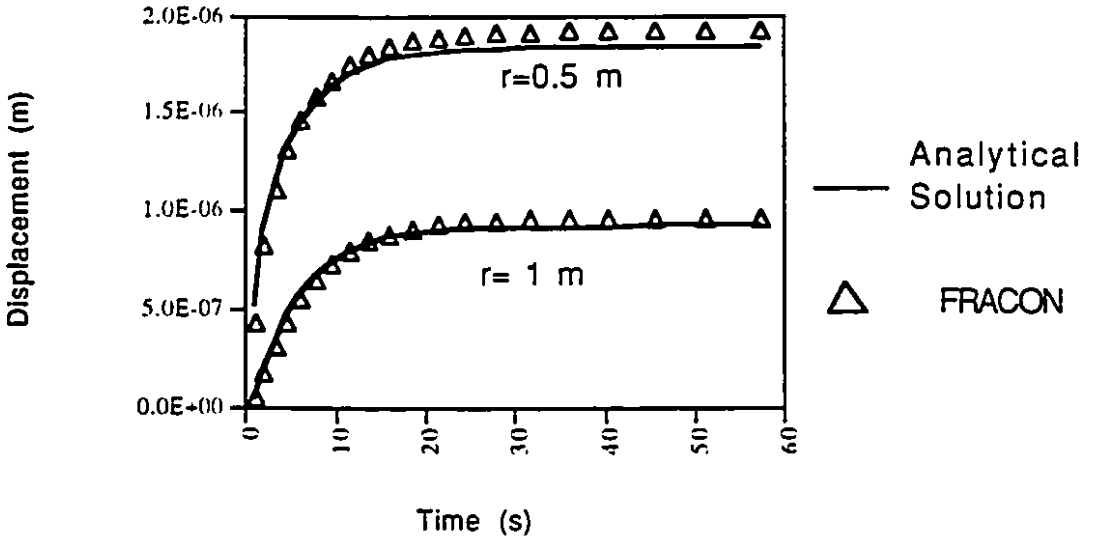

Figure 4.20 Vertical displacement in the joint

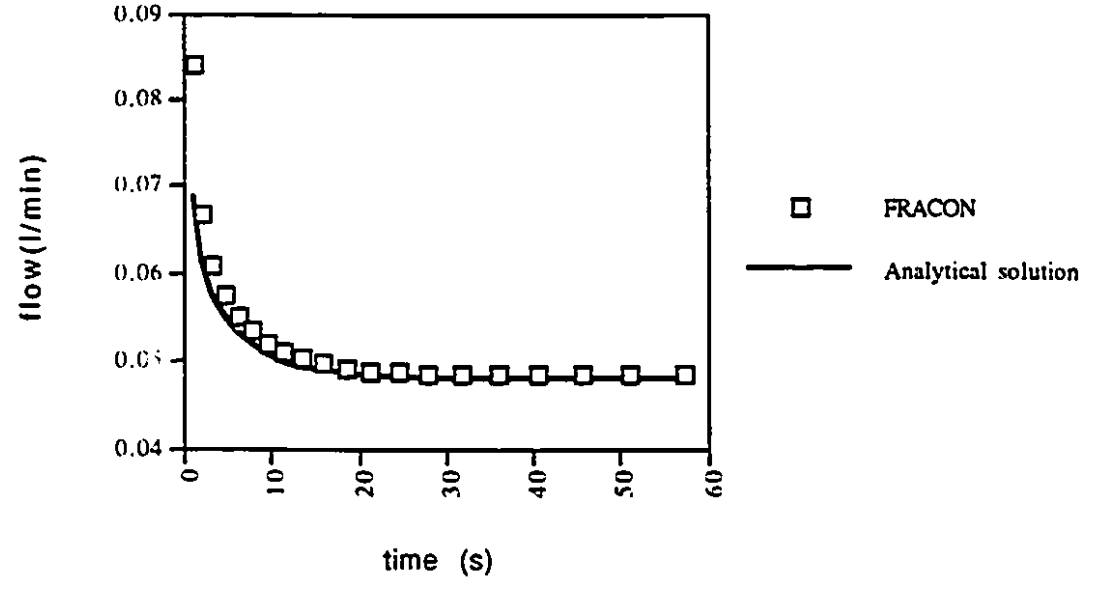

Figure 4.21 Flow from the sealed borehole section into the joint

4.8 Conclusion

Verification is an important aspect of modern computational modelling exercises. For example, in the context of nuclear fuel waste management, the safety performance of NFW disposal systems is assessed with computer codes. These codes should be extensively tested for accuracy. Code verification is the first step in building confidence in the adequacy of a computer code as a tool to perform safety assessment. The next step in building this confidence is by comparing the code's results with experimental data, and this will be the subject of chapters 5 and 7.

The availability of analytical solutions is a necessary prerequisite to perform code verification. Due to the present focus on numerical methods among the majority of investigators, analytical solutions for non-isothermal consolidation problems are scarce. To our knowledge, the only solutions available for non-isothermal consolidation problems are the ones developed by Booker and Savvidou (1985) for unfractured saturated poroelastic media. These solutions were presented in this chapter. To our knowledge, no analytical solution exist for thermal consolidation effects in joints. Due to the importance of code verification, we feel that more emphasis should be brought to mathematical methods in future investigations.

In this chapter, we have compiled a series of verification problems that include both isothermal and non-isothermal effects. For these problems, good comparison both from the point of view of trends and actual magnitudes, was obtained between the numerical results of the FRACON code and the analytical results. The results presented in this chapter are considered an important development since the verification problems which were presented can constitute a set of benchmark problems for other code developers.

CHAPTER 5

SIMULATION OF A LABORATORY EXPERIMENT ON AN UNFRACTURED CEMENTITIOUS MATERIAL

In order to validate the extended theory of Biot's consolidation presented in chapter 2 for unfractured porous rock, a laboratory experiment involving the heating of a saturated synthetic rock was performed at the civil engineering laboratory at Carleton University (Selvadurai, 1994). Experimental investigations of coupled T-H-M processes in unfractured rock are very rare. In this chapter we present a description of this experiment and its simulation with the FRACON code.

5.1 Description of the experiment

Complete descriptions of the experimental details and procedures are given by Selvadurai (1994). A cylinder, 50 cm in diameter and 46 cm in height was cast with a special mixture of cementitious SIKA grout using a sono-tube as a mould for casting the cylinder. The SIKA grout was chosen due to its high degree of workability and low shrinkage potential. Three pore pressure tranducers were positioned along the axis of

the mould with thin plastic string harnesses prior to placing the SIKA grout. They were located at distances of 16 mm, 34 mm and 72 mm from the surface of the cylindrical block where a heater would be emplaced. The details of the pore pressure transducers are shown in figure 5.1. Type K thermocouples were also positioned close to the pore pressure transducers and at salient points close to the heater.

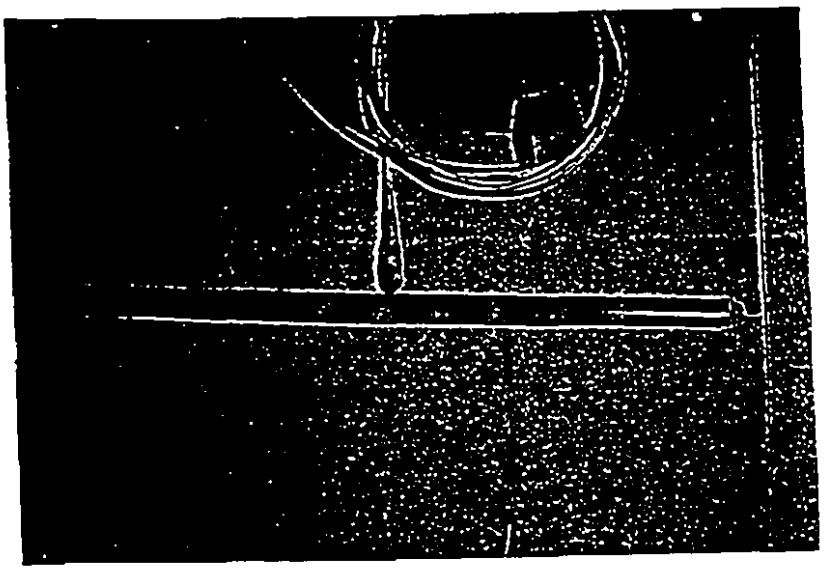

(a) ALD–MPM Miniature Transducer

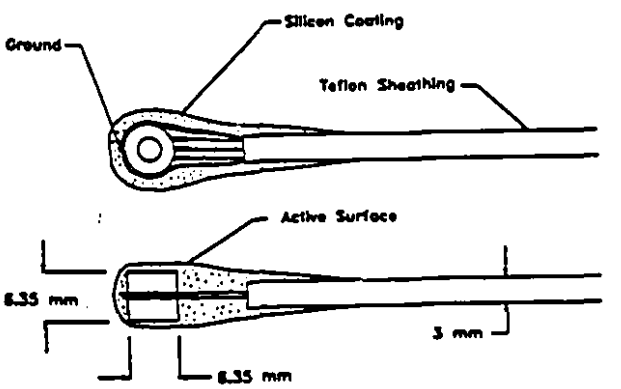

(b) Dimensions of the Pressure Transducer

Figure 5.1 Pore pressure transducers used in the heated cylinder experiment (from Selvadurai, 1994)

The grout was mixed with sand in a rotary mixer and wet sieved to remove particles larger than 5 mm. The mixture was then poured into the mould and the plastic wire harnesses were removed from the grout mixture at the completion of pouring. The mould was removed after 10 days of curing in a moist atmosphere. After an additional 18-day curing period, the cylinder was vacuum saturated. The cylinder was then immersed in water and a heat source was applied at the surface. Temperatures and pore pressures were continuously recorded by a computerized data acquisition system during the experiment.

5.2 Numerical simulation

The properties of the grout material were measured separately by conducting tests on small samples made from the same grout mixture used for casting the cylinder:

Thermal conductivity: κ = 0.563 W/m/^{o}C

Heat capacity: $\rho C = 2 \times 10^{6}$ J/m^{3}/^{o}C

Poisson ratio: ν=0.24; Young's modulus E = 26.65 GPa.

Coefficient of volumetric thermal expansion of the dry grout: 2×10^{-5}/^{o}C

Hydraulic conductivity : 10^{-14} to 10^{-12} m/s

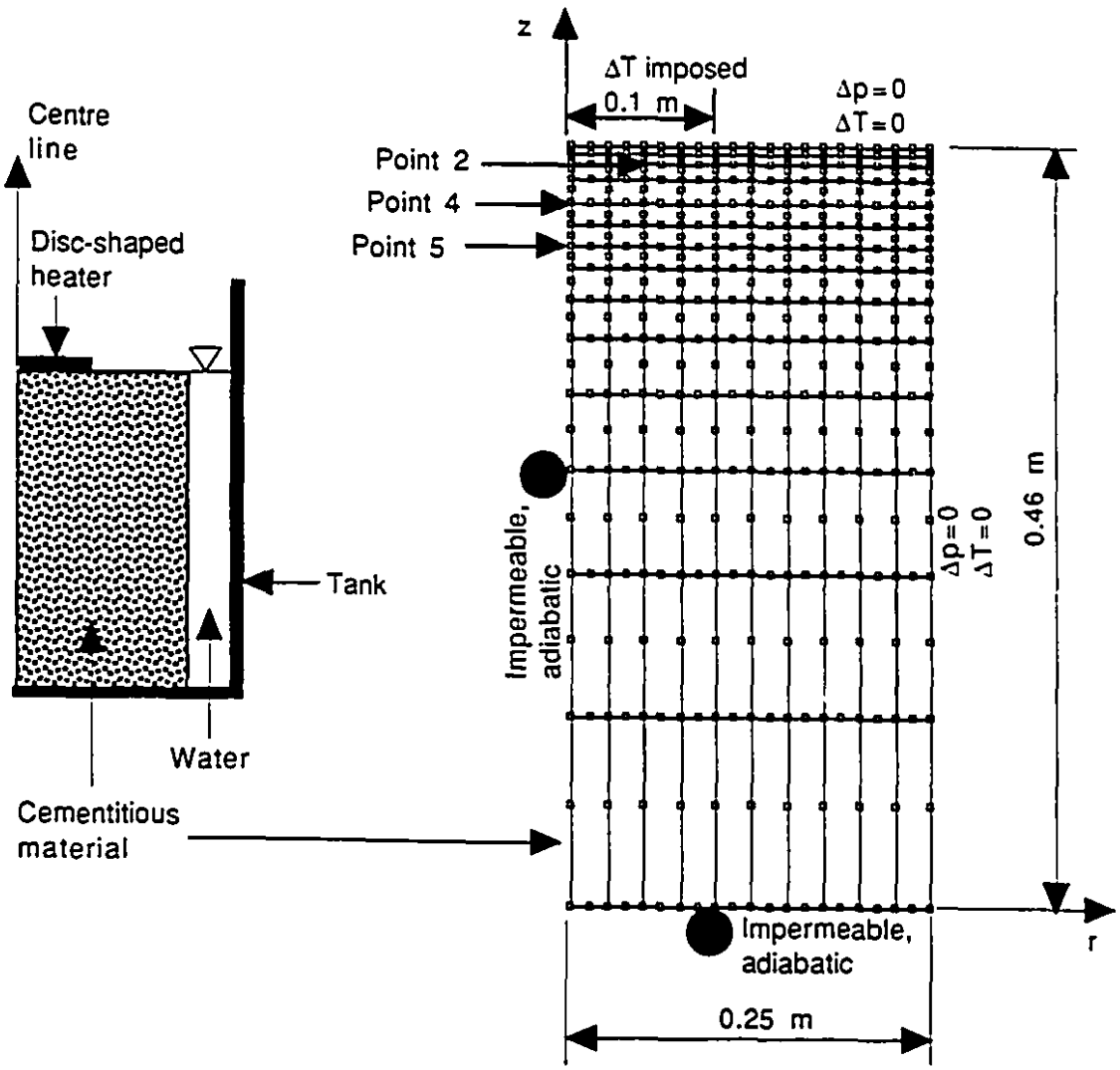

Figure 5.2 Heated Cylinder - Finite element mesh

We have simulated this experiment with the FRACON code, using the above values as input data. The physical setup of the experiment is shown in figure 5.2. The axisymmetric finite element mesh and the relevant boundary conditions are also shown in Figure 5.2. Since the measured value of the hydraulic conductivity is very low, undrained conditions are assumed in the analysis. The values for the calculated temperature agree well with the experimental results (Figure 5.3). In order to compare the calculated pore pressure with the experimental results, the assumption of slightly imperfect saturation, has to be made. This assumption results in a modified value of compressibility of the air/water mixture in the pores, as described below.

When the degree of saturation Sr is high (80%<Sr<100%) one can neglect capillary and surface tension effects (Vaziri et al., 1992). The porewater/air mixture could then be considered as a homogeneous single phase fluid, albeit with a higher compressibility than pure water. The relationship between the compressibility of the equivalent single phase pore fluid and the degree of saturation could be derived as follows.

Consider a volume V of the porous medium, with a volume V_v of voids. The void space is occupied partially with water and partially with air. By definition:

$$V_w = V_v\, Sr \tag{5.1}$$

$$V_a = V_v\,(1-Sr) \tag{5.2}$$

where V_w and V_a are respectively the volumes of water and air.

When a pressure dp is applied to the water/air mixture, a volumetric compression in

the voids dV_v results, such that:

$$\frac{dV_v}{V_v} = \frac{dV_w}{V_w} Sr + \frac{dV_a}{V_a} (1-Sr) \qquad (5.3)$$

The compressibility of the air/water mixture is, by definition:

$$C_{aw} = \frac{1}{V_v} \frac{dV_v}{dp} \qquad (5.4)$$

From (5.3):

$$C_{aw} = C_w Sr + C_a(1-Sr) \qquad (5.5)$$

where C_{aw}, C_w, C_a are the compressibilities of, respectively, the air/water mixture, water and air.

Let us assume that the law of ideal gas is valid for air:

$$p_{abs} V_a = MRT \qquad (5.6)$$

where M is the number of moles, R is the universal gas constant, T is the absolute temperature (°K) and p_{abs} is the absolute pressure :

$$p_{abs} = p_{atm} + p \qquad (5.7)$$

where p_{atm} is the atmospheric pressure and p is the relative pressure.

Differentiating equation (5.6) with respect to p, one obtains:

$$C_a = \frac{1}{V_a}\frac{dV_a}{dp} = -\frac{1}{p_{abs}} \qquad (5.8)$$

Defining compression as positive, and substituting the value of p_{abs} from equation (5.7) into (5.8), we obtain:

$$C_a = \frac{1}{p_{atm} + p} \qquad (5.9)$$

Equation (5.5) then becomes :

$$C_{aw} = C_w Sr + \frac{1-Sr}{p_{atm} + p} \qquad (5.10)$$

In the governing equation (2.32) , the bulk modulus of the pore fluid could now be defined as:

$$K_f = 1/C_{aw} \qquad (5.11)$$

The value of K_f would depend on the unknown p, making the equation nonlinear. A direct iteration method was incorporated in the FRACON code to handle this nonlinear behaviour.

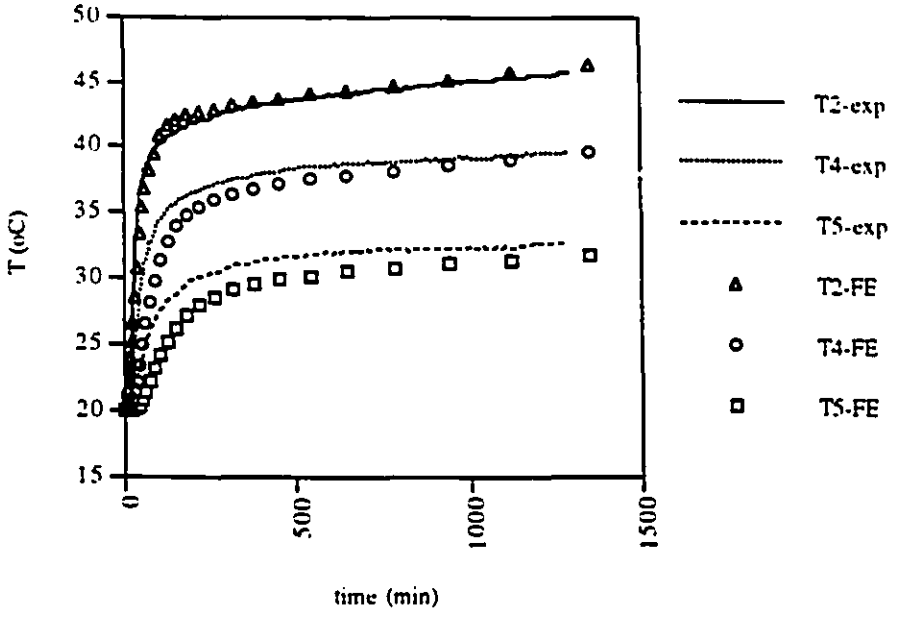

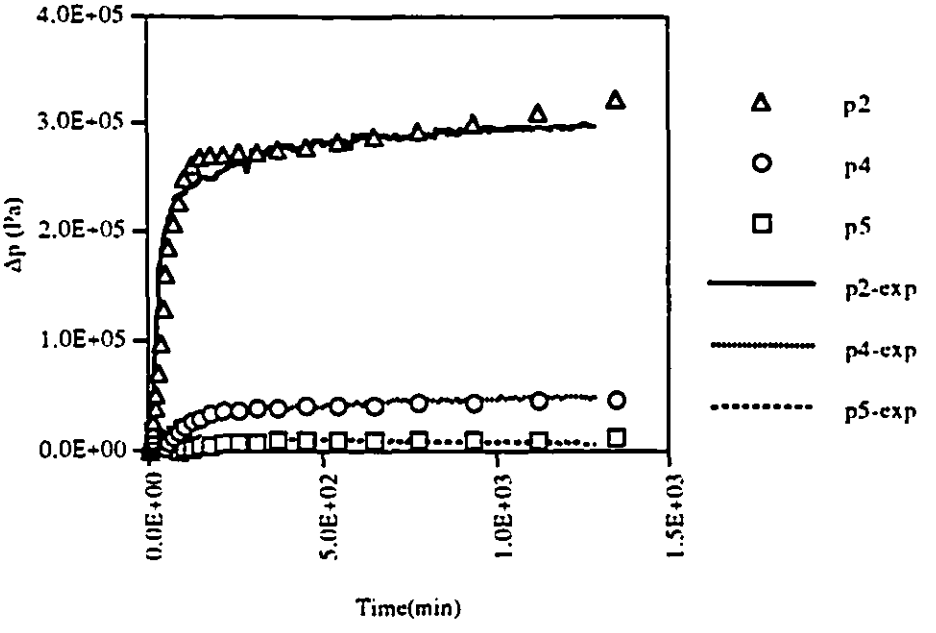

Figure 5.3 Heated cylinder - temperature and pore pressure evolution

It is assumed that the degree of saturation of the cylindrical block varies from 94% to 99% , with a higher degree of saturation near the outer surface. The top three horizontal layers of elements surrounding point 2 (figure 5.2) are assigned a value of Sr=99%; the next two layers of elements surrounding point 4 are assigned a value of Sr=97.5%; and the remaining elements are assumed to have a value of Sr=94%. With these modifications to the degree of saturation, a good match is obtained between the calculated and measured pore pressure values (compression is considered positive) as shown in Figure 5.3. Figure 5.4 shows that the absolute value of the pore pressure is sensitive to Sr, while the time transient is not much affected.

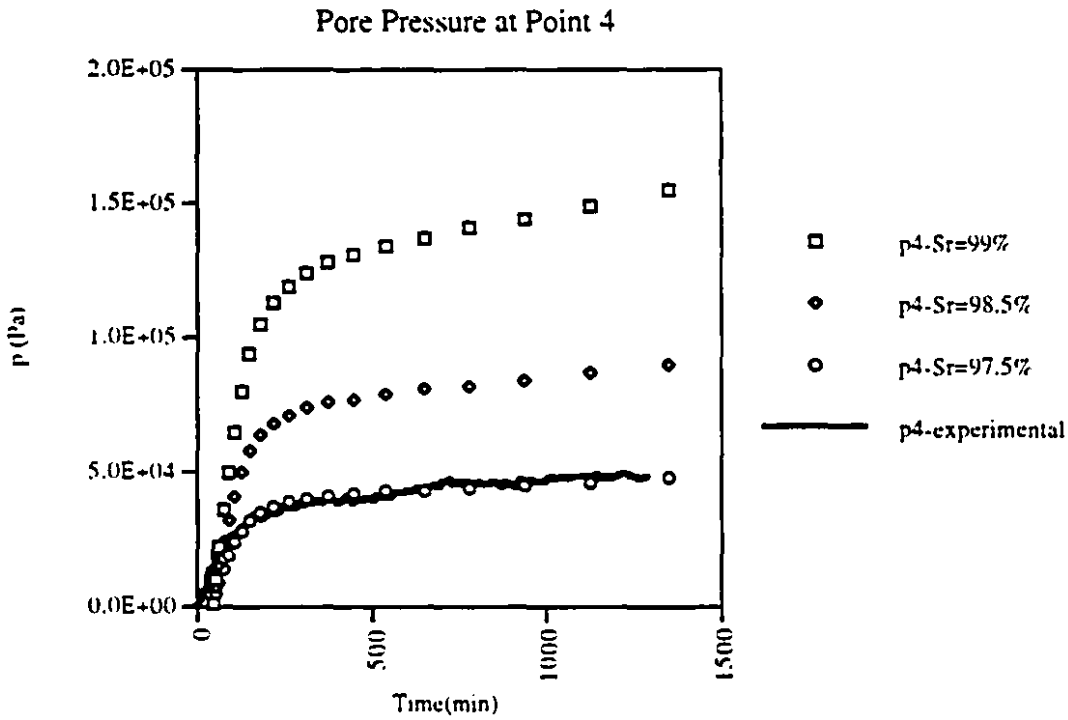

Figure 5.4 Heated cylinder - Effect of degree of saturation on pore pressure

5.3 Conclusions

Thermally induced pore pressure increases result in a reduction of the normal effective stresses and could adversely affect the strength of geomaterials. Although these increases have been experimentally observed for clays and could be predicted by the theory of thermal consolidation (see e.g. Hueckel et al., 1987), to our knowledge this phenomenon has never been experimentally observed in rocks. A unique experiment to investigate coupled T-H-M processes in a cementitious porous material, used to simulate hard porous rocks, was briefly described in this chapter. The results of the experiment show that thermally induced pore pressure increases can indeed occur in rock-type materials. It is shown that the theory of thermal consolidation implemented into the FRACON code is capable of simulating these pore pressure increases. Due to the imperfect saturation of the pores, we have proposed a new procedure to interpret effects of slightly imperfect saturation, by assuming that the mixture of water and air in the pores could be considered as an equivalent single phase pore fluid. This procedure is shown to be well supported by the good comparison between the calculated and experimental results.

CHAPTER 6

A MODEL FOR THE MECHANICAL AND HYDRAULIC BEHAVIOUR OF ROCK JOINTS

6.1 Overview of models for the mechanical and hydraulic behaviour of rock joints

Discontinuities in rock masses, which shall be referred to as "joints" in this thesis, constitute planes of weakness in the rock mass from the point of view of its mechanical behaviour. Joints have critical importance in NFW disposal, since they are the preferred paths for contaminant transport. Under external loads, sliding along the joints is likely to occur. Due to the presence of asperities at the joint surfaces, dilation usually accompanies the shearing process, leading to an increase in the joint aperture. As a consequence, the joint becomes more permeable. The asperities of the joint walls have finite strength; during shear, mechanical degradation of these asperities occurs, and dilation of the joint would cease at later stages of the shearing process. In this process, gouge material is being produced by the damage of the asperities and the accumulation of the gouge material can result in the reduction of flow in the joint. The very limited number of experiments (Bandis

et al., 1985; Makurat et al., 1990; Benjelloun, 1991) which investigate the effects of shear on joint permeability show that the rate of increase of the permeability slows down as shearing proceeds and in later stages, the permeability could decrease as a result of gouge production .

Patton (1966) performed experiments on artificial joints with regular "saw-tooth shaped" asperities moulded with plaster of Paris. He proposed a bilinear model of a shear strength criterion for the joint; at low normal stress, the joint shows dilation during shear due to overriding of the asperities; at high normal stress, shearing through the asperities occurs and not much dilation is observed. Ladanyi and Archambault (1970) , Jaeger (1971), Barton and Choubey (1977) and Bandis et al. (1981) proposed similar strength criteria, with a smooth transition between the two extreme types of response proposed by Patton (1966). Barton and Choubey (1977), and Bandis et al (1981) introduced the empirical coefficients JRC (Joint Roughness Coefficient) and JCS (Joint Compressive Strength) in their strength criterion. These empirical coefficients are easily determined in the laboratory or in-situ and they are a measure of the roughness of the joint surface (JRC) and the strength of the asperities (JCS). Empirical relations are proposed by these authors in order to include scale-dependency of JRC and JCS. The above strength criteria delineate the state of stress that separates pre-sliding and post-sliding of the joints. In order to predict the stress-strain behaviour of joints in both stages, numerous constitutive relationships have been proposed. These relationships could be categorized into two main classes. The incremental relationships (Goodman, 1976; Goodman and Dubois, 1972; Heuze, 1979; Heuze and Barbour, 1982 ; Leichnitz, 1985 ; Barton et al., 1985; Boulon and Nova, 1990 ; Benjelloun, 1991) consist of piecewise linear relationship between the increment of stress and the increment of strain. These relationships are usually developed from direct shear tests under constant normal stress and their use under different load paths is not

straightforward. Graphical methods to use these models to predict shear behaviour under constrained dilation (or constant normal stiffness) have been proposed with some success (Archambault et al., 1990; Amadei and Saeb, 1990; Skinas et al, 1990). Boulon and Nova (1990) and Benjelloun (1991) proposed an incremental approach with directional dependency. In this approach, the stress-strain matrices are determined from elementary stress paths derived from laboratory tests (such as shear under constant normal stress conditions). A weighted interpolation procedure between the elementary stress paths is used to determine the incremental stress-strain matrix for other stress paths. The second category of constitutive relationships are the elasto-plastic relationships, derived from the theory of plasticity. The models which fall into this class assume that before sliding, the deformations are elastic (recoverable). Post-sliding behaviour is characterized by plastic (irrecoverable) deformations. The state of stress that separates elastic from plastic behaviour is defined by appeal to a yield criterion. For example, Roberds and Einstein (1978) used the strength criterion proposed by Patton (1966) as the yield criterion to formulate their elasto-plastic model. Strain-softening (decrease in shear stress in the plastic stage) often found in experimental behaviour of joints could not be predicted from the model proposed by Roberds and Einstein (1978). Numerous elasto-plastic models exist in the literature. These include the formulations given by Ghaboussi et al. (1973), Hsu Yun (1979), Pande and Xiong (1982), Desai and Fishman (1987) and Plesha (1987). Reference to further work is also given by Selvadurai and Boulon (1995). The elasto-plastic approach has a particular appeal since different load paths and directions could be accommodated. Among the above models, the one proposed by Plesha (1987) is particularly attractive due to its simplicity and its ability to capture certain fundamental aspects of the mechanical behaviour of real joints, such as dilation under shear and strain softening due to surface asperity degradation.

For predicting the hydraulic behaviour of rock joints, the parallel plate model, developed from the application of the Navier-Stokes equation for laminar incompressible flow between two parallel smooth plates is employed. This procedure is widely used to calculate the effective permeability k of a fracture (see e.g. Benjelloun, 1991). The permeability of the joint is thus expressed as a function of its effective opening to fluid flow, called the hydraulic aperture. Since natural fractures are quite dissimilar to ideal parallel plates, the hydraulic aperture of the fracture is not equal to its mechanical aperture. Empirical relationships between the mechanical and hydraulic apertures were proposed by Barton (1982), Elliot et al. (1985), Witherspoon et al. (1979), Benjelloun (1991) and Boulon et al. (1993). The effect of gouge production on the permeability of the joint, however, is not accounted for in these relationships.

In this chapter, we employ the methodology proposed by Plesha (1987), based on the classical theory of plasticity, to formulate the stress-strain relationship for a rock joint. We illustrate a procedure whereby most of the parameters of the constitutive relationship for a joint could be estimated from two widely used and easily measurable empirical coefficients proposed by Barton and Choubey (1977) and Bandis et al. (1981); namely, the JRC (joint roughness coefficient) and JCS (joint compressive strength). In order to derive a relationship between the permeability of the joint and its mechanical aperture, we further assume that gouge production during the shearing of the joint is related to the plastic work. The extended version of the model proposed by Plesha (1987) is implemented in the FRACON code. This chapter is restricted to the analysis of joints without infilling material. Temperature effects on the strength of the joint are assumed to be negligible. Based on the experimental data from Stesky et al. (1974), this seems to be a justifiable assumption, at least for temperatures below 100°C.

6.2 Elastoplastic formulation for the mechanical behaviour of rock joints

6.2.1 Patton's saw-tooth model

The surface asperities of dilatant rock joints are irregular in shape and height. Nevertheless, their basic mechanical behaviour could be explained by assuming an idealized two-dimensional saw-tooth pattern as proposed by Patton (1966). This idealization is adopted by Plesha (1987) and several other researchers (e.g. Roberds and Einstein, 1978). Thus it is useful to review the basic concept of the model attributed to Patton (1966).

Consider a joint with perfectly planar contact surfaces (figure 6.1), subjected to a normal compressive stress σ and a shear stress τ. Sliding will not occur if:

$$|\tau| < (-\sigma) \tan \phi \qquad (6.1)$$

where $\tan \phi$ is the coefficient of friction between the two contact planes. This is the basic Coulomb friction model for non-dilatant behaviour.

To formulate the mechanical response of the joint in the context of the theory of plasticity, it is necessary to define a criterion at which yield occurs at the joint. For an interface exhibiting Coulomb friction, we have:

$$F(\tau, \sigma) = |\tau| + \sigma \tan \phi \qquad (6.2)$$

such that when F=0, sliding occurs, resulting in irrecoverable (plastic) deformation.

We introduce the relative displacement between the two adjoining planes constituting the interface, such that, $u=u_1$ is the relative displacement in the shear direction (direction 1) and $v=u_2$ is the relative displacement in the normal direction (direction 2). When F=0, increments of stress will give rise to increments of plastic deformation. In order to determine the direction and magnitude of plastic deformation, it is necessary to define a plastic potential function $Q=Q(\tau, \sigma)$ such that:

$$du_i^p = d\lambda \frac{\partial Q}{\partial \sigma_i} \tag{6.3}$$

where i=1,2: $\sigma_1 = \tau$ and $\sigma_2=\sigma$: du_i^p are the plastic components of the relative displacement at the surface of the joint and $d\lambda$ is a scalar multiplier.

By imposing the constraint that only shear traction can produce permanent deformation due to sliding, Michalowski and Mroz (1978) proposed that, in the case of surfaces in perfectly plane contact:

$$Q=|\tau| \tag{6.4}$$

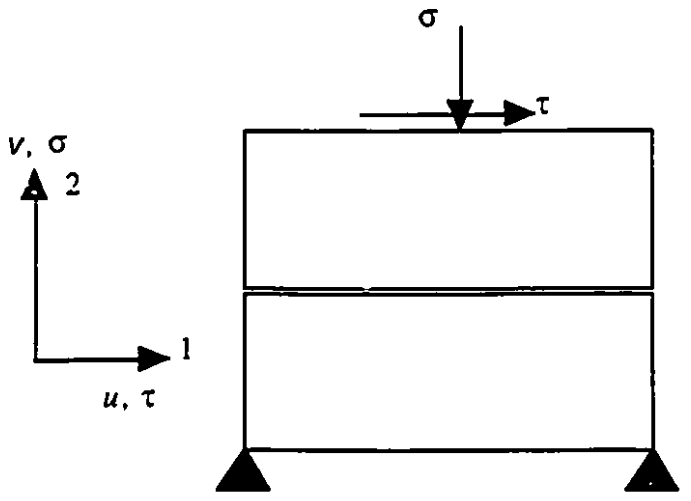

a) Perfectly plane joint surfaces

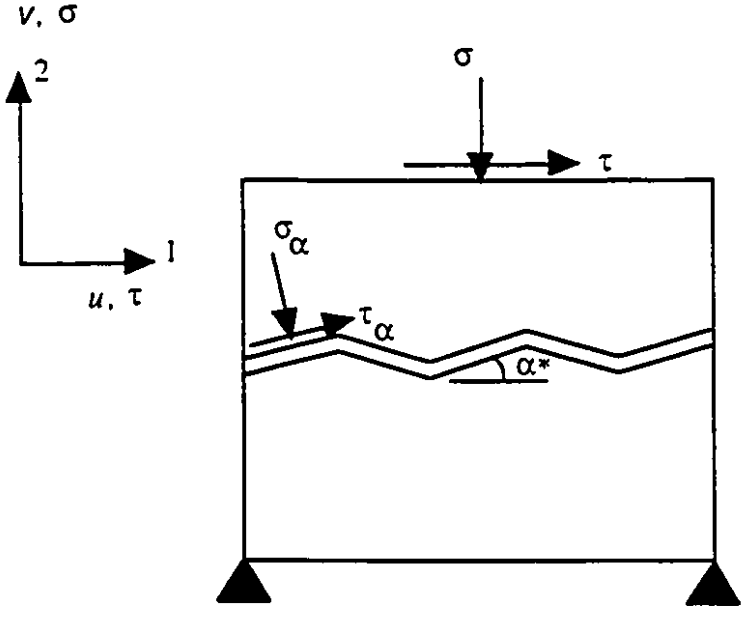

b) Regular saw-tooth joint surfaces

Figure 6.1 Patton's (1966) joint model

In Patton's model shown Figure 6.1, the asperities have regular angles of inclination $\alpha*$ with respect to the horizontal direction. Along a typical asperity inclined at angle $\alpha*$, the relationship between the "macro" values of the stresses τ and σ and the "local" or "micro" values of the stresses τ_α and σ_α can be obtained by appeal to local equilibrium at the inclined sliding plane: i.e.:

$$\tau_\alpha = (\tau \cos\alpha* + \sigma \sin\alpha*) \cos\alpha* \tag{6.5}$$

$$\sigma_\alpha = (\tau \cos\alpha* - \sigma \sin\alpha*) \cos\alpha* \tag{6.6}$$

Movement will start along the asperity if according to (6.1):

$$|\tau_\alpha| = -\sigma_\alpha \tan\phi \tag{6.7}$$

And thus the yield criterion for the saw-tooth joint model is:

$$F = |\sigma \sin\alpha* + \tau \cos\alpha*| + \tan\phi\,(\tau \cos\alpha* - \sigma \sin\alpha*) \tag{6.8}$$

Similarly, the plastic potential function is defined as:

$$Q = |\sigma \sin\alpha* + \tau \cos\alpha*| \tag{6.9}$$

It is noted that as the asperity angle $\alpha*$ reduces to zero, equations (6.8) and (6.9) reduce to the results of equations (6.2) and (6.4) applicable to a joint which exhibit Coulomb friction.

6.2.2 Derivation of the elasto-plastic stiffness matrix of the model by Plesha

In the formulation presented by Plesha (1987), sliding along the asperities is considered. When the magnitude of the applied shear stress is such that F, as defined in equation (6.8), is less than zero, only elastic deformations in the shear direction take place. Plastic or irrecoverable deformations in both shear and normal directions take place when F=0. The total increment of relative displacement at the joint, du_i, in this case, is the sum of an elastic and a plastic components: i.e.

$$du_i = du_i^e + du_i^p \tag{6.10}$$

where the superscripts e and p respectively stand for elastic and plastic.

When plastic displacements occur, the asperities of the joint are damaged, resulting in a decrease of the asperity angle. Plesha (1987) assumes that the asperity angle decreases as an exponential function of the plastic work produced by shear:

$$\alpha^* = \alpha^*_0 \exp\left(-\int_0^{W^P} c\, dW^P\right) \tag{6.11}$$

where α^*_0 is the original asperity angle, c is a degradation coefficient and W^P is the plastic work produced by the shear stress, whose increment is given by:

$$dW^P = \tau\, du^P \tag{6.12}$$

From the consideration of asperity damage, strain softening behaviour will now occur in

the joint during plastic deformation, i.e. both the yield surface and the potential surface as defined respectively by equations (6.8) and (6.9) will shrink in the τ- σ stress space. Both F and Q will now be functions of not only τ, σ but also of the plastic work (i.e. $F=F(\tau, \sigma, W^P)$ and $Q=Q(\tau, \sigma, W^P)$.

The increment of stress $d\sigma_i$ is related to the increment of elastic displacement at the joint by:

$$d\sigma_i = d^e_{ij}\, du^e_j \tag{6.13}$$

where d^e_{ij} is a matrix of elastic stiffnesses (Pa/m in SI units)

Combining (6.3), (6.10) and (6.13), we obtain:

$$d\sigma_i = d^e_{ij}(du_j - d\lambda\frac{\partial Q}{\partial \sigma_j}) \tag{6.14}$$

At the onset of yield, F=0 and dF=0; consequently :

$$dF = \frac{\partial F}{\partial \sigma_i}d\sigma_i + \frac{\partial F}{\partial W^P}dW^P = 0 \tag{6.15}$$

From the definition of the plastic work, equation (6.14) is equivalent to the following expression:

$$\frac{\partial F}{\partial \sigma_i}d\sigma_i + \frac{\partial F}{\partial W^P}\tau du^P = 0 \tag{6.16}$$

And from equation (6.14):

$$\frac{\partial F}{\partial \sigma_i} d_{ij}^e (du_j - d\lambda \frac{\partial Q}{\partial \sigma_j}) + \frac{\partial F}{\partial W^p} \tau du^p = 0 \tag{6.17}$$

From equation (6.17):

$$d\lambda = \frac{1}{\psi - H} \frac{\partial F}{\partial \sigma_i} d_{ij}^e du_j \tag{6.18}$$

with:

$$\psi = \frac{\partial F}{\partial \sigma_l} d_{lm}^e \frac{\partial Q}{\partial \sigma_m} \tag{6.19}$$

and:

$$H = \frac{\partial F}{\partial W^p} \tau \frac{\partial Q}{\partial \tau} \tag{6.20}$$

Substituting equation (6.18) into equation (6.14), one obtains:

$$d\sigma_i = d_{ij}^{ep} du_j \tag{6.21}$$

where d_{ij}^{ep} is the elasto–plastic stiffness matrix, given by:

$$d_{ij}^{ep} = d_{ij}^e - \frac{1}{\psi - H} \frac{\partial Q}{\partial \sigma_l} d_{il}^e d_{mj}^e \frac{\partial F}{\partial \sigma_m} \tag{6.22}$$

With explicit expressions of F and Q as given in equations (6.8) and (6.9), the elasto-plastic stiffness matrix could be explicitly formulated as a function of the current stress level by using equation (6.22). The coefficients of the [D] matrices in equations (3.54) and

(3.71) of chapter 3 are obtained by multiplying the elasto-plastic stiffnesses in equation (6.22) by the joint thickness b.

6.2.3 Parameters of the Plesha's model

The parameters required by the model proposed by Plesha (1987) are the elastic stiffness constants, the degradation factor c, the initial asperity angle α^*_0 and the friction angle ϕ. Usually, one assumes that[1] :

$$d^e_{11} = k_s$$
$$d^e_{22} = k_n$$
$$d^e_{12} = d^e_{21} = 0$$

where k_s and k_n are respectively the elastic shear and normal stiffness.

Plesha (1987) estimated the parameters of the model by calibrating the results of experimental data derived from shear test under constant normal stress. We propose here that most of these parameters can also be estimated from the Barton's empirical coefficients JRC and JCS. First, we note that the surface asperities in real joints do not follow a regular

---

[1] The rationale for the off-diagonal elastic stiffnesses to be zero is provided, for example by Plesha (1987). For example, suppose that an increment of elastic shear displacement du^e is imposed on the joint. According to equation (6.13), the increment in normal stress will be:
$d\sigma = d^e_{21}\, du^e$
Because the contact surface is macroscopically smooth, the same change in $d\sigma$ should result when an increment $-du^e$ is imposed. Consequently:
$d^e_{21} = 0$

pattern as idealized by Patton (1966) and Plesha (1987) (figure 6.2). Several orders of irregularities exist, and each order will be activated depending on the size of the sample and the magnitude of the normal stress. For high normal stresses, the higher-order asperities will be subjected to through-shear and sliding will occur only along the lower order asperities (with lower effective angle α^*). Similarly, for larger joint samples, the lower order asperities will be activated. It is clear from the above discussion that the effective asperity angle for real joints will depend on the size of the joint, the magnitude of the normal stress, and the strength of the joint wall material. These factors could be taken into account if one adopts the Barton - Bandis empirical expression for the peak shear envelope as the yield criterion:

$$|\tau| + \sigma \tan\left(\text{JRC } \text{Log}_{10}\left(\frac{\text{JCS}}{\sigma}\right) + \phi\right) = 0 \tag{6.23}$$

Before the start of asperity degradation, we note that the yield condition given by equation (6.8) can be rewritten as:

$$\begin{aligned} |\tau| + \sigma \tan(\phi + \alpha^*_0) &= 0 \quad \text{when } \sigma \sin\alpha^*_0 + \tau \cos\alpha^*_0 > 0 \\ |\tau| + \sigma \tan(\phi - \alpha^*_0) &= 0 \quad \text{when } \sigma \sin\alpha^*_0 + \tau \cos\alpha^*_0 < 0 \end{aligned} \tag{6.24}$$

Assuming that no asperity degradation occurs before the peak shear stress is mobilized and by comparing equations (6.23) and (6.24), we can write:

$$\alpha^*_0 = \text{JRC } \text{Log}_{10}\left(\frac{\text{JCS}}{\sigma}\right) \tag{6.25}$$

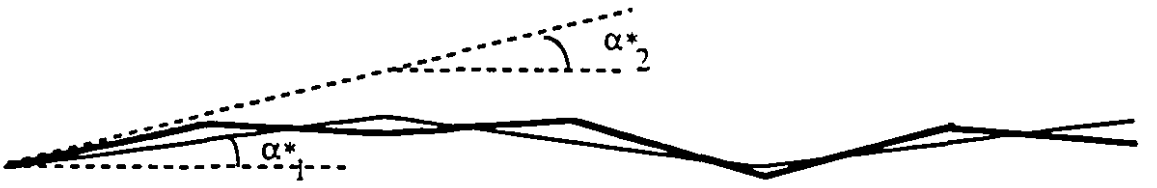

α^*_1 : angle of first order asperities

α^*_2 : angle of second order asperities

Figure 6.2 Schematic illustration of the many orders of asperities for real joints

The coefficients JRC (dimensionless) and JCS (MPa) and the friction angle ϕ can be easily estimated from two tests: the tilt test and the Schmidt hammer test. To determine ϕ, an artificial clean joint is prepared by diamond-sawing of a rock specimen containing the real joint, and sandblasting the surfaces. The jointed rock specimen is then tilted until sliding occurs along the clean joint. The tilt angle measured will be equal to ϕ_b. The angle ϕ_b is assumed to reflect pure frictional resistance of a clean (unweathered) planar surface. The friction angle ϕ for the real joint also reflects pure frictional behaviour. Nevertheless, the real joint contains gouge material originating from the failure of surface asperities. From the results of 135 shear tests on natural joints, Barton and Choubey (1977) has proposed the following empirical relationship between ϕ and ϕ_b: i.e.

$$\phi = (\phi_b - 20) + 20(r/R) \qquad (6.26)$$

where, R and r are rebound value (expressed in units of m) from the Schmidt hammer test

performed respectively on a clean, dry unweathered surface and on a wet joint surface.

The joint wall compressive strength JCS is obtained from a simple empirical relation with the Schmidt rebound value:

$$\text{Log}_{10}\,\text{JCS} = 0.00088\rho R + 1.01 \qquad (6.27)$$

Where JCS is in MPa, ρ is the density of the dry rock in kN/m^3.

The value of JRC, on the other hand, is determined from the tilt test, by using equation (6.23)

$$\text{JRC} = (\beta_t - \phi)/\log\,(\text{JCS}/\sigma_0) \qquad (6.28)$$

where β_t is the tilt angle when sliding occurs and σ_o is the self-weight induced normal stress acting on the joint, at the instant of sliding.

The parameters JRC and JCS are both scale-dependent. Barton et al. (1985) proposed the following empirical relations to account for scale effects:

$$\text{JRC} = \text{JRC}_0\left(\frac{L}{L_0}\right)^{-0.02\,\text{JRC}_0} \qquad (6.29)$$

$$\text{JCS} = \text{JCS}_0\left(\frac{L}{L_0}\right)^{-0.03\,\text{JRC}_0} \qquad (6.30)$$

Where JRC_0 and JCS_0 are laboratory scale values, for joints with nominal size L_0= 100 mm and JRC and JCS are values for larger samples, of size L.

Barton et al. (1985) also observed that u_{peak} (the shear displacement corresponding to the

peak shear stress τ_{peak}, under constant normal stress conditions) is independent of the normal stress but is scale dependent: i.e.

$$u_{peak} = \frac{L}{500}\left(\frac{JRC}{L}\right)^{0.33} \tag{6.31}$$

Assuming a linear elastic response of the joint up to the peak shear stress, we obtain, from equations (6.23) and (6.31), an expression for the elastic shear stiffness k_s as follows:

$$k_s = \frac{|\tau_{peak}|}{u_{peak}} = \frac{\sigma \tan\left(JRC\ Log_{10}\left(\frac{JCS}{\sigma}\right) + \phi\right)}{\frac{L}{500}\left(\frac{JRC}{L}\right)^{0.33}} \tag{6.32}$$

The normal stiffness k_n can be determined by performing simple compression tests on jointed rock specimens. The most comprehensive experimental investigations on the normal closure behaviour of joints under applied normal stresses are due to Bandis et al. (1981). In these studies, 64 pairs of specimens, with a wide range or rock types and surface roughness were tested. Each pair of specimens consisted of one jointed specimen and one unjointed specimen. Normal compression tests were performed on both specimens. The deformation of the unjointed specimen was subtracted from the one of the jointed specimen in order to obtain the net deformation properties of the joint. Typically, several cycles of loading-unloading were performed. Strong hysteresis was observed for the first few cycles and the hysteresis progressively disappeared with the number of cycles. The third or fourth cycles are generally considered to be representative of in-situ conditions. The normal stress-closure curves have the shape of steep hyperbolae. Several authors (Goodman, 1976 ; Bandis et al., 1981) adopt hyperbolic relations to describe these experimental curves. For example, Bandis et al. (1981) proposed the following hyperbolic relationship

(figure 6.3):

$$\sigma = k_{ni}\frac{v}{1-v/v_m} \tag{6.33}$$

where k_{ni} is the normal stiffness at zero normal stress, and v_m is the maximum closure of the joint.

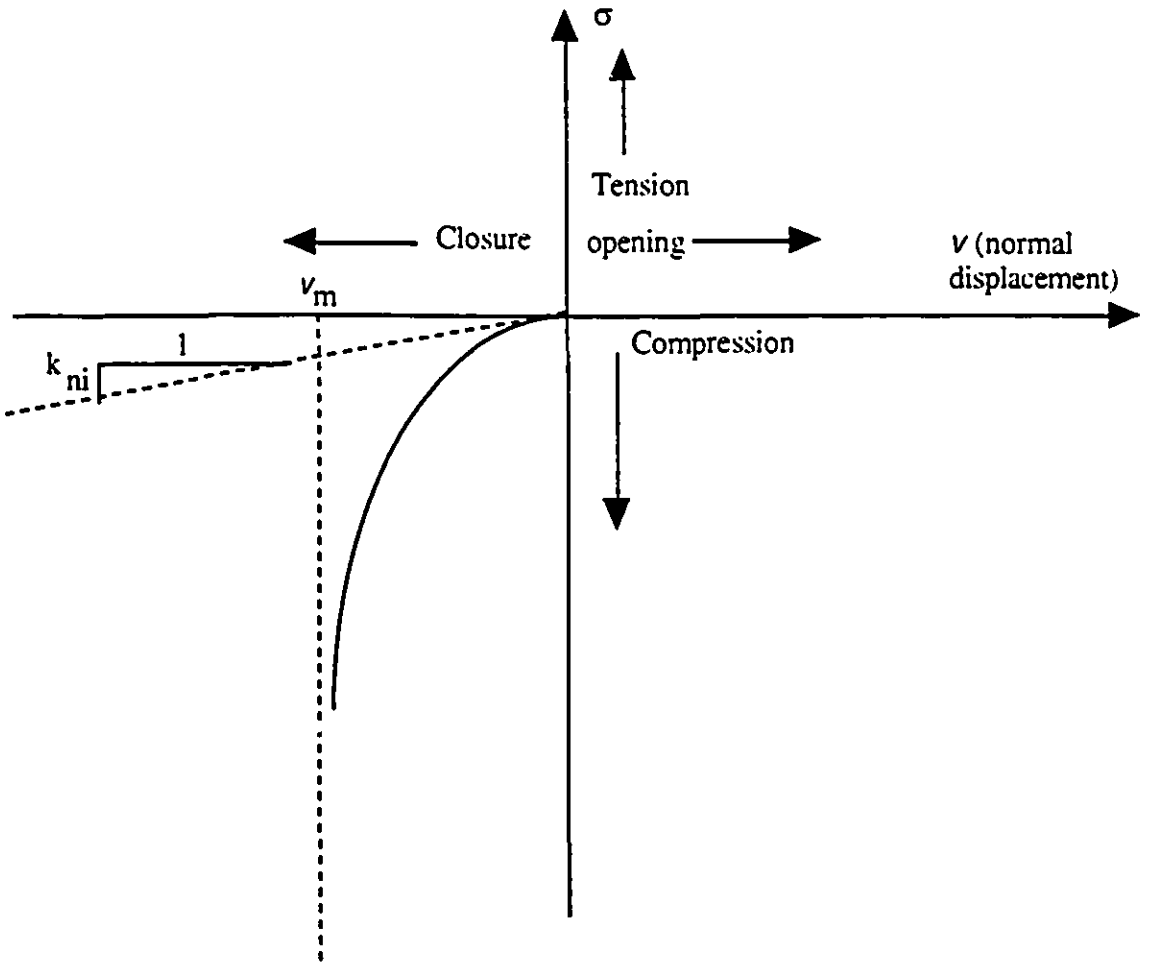

Figure 6.3 Hyperbolic relationship for normal behaviour of rock joints

The normal stiffness at any level of normal stress is then:

$$k_n = \frac{d\sigma}{dv} = k_{ni}\left(1 - \frac{\sigma}{v_m k_{ni} + \sigma}\right)^{-2} \qquad (6.34)$$

The parameters k_{ni} and v_m that enter into equation (6.34) are best determined by performing simple compression tests on jointed rock samples.

The remaining parameter required for the model is the degradation coefficient c. Limited experimental data show that c is a function of the normal stress. Hutson and Dowding (1990) and Qiu et al. (1993) have experimentally found that the coefficient c increases with the normal stress, while Benjelloun (1991) has found the reverse trend. Obviously, more experimental data is needed in order to establish correlations between c, the normal stress and also possibly the JRC and JCS coefficients. In this thesis, we use a calibration procedure to establish the relation between c and σ (cf. chapter 7).

6.3 Joint Hydraulic Behaviour

The parallel plate model, developed by the application of the Navier-Stokes equation for laminar incompressible flow between two parallel smooth plates, is usually used to calculate the permeability k of the joint (see e.g. Benjelloun, 1991): i.e.

$$k = e_h^2/12 \qquad (6.35)$$

where e_h is the hydraulic aperture of the joint.

Since natural fractures are quite dissimilar to ideal parallel plates, the hydraulic aperture of the joint is not equal to its mechanical aperture. Barton (1982) proposed the following empirical relationship to estimate the hydraulic aperture from the mechanical aperture:

$$e_h = \frac{e_m^2}{JRC^{2.5}} \tag{6.36}$$

where e_h is in μm, e_m (also in μm) is the mechanical aperture of the joint.

Elliot et al. (1985) and Witherspoon et al. (1979) proposed a linear relationship between the hydraulic and mechanical apertures:

$$e_h = e_{h0} + f\,\Delta e_m \tag{6.37}$$

where e_{h0} is the initial hydraulic aperture, Δe_m is the variation in mechanical aperture due to the combined effects of compression and shear as discussed in section 6.2 and f is a proportionality factor. Benjelloun (1991) experimentally confirmed the validity of equation (6.37) and found that f varies between 0.5 to 1. This factor comes from the roughness of the joint walls. A factor f=1 applies to the limiting ideal case of parallel smooth plates; this situation prevails only when the joint is relatively open, with apertures of the order of mm. For most other cases, f<1. The geometry of the flow path has an important influence on f. For rectilinear laminar flow, f is generally close to 0.8 and for radial flow, f is close to 0.5 (Benjelloun, 1991).

In this thesis, we adopt the linear relationship between the hydraulic and mechanical apertures given in equation (6.37). During the shearing of a joint, dilation occurs as

discussed in section 6.2. This dilation results in an increase of the mechanical aperture Δe_m. Equations (6.35) and (6.37) indicate that the permeability of the joint should increase with joint shear. Bandis et al. (1985) experimentally observed such an increase in permeability. Nevertheless at later stages of shearing, the permeability of the joint decreases. This latter observation is attributed to the effect of gouge production due to asperity breakage, that could not be explained by the existing models, similar to those defined by equations (6.36) and (6.37). In order to simulate the effect of gouge production on the joint permeability, we assume that this effect is related to the plastic work due to shear. Adopting the form of the relation proposed by Plesha (equation 6.11), we assume that the factor f in equation (6.37) is related to the plastic work produced by the shear forces according to the following equation:

$$f = f_0 \exp\left(-\int_0^{W^p} c_f dW^p\right) \tag{6.38}$$

where c_f is a gouge production factor. It is very likely that the additional parameters f_0 and c_f introduced in this section could be empirically related to JRC, JCS and σ. A detailed experimental program will be needed in order to arrive at specific correlations.

CHAPTER 7

SIMULATION OF LABORATORY AND FIELD EXPERIMENTS ON JOINTS AND JOINTED ROCK

The joint model described in chapter 6 was implemented in the finite element code FRACON. In this chapter, we show the use of the FRACON code to simulate some laboratory and field experiments on rock joints and jointed rock masses.

In order to be consistent with the usual convention in rock and soil mechanics, compressive normal stresses and pore pressures are considered positive in this chapter and also in chapter 8.

7.1 Shear under constant normal stress

Most laboratory experiments on joints are performed under constant normal stress conditions. These conditions apply mainly to geomechanical problems associated with rock slope stability, where the focus is on the analysis of the sliding movement of rock blocks near the surface of a slope. The constant normal stresses across the joints between these blocks is due to the weight of the blocks themselves.

We show here the simulation of experiments involving shear under constant normal stress performed by Skinas et al. (1990). The tests were conducted on 15x10 cm model joints. These joints were cast from natural joint surfaces, using a brittle, artificial material consisting of a sand-barytes-cement mixture. Skinas et al. (1990) showed experimental results for joints with the following properties:

JRC=9, 12, 15 and 18

JCS=28 MPa

$\phi = 37^{o}$

We perform a simulation with the FRACON code of the tests performed on the joint with JRC=9. The input data to the FRACON code are:

JRC = 9

JCS=28 MPa

$\phi = 37^{o}$

Three levels of normal stress are considered: 1, 2 and 5 MPa. In order to obtain a good fit between the calculated and experimental results, different values of the asperity degradation coefficient c are assumed for different normal stress values: 1.1×10^{-4} m/N (σ=1Mpa), 0.4×10^{-4} m/N (σ=2MPa), 0.25×10^{-4} (σ=5MPa) m/N. The above values of c are plotted as a function of the ratio of the normal stress to the atmospheric pressure in figure 7.1. The equation of the best fit curve is also shown in figure 7.1. Figure 7.1 shows that the asperity degradation coefficient decreases with increasing compressive normal stress. This

observation is consistent with experimental results obtained by Benjelloun (1991). However, as mentioned in chapter 6, Hutson and Dowding (1990) and Qiu et al. (1993) observed the reverse trend.

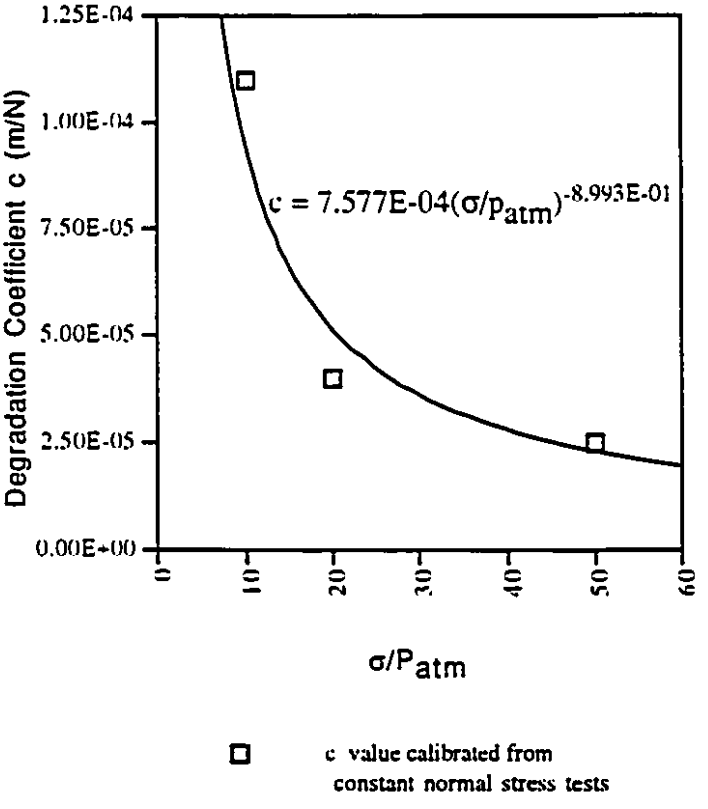

P_{atm} is the atmospheric pressure (P_{atm} =10^5 Pa)

Figure 7.1 Variation of asperity degradation coefficient with normal stress

The finite element model consists of one single joint element (Figure 7.2). Constant normal stresses are applied on the element, and shear displacement are imposed on the appropriate nodes. In figure 7.2, it is noted that, as in the previous chapters, u,v denote the absolute displacements while u, v denote the relative displacements between the walls of the joint.

The results for shear stress versus shear displacement are shown in Figure 7.3. A reasonably close fit is obtained between the results derived from the numerical modelling and the experimental results. Figure 7.3 shows that the shear strength of the joint increases with the normal stress level. On the other hand, the displacement value corresponding to the peak shear stress does not depend on the normal stress level, but only on the size of the joint sample (cf. equation 6.31). These observations are also consistent with experimental results obtained by other researchers (e.g. Bandis et al., 1981; Benjelloun, 1991).

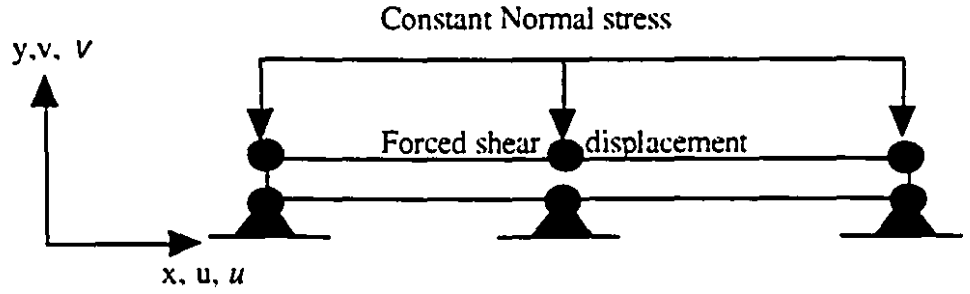

u,v : absolute displacements
u,v : relative displacements in the joint

Figure 7.2 Finite element model for joint shear under constant normal stress condition

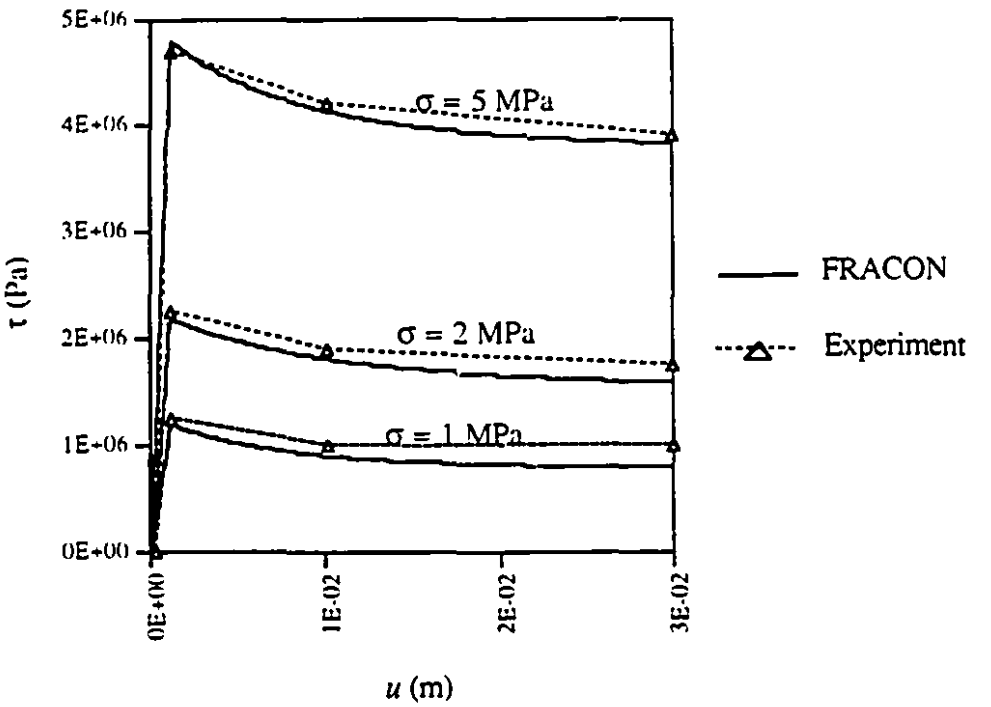

Figure 7.3 Shear under constant normal stress -Shear stress (τ) vs shear displacement (u)

The joint dilation due to shear is shown in Figure 7.4. For a value of the normal stress of 1 MPa, the FRACON code overpredicts dilation by approximately 15% when compared to the experimental results. This might be due to an inherent feature of the implementation of the model of Plesha (1987) into the FRACON code, in the sense that the model does not allow the joint surfaces to approach one another as the asperities are degraded. Plesha (1995) included this damage deformation in a recent version of his model. The FRACON code nevertheless correctly predicts decreasing dilation with increasing normal stress, as found experimentally by numerous researchers (e.g. Bandis et al, 1981; Benjelloun, 1991). No experimental data were given by Skinas et al (1990) for dilation at normal stress values

of 2 MPa and 5 MPa.

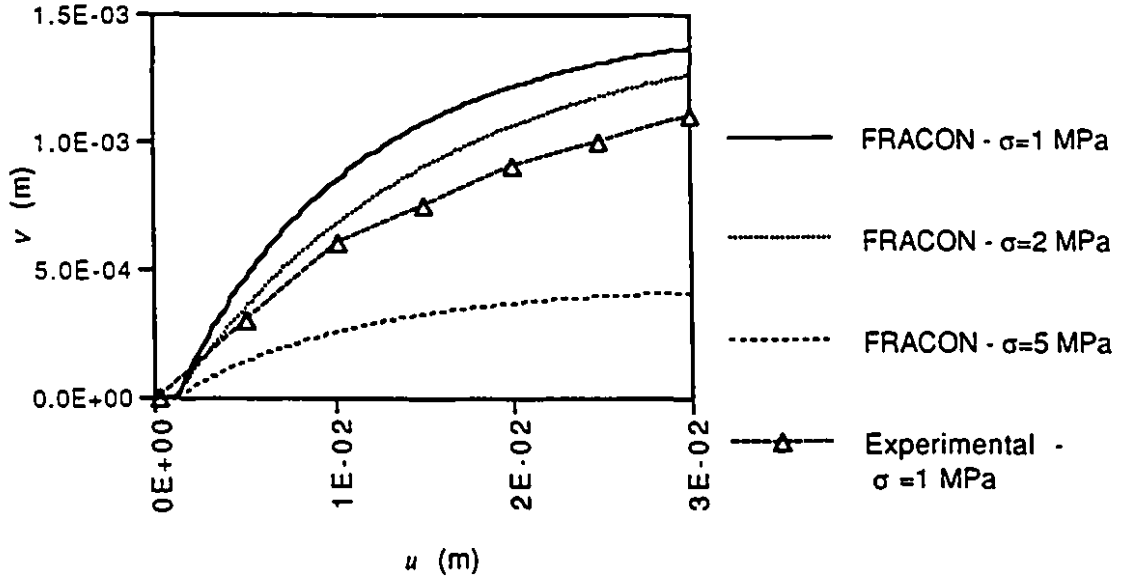

Figure 7.4 Shear behaviour under constant normal stress conditions- Joint Dilation

Figures 7.5, 7.6 and 7.7 illustrate the effects of degradation on the joint behaviour, for a typical case (normal stress of 1 MPa). From Figure 7.5, it may be observed that the joint will behave in an elastic-perfectly plastic fashion if there is no degradation (c=0). For this latter case, Figure 7.6 shows that dilation of the joint will take place indefinitely at a constant rate, while this rate will decrease and tend to zero if degradation is considered. Figure 7.7 shows that due to degradation (case when c=1.1x10-4 m/N), the asperity angle gradually tends to zero.

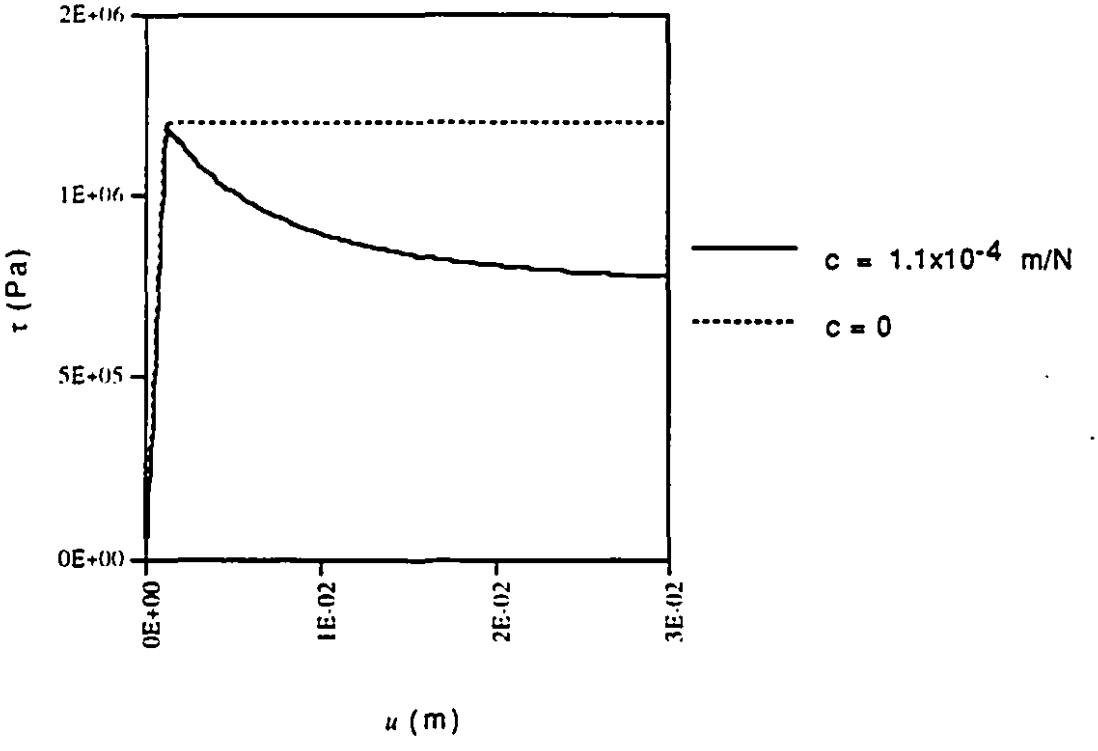

Figure 7.5 Effects of degradation on shear stress

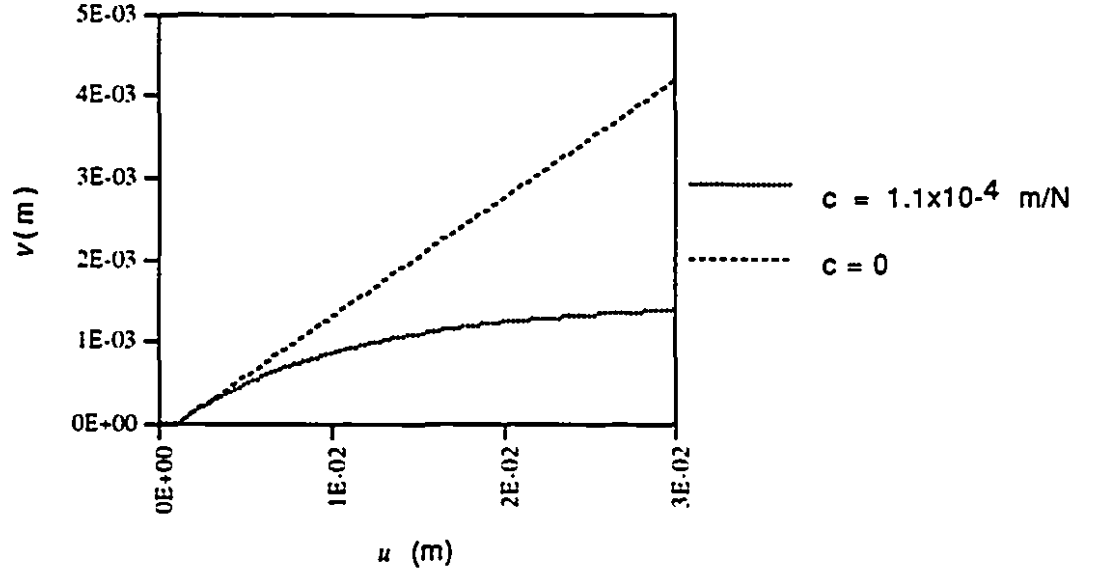

Figure 7.6 Effects of degradation on dilation

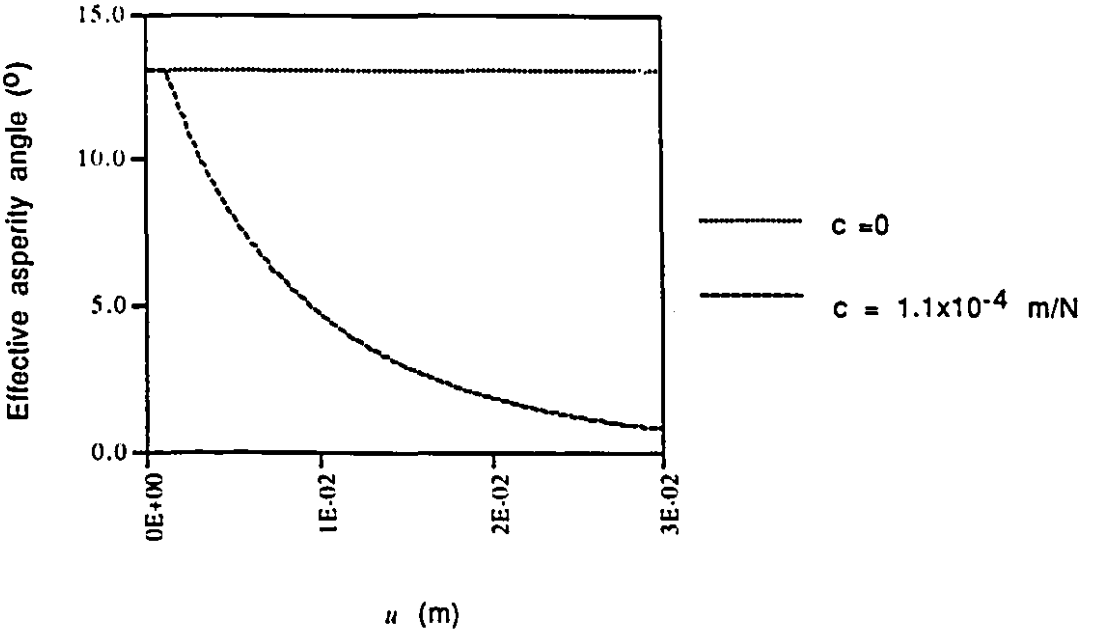

Figure 7.7 Effects of degradation on the asperity angle

7.2 Shear under constant stiffness

Skinas et al. (1990) also presented results of shear tests performed under constant external stiffness conditions. The external stiffness variations were achieved by incorporating springs of different stiffnesses which restrained normal movement of the joint samples. The joints were then sheared by the application of a force in the shear (horizontal) direction. These test conditions correspond to the situation that can be encountered in rock joints located at some depth within a rock mass. In this situation, the tendency for dilation of the joints is restricted by both the normal stresses on the joint and the stiffness of the surrounding rock mass. We perform simulation of these tests under external spring

stiffnesses of 1.03, 3.33 and 13.33 GPa/m and an initial normal stress of 1 MPa. The joint sample has properties similar to those described in the previous section. In particular, the degradation coefficient is assumed to vary according to a power law of the normal stress as shown in figure 7.1. The coefficients of this power function are estimated by the best fit curve derived from the discrete calibrated values obtained from the simulation of the shear tests under constant normal stress. The normal stiffness of the joint, which does not play a role in the previous case, has to be taken into account under the current conditions. In the absence of experimental data, we assumed that k_n is given by equation (6.34), with k_{ni} = $2x10^9$ Pa/m and $v_m = 8x10^{-4}$ m.

The finite element model used in the FRACON code is shown in figure 7.8. The stiffness of the springs is simulated by an eight-noded element which has elastic properties and height H equivalent to the corresponding spring stiffness K_n:

H = 1 m

E = 1.033 GPa (for K_n=1.033 GPa/m), 3.33 GPa (K_n=3.33 GPa/m), 13.33 GPa (K_n=13.33 GPa/m)

v=0

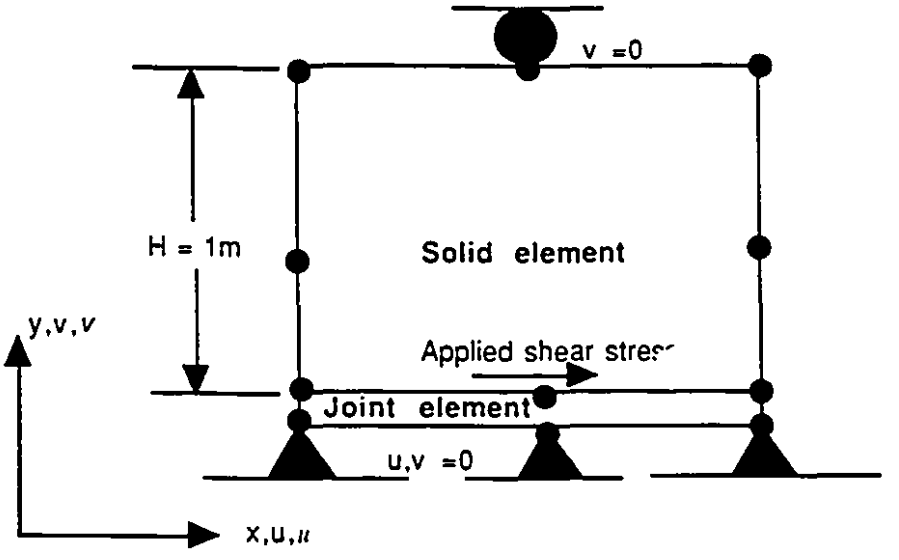

Figure 7.8 Finite element model for shear under constant normal stiffness condition

Shear stress and normal stress are shown in figure 7.9. Good to fair agreement is obtained between the FRACON results and the experimental data. Both set of results show that the stiffness of the external springs, because it restrains dilation, results in a "strengthening" of the joint. It is important to note that the pre-yield behaviour of the joints is essentially the same for all values of external stiffness. The post-yield behaviour shows a completely different picture. For zero external stiffness (which is equivalent to constant normal stress conditions), the shear stress decreases due to asperity degradation. This is the strain softening behaviour discussed in the previous section. When the external stiffness increases, the joint exhibits a strain hardening response. As shown in figure 7.9, both the shear and normal stresses increase when shearing continues beyond the yield point.

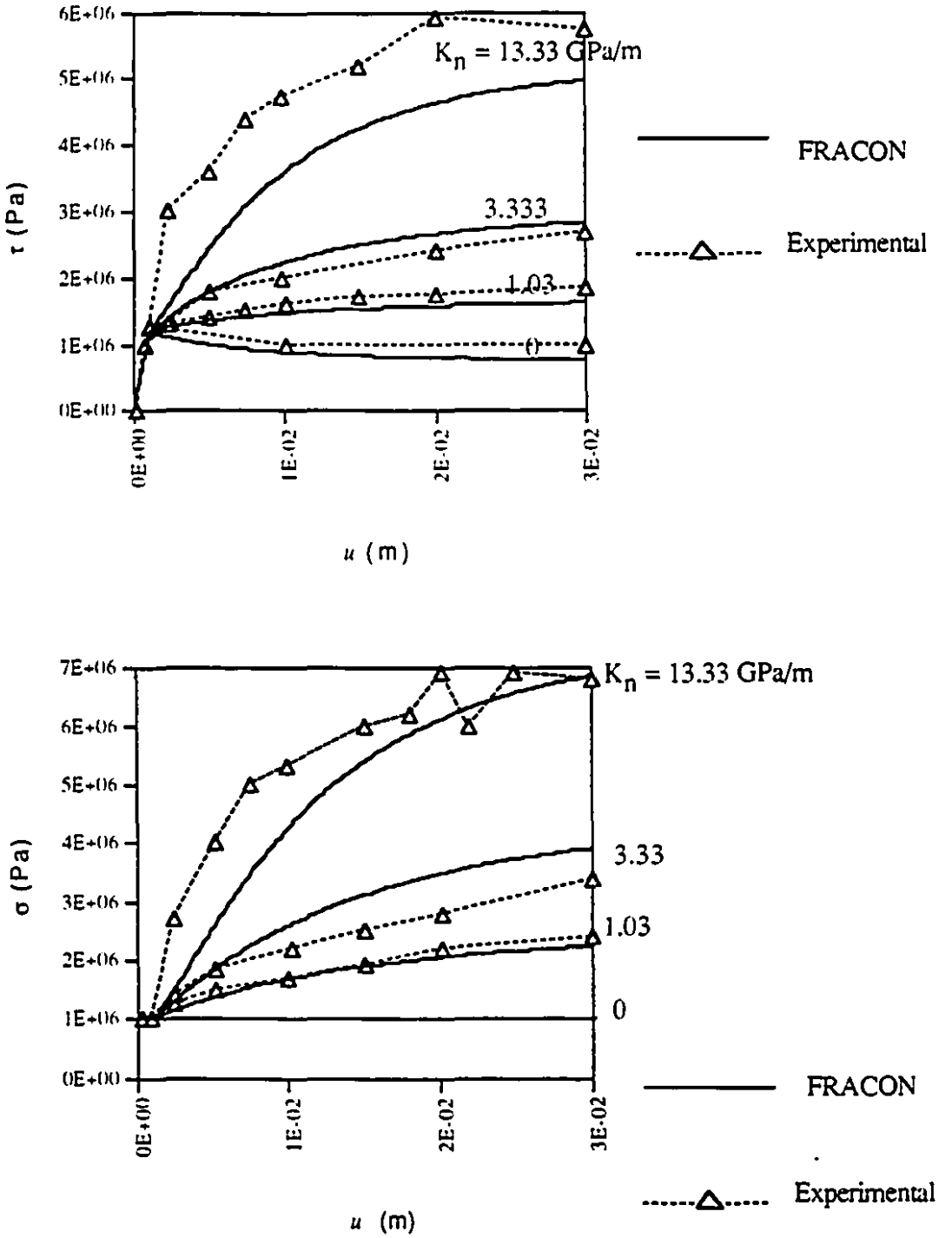

Figure 7.9 Joint behaviour under constant normal stiffness conditions

7.3 Effects of shear on joint permeability

Bandis et al. (1985) showed results of hydro-mechanical experiments performed on rock joints composed of gneiss. The experimental configuration was a biaxial cell (Figure 7.10). The joint sample was first consolidated without shear by equally increasing the values of the normal stresses σ_1 and σ_2 . The joint was then sheared by maintaining one load constant and increasing the other one. At specific values of the shear displacement, the permeability of the joint was determined by injecting water through the joint and measuring the flow rate. Bandis et al. (1985) recorded the evolution of the joint permeability with increasing shear displacement. Although both the normal and shear stresses varied during the experiment, Bandis et al. (1985) assumed constant normal stress conditions to simulate the evolution of joint permeability during one typical experiment. The assumed constant normal stress was the average value of the actual normal stress. In this chapter, we also computationally simulate the experiment by assuming constant normal stress conditions. The finite element model used in the FRACON simulation is the same as the one shown in Figure 7.2, with the same boundary conditions. The following values of joint properties were estimated by Bandis et al. (1985) and are used as input to the simulation :

JRC = 7

JCS = 110 MPa

Joint length: L= 0.15 m

Average normal stress: 1.5 MPa

In addition to the above values, an asperity degradation factor c=1.5x10-4 m/N is assumed.

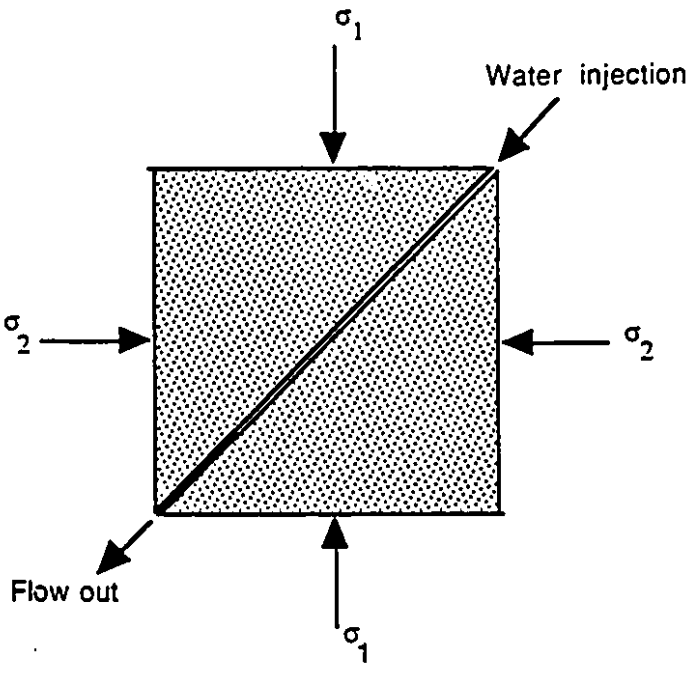

Figure 7.10 Schematics of the hydromechanical experiments performed by Bandis et al. (1985) and Makurat et al .(1990)

When sheared the joint dilates. The dilation calculated by FRACON is shown in Figure 7.11. This dilation is accompanied initially by a corresponding increase in the permeability of the joint (Figure 7.12). However, this permeability decreases later on due to gouge produced by joint asperity breakage. Bandis et al. (1985) could not simulate this permeability decrease (Figure 7.12), using Barton's (1982) model (cf. equation 6.32). The FRACON code simulation, with a gouge production factor $c_f = 0$, produces similar results to those presented by Bandis et al. (1985). Assuming $f_0 = 1$ and $c_f = 0.001$ m/N (cf. equation 6.34), the *trends* in the permeability variations predicted by the FRACON code agree relatively well with the experimental results. Most importantly, the tendency for the

reduction in the permeability of the joint with increasing shear is correctly predicted.

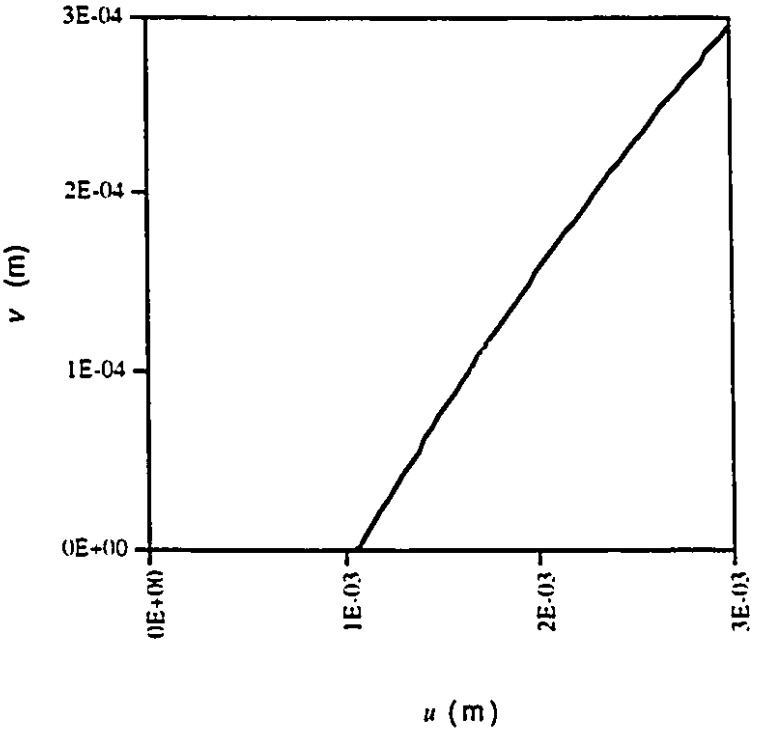

Figure 7.11 Shear dilation calculated via the FRACON code for Bandis et al. (1985) experiment

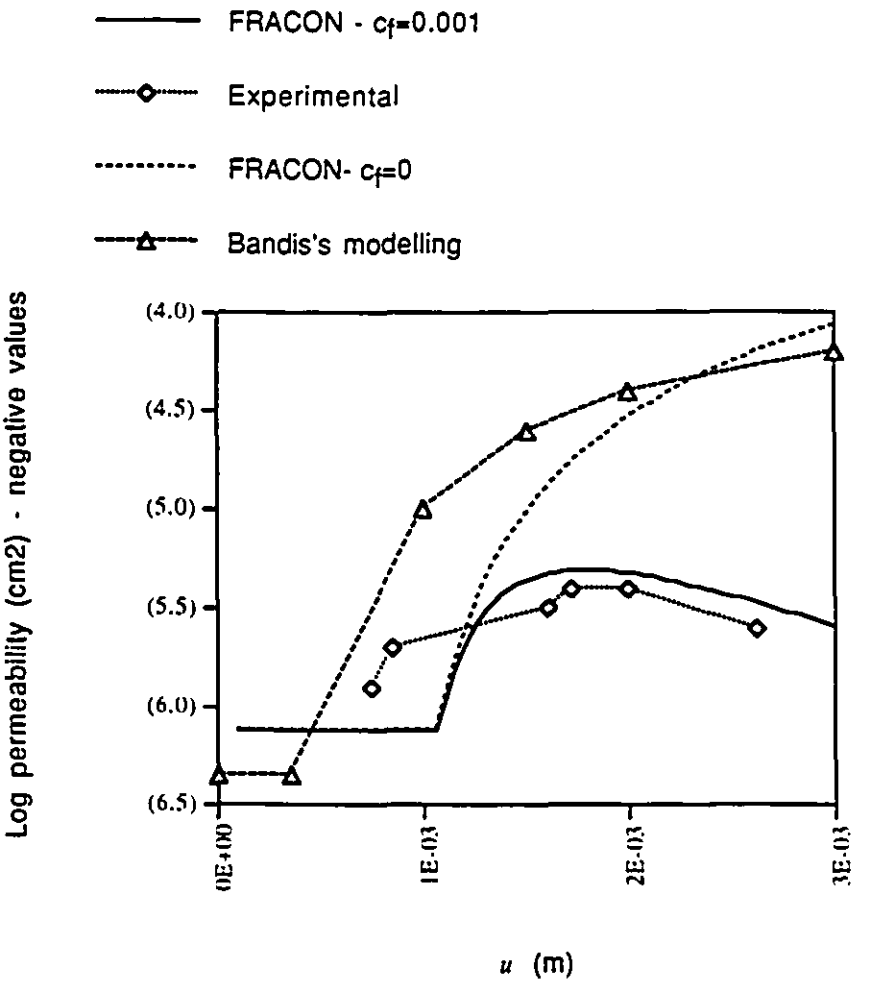

Figure 7.12 Effects of shear on joint permeability - Bandis et al. (1985) experiment

7.4 Scale effects

Bandis et al. (1981) studied scale effects on joints by making identical pairs of replicas of natural joints, using a brittle model material. These artificial joint samples were tested full-size or were divided into smaller samples for separate testing. The tests performed were shear tests under constant normal stress conditions.

In this study, the scale effects in the tests conducted by Bandis et al. (1981) are simulated by using the properties given in their studies:

L_0= 6 cm

JRC_0 = 16.7

JCS_0 = 2 Mpa

Normal stress = 24.5 kPa

Scale effects are simulated with the FRACON code by the use of the empirical equations (6.29) and (6.30) for JRC and JCS respectively. The finite element mesh used in the study is similar to the one shown in figure 7.2.

Figure 7.13 shows that the FRACON code correctly predicts that with increasing size, the strain softening phenomena are less pronounced, i.e. the joint behaviour becomes less brittle. With increasing size, the shear stiffness prior to failure decreases and the displacement required to reach the peak shear stress increases. For larger specimens, the shear strength of the joint is underestimated by the numerical modelling, with a maximum discrepancy of approximately 20% .

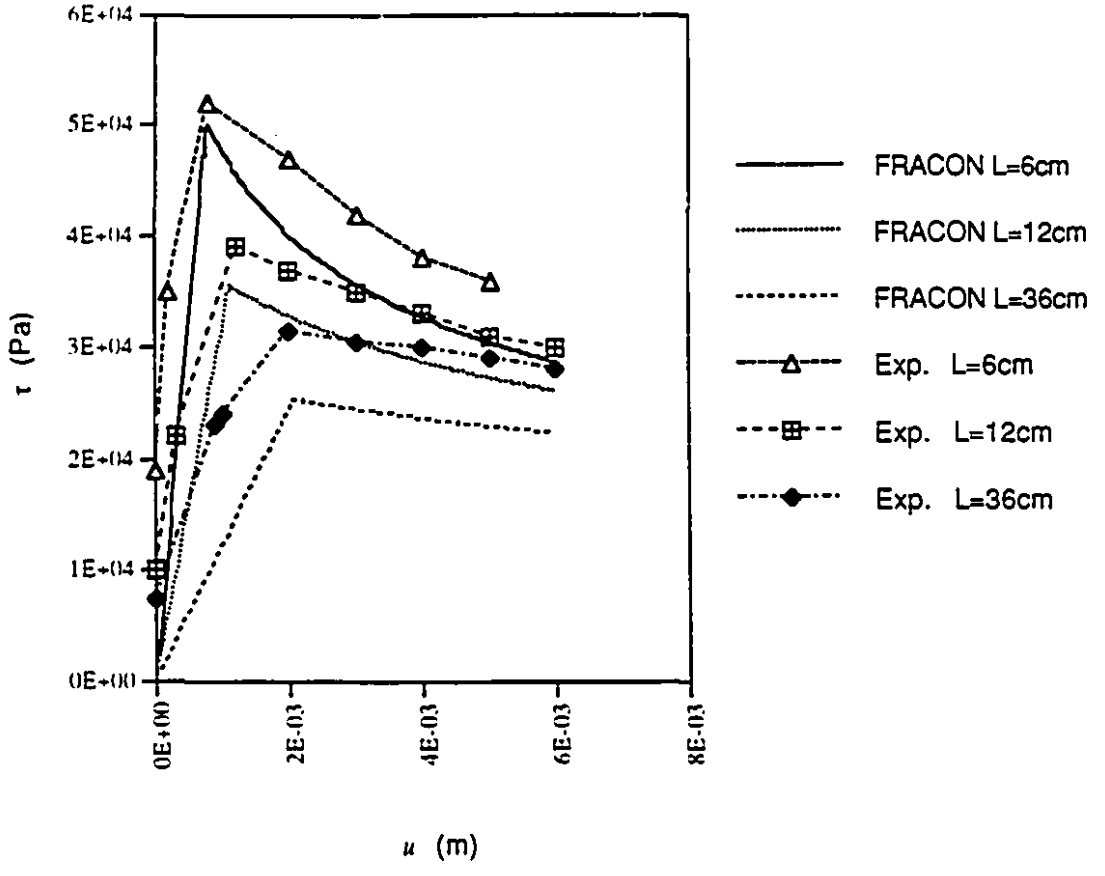

Figure 7.13 Scale effects on joint shear

Figure 7.14 shows scale effects on joint dilation. The FRACON code correctly predicts a decrease in shear dilation with larger samples. The experimental data shows that dilation starts before the peak shear stress is attained. As can be seen in Figure 7.14, the model by Plesha (1987) incorporated in the FRACON code assumes linear elastic behaviour in the pre-peak phase. Thus dilation is predicted to occur only after when the peak shear stress is attained. For reasons already discussed in section 7.1, with the smaller joint samples, the FRACON code overpredicts the dilation value.

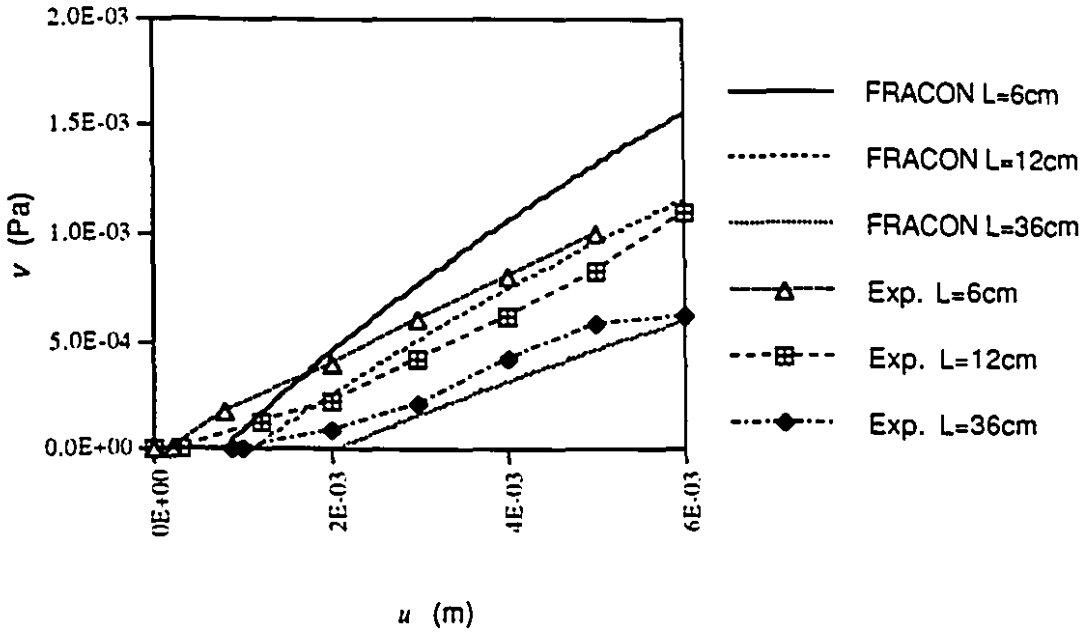

Figure 7.14 Scale effects on joint dilation

7.5 Simulation of field injection tests

The International project, DECOVALEX (SKI, 1993), was initiated in 1991, with the objective of developing, verifying and validating computer models for simulating the Thermal-Hydrological-Mechanical (THM) response of fractured hard rocks. Simulation problems are pre-defined to allow the researchers to develop models and to compare predictions with a variety of computational solutions, analytical solutions and experimental data. One such problem of DECOVALEX, called test case no. 6 (TC6), consists of the simulation of field borehole injection tests conducted in a single horizontal fracture (Rutqvist, 1993). A vertical borehole, 56 mm in diameter, was drilled in hard crystalline

rock, at the Lulea University of Technology, Sweden. The borehole intersected a horizontal fracture at a depth of 356.7 m. A 65 cm section of the borehole, containing the fracture, was isolated by packers. Three types of injection tests were performed by pumping water into the isolated section according to the following methods:

The pulse test: this consists of instantaneously raising the pressure in the isolated section and then "shutting in" the pressure within the sealed section. The pressure in the isolated section will decay to the original pressure as flow through the fracture takes place. The test results are presented in the form of the variation of the pressure in the borehole with time.

The hydraulic jacking test: this consists of raising the pressure in the section in a stepwise manner and measuring the rate of water injection into the section. Each pressure level is maintained for a period of approximately one to two minutes, in order to achieve an apparent steady flow rate, before increasing the pressure to the next level. The test results are presented as pressure versus flow rates.

The constant pressure test: this consists of increasing the pressure in the section to a certain level and then maintaining it constant during the entire test. The flow rate versus time is monitored. In the present case, a constant pressure of approximately p = 11.4 MPa is maintained for more than 10 minutes in the isolated borehole section.

A characteristic nonlinear coupled hydraulic/mechanical behaviour of the rock mass/ fracture system is apparent in its response to the borehole injection tests (Rutqvist et al., 1990). This behaviour can be interpreted in the context of Biot's theory of consolidation, and could thus be simulated with the FRACON code. We present here the simulation results for TC6, with the finite element code FRACON.

7.5.1 Measured data

The following properties of the intact rock were obtained from laboratory tests on drill rock cores:

Young's modulus: E = 80 GPa

Poisson's ratio: v = 0.25

Density: 2800 kg/m^3

Compression tests on a core containing a joint was performed and typical curves of normal stress versus normal displacement of the joint were obtained. A cyclic loading procedure was adopted; the third loading/unloading cycle is generally considered representative of in-situ conditions. The unloading curve from the third cycle is shown in figure 7.15. We only show the unloading curve because during the injection tests, the pore pressure increases and thus the normal effective stress across the joint decreases. The in-situ total normal stress across the joint was estimated to be between 8 and 10 MPa. The total normal stress due to the weight of the overburden is equal to 9.9 MPa at the depth of the joint and falls into the estimated range of the in-situ normal stress . The joint radius was roughly estimated to be in the 1 m - 5 m range.

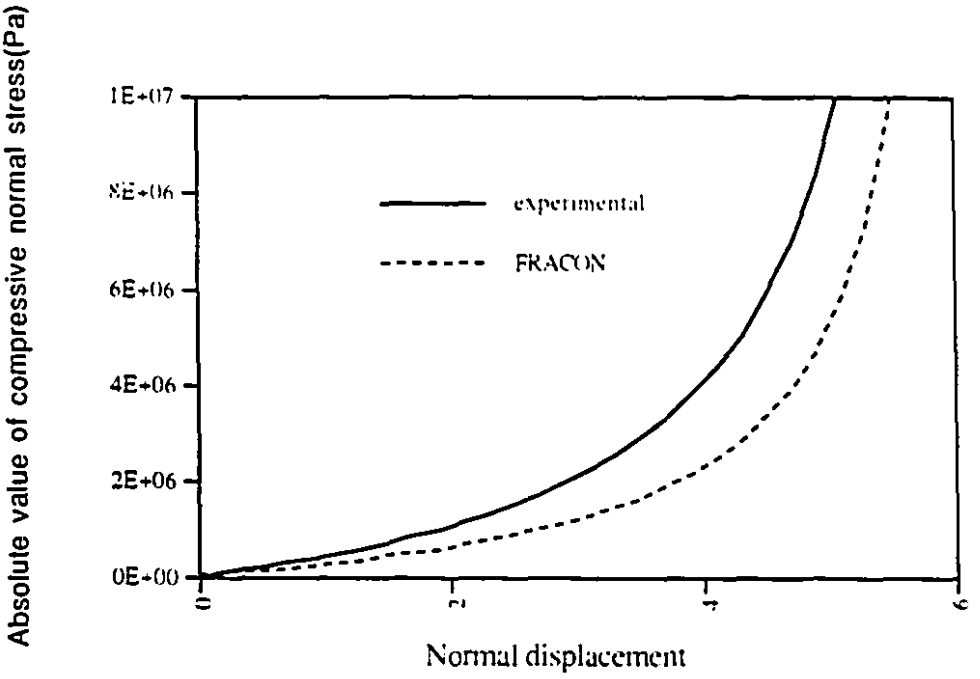

Figure 7.15 Normal Stress vs Normal Displacement relationship for fracture

7.5.2 Input Data

The finite element mesh with the assumed boundary conditions is shown in figure 7.16 . Axisymmetric conditions are assumed.

A calibration procedure is performed by varying the properties of the rock mass and the joint within a representative range. The following set of input parameters used in the FRACON simulation provides the best fit between calculated and experimental results:

Young's modulus of rock mass: E = 70 GPa

Poisson's ratio of rock mass: $\nu = 0.25$

Permeability of rock mass: 10^{-19} m^2

radius of fracture : 4.9 m

The Young's modulus of the rock mass used in the analysis (70 GPa) is slightly lower than the value obtained from an intact core (80 GPa). This is considered to be a reasonable assumption due to scale effects and the likely presence of microcracks in the rock mass. The normal stress-normal displacement relationship for the fracture is assumed to follow a hyperbolic function, equation (6.33), as shown in figure 7.15. The experimental curve (for unloading during the third cycle of the laboratory experiment) shows a stiffer behaviour of the fracture than the one assumed in the FRACON simulation. Due to scale effects, a less rigid in-situ behaviour as used in the FRACON analysis is considered a reasonable assumption.

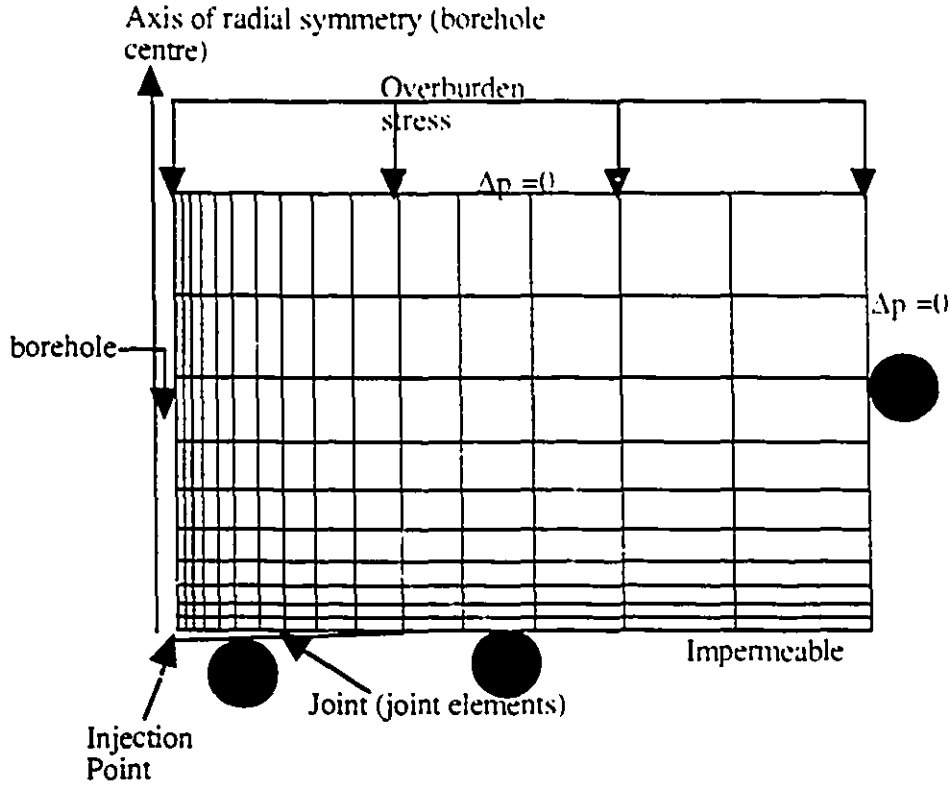

Mesh dimension 15 m horizontal x 10 m vertical

Figure 7.16 Finite element mesh for borehole injection tests

The parallel plate model, developed from the application of the Navier-Stokes equation for laminar incompressible flow between two parallel smooth plates, is used to calculate the permeability k of the fracture (cf. equation 6.35). Equation (6.37) that relates the hydraulic aperture of the fracture to its mechanical aperture is adopted:

$$eh = eh_0 + f\,\Delta em \qquad (7.1)$$

where eh_0 is the initial hydraulic aperture, Δem is the variation in mechanical aperture and f is a correction factor that varies from 0.5 to 1 (as suggested by Benjelloun, 1991).

In the FRACON simulation of the borehole injection tests, we used:

eh_0 = 17 μm

f=1.

The in-situ total normal stress in the FRACON simulation is assumed to be 8.6 MPa and is 15% lower than the stress due to the weight of the overburden.

The hydraulic conditions at the outer radius of the joint are dictated by the permeability of the rock mass. As the pressure propagates outward from the injection point, the pressure at the outer radius of the joint increases from an initial ambient value to a value that should be lower than the initial normal stress (any higher pressure is not admissible, since the rock mass is assumed to have negligible tensile strength and fracture toughness). In the FRACON code, an internal control was included to impose a higher limit of p= 8.6 MPa at the nodes corresponding to the outer radius of the joint.

7.5.3 Simulation results for pulse test

For the pulse test, an additional "fluid element" was added to the finite element mesh of figure 7.16, at the injection point. This element is in fact a joint element, with very high permeability, with a volume equal to that of the sealed section (0.00062 m^3) and with a compressibility equal to the measured combined compliance of the water and the equipment (2.2×10^{-9} Pa^{-1}). The calculated pressure at the injection point compares very well with the experimental one, as shown in figure 7.17.

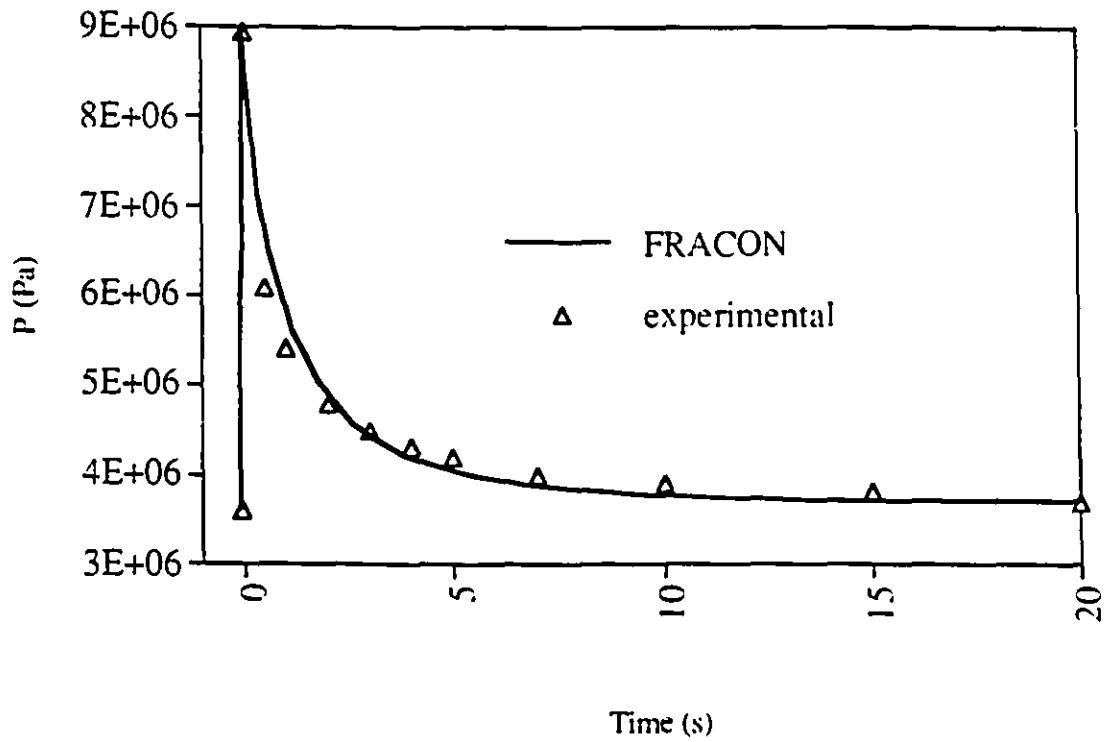

Figure 7.17 Pressure at injection point - Pulse Test

7.5.4 Simulation results for Hydraulic Jacking Test

In figure 7.18 , the results of the FRACON simulation are compared to the experimental results of the hydraulic jacking test. Satisfactory agreement between the simulated and the experimental data is observed. Both sets of data show that at injection pressures below the in-situ total normal stress across the joint, the flow rate is quite low. The resistance to opening of the joint at low injection pressures comes mainly from the normal stiffness, without any significant contribution from the surrounding rock mass. For pressures above the in-situ normal stress, the joint normal stiffness is very low and the aperture of the joint increases drastically, resulting in a very rapid increase of its permeability and,

consequently, of the flow rate. The rigidity of the system in the latter case is almost entirely due to the rigidity of the surrounding rock mass.

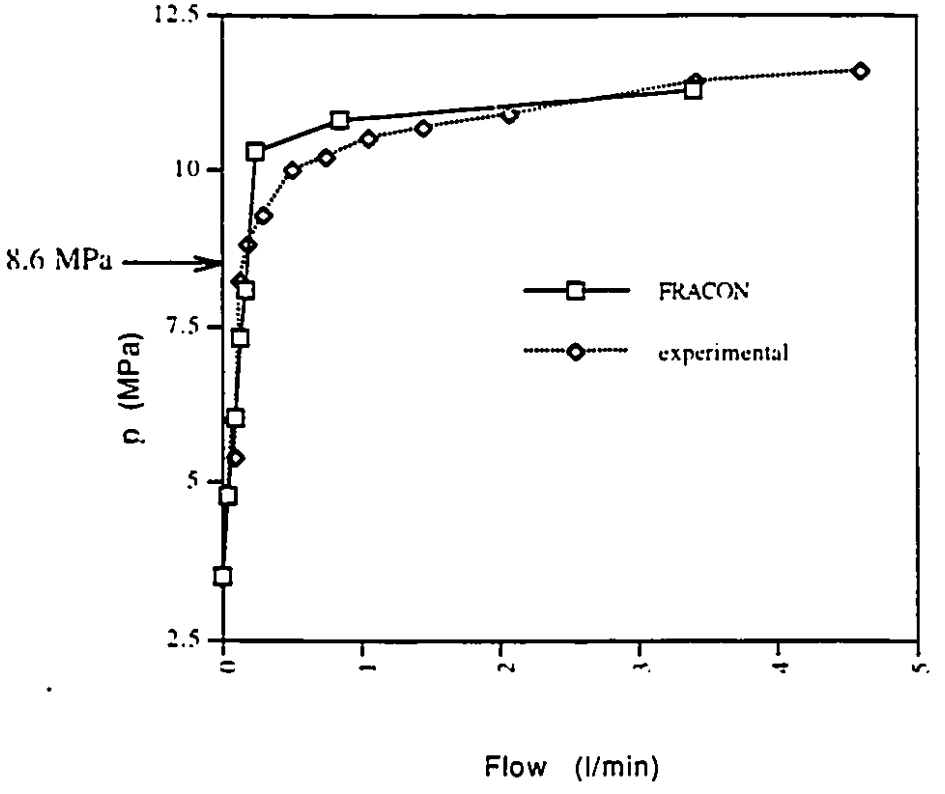

Figure 7.18 Hydraulic jacking test

The transition from low to high flows derived from the FRACON simulation happens more abruptly and at higher injection pressures as compared to the experimental data. It is likely that this is primarily due to the fact that there is no account for fracture propagation in the FRACON simulation. As noted before, in the FRACON simulation the outer periphery of the joint is fixed in space and the pressure at this location is artificially subjected to a higher

limit equal to the normal in-situ stress. The FRACON code always checks for the value of pressure at this location; when the higher limit is reached, the pressure at this location is maintained constant at that value for subsequent time steps and the flow rate is thus bounded by this imposed hydraulic condition. In reality, an outward fracture propagation is likely to happen, resulting in an increase in the radius and the aperture of the joint and allowing for an increase in the flow rate.

7.5.5 Simulation results for constant pressure test

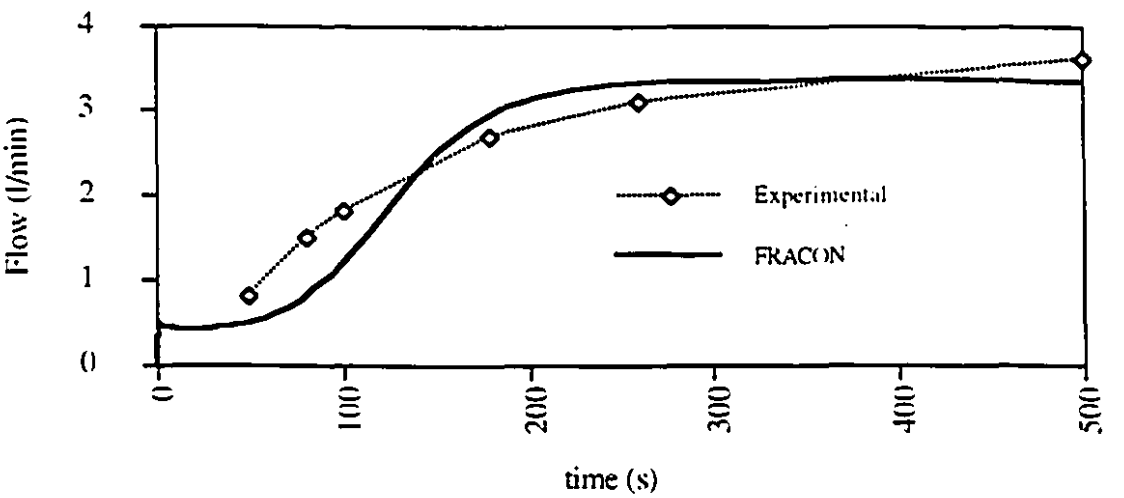

Figure 7.19 Constant pressure test

In figure 7.19, the FRACON results are compared with the experimental results for the constant pressure test. Again the simulated results are consistent with the experimental data. For a joint with constant permeability, analytical solutions (see e.g. Crank, 1975) show that the flow rate sharply increases very early in time, since the hydraulic gradient is very

high. This flow then gradually decreases to a steady state-value, as the pore pressure is dissipated radially into the fracture. Both the experimental and simulated results show that the above behaviour occurs only at the early stage, lasting approximately 60 s, during which the high pressure at the injection point has insufficient time to propagate radially towards the outer boundary of the fracture. After that early stage, a gradual increase of the flow rate is observed. This type of behaviour is indicative of the nonlinear nature of the mechanical/hydraulic processes that prevail during the test, because of the high water pressure (injection pressure of p =11.5 MPa, higher than the in-situ normal stress of 8.6 MPa). The high pressure of the injected water leads to a drastic opening of the fracture (maximum opening of 70 μm compared to an initial hydraulic aperture of 17 μm), resulting in an increase of its permeability by several orders of magnitude. Consequently, the flow rate increases with time and reaches a steady-state value when the aperture distribution in the fracture reaches a stable value, as shown in figure 7.19.

As compared to the experimental data, the FRACON results shows a steeper increase in the flow rate and a lower steady state flow value, during the highly nonlinear phase. We believe that this comes from the fact that crack propagation at the outer radius of the joint could not be simulated with the code, as explained earlier.

7.5.6 Sensitivity of simulated results to some key parameters

In sections 7.5.3, 7.5.4 and 7.5.5, we only showed the results from the set of input data that provides the best comparison between the calculated and the experimental results. In order to arrive to these best fit results, numerous simulations with different sets of input data had to be performed. For the pulse test, the joint aperture does not change much due to the short duration of the test. Consequently, we found that the results of the pulse test are

most sensitive to the initial hydraulic aperture. Higher values of this parameter result in faster pressure dissipations in the isolated borehole section. For the hydraulic jacking and constant pressure tests, the results are very sensitive to the initial in-situ normal stress, the Young's modulus of the rock mass and the joint radius. These parameters determine the rigidity of the system at high injection pressures, directly influence the degree of opening of the joint and, consequently, affect the flow rate through the joint. Lower values of the initial in-situ normal stress and of the Young's modulus of the rock mass, and higher values of the joint radius all result in higher flow rates for the constant pressure test and the hydraulic jacking test. For the hydraulic jacking test, the transition pressure from low flow rates to high flow rates is lower for lower initial in-situ normal stress. To a lesser degree than the above factors, higher permeability values of the rock mass result in higher flow rates for the constant pressure and hydraulic jacking tests. Due to a more significant amount of water diffusing tranversely from the joint into the surrounding rock mass, the time for longitudinal pressure propagation in the joint is longer. Thus the steady-state value of flow, for the constant pressure test, is reached at later times as compared to cases with lower rock mass permeability.

7.6 Conclusions

The joint model developed in chapter 6 has been implemented in the finite element code FRACON. In this chapter, we have shown the use of the code to simulate several laboratory experiments: shear tests under constant normal stress and under constant normal stiffness conditions performed by Skinas et al. (1990); and coupled shear-flow experiments performed by Bandis et al. (1985). The model performs quite satisfactorily in simulating the trends observed in the above experiments. Scale effects, as evidenced from the

experimental results of Bandis et al. (1981) , are also correctly predicted by the proposed model. To better predict dilation, the model could be improved by incorporating a damage deformation component as suggested by Plesha (1995) and by assuming that plasticity phenomena can also occur prior to the attainment of the peak shear stress.

The FRACON code was also used to simulate several borehole injection tests conducted in a natural fracture. The code successfully predicted the significantly nonlinear nature of the coupling between flow and mechanical processes that prevail in these tests.

CHAPTER 8

APPLICATIONS TO NUCLEAR FUEL WASTE DISPOSAL

The Canadian concept for the disposal of heat emitting high level Nuclear Fuel Waste (NFW) involves the deep burial of the wastes in a plutonic rock mass of the Canadian Shield. Due to the longevity of the radioisotopes, a NFW disposal system is required to provide protection to human health and the environment from the hazards of contaminant release which could last for tens of thousands of years. The plutonic rock mass is a major barrier against contaminant release to the environment. In this chapter, we present certain scoping calculations with the FRACON code to assess the impact on the performance of the natural geological barrier due to the following: a future glaciation scenario and the influence of radiogenic heat produced from the wastes. The Nuclear Fuel Waste Disposal program in Canada is in an early stage of concept feasibility studies. A specific site that would host a NFW repository is yet to be selected. Consequently, the scenarios modelled here are meant to be indicative of generic conditions applicable to a hypothetical site. In that context, the use of simple but conservative assumptions in building scenarios in order to assess the robustness of the concept is thought to be preferable to sophisticated assumptions which do not have site-specific data to support them. The regulatory document R-104 (Atomic Energy Control Board, 1987) requires that the safety of the repository has to be

demonstrated for the first 10000 years. It is with this time frame in mind, that the analyses presented in this chapter are performed.

Throughout this chapter, compressive stresses and pore water pressure are considered positive according to the usual convention in rock and soil mechanics.

8.1 Rock mass reponse to radiogenic heat from a nuclear fuel waste repository

8.1.1 Conceptual and finite element models of a hypothetical NFW repository

A plutonic rock mass of the Canadian Shield that would contain a NFW repository would ideally be competent, mostly unfractured with the presence of few major fracture zones which are easily distinguishable from the competent rock mass. Field data from the Underground Research Laboratory (AECL, 1994 a,b and c) at Whiteshell, Manitoba, indicate that near the ground surface (up to 200 to 500 m deep), the rock mass is moderately fractured and contains networks of interconnected joints. However, at greater depths, the field data suggest that the rock mass is of very good quality and contains few discernible fractures outside the major fracture zones (figure 8.1). This relatively unfractured competent rock is also referred to as "sparsely fractured" rock. We will refer to this sparsely fractured rock mass as "competent" rock in this chapter. In the competent rock, water moves in a network of pores, microcracks and sparsely distributed joints which are generally not interconnected. The major fracture zones are defined as zones of fractured, broken rocks, which are hundreds of metres (or more) long and tens of metres (or more) thick. These fracture zones usually have very different mechanical and

hydrogeological characteristics when compared with the remaining competent rock mass. Usually they are more hydraulically conductive and prone to shearing under large external loads, such as the weight of a glacier or the heat generated by the wastes.

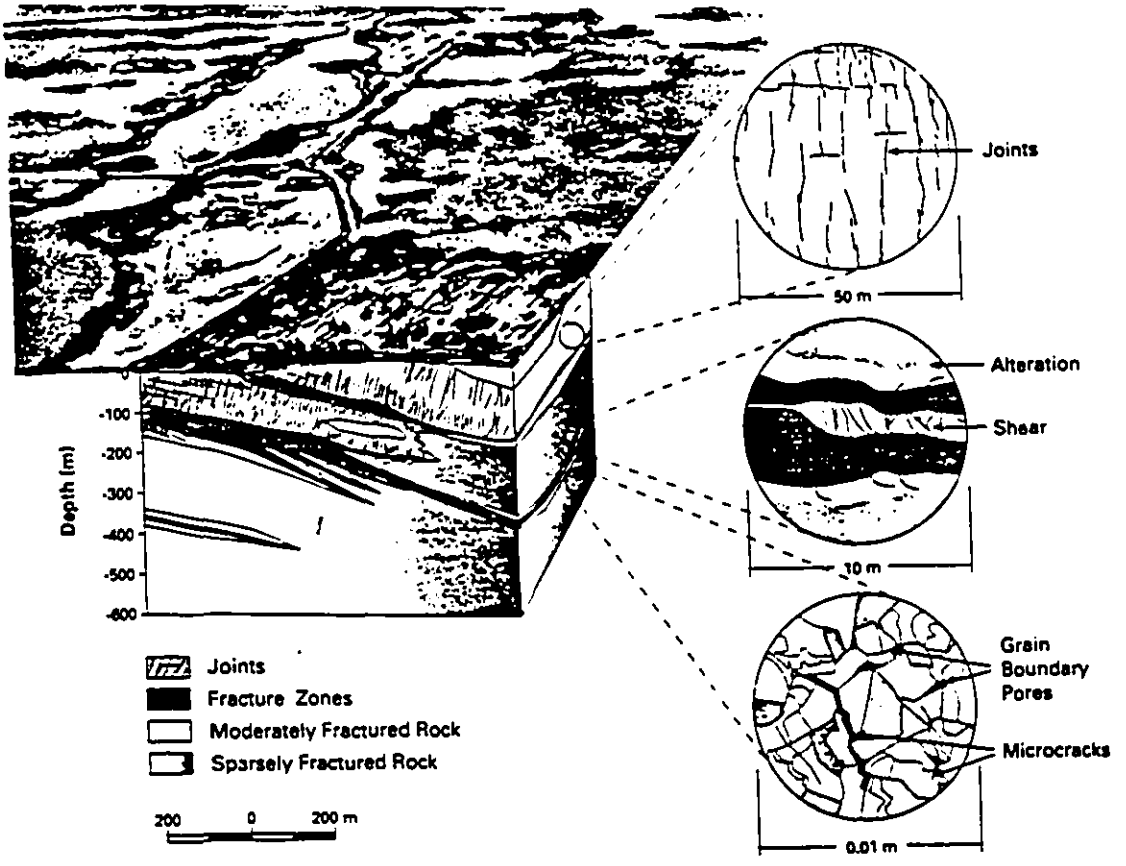

Figure 8.1 Schematic of rock structure for competent rock, moderately fractured rock and fracture zones (from AECL, 1994-a)

A hypothetical repository situated at a depth of 1000 m in a typical pluton of the Canadian Shield is considered in this section. The repository occupies an area of 2000 m by 2000 m. The total amount of wastes contained in the repository, will result in an initial heat generation rate (per unit area of the repository) of 10.4 W/m^2. This rate decays to 95% after

1 year, 80% after 1000 years and less than 10% after 10000 years, due to the decay in radioactivity of the wastes (figure 8.2). The above dimensions of the hypothetical repository and its heat characteristics basically follow the conceptual design of AECL (1994-b).

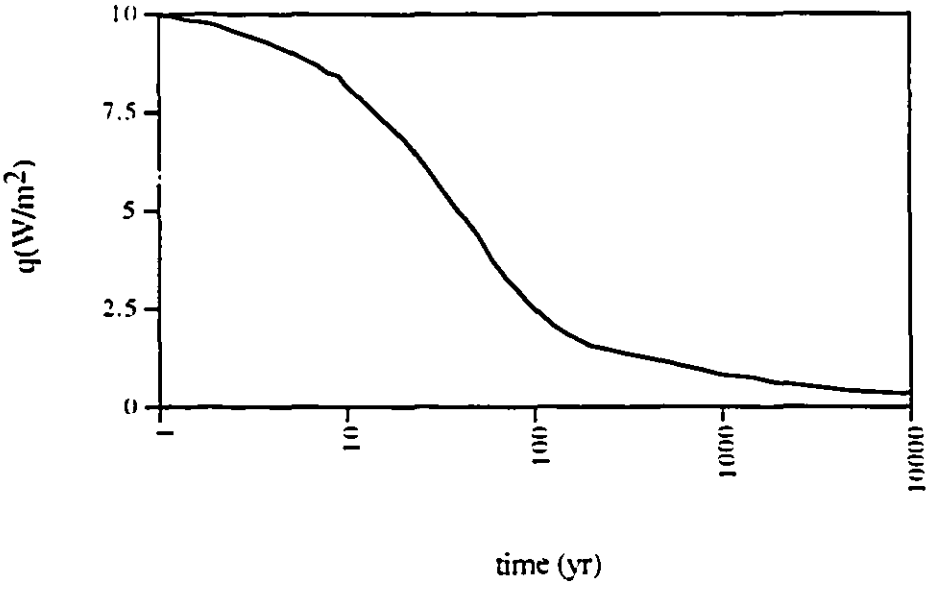

Figure 8.2 Radiogenic heat output from the waste repository

We assume that the repository is located in a competent rock mass disrupted by the presence of two vertical fracture zones, 20 m thick, at 100 m from two opposite edges of the repository. Assuming plane strain conditions, the rock mass response was simulated with the FRACON code. It is shown by AECL (1994-b), that the plane strain simplification will result in slightly higher temperatures and thermally induced stresses, as compared to the more realistic 3-D problem. Consequently, the analysis shown here is considered to be

conservative and the approach used is consistent with the objective described in the introduction of this chapter. The finite element mesh used in the study is shown in Figure 8.3. Eight-noded isoparametric elements are used to represent the rock mass while six-noded joint elements are used to represent the fracture zone. The boundary conditions invoked in the analysis are also shown in Figure 8.3. Due to the assumed symmetry conditions, only half of the repository is considered.

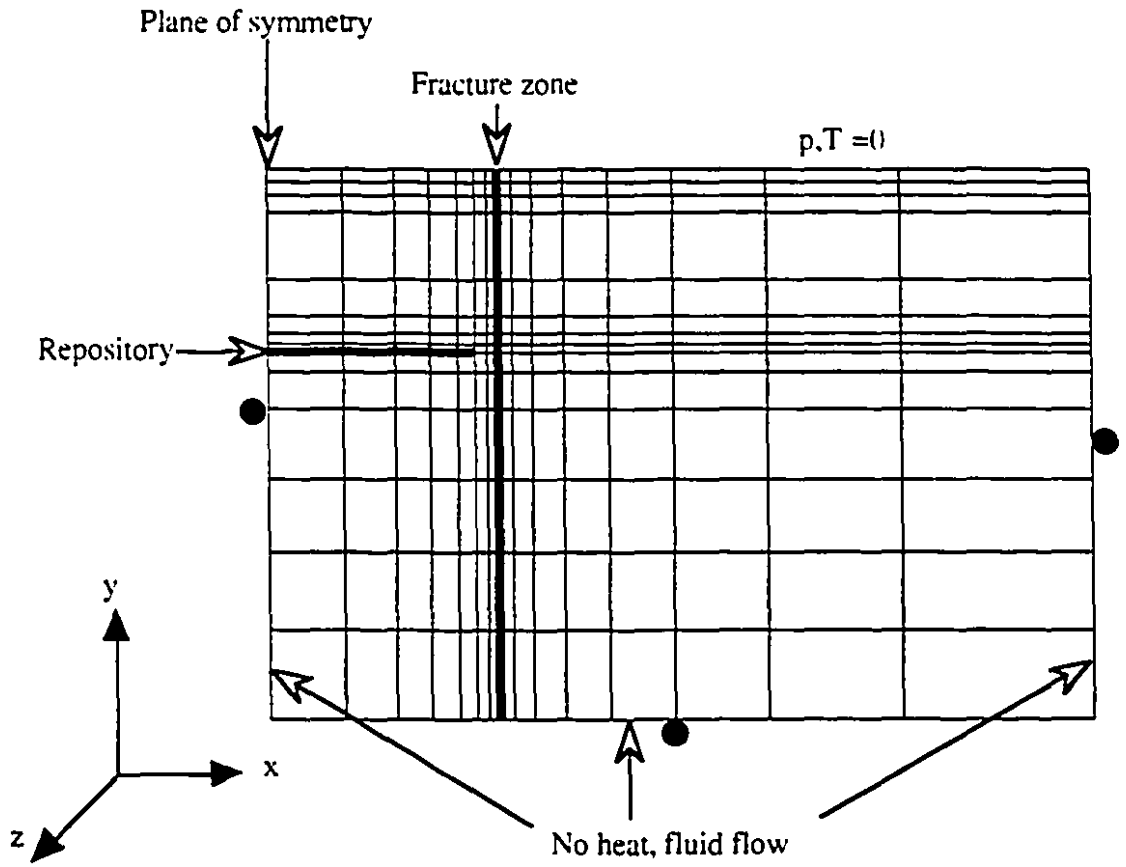

Figure 8.3 Finite element mesh for waste repository

8.1.2 Assumed properties of rock mass and fracture zones - Reference case

For the reference case analysis the following properties of the rock mass and the fracture zone are assumed:

For the rock mass:

permeability k: 10^{-18} m^2

Young's modulus E: 35×10^9 Pa

Poisson's ratio ν: 0.2

Effective porosity n: 0.005

For the fracture zone:

permeability k: 10^{-15} m^2

Shear stiffness $D_s = 35 \times 10^6$ Pa

Normal stiffness $D_n = 35 \times 10^8$ Pa

The thermal properties for both the rock mass and the fracture zone are assumed to be:

$\kappa = 3$ W/m/°C

C= 845 J/kg/°C

Physical property of pore water, solid grains and solid matrix:

Compressibility of water $c_f = 1/K_f = 4.5 \times 10^{-10}$ Pa^{-1}

Compressibility of the solid grains $c_s = 1/K_s = 2 \times 10^{-11}$ Pa^{-1}

density of solid grains: ρ_s=2700 kg/m^3,

density of pore water: ρ_f=1000 kg/m^3,

Coefficient of thermal expansion of solid matrix and solid grains: $\beta' = \beta_s = 0.24 \times 10^{-4}$ $^oC^{-1}$

Coefficient of thermal expansion of pore water: $\beta_f = 0.4 \times 10^{-3}$ $^oC^{-1}$

The above thermal/mechanical/hydraulic properties of the rock mass are considered typical for competent plutonic rock masses of the Canadian Shield (Gale, 1982; AECL, 1994-b, c). Much more uncertainties exist for the definition of properties for fracture zones. The shear and normal stiffness values of fracture zones in the Canadian Shield are largely unknown because of the lack of field measurements to determine these mechanical properties. Permeability values, on the other hand, which have been estimated for fracture zones at the Underground Research Laboratory site, vary in a range of 10^{-12} m^2 - 10^{-17} m^2 (AECL, 1994-c). The value of permeability for the fracture zone used in the reference case analysis corresponds roughly to the mean value of the above range. It is noted that for water at 15 ^{o}C, the hydraulic conductivity values (in m/s) is 7 orders of magnitude higher than the values of permeability (in m^2). For example a value of permeability of 10^{-12} m^2 would correspond to a hydraulic conductivity of 10^{-5} m/s . For the sake of simplicity consistent with the generic site discussed earlier, all properties are assumed constant and only linear elastic analyses are performed in this chapter. In particular, due to the lack of data on the mechanical properties of the fracture zones, the elasto-plastic joint model discussed in chapters 6 and 7 is not used in this study.

8.1.3 Results for reference case analysis with the FRACON code

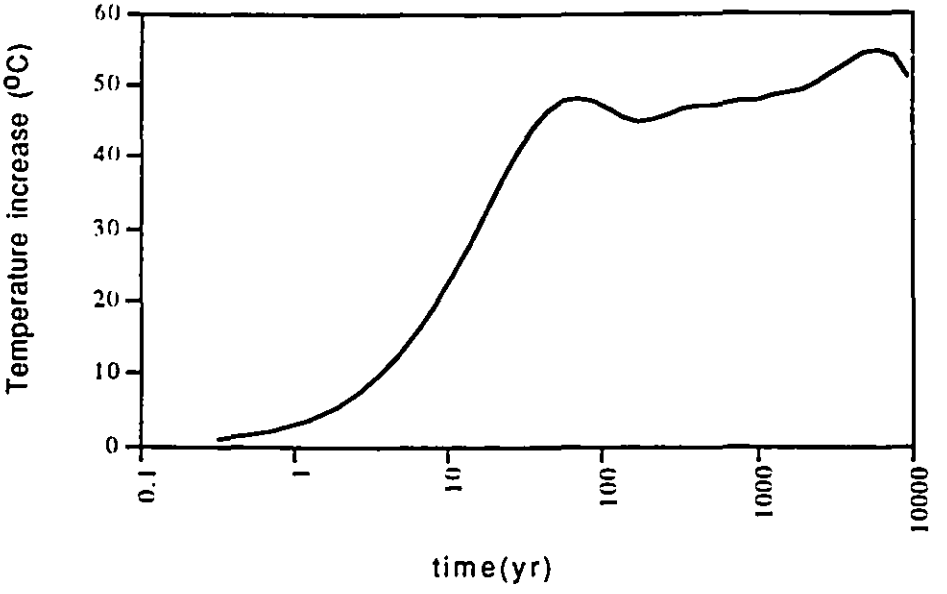

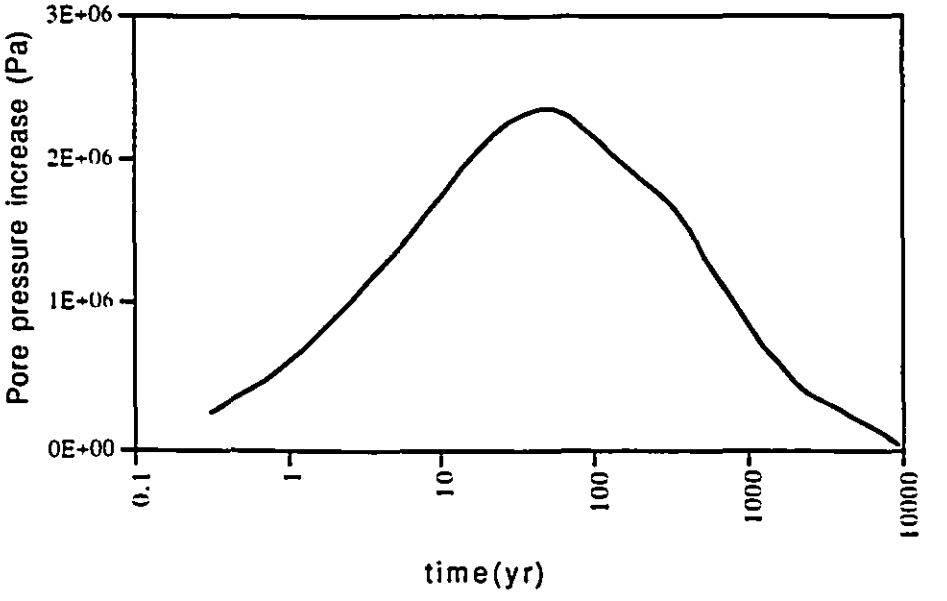

Figure 8.4 Time-dependent variations of pore pressure and temperature at the centre of the repository - Reference case

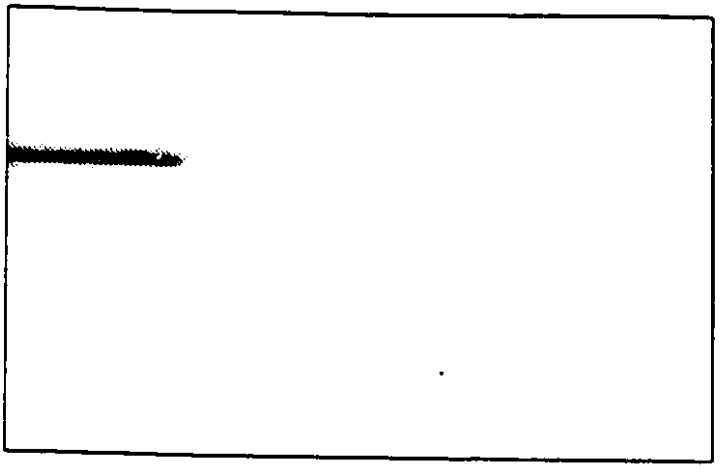

Temperature Field - 70 years

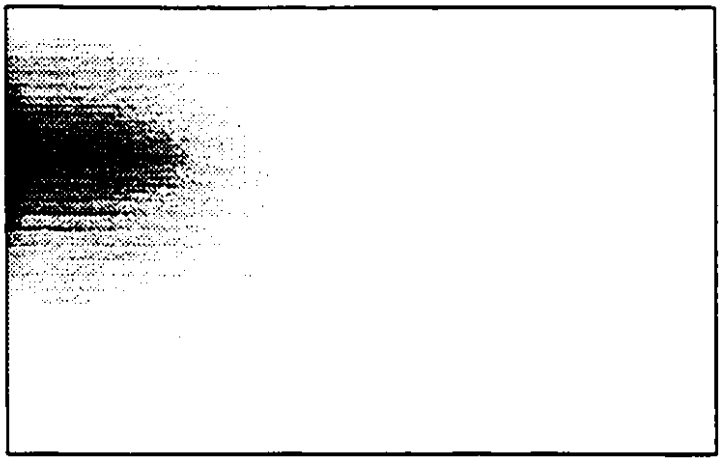

Temperature Field - 5000 years

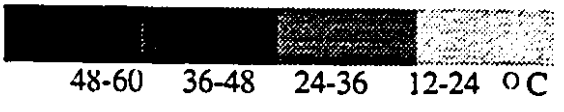

Figure 8.5 Typical temperature contours around the NFW repository

The temperature and the pore pressure increases at the centre of the repository are shown in figure 8.4. The temperature increase shows two peaks, 50°C at 70 years and 55°C at 5000 years; this is consistent with results of others (AECL, 1994-b). The presence of two thermal peaks is due to the nature of the heat output from the fuel wastes. The first peak is due to short-lived radio-isotopes which generate heat at a high rate but for short time periods; the second peak is due to longer-lived isotopes that generate heat at lower rates but for much longer times. Temperature contours are shown in figure 8.5 for the two times corresponding to the temperature peaks at the centre of the repository. It could be seen that at 70 years, the perturbation in the temperature is limited to a rock mass approximately 200 m thick surrounding the repository. At 5000 years, the thermal perturbation extends to the ground surface.

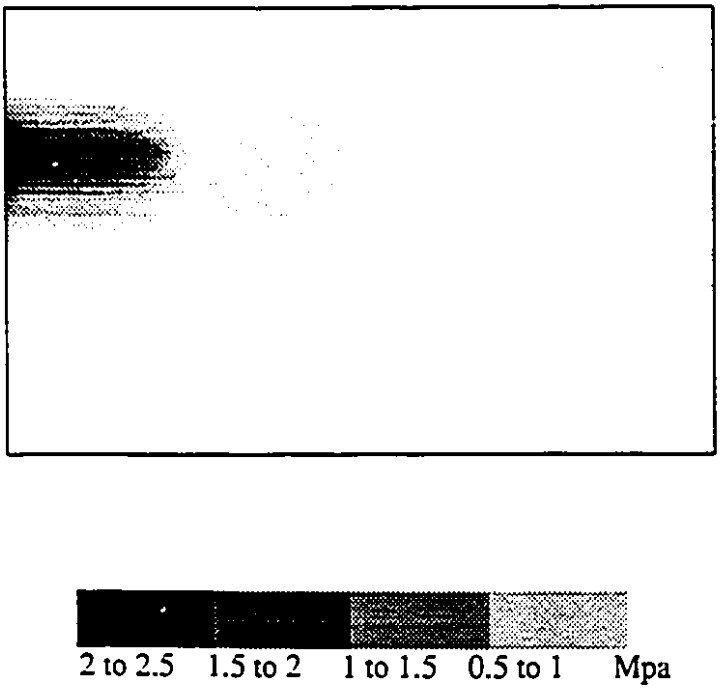

Figure 8.6 Typical pore pressure contours around the repository- Reference case

The pore pressure increase in the centre of the repository shows a peak of approximately 2.5 MPa at 55 years (figure 8.4). This pore pressure increase is due to the fact that the thermal expansion coefficient of the water is higher than that of the solid matrix. Due to the low permeability of the medium, drainage is slow and the pore water expansion is impeded, resulting in pore pressure increases at the initial stages. At the later stages, migration of water from the heat source takes place gradually allowing the pore pressure to dissipate. Typical contours of pore pressure increases are shown in Figure 8.6 (at 55 years). These pore pressure contours suggest that high hydraulic gradients are thermally induced in the vicinity of the repository. These gradients can attain values of up to 100% (i.e. several orders of magnitude higher than typical regional gradients in the Canadian Shield which are in the order of 0.1%) resulting in increased groundwater velocities diverging from the repository. The existing groundwater regimes will therefore be significantly modified by the thermal pulse. It can also be observed that the fracture zone acts as a drainage feature and would constitute a preferential pathway for the movement of groundwater to the surface. Another implication of these high pore pressures is that effective stresses will be reduced, possibly resulting in either a reduction of the strength of both the competent rock mass and the fracture zones or in the creation of new fractures.

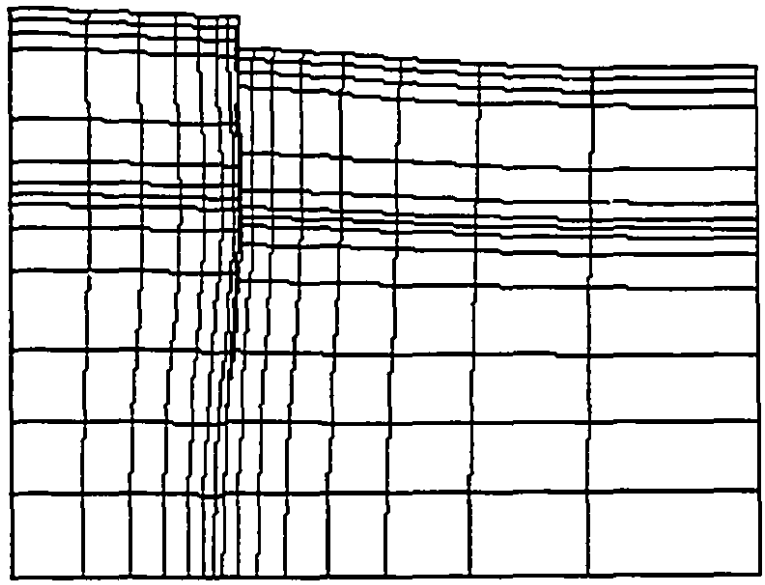

Figure 8.7 Deformed configuration of the mesh - Reference case

A typical deformed configuration of the modelled region is shown in Figure 8.7. These results indicate that shear movements are induced in the fracture zone, an uplift of the ground surface is induced directly above the repository and thermal expansion of the rock matrix takes place around the repository. These displacements are relatively small (maximum value of 50 cm), but can induce significant disturbances to the stress regime and as a consequence, the structural integrity of the rock mass in the vicinity of the repository has to be further assessed. We will now have a closer look at the thermally induced perturbations to the stress and groundwater regimes in the rock mass and in the fracture zone.

Herget (1980) reported a compilation of in-situ stress measurements in the Canadian Shield. In the majority of cases, the minor principal stress corresponds to the vertical

stress, which is primarily due to the weight of the overburden. The major principal stress is oriented in a horizontal direction, and is mainly due to tectonic forces. Herget (1980) proposed the following equations for estimating the in-situ stresses:

$$\sigma_v = 0.0265\ h \quad (Mpa) \tag{8.1}$$

$$\sigma_{ha} = 6.67 + 0.0302\ h \quad (Mpa) \tag{8.2}$$

$$\sigma_{he} = 12.36 + 0.0586\ h \quad (Mpa) \tag{8.3}$$

where σ_v is the vertical stress; σ_{ha} is the average value of the horizontal stress for the Canadian Shield and σ_{he} is the higher values of horizontal stress in the range of values reported by Herget (1980); and h is the depth below the ground surface (in units of m). In equations (8.1)-(8.3), total stresses (as opposed to effective stresses) are considered.

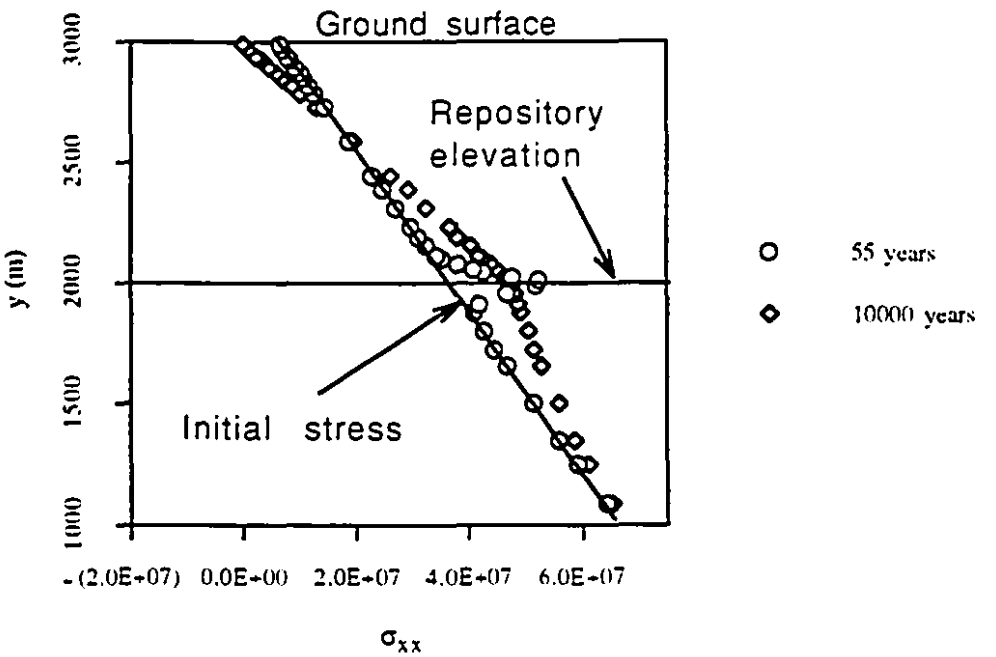

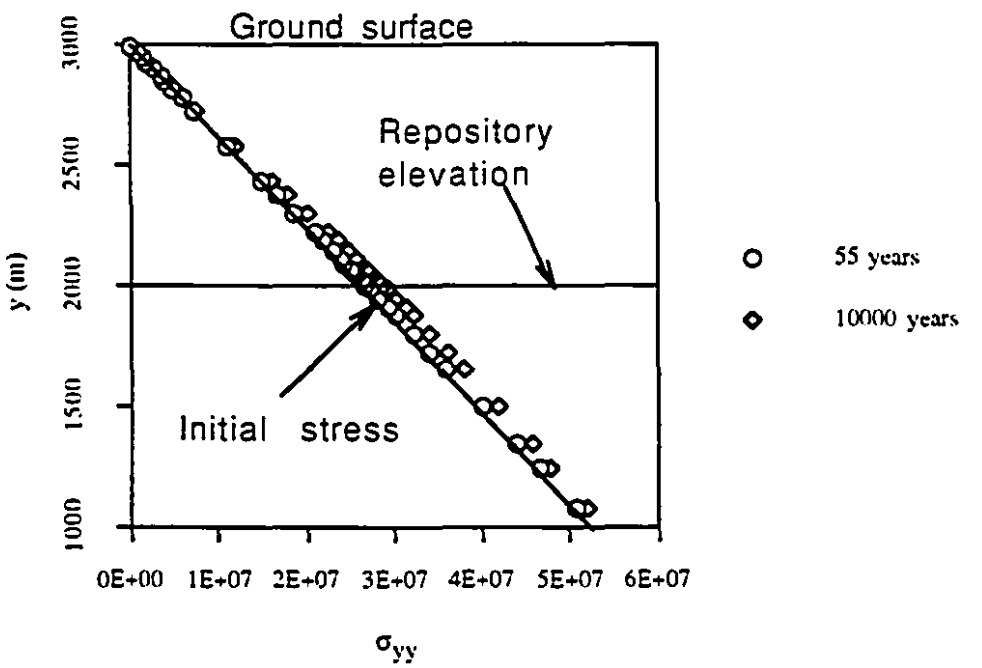

Figure 8.8 Vertical profile of total stresses near centre of repository - Reference case

The heat generated by the wastes will change the above original in-situ state of stress. The total vertical and horizontal stresses along a vertical section through the centre of the repository are shown in figure 8.8 at two specific times: 55 years after wastes emplacement, when the thermally induced pore pressure is at its peak, and at 10000 years when the temperature at the centre of the repository is near its second peak and the thermal perturbation extends to the ground surface. In figure 8.8, the x coordinate corresponds to the horizontal direction, the y coordinate corresponds to the vertical direction, and the initial stress distribution is assumed to follow Herget's values for average conditions, defined by equations (8.1) and (8.2). Figure 8.8 shows that along a vertical section through the centre of the repository, the vertical stresses are not significantly changed while more important changes are found for the horizontal stresses. The results shown in figure 8.8 are consistent qualitatively and quantitatively to results given by AECL (1994-b). However, in contrast to the analyses by AECL (1994-b), in order to assess the rock mass failure conditions, we will consider effective stresses instead of total stresses, as follows.

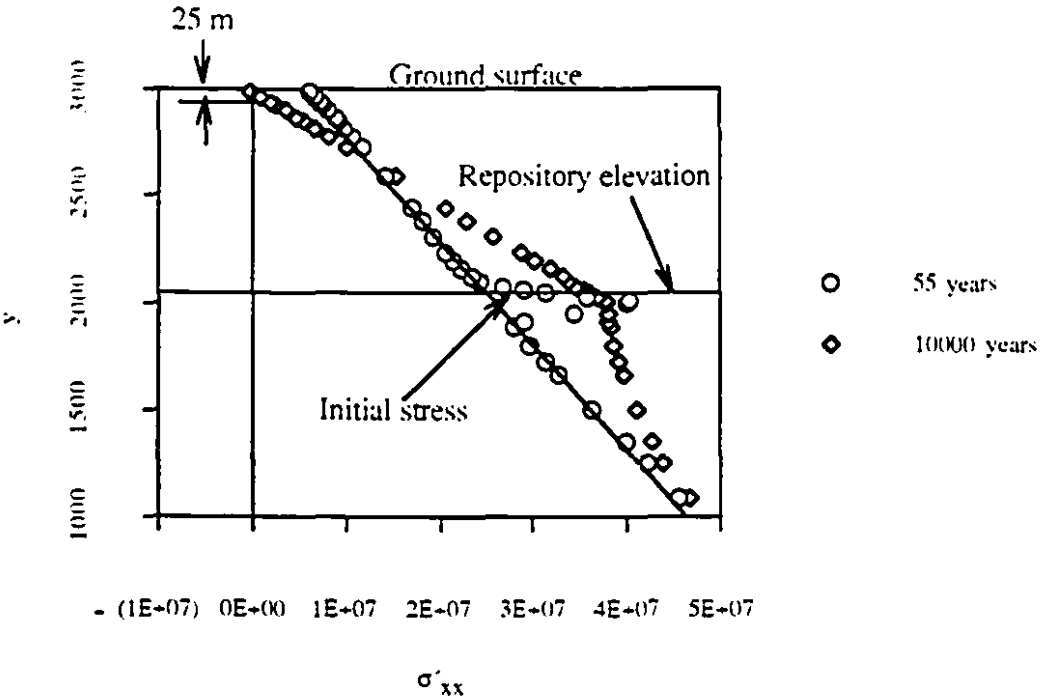

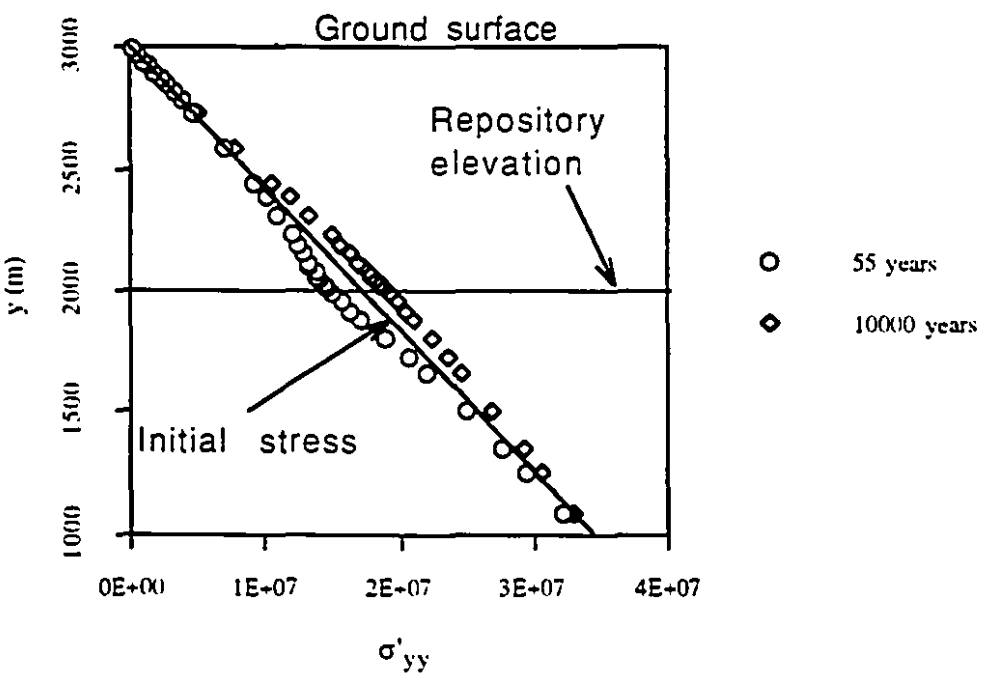

Figure 8.9 Vertical profile of effective stresses near centre of repository - Reference case

Figure 8.9 shows that due to thermal effects, along a vertical section through the centre of the repository, the horizontal effective stress increases in the vicinity of the repository, while it decreases near the surface. At 10000 years, a zone of tensile stresses could be seen to have formed down to a depth of approximately 25 m from the surface. Horizontally this zone would approximately occupy an area of 200mx200 m above the centre of the repository. If the tensile strength of rock is neglected, it is likely that vertical fractures will form in this zone. The zone of tensile cracking has limited extent. This zone is at a distance of 975 m from the repository and is not expected to significantly influence the groundwater flow field in the vicinity of the repository. Figure 8.9 also shows that the effective vertical stresses in the rock mass along a vertical section through the centre of the repository decreases at early times (55 years) due to the pore pressure buildup shown in figure 8.6. As the pore pressure dissipates, the effective vertical stresses gradually increase and become more compressive due to thermal effects.

The competent rock mass between the edge of the repository and the fracture zone is of particular importance, since it is part ot the groundwater flow path with the minimum travel time to the ground surface. Figures 8.10 to 8.14 shows the evolution of effective stresses at four points located in that envelope of competent rock (point 2 at the edge of the repository: point 3 at a distance of 63 m from the repository and 37 m from the fracture zone: point 4 at 19 m from the fracture zone: and point 5 adjacent to the fracture zone) and at the centre of the repository (point 1). Since the shear stresses are small, it is evident (from figures 8.10-8.14) that the minor principal stress is practically equal to the vertical stress, while the major principal stress would be practically horizontal, either in the z direction (perpendicular to the plane of the model), in the vicinity of the repository (point 1 and 2) or in the x direction at points closer to the fracture zone (points 3, 4 and 5).

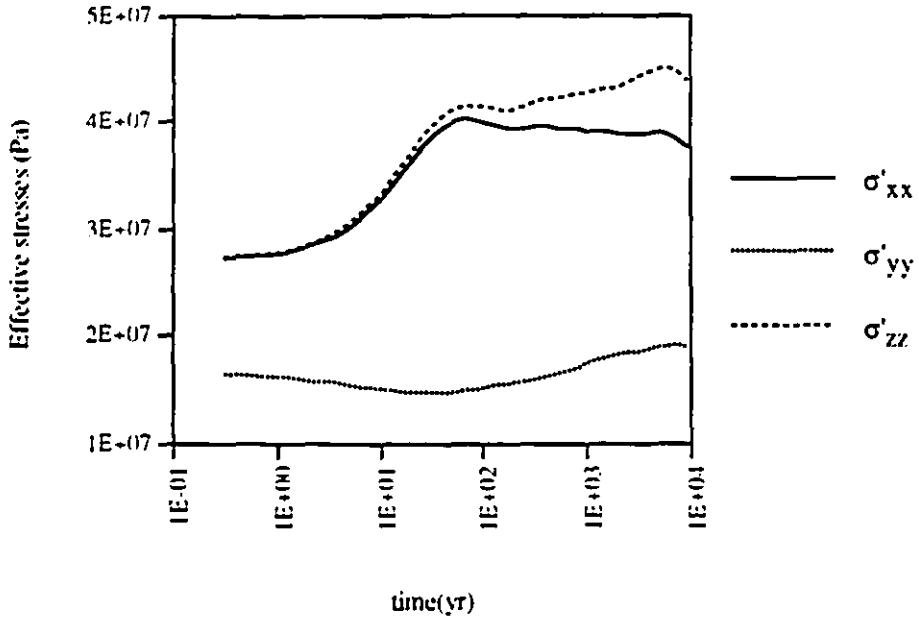

Figure 8.10 Stress evolution at Point 1, near centre of repository - Reference case

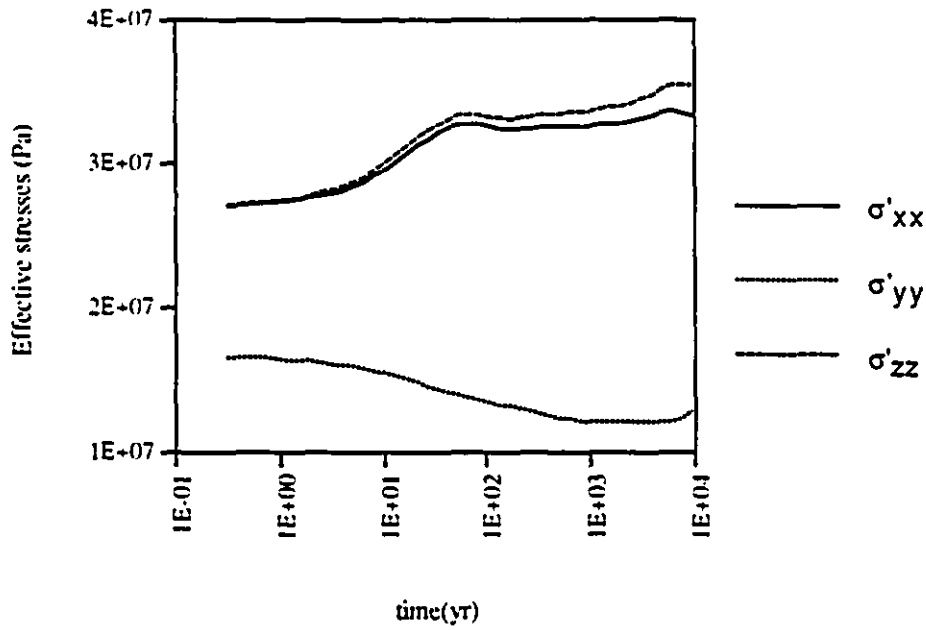

Figure 8.11 Stress evolution at Point 2, at edge of repository - Reference case

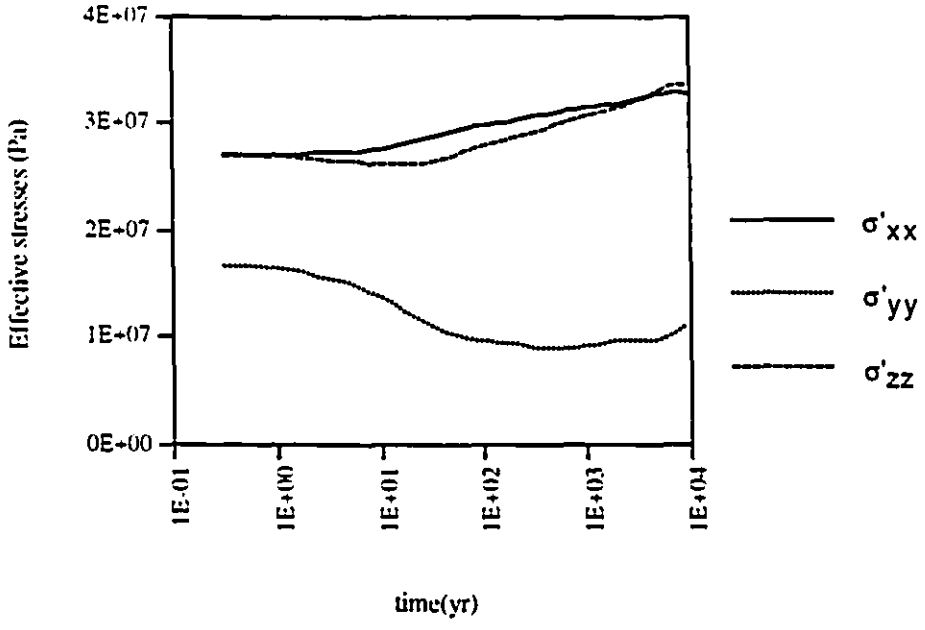

Figure 8.12 Stress evolution at Point 3 (63 m from edge of repository) - Reference case

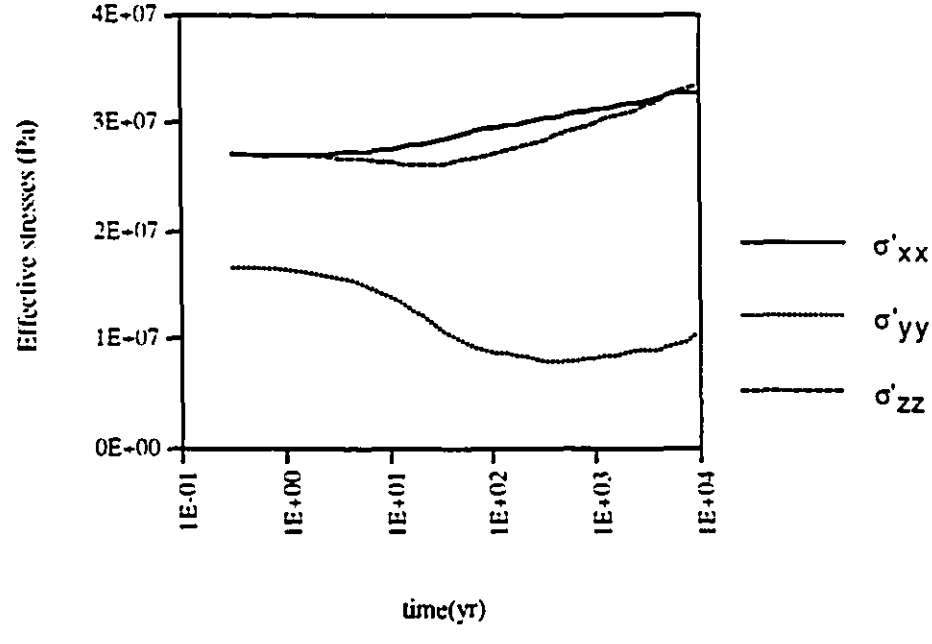

Figure 8.13 Stress evolution at Point 4 (19 m from fault zone) - Reference case

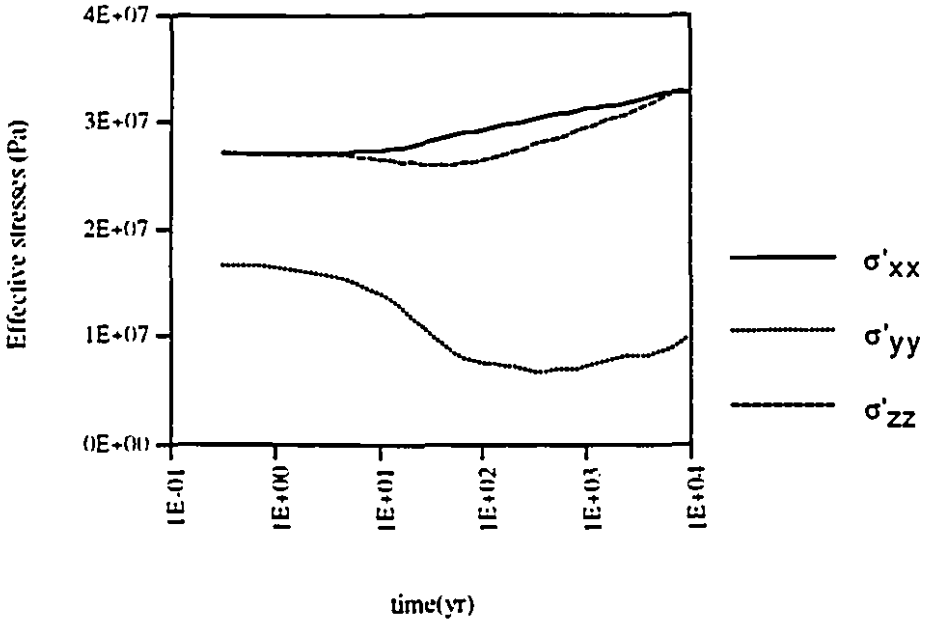

Figure 8.14 Stress evolution at Point 5 (adjacent to fracture zone) - Reference case

In order to verify whether the above stresses will result in fracturing of the competent rock mass , the empirical Hoek and Brown (1988) failure criterion was adopted:

$$\sigma'_{1f} = \sigma'_3 + \sqrt{m\sigma_c\sigma'_3 + s\sigma_c^2} \qquad (8.4)$$

In which:

σ'_{1f} is the effective major principal stress at failure.

σ'_3 is the effective minor principal stress

σ_c is the uniaxial compressive strength of intact samples of the rock mass

m , s are empirical constants.

The above criterion was formulated in terms of effective stresses, since these stresses govern the mechanical behaviour of saturated geological materials. The following values were adopted (AECL,1994-b) in the computations:

σ_c = 190 MPa

m=17.5, s=0.19

The above values suggest a rock mass with a "very good quality" designation (Hoek and Brown, 1988). Using the above values, it is found that the major principal stress at points 1 to 5 have a maximum value of approximately 45 MPa and at all times are lower than the major principal stress at failure given by the Hoek and Brown criterion (minimum value of approximately 160 MPa). If the initial in-situ horizontal stress is assumed to be in the upper bound (equation 8.3) of the envelope given by Herget (1980) instead of the average value (equation 8.2), the maximum value of the major principal stress would be approximately 80 MPa. For this condition, there is still a high margin of safety against failure of the competent rock mass surrounding the repository.

It is assumed that in the fracture zone, failure is governed by the Mohr-Coulomb failure criterion : i.e.

$$\tau_f = \sigma' \tan\Phi' + c' \qquad (8.5)$$

where:

τ_f is the shear stress at failure

σ' is the effective normal stress acting across the fracture zone

c' and ϕ' are respectively the effective values of the cohesion and the angle of internal friction

AECL (1994-b) has reviewed the data available for the values c' and ϕ' for fracture zones in granite and has proposed the following ranges:

ϕ': 25 to 40°

c': 0 to 240 kPa

As a conservative estimate of these parameters, we assume that $c' = 0$ and $\phi' = 33°$. It is observed that the shear stress levels in the fracture zone are at all times below the shear stress at failure according to the Mohr-Coulomb criterion.

The thermally induced pore pressure triggers outward flow from the repository. In order to assess the rate of migration of potentially contaminated groundwater, the trajectories of water particles from points near the centre and from the edge of the repository are calculated according to the equations:

$$x(t) = x_0 + \int_0^t v_x(x,y,t)\, dt \tag{8.6}$$

$$y(t) = y_0 + \int_0^t v_y(x,y,t)\, dt \tag{8.7}$$

where :

$x(t)$ and $y(t)$ are the coordinates of the particle position at time t, x_0 and y_0 are the

coordinates of the particle position at time 0, and:

$$v_x(x,y,t) = -\frac{k}{n\,\mu}\frac{\partial p}{\partial x} \tag{8.8}$$

$$v_y(x,y,t) = -\frac{k}{n\,\mu}\frac{\partial p}{\partial y} \tag{8.9}$$

where k is the permeability of the rock mass, μ is the viscosity of water, n is the porosity of the rock mass and p is the pore pressure (positive in compression).

The calculated trajectories of groundwater movement during 10000 years are shown in figures 8.15 a and b. At 10000 years, the water particle from near the centre of the repository travels approximately 10 m in an upward direction and 6m in a horizontal direction (towards the fault zone). The particle from the edge of the repository travels mostly in a horizontal direction towards the fracture zone. Once a water particle has reached a fracture zone, it will migrate relatively quickly to the ground surface. At 10000 years, the particle from the edge of the repository has travelled a horizontal distance of approximately 30 m but is still 70 m away from the fracture zone. From the above discussion, it is evident that for the rock mass properties assumed in this hypothetical repository scenario, a zone of competent sparsely fractured rock of 100m between the repository and a major fracture zone would provide an effective barrier for contaminant migration due to thermally induced groundwater flow.

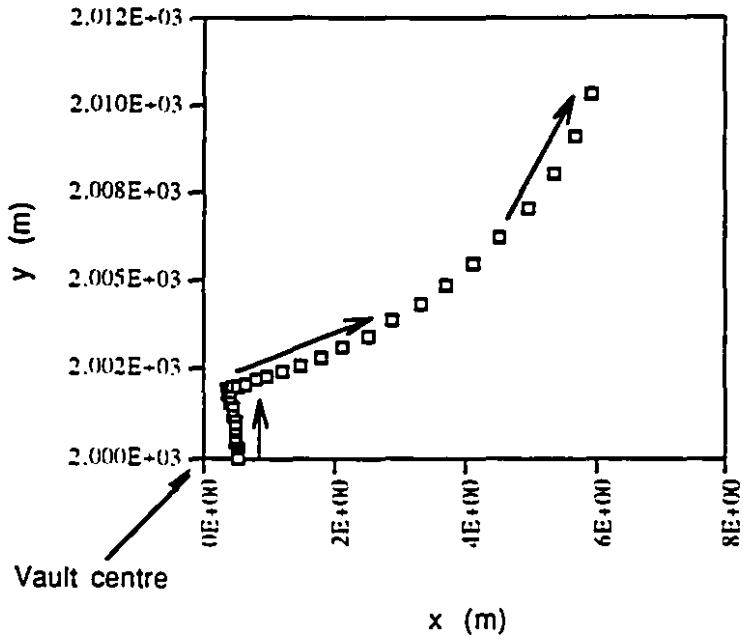

a) Near centre of repository

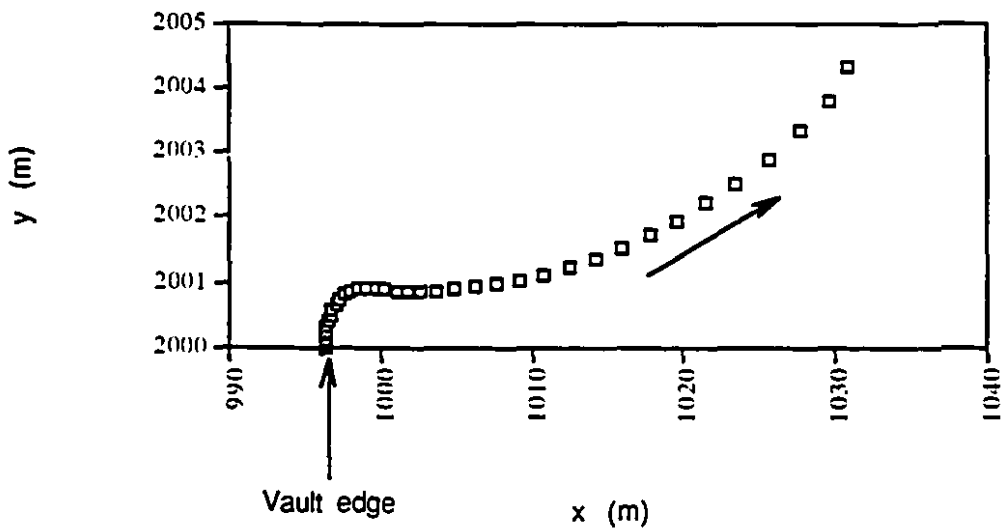

b) from edge of repository

Figure 8.15 Water particle trajectories - reference case

8.1.4 Parametric study

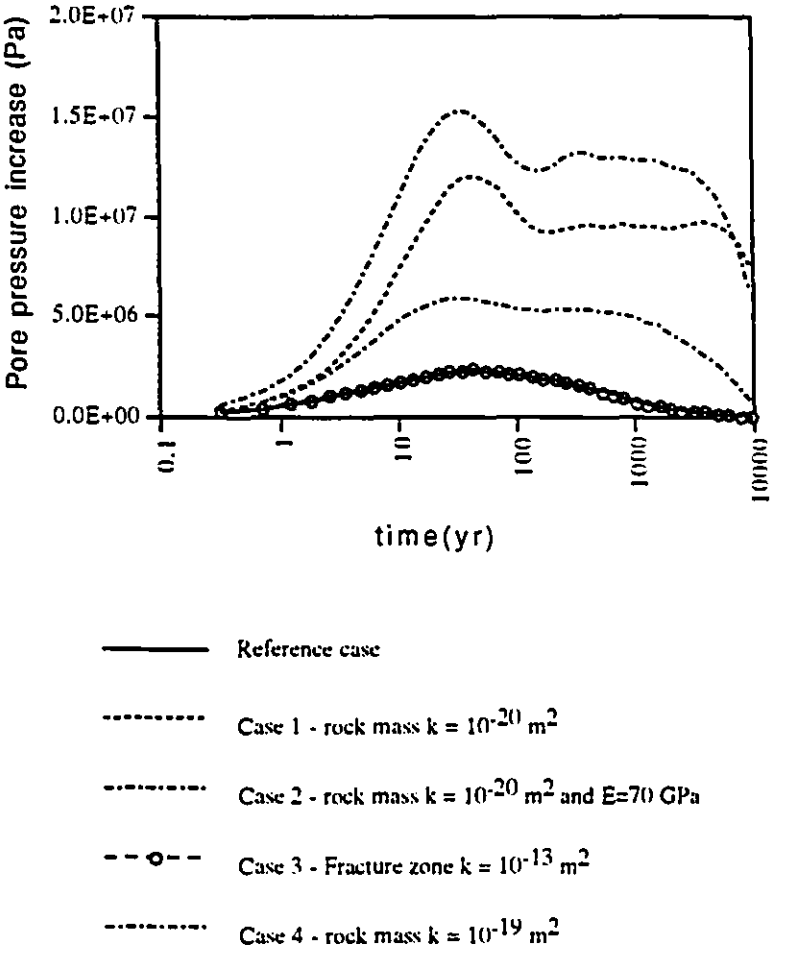

Figure 8.16 Effects of permeability and Young's modulus on pore pressure

The effects of rock mass permeability, fracture zone permeability and rock mass Young's modulus are evaluated by considering the following cases, which are in every way similar to the above reference case except for the following differences:

- case 1: rock mass permeability: 10^{-20} m^2 (2 orders of magnitude lower than in the reference case)

- case 2: rock mass permeability : 10^{-20} m^2 and E=70 Gpa (2 times higher than in the reference case)

- case 3: fracture zone permeability 10^{-13} m^2 (2 orders of magnitude higher than in the reference case)

- case 4: rock mass permeability: 10^{-19} m^2 (1 order of magnitude lower than in the reference case)

Figure 8.16 presents a comparison of the pore pressure at the centre of the repository for all the separate cases. It can be seen that decreases in the rock mass permeability (case 1 and 4) results in substantial increases in the peak pore pressure. The thermally induced pore pressure would remain high for longer durations when compared to the reference case. A decrease in the permeability combined with an increase in the Young's modulus of the rock mass (case 2) results in a further increase in the pore pressure, which would be six times higher than in the reference case. An increase in the permeability of the fracture zone by two orders of magnitude (case 3) does not have any discernible influence on the pore pressure in the centre of the vault.

Case 2 is the most critical for rock mass stability, since the high thermally induced pore pressure (up to 15 MPa) would substantially reduce the minor effective principal stress (σ'_{yy}). Figure 8.17 shows the stress evolution at point 3, at a distance of 37 m from the fracture zone. It may be noted that in this case the effective vertical stress becomes tensile ($\sigma'_{yy}<0$). This tension zone is found to extend from the fracture zone to approximately a distance of 50 m towards the edge of the repository. Horizontal cracks would form in the

tension zone and the original envelope of 100 m of competent rock which existed between the repository and the fracture zone could be reduced to 50 m.

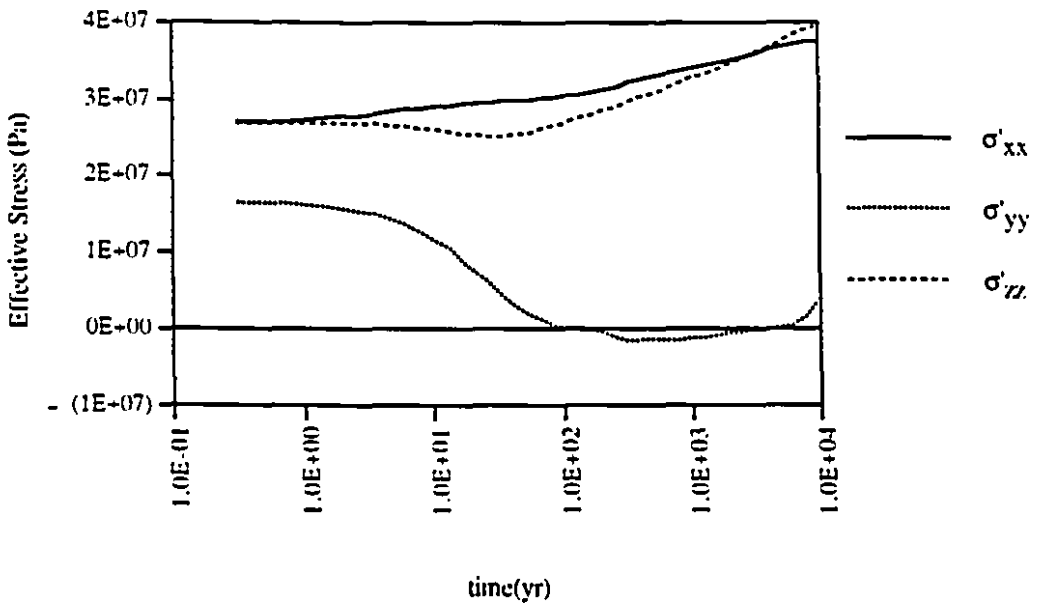

Figure 8.17 Stress evolution at point 3 at 37 m from fracture zone - Case 2

In figure 8.18, the flow paths of a particle of water from the edge of the repository are compared for the different cases. Although the pore pressure and the hydraulic gradients are higher for cases 1 and 2 (when compared with the reference case), the water particle has only moved a horizontal distance of approximately 10 m towards the fracture zone in 10000 years (compared to more than 30 m for the reference case), due to the significantly lower permeability of the rock mass. With an increase in the permeability of the fracture

zone (case 3), it exhibits a stronger drainage effect . As a consequence, the flow path becomes more horizontal and the path length is slightly increased compared with the reference case. For case 4, although the permeability of the rock mass is ten times lower compared to the reference case, the travel distance for a particle of water is not significantly reduced, since the thermally induced hydraulic gradients are much higher.

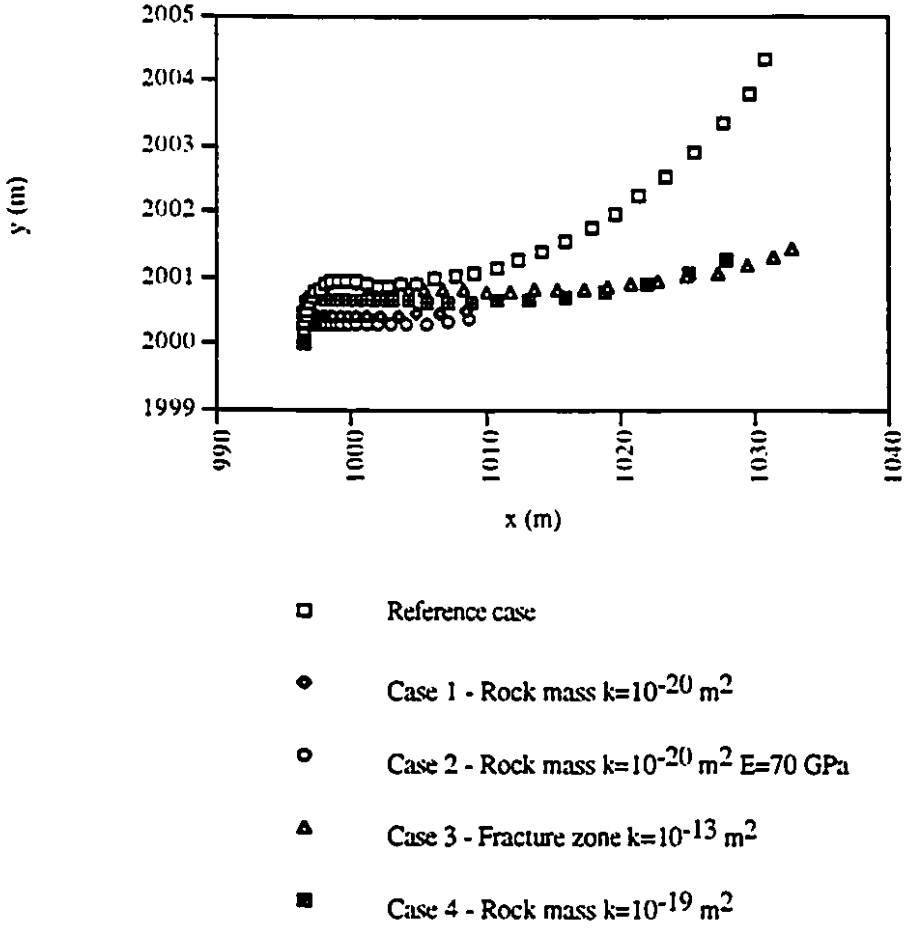

Figure 8. 18 Comparison of flow paths of water particle from edge of repository

8.2 Glaciation impacts on a nuclear fuel waste repository

Geologists expect that in approximately 10000 to 20000 years, the Canadian Shield could be exposed to a new glaciation period, similar to the ones that occured cyclically during the past. An ice cap could impose a load on the ground surface of up to 30 MPa near the centre of the cap and 15 MPa near the edges. If an ice cap forms on the ground surface above a NFW repository, the load due to its weight can significantly affect the structural and hydrogeological characteristics of the rock mass containing the repository. The FRACON code was used to model the impact of a glaciation scenario on the performance of a NFW repository.

When a rock mass is subjected to glacial loading, it will respond both mechanically and hydraulically in a coupled manner. Furthermore, even for temperatures below zero, the pore fluid will be unfrozen due to its salinity and due to the high pressures exerted by the glacier. Based on a review of geological studies of past glaciation events (Nguyen et al., 1993), it is inferred that a future glacier could cover up to half of the Northern hemisphere. The ice is thickest in the centre, around 3 km, resulting in a load of 30 MPa on the ground surface; near the edges the thickness would be about 1.5 km, with a resulting pressure of 15 MPa. The response of the rock mass hosting a NFW repository to ice loading will be different depending on its location (far away from or near the edges of the glacier) not only because of the difference in magnitude of the loads associated with variable ice thicknesses, but also due to the different hydraulic and structural boundary conditions applicable to each case. Mathematical modelling of both cases with the FRACON code has been reported by Nguyen et al. (1993). The most critical scenario for the performance of the repository is the one when it is located immediately at the edge of a glacier. This scenario is reported in this chapter.

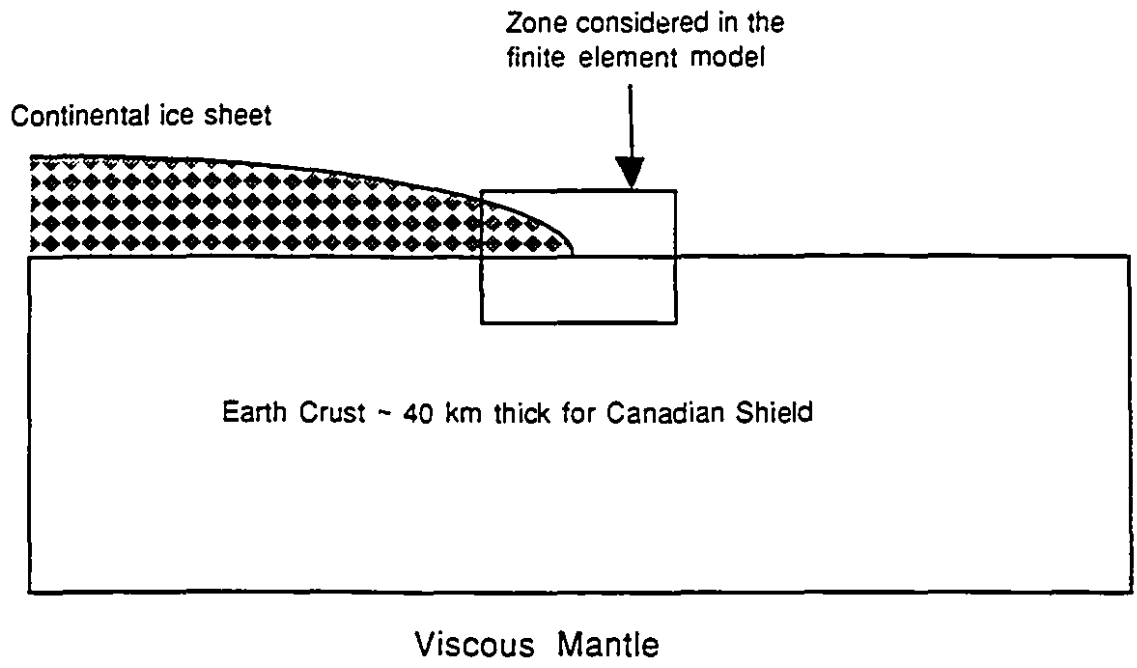

Figure 8.19 Conceptual Model for a glaciation scenario

The conceptual model for a glaciation scenario is illustrated in figure 8.19. Under the load of the glacier, geologists estimate from past glaciation periods that the surface of the earth will be depressed by up to 1 km. This downward movement is primarily attributed to the flow of the viscous mantle (Cathles III, 1969; Walcott, 1970 a and b; Selvadurai, 1979). In this study, we are primarily interested in the mechanical and hydrogeological disturbances in the upper part of the earth crust, where a NFW repository might be located.

The finite element model for the region of the earth's crust near the toe of the glacier is shown in figure 8.20. Only the upper 5 km of the crust is represented; it is assumed that the

deeper portion of the crust is impermeable and behaves as a rigid body. Consequently, the lower boundary is assumed to be impermeable. Since we are only interested in the relative deformations in the crust (and not in the absolute movement which is due mainly to the flow of the mantle) the lower boundary is also considered to be fixed in the vertical direction. We further assume that the interface between the crust and the mantle is relatively smooth. Consequently, the lower boundary is assumed to be free of shear traction. Considering the lateral extent of the ice sheet, the left boundary of the geological medium is fixed in the horizontal direction. The upper boundary of the modelled region is assumed to be free draining. The ice loading is represented by a normal load of stress intensity 15 MPa applied at the ground surface. Vincent and Prest (1987) have estimated that the rate of advance of a continental glacier is of the order of 0.1km/year (i.e. quite rapid when compared to the transient period of hydrological/mechanical disturbances that it would induce in the upper crust). It is therefore assumed that the glacial loads can be modelled as a normal surface load of intensity 15 MPa which is imposed instantaneously and has a time variation in the form of a Heaviside step function.

In this analysis, we assume that the glacial surcharge load extends to the position of the vertical fracture zone. The fracture zone is 20 m thick and extends to the entire depth of the model. Joint elements are used to simulate the fracture zone and solid isoparametric elements are used to simulate the unfractured rock mass. The location of the fracture zone at the edge of the glacier is a conservative assumption, since the rate of groundwater flow is expected to be higher near the edge of the glacier where a hypothetical repository is located. The mechanical/hydraulic properties of the rock mass and the fracture zone used in this analysis are the same as the ones used in the reference case cited in section 9.1.2.

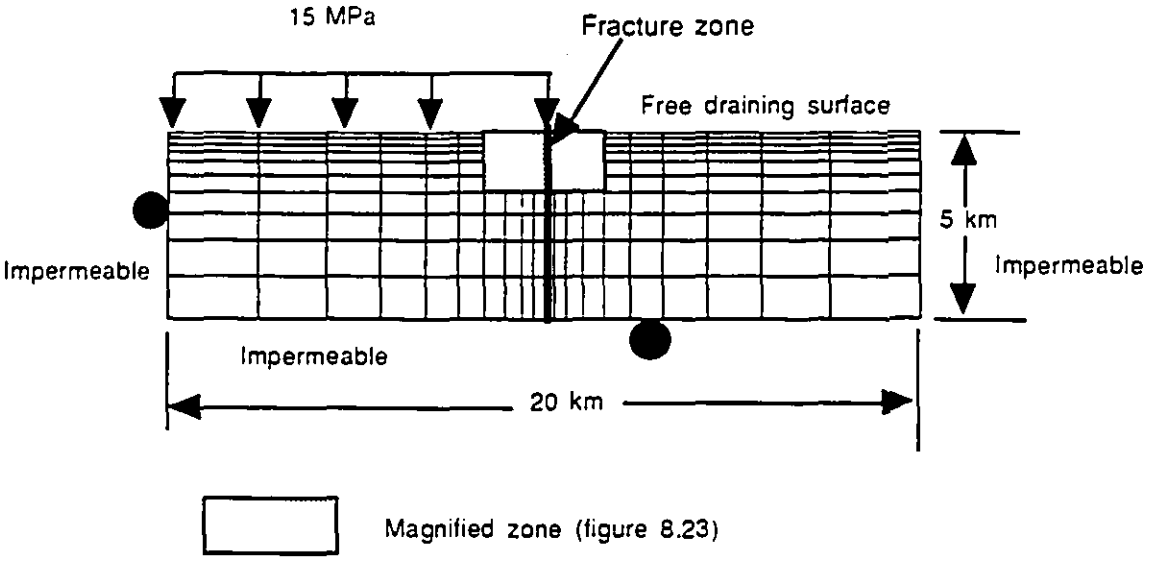

Figure 8.20 Finite element model for glaciation impact study

Also, for simplicity consistent with the generic site discussed earlier, the properties of both the competent rock mass and the fracture zone are assumed to be uniform with depth. Furthermore, both the competent rock mass and the fracture zone are assumed to be linearly elastic.

A typical deformed configuration of the mesh is shown in figure 8.21. It can be seen that a discontinuity in the displacement field is created at the fracture zone. It could also be inferred that the glacier might induce high shear stress in the fracture zone and significantly perturb the existing equilibrium stress distribution in the competent rock mass, especially near the toe of the ice sheet.

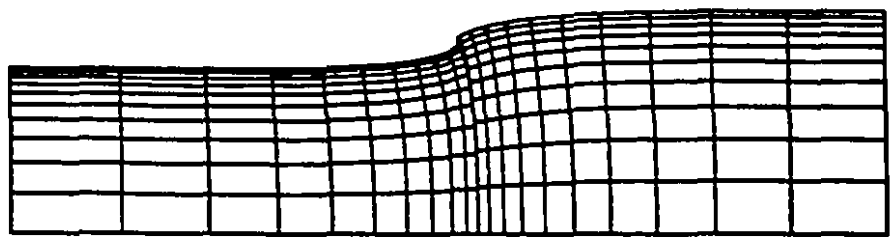

Figure 8.21 Deformed shape of the repository host rock due to glacier

We assume that the Mohr-Coulomb criterion is applicable to the fracture zone, and that the Hoek-Brown failure criterion is applicable to the competent rock mass. We use typical values of parameters for these criteria and typical values of initial in-situ stresses utilized in section 8.1.3. The results from the finite element simulation indicate that the stresses induced by the glacier combined with the initial in-situ stresses could result in failure of both the fracture zone and the rock mass at depths less than 200 m.

Typical contours of excess pore pressure are shown in figure 8.22. It can be seen that the fracture zone acts like a hydraulic sink and would constitute a discharge conduit for the migration of groundwater to the surface. These contours also suggest that high hydraulic gradients are induced by the glacier. These gradients could reach maximum of the order of 100% (several orders of magnitude higher than normal regional gradients). In order to assess the effects of these high gradients on contaminant migration from a repository located near the edges of the glacier, the trajectories of typical particles of water are calculated, according to equations (8.6)-(8.9).

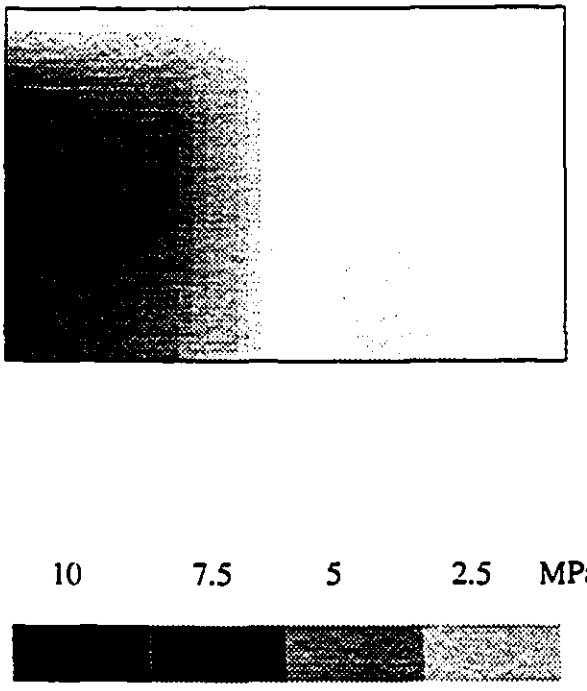

Figure 8.22 Glaciation impact - Typical excess pore pressure contours

Typical migration paths for particles of water are shown in Figure 8.23. Particles 1 and 2 are at a depth of 500 m; particles 3 and 4 are at a depth of 1000 m. Particles 1 and 3 are located 200 m from the fracture zone, while 2 and 4 are located 100 m from the fracture zone. After 20,000 years particles 1, 2 and 3 have travelled a distance of less than 100 m and have not reached the fracture zone. Particle 4 reaches the fracture zone in about 6,000 years.

The main findings from this rather elementary idealized model are consistent with the

geologists' observations on the effects of past glaciations, as follows:

- structural failure in competent rock masses and fracture zones reactivation would likely happen in the upper few hundred metres of the earth crust only

- the groundwater regime is profoundly perturbed

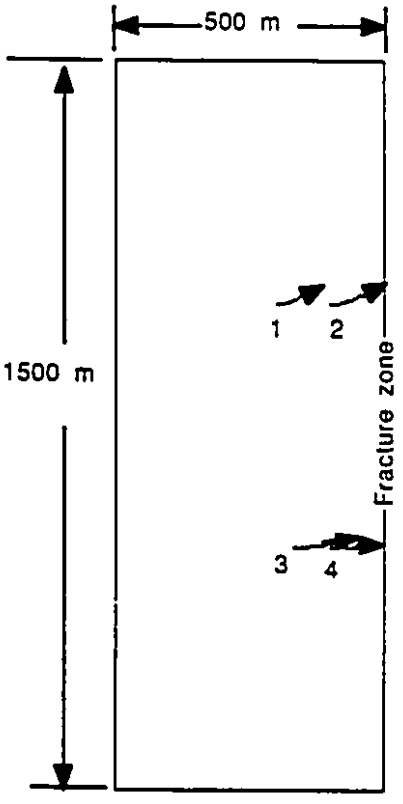

Figure 8.23 Glaciation impact - Typical water particle trajectories

8.3 Conclusions

The FRACON code was used for the preliminary assessments of the impact of the heat generated by nuclear fuel wastes and of glaciation loads on a sparsely fractured plutonic rock mass, representative of conditions that can be encountered in the Canadian Shield. The thermal, mechanical and hydrological disturbances due to these two factors were traditionally analyzed by neglecting the coupling between the T-H-M processes. From the scoping calculations shown in this chapter, where this coupling is considered, several new results were found:

- both the heat pulse generated by the wastes, and the loads associated with a future ice age have the ability to significantly perturb the groundwater and stress regimes in the host rock.

- Both the pore pressure generated by a glacier and the heat generated by the wastes can accelerate the movement of contaminated water to the ground surface. In ten thousand years, this accelerated rate results in flow distances of tens of metres (due to heat effects) to more than 100 m (due to glacier) in addition to any flow distance dictated by the natural hydraulic gradient that existed prior to the thermal and glacial loadings.

- Very low permeability of the rock mass will not always ensure lower groundwater flow rate since the thermally induced hydraulic gradients are higher for lower permeabilities. In some extreme cases, when a low permeability is combined to a high Young's modulus of the rock mass, the high pore pressure generated by the waste heat can induce tensile cracks in the rock mass, and the buffering distance provided between the repository and a fracture zone could be reduced .

A waste repository should ideally be located in a competent sparsely fractured rock mass, at a "safe" distance from major hydraulic conduits such as highly permeable fracture zones. The basis for the minimum distances between these hydraulic features and the repository should be established by consideration of the thermal/hydraulic disturbances due to the thermal pulse and future geological events such as glaciation. The regulatory document R-104 (Atomic Energy Control Board, 1987) requires that the safety of the repository has to be demonstrated for the first 10000 years. Considering coupled T-H-M processes, the analyses performed in this chapter suggest that the thickness of the envelope of competent rock between the repository and a fracture zone should be at least 100 m. However, there are practical limitations in providing such an envelope. It would be difficult to find large regions of competent rock in the Canadian Shield that could contain a 4 square kilometre repository and at the same time provide a minimal distance of 100 m between the repository and major fracture zones. Lower order fractures, of thickness up to 1 cm, cannot be detected by present geophysical site investigation techniques. The undetected fractures in the competent rock envelope could be extended by T-H-M processes to provide preferential groundwater flow paths and the implications of such contaminant transport processes have to be further assessed. From the above uncertainties pertaining to the competent rock envelope, it would seem advisable that more reliance should be brought to engineered barriers such as the container, the buffer and the backfill.

By analyzing the thermal, stress and flow regimes of a rock mass without considering the influences of coupling between these processes, it is likely that some safety features of importance to a repository could be unwittingly omitted. It is recommended that detailed, site-specific assessment of a future repository should be conducted by taking into account the coupled nature of thermal-mechanical and hydrological processes.

CHAPTER 9

CONCLUSIONS AND RECOMMENDATIONS

9.1 Conclusions

The equations governing coupled Thermal-Hydrological- Mechanical processes in saturated geological media were derived by the generalization of Biot's classical theory of consolidation of a poroelastic medium. These governing equations were expressed in terms of clearly defined physical parameters and a detailed description of the assumptions used in the developments was provided. Since the compressibilities of the pore fluid and the solid grains were taken into account in the derivation of the governing equations, the theory of coupled T-H-M processes thus formulated is particularly applicable to both saturated rocks and soils, where in the latter effects of compressibility are usually neglected.

In order to numerically solve the governing equations, the finite element method was used. A finite element computer code, FRACON, was developed to examine both plane strain and axisymmetric problems. Eight-noded isoparametric elements were developed to represent the unfractured regions of a geological medium, while special six-noded joint elements were developed to simulate discrete joints. The unfractured regions of a geological medium were assumed to exhibit linear elastic behaviour. The joints were assumed to exhibit both linear elastic or nonlinear elasto-plastic behaviour. For the development of these two types of elements, polynomials were used as shape functions. The shape

functions used to describe the variations in the pressure and temperature fields are one order lower than those used for the displacement field. It was shown that spatial oscillations of the calculated pore pressure can be minimized with these element formulations.

The development of the FRACON code followed an extensive procedure of code verification via analytical solutions and code-to-code comparison. A set of benchmark problems was defined and could be used by other investigators to perform code verification for similar coupled T-H-M computer codes.

Irregular asperities are present on the surfaces of a natural rock joint. During shearing, the joint dilates as a result of ride up at the asperities. Also, the shearing process can result in breakage of the asperities, resulting in the decrease of the dilation rate and strain softening of the joint. In order to reproduce the above fundamental aspects of the mechanical behaviour, the classical incremental theory of plasticity applicable to nonlinear interfaces was used to formulate the stress-strain relationship for the joint. The two-dimensional local geometry of the joint surfaces was idealized by a series of regular asperities with constant effective angle with respect to the shear direction. Following the work by Plesha (1987), it was assumed that asperity damage can be related to the plastic work of the shear stress. As a consequence, the asperity angle was assumed to be a decaying exponential function of this plastic work of the shear stress at the joint. In this thesis, the above concept was extended to describe the hydraulic behaviour of the joint in the following manner. Dilation of a joint during shear leads to an increase of its permeability at the initial stages. At later stages, as gouge is produced from breakage of the asperities, the flow path will be impeded and this process has the overall tendency to decrease the permeability of the joint. The results of limited experimental work available in the literature indicate that shearing of the

joint leads to an initial increase followed by a decrease of the joint permeability. Existing models for the hydraulic behaviour of joints do not allow for the prediction of the above phenomenon. In the present work, the increase in the hydraulic aperture was assumed to be proportional to the increase in the mechanical aperture. The results of several experimental investigations in the literature have confirmed this assumption. These investigations also showed that the factor of proportionality f between the hydraulic aperture and the mechanical aperture varies between 0.5 and 1.0 depending on the geometry of the flow direction. In this thesis, we assumed that gouge production is due to the plastic work from the shear stress, and thus the factor f was assumed to be a decaying exponential function of the plastic work. The parameters of the proposed joint model could be back-calculated from shear tests under constant normal stress conditions with permeability measurement and normal closure tests. Alternatively, most of these parameters could be estimated from the empirical coefficients JRC and JCS. Using the latter approach, the influence of the normal stress on dilation and scale effects become integral aspects of the proposed model.

The FRACON code was used to interpret a wide range of laboratory and field experiments, including the following:

- coupled T-H-M laboratory heater experiment on a cylinder of cementitious material with low permeability
- laboratory experiments on joint shear behaviour under constant normal stress and constant normal stiffness conditions
- coupled shear-flow laboratory experiment on a joint
- field experiments of fluid injection in a horizontal fracture in a granitic rock mass

The laboratory experiment on the block of cementitious material showed that owing to thermal effects, the pore pressure increases as a consequence of the differences in the

thermal expansion between the pore water and the solid matrix. This effect is also valid for slightly imperfect saturation of the pores. Using the FRACON code, we were able to predict the trends observed in the experiment.

The FRACON code with the elasto-plastic joint model was also used to simulate several laboratory experiments involving rock joints. These are: shear tests under constant normal stress and under constant normal stiffness conditions; and coupled shear-flow experiments performed by other researchers. The model performed quite satisfactorily in simulating the trends observed in the above experiments. For joint shear under constant normal stress, phenomena such as the post peak strain softening and joint dilation were correctly predicted. Scale effects and the effects of the normal stress were also correctly predicted by the proposed model. For joint shear under constant normal stiffness, the strengthening of the joint and decreased dilation were well simulated by the model. For the coupled shear flow-experiments, the model correctly predicted an initial increase in the joint permeability due to shear dilation followed by a decrease in the permeability due to subsequent gouge production.

The FRACON code was used to simulate field injection tests conducted in a horizontal fracture in a granitic rock mass. Due to the high pressure of the injected fluid, nonlinear coupled H-M behaviour prevailed during most of these tests. For a fracture with constant permeability, analytical solutions (e.g. Crank, 1975) shows that when the fluid pressure in the sealed borehole section is kept constant, the flow rate sharply increases very early in time due to the high hydraulic gradients. This flow then gradually decreases to a steady state-value, as fluid migration takes place radially into the fracture. The experimental results showed that the above behaviour occurs only at the early stage, lasting approximately 60 s, during which the high pressure at the injection point has insufficient time to propagate

outward to the periphery of the fracture. Subsequent to this early stage, a gradual increase of the flow rate takes place. The above behaviour is indicative of the nonlinear nature of the mechanical/hydraulic processes that prevail during these types of test, because of the high pressure of the injected water (higher than the in-situ normal stress). The high pressure of the injected water leads to a drastic opening of the fracture, resulting in an increase in its permeability by several orders of magnitude. Consequently, the flow rate increases with time and reaches a steady-state value when the aperture distribution in the fracture reaches a stable value. We were able to simulate this nonlinear coupled M-H behaviour.

Lastly, the FRACON code was used to simulate the coupled T-H-M response of a plutonic rock mass typical of the Canadian Shield to two factors: the radiogenic heat generated from a hypothetical nuclear fuel wastes repository and the loads imposed by a glacier during a future glaciation period. The regulatory document R-104 (AECB, 1987) requires that the safety of such a repository has to be demonstrated for the first 10000 years. The current conceptual design by Atomic Energy of Canada Ltd (AECL, 1994-a) establishes a 'protection zone' of sparsely fractured, competent rock of width 50 m between the wastes and a major fracture zone. This distance was determined without the considerations of coupled T-H-M processes. Taking into account the coupling of these processes, we observed that, due to the increase in pore water pressure generated by radiogenic heat and the load of a glacier, the mechanical/hydraulic regimes of the rock mass could be significantly changed by these two factors. From the results of the analyses performed in chapter 8, we observed that, some severe combinations of site conditions and rock mass properties might necessitate an increase of the thickness of the "protection zone" to 100 m. There are however several practical limitations in providing such an envelope. It is unlikely that a site could be found in the Canadian Shield, with large regions of competent rock that could contain a repository of 4 km^2 and at the same time provide a minimal distance of 50

to 100 m between the repository and a major fracture zone. Present geophysical site investigation techniques do not allow the detection of lower order fractures, of thickness up to 1 cm. The undetected fractures in the competent rock envelope would constitute preferential groundwater flow paths and the implications on contaminant transport has to be further assessed. A research program, partly sponsored by the AECB, has recently been initiated at McGill University (Selvadurai, 1995-b), to perform coupled T-H-M laboratory tests on natural granitic rock joints with a view to address the previous point. If a minimum envelope of competent rock could not be practically provided due to all the above considerations, more reliance should be placed on engineered barriers such as the container, the buffer and the backfill. It is recommended that the safety assessment of a future nuclear fuel wastes repository should be performed taking into account the coupled nature of T-H-M processes.

9.2 Recommendations for future studies

A key component of the research in coupled T-H-M processes is the development of laboratory and field experiments which can investigate T-H-M processes under controlled conditions. Such experiments should be conducted in conjunction with the development of computational models.

A multi-year research program has been initiated at the Department of Civil Engineering and Applied Mechanics of McGill University to further our understanding of the coupled T-H-M behaviour of rock joints. The conceptual experimental set-up is illustrated in figure 9.1. Granitic rock samples with induced joints will be tested. A central borehole will be provided in the sample, and a pore pressure transducer will be positioned in the borehole.

A combination of shear and normal stress will first be imposed by the actuator, and the normal and shear displacements will be monitored. The jointed rock sample will then be heated. Due to heating, the water pressure in the central borehole will increase and subsequently decay. The water pressure transient will be continuously monitored by the pressure transducer. A small scale experiment which utilizes this concept has already been investigated by Selvadurai and Carnaffan (1995). The shape of this pressure transient will bear the coupled T-M-H signature of both the joint and the intact rock. The thermal, mechanical and hydraulic properties of both the intact rock and the joint will be measured before the actual performance of the above experiments. It is recommended that the FRACON code be used to perform Class A predictions of the experiments (i.e. predictions made prior to the testing). These investigations should be complemented by post-experimental simulations to improve the modelling and minimize any differences between experimental and predicted results. The refinement of the joint model proposed in this thesis could also be performed during this research program. In particular, the two parameters which could not be expressed as empirical functions of JRC and JCS at the present time are the asperity degradation factor, c, and the gouge production factor, c_f. It is recommended that such correlations be established in this research program. The joint model could be improved by including a damage deformation component as suggested by Plesha (1985) and by assuming that plasticity phenomena can also occur prior to the attainment of the peak shear stress.

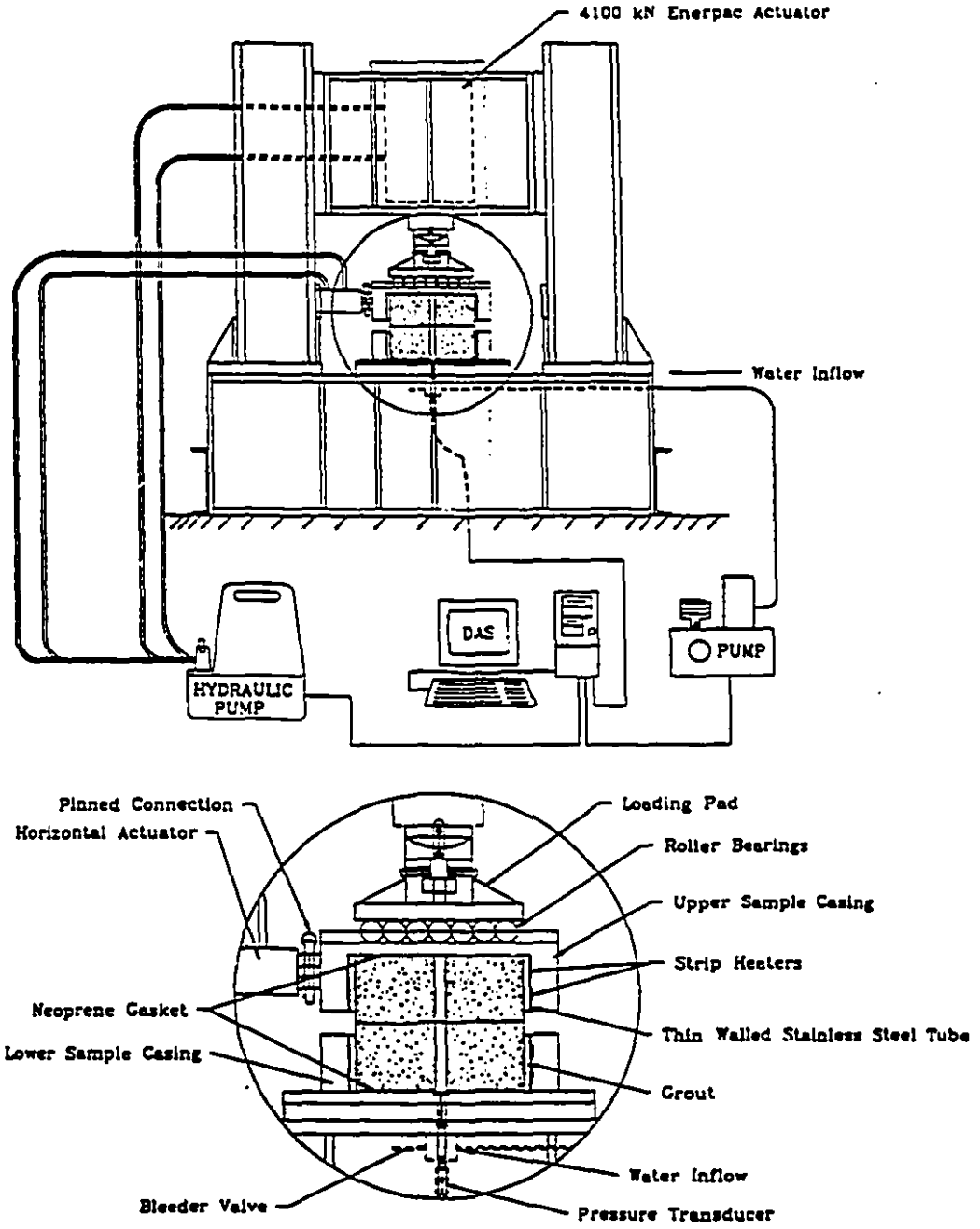

Figure 9.1 T-H-M laboratory experiment on jointed granite (from Selvadurai, 1995-b)

Field tests of coupled T-H-M processes in both fractured rock and buffer are also planned by other researchers. The Japanese research organization PNC is planning an experiment at the Kamaishi mine, located in the Iwate prefecture, 600 km North of Tokyo. A room of the mine will be used for this experiment. A heater will be emplaced in a trench excavated from the floor of the room. A buffer material will be subsequently compacted around the heater in the trench. The geology of the granitic rock mass around the rooms is known and the fractures have been mapped. Thermistors, pressure transducers and strain gauges will be positioned in the buffer and in the rock mass to measure the coupled T-H-M response of the system to heating. The performance of this experiment and its mathematical simulation will take several years and will be part of the international project DECOVALEX. It is recommended that the FRACON code be further developed to simulate the Kamaishi mine experiment. Three-dimensional effects as well as nonlinear stress-strain behaviour of buffer material could be included in order to simulate the above experiment.

REFERENCES

Agbezuge L.K. and H. Deresiewicz, 1974, ' On the indentation of a consolidating half-space', Israel J. Technol., **12**, 322-338.

Aboustit B.L., S.H. Advani and J.K. Lee, 1985, 'Variational principles and finite element simulations for thermo-elastic consolidation', Int. J. Num. An. Methods in Geomech., **9**,49-69.

Ahmad M. and Y. Bangash, 1987, ' A 3-D bond analysis using FEs', Computers and Structures, **25**, 281-296.

Amadei B. and S. Saeb, 1990, ' Constitutive models of rock joints', Proc. of the Int. Symp. on Rock Joints, Loen, Norway, Balkema.

Anderson H.W. and R.L.Dopp, 1966, ' FEM applied to rock mechanics', Proc. 1st Int. Soc. Rock Mech. Congr., Lisbon, **2**, 317-321.

Archambault G., M. Fortin, D.E. Gill, M. Aubertin and B. Ladanyi, 1990, ' Experimental investigations for an algorithm simulating the effect of variable normal stiffness on discontinuities shear strength', Proc. of the Int. Symp. on Rock Joints, Loen, Norway, Balkema.

Atomic Energy Control Board, 1987, ' Regulatory policy statement. Regulatory objectives, requirements and guidelines for the disposal of radioactive wastes - long term aspect',

AECB regulatory document R-104, Ottawa.

Atomic Energy of Canada Ltd., 1994-a, ' Environmental Impact statement on the concept for disposal of Canada's nuclear fuel waste', AECL-10711,COG-93-1.

Atomic Energy of Canada Ltd., 1994-b, ' The disposal of Canada's nuclear fuel waste: engineering for a disposal facility', AECL-10715, COG-93-5.

Atomic Energy of Canada Ltd., 1994-c, ' The disposal of Canada's nuclear fuel waste: the Geosphere model for postclosure assessment', AECL-10795, COG-93-9.

Bandis S., A. C. Lumsden and N. Barton, 1981, ' Experimental studies of scale effects on the shear behaviour of rock joints', Int. J. Rock Mech. Min. Sci. and Geomech. Abst., **18**, 1-21.

S. Bandis, A. Makurat and G. Vik, 1985, ' Predicted and measured hydraulic conductivity of rock joints', Proc. of the Int. Symp. on Fundamentals of Rock Joints, Bjorkliden, Sweden, Balkema.

Barton N., 1982, ' Modeling rock joint behavior from in situ block tests: implications for nuclear waste repository design', Office of Nuclear Waste Isolation Report ONWI-308.

Barton N. and V. Choubey, 1977, ' The shear strength of rock joints in theory and practice', Rock Mechanics,**10**, 1-54.

Barton N., S. Bandis and K. Bakhtar, 1985, 'Strength, deformation and conductivity

coupling of rock joints', Int. J. rock Mech. Min. Sci. and Geomech. Abstr., **22**, no.3, 121-140.

Bear J., 1972, ' Dynamics of fluids in porous media', Elsevier.

Bear J. and M.Y. Corapcioglu, 1981, ' A mathematical model for consolidation in a thermoelastic aquifer due to hot water injection or pumping', Water Resources Research, **17**, 723-736.

Beer G., 1985, ' An isoparametric joint/interface element for finite element analysis', Int. J. Num. Meth. Eng., **21**, 585-600.

Benjelloun Z.H., 1991, ' Etude Experimentale et Modélisation du Comportement Hydromécanique des Joints Rocheux', Thèse de doctorat, Université Joseph Fourier, Grenoble I.

Biot M. A., 1941, ' General theory of three dimensional consolidation', J. Appl. Phys., **12**, 155-164.

Biot M. A., 1955,' Theory of elasticity and consolidation for a porous anisotropic solid', J. Appl. Phys., **26**, 182-185.

Biot M. A., 1956, ' Theory of deformation of a porous viscoelastic anisotropic solid', J. Appl. Phys., **27**, 459-467.

Bishop A.W., 1973 , ' The influence of an undrained change in stress on the pore pressure

in porous media of low compressibility', Geotechnique, 435-442.

Booker J.R. and J.C. Small, 1985, ' An investigation of the stability of numerical solution of Biot's equations of consolidation', Int.J. Solids Struct., **11**, 907-917.

Booker J.R. and C. Savvidou, 1985, Consolidation around a point heat source, Int. J. Num. and Analytical Methods in Geomechanics, **9**, 173-184 (1985).

Borsetto M., G. Carradori and R. Ribacchi, 1981, ' Coupled seepage, heat transfer and stress analysis with application to geothermal problems', in Numerical methods in heat transfer, ed. by R.W. Lewis, K. Morgan and O.C. Zienkiewicz, John Wiley & Sons, 233-259.

Boulon M. and R. Nova, 1990, ' Modelling of soil-structure interface behaviour - a comparison between elastoplastic and rate type laws', Computers and Geotechnics, **9**, 21-46.

Boulon M., A.P.S. Selvadurai, H. Benjelloun and B. Feuga, 1993, ' Influence of rock joint degradation on hydraulic conductivity', Int. J. Rock Mech. Min. Sci. & Geomech. Abst., **30** (7), 1311-1317.

Brebbia C.A. (ed.), 1984, ' Topics in boundary element research', Springer-Verlag.

Britto A.M., C. Savvidou, D.V. Maddocks, M.J. Gunn and J.R. Booker, 1989, ' Numerical and centrifuge modelling of coupled heat flow and consolidation around hot cylinders buried in clay', Geotechnique, **39** (1), 13-25.

Bruggeman J.R., C.N. Zanger and J.H.A. Brahtz, 1939, ' Memorandum to Chief Designing Engineers: notes on analytical soil mechanics', US Department of the Interior Technical Memorandum no. 592.

Carol I. and E.E. Alonso, 1983, ' A new joint element for the analysis of fractured rock', Proc. 5th Int. Conf. Rock mech. Melbourne, F147-F151.

Case J.B. and P.C. Kelsall, 1987, ' Coupled processes in repository sealing', in Coupled Processes Associated with Nuclear Waste Repositories, edited by C.F. Tsang, 591-604, Academic Press Inc.

Cathles III, L.M., 1969 , ' The viscosity of the Earth's Mantle', Princeton University Press.

Cedergren H.R., 1967, ' Seepage, drainage and flow nets', John Wiley and Sons.

Chen W.F. and G.Y. Baladi, 1985, ' Soil Plasticity: Theory and Implementation', Elsevier Science Publishers B.V., New York.

Cheng A.H.D and J.A. Liggett, 1984-a, ' Boundary integral equation method for linear porous elasticity with applications to soil consolidation', Int. J. Num. Meth. Eng., 20, 255-278.

Cheng A.H.D and J.A. Liggett, 1984-b, ' Boundary integral equation method for linear porous elasticity with applications to fracture propagation', Int. J. Num. Meth. Eng., 20, 279-296.

Cheng A.H.D and M. Predeleanu, 1987, ' Transient boundary element formulation for linear porous elasticity with applicvations to soil consolidation', Appl. Math. Modelling, **11**.

Chiarelli C. and J.R. Booker, 1975, ' The time-settlement behavior of a rigid die resting on a deep clay layer', Quart. J. Mech. Appl. Math., **28**, 317-328.

Christian J.T., 1977, ' Two- and three-dimensional consolidation', in Numerical methods in geotechnical engineering, ed. C.S. Desai and J.T. Christian, McGraw Hill, 399-426.

Christian J.T. and J.W. Boehmer, 1970, ' Plane strain consolidation by finite elements', J. Soil Mech. and Found. Div., ASCE, **95** (SM1), 285-312.

Cook N.G.W., 1987, ' Coupled processes in geomechanics', In Coupled Processes Associated with Nuclear Waste Repositories , edited by C.F. Tsang, 39-66, Academic Press Inc.

Crank J., 1975, ' The mathemetics of diffusion', second edition, Oxford University Press.

Cryer C.W., 1963, ' A comparison of the three-dimensional consolidation theories of Biot and Terzaghi', Quart. J. of mech. and appl. math., **16**, 401-412.

Darcy H., 1856, ' Les fontaines publiques de Dijon', Victor Dalmont, Paris.

Desai C.S. and H.J. Siriwardane, 1984, ' Constitutive laws for engineering materials with

emphasis on geologic materials', Prentic-Hall Inc, Englewood Cliffs.

Desai C.S., M.M. Zaman, J.J. Lightner and H.J. Siriwardane, 1984, ' Thin layer element for interfaces and joints, Int. Journal for Num and Analy. Methods in Geomech.,8, 19-43.

Desai C.S. and Nagaraj B.K., 1986, ' Constitutive modelling for interfaces under cyclic loading', in Mechanics of Material Interfaces (Selvadurai, A.P.S. and G.Z. Voyiadjis, Eds.), II, Studies in Applied Mechanics, Elsevier, 97-108.

Desai C.S. and K.L. Fishman, 1987, ' Constitutive models for rocks and discontinuities', Proc. 28th US Symposium on Rock Mechanics, Tucson, Arizona.

Elliot G.M., E.T. Brown, P.I. Boodt and J.A. Hudson, 1985, ' Hydrochemical behaviour of joints in the Carmenelis granite, SW England', Proc. of the Int. Symp. on Fundamentals of Rock Joints, Bjorkliden, Sweden, A.A. Balkema, Rotterdam.

Frank P., A. Guenot and P. Humbert, 1982, ' Numerical analysis of contacts in geomechanics', Proc. 4th Int. Conf. Num. Meth. in Geomech., ed. by Z. Eisentein, Edmonton, 1, 37-45.

Franklin J.A. and M.B. Dusseault, 1989, ' Rock Engineering', McGraw Hill.

Freeze R.A. and Cherry J.A., 1979, ' Groundwater', Prentice Hall.

Gale J.E., 1982, 'Assessing the permeability characteristics of fractured rock', in Recent

Trends in Hydrogeology, the Geological Society of America, Boulder, Colorado.

Galerkin B.G., 1915, ' Series solution of some problems of elastic equilibrium of rods and plates' (Russian), Vestn. Inzh. Tech., **19**, 897-908.

Gaszynski J. and G. Szefer, 1978, ' Axisymmetric problem of the punch for the consolidating semi-space with mixed boundary permeability conditions', Archiwum Mechaniki Stosowanej, **30**, 17-26.

Gens A., I. Carol and E.E. Alonso, 1995, ' Rock joints: FEM implementation and applications', in Mechanics of geomaterial interfaces, edited by A P S Selvadurai and M Boulon, Elsevier (1995).

Ghaboussi J. and E.L.Wilson, 1973, ' Flow of compressible fluid in porous elastic media', Int. J. for Num. Meth. in Eng., **5**, 419-442.

Ghaboussi J., E.L. Wilson and J. Isenberg, 1973, ' Finite Elements for rock joints and interfaces', J. Soil Mech. Fdn. Div. Proc. ASCE, **99**, 833-848.

Gibson R.E., K. Knight and P.W. Taylor, 1963, ' A critical experiment to examine theories of three-dimensinal consolidation', proc. European conf. soil mech. and found. eng., Weisbaden, **1**, 69-76.

Gibson R.E., R.L. Schiffman and S.L. Pu , 1968, ' Plane strain and axially symmetric consolidation of a clay layer on a smooth impervious base', Quart. J. Mech. Appl. Math., **23**, 505-520.

Goodman R.E., R.L. Taylor and T.L. Brekke, 1968, ' A model for the mechanics of jointed rock', *J.* Soil Mech. Fdn. Div. Proc. ASCE, **94**, 637-659.

Goodman R.E. and J. Dubois, 1972, ' Duplication of dilatancy in analysis of jointed rock', J. of the soil mech. and found. div., ASCE, **SM4**, 399-422.

Goodman R.E., 1976, ' Methods of geological engineering in discontinuous rocks', West Publishing Company, New York.

Griffiths D.V., 1985, ' Numerical modelling of interfaces using conventional finite elements', Proc.5th Int. Conf. Num. Meth. in Geomech., Nagoya, 2, 837-844.

Guvanasen V. and T. Chan, 1991, ' Three-dimensional finite element solution for heat and fluid transport in deformable rock mass with discrete fractures', proc. Int. Conf. on computer methods and advances in geomechanics, Cairns, Australia, 1547-1552, Balkema.

Guvanasen V. and T. Chan, 1995, ' A new three-dimensional analysis of hysteretic thermo-hydro-mechanical deformations of fractured rock mass with dilatancy in fractures', in Mechanics of jointed and faulted rock, edited by H.P. Rossmanith, MJFR-2, 437-442, Balkema.

Hassanizadeh M. and W.G. Gray, 1979, 'General conservation equations for multiphase systems 2: Mass momentum energy and entropy equations', Adv. Water Res., 2, 191-203

Herget G., 1980 , 'Regional stresses in the Canadian Shield', Proceedings of the 13th Canadian Rock Mechanics Symposium, CIMM.

Hubbert M.K., 1940, 'The theory of ground water motion', J. Geol., **48**, 785-944.

Heuze F.E., 1979, ' Dilatant effects of rock joints', Proc. of 4th congress of Int. Society of Rock Mech. , Montreux, Switzerland.

Heuze F.E. and T.G.Barbour, 1982, ' New models for rock joints and interfaces', J. of Geotechn. Eng. Div., Proc. ASCE, **108, GT5**, 757-776.

Hickox C.E. and H.A.Watts, 1980, " Steady thermal convection from a concentrated source in a porous medium', trans. ASME, **102**, 248-253.

Hoek E. and E.T. Brown, 1988, ' The Hoek-Brown failure criterion - a 1988 update', Proc. 15th Can. Rock Mech. Symposium.

Hsu-Jun K., 1979, ' Nonlinear analysis of the mechanical properties of joint and weak intercalation in rock ', Proc. 3rd Int. Conf. on Num. Methods in Geomechanics, Aachen, Germany.

Huang N.C. , A.A. Szewczyk and Y.C. Li, 1990, ' Variational principles and finite element method for stress analysis of porous media', Int. J. Num. An. Meth. in Geomech., **14**, 1-26.

Hueckel T., M. Borsetto and A. Peano, 1987, ' Modelling of coupled thermo-elastoplastic-hydraulic response of clays subjected to nuclear waste heat', in Numerical methods for transient and coupled problems, edited by R.W. Lewis, E. Hinton, P. Bettess and B.A. Schrefler, John Wiley & Sons, 213-235.

Hutson R.W. and C.H. Dowding, 1990, 'Joint asperity degradation during cyclic shear', Int. J. Rock Mech. Mining Sci. and Geom. abstr., 27, 109-119.

Huyakorn P.S. and G.F. Pinder, 1983, ' Computational methods in subsurface flow', Academic Press.

Hwang C.T., N.R. Morgenstern and D.W. Murray, 1971, ' On solutions of plane strain consolidation problems by finite element methods', Canadian Geotechnical Journal, 8, 110- 118.

Jaeger J.G., 1971, ' Friction of rocks and stability of rock slopes', Geotechnique, 21 (2), pp 97-134.

Ladanyi B. and G. Archambault, 1970, ' Simulation of shear behaviour of a jointed rock mass', Proc. of the 11th Symp. Roch. Mech., American Institute of Mechanical Engineers, New York.

Lan Q. and A.P.S. Selvadurai, 1995, ' Interacting punches on a poroelastic half-space', submitted to Quart. J. of Mech. and Appl. Math.

Leichnitz W. , 1985, ' Mechanical Properties of rock joints', Int. J. Rock Mech. Min. Sci. and Geomch. Abst., 22, 313-321.

Lewis R.W. and B.A. Schrefler, 1987, ' The Finite element method in the deformation and consolidation of porous media ', John Wiley & Sons.

Mandel J., 1950, ' Etude mathématique de la consolidation des sols', actes du colloque international de mécanique, Poitier, France, **4**, 9-19.

Mandel J., 1953, ' Consolidation des sols (étude mathématique), Geotechnique, **3**, 287-299.

Makurat A., N. Barton, N.S. Rad and S. Bandis, 1990, ' Joint conductivity variation due to normal and shear deformation', Proc. of the Int. Symp. on Rock Joints, Loen, Norway, Balkema.

Marsily G., 1987, ' An overview of Coupled Processes with emphasis on Geohydrology', in Coupled Processes Associated with Nuclear Waste Repositories, edited by C.F. Tsang, 27-37, Academic Press Inc (1987).

McNamee, J. and R.E. Gibson, 1960, ' Plane strain and axially symmetric problems of the consolidation of a semi-infinite clay stratum', Quart. J. Mech. and Applied Math., **13**, 210-227.

Michalowski R. and Z. Mroz, 1978, ' Associated and non-associated sliding rules in contact friction problems', Arch. Mech., **30**, 259-276.

Ngo D. and A.C. Scordelis, 1967, ' Finite element analysis of reinforced concrete beams', ACI journal, Proc., **64**, no.3, 162-168.

Nguyen T.S., 1991, 'Thermal-mechanical-hydrological coupling for a radioactive waste repository', proc. 44th Can. Geot. Conf., Calgary, paper no. 67.

Nguyen T.S., V. Poliscuk and A.P.S. Selvadurai, 1993, ' Effects of glaciation on a nuclear fuel waste repository', Proc. Can. Geot. Conf., Saskatoon, 79-88.

Noorishad J., P.A. Witherspoon and T.L. Brekke, 1971, ' A method for coupled stress and flow analysis of fractured rock masses', Geotechnical Engineering Publication No. 71-6, University of California, Berkeley.

Noorishad J., C.F. Tsang and P.A. Witherspoon, 1984, ' Coupled Thermal-Hydraulic-Mechanical phenomena in saturated fractured porous rocks: numerical approach', J. Geophysical Research, **89** (B12), 10362-10373.

Noorishad J. and C.F. Tsang, 1987, ' Simulation of coupled thermal-hydraulic-mechanical interactions in fluid injection into fractured rocks', in Coupled Processes Associated with Nuclear Waste Repositories, edited by C.F. Tsang, 673-678, Academic Press Inc.

Ogata A., 1970, ' Theory of dispersion in a granular medium', U.S. Geol. Surv. Prof. Paper 411-I.

Onishi Y., Shibata H. and Kobayashi A., 1987, ' Development of finite element code for the analysis of coupled thermo-hydro-mechanical behaviors of a saturated-unsaturated medium' , in Coupled Processes Associated with Nuclear Waste Repositories, edited by C.F. Tsang, 679-698, Academic Press Inc.

Onishi Y., S. Akiyama, M. Nishigaki and A. Kobayashi, 1990, ' Three-dimensional coupled thermo-hydraulic-mechanical analysis code with PCG method', proc. GEOVAL-1990, OECD, Paris.

Pande G.N. and K.G. Sharma, 1979, ' On joint/interface elements and associated problems of numerical ill-conditioning', Int. Journal for Num. and Analy. Methods in Geomech., 3, 293-300.

Pande G.N. and W. Xiong, 1982, ' An improved multilaminate model of jointed rock masses', in Numerical Models in Geomechanics, A.A.Balkema, Rotterdam, 218-226 (1982)

Pande G.N., G. Beer and J.R. Williams, 1990, ' Numerical methods in Rock Mechanics', John Wiley & Sons Lt.

Patton F.D., 1966, ' Multiple modes of shear failure in rock', Proc. of 1st Congress of Int. Society of Rock Mech. , Lisbon, 1.509-513 (1966).

Plesha M.E., 1987, ' Constitutive models for rock discontinuities with dilatancy and surface degradation', Int. Journal for Num. and Analy. Methods in Geomech., 11, 345-362.

Plesha M.E., 1995, ' Rock joints: theory, constitutive equations', in Mechanics of geomaterial interfaces, edited by A P S Selvadurai and M Boulon, Elsevier.

Peano A. (ed.), 1995, Special Issue of Engineering Geology, on ' Thermomechanics of clays and clay barriers'

Pinder G.F. and W.G. Gray, 1977, ' Finite element simulation in subsurface hydrology', Academic Press Inc.

Pusch R. (ed.), 1990, Special Issue of Engineering Geology, on 'Artificial clay barriers for high level radioactive waste repositories'.

Qiu X., M.E. Plesha, B.C. Haimson and X. Huang, 1993, ' An investigation of the mechanics of rock joints -- part II, analytic investigation', Int. J. Rock Mech. Mining Sci. and Geom. abstr., **30**, 271-287.

Rae J., P.C. Robinson and L.M. Wickens, 1983, ' Coupled Heat and groundwater flow in porous rock', in Numerical methods in heat transfer, ed. R.W. Lewis, K. Morgan and B.A. Schrefler, John Wiley & Sons Ltd, **II**, 343-367.

Rice J.R. and M.P. Cleary, 1976, ' Some basic stress diffusion solutions for fluid-saturated elastic porous media with compressible constituent', Rev. Geophys. Space Phys., **14**, 227-241.

Rutqvist, J., Ljunggren, C., Stephansson, O., Noorishad, J. and Tsang, C. F., 1990, ' Theoretical and Field Investigations of Fracture Hydromechanical Response under Fluid Injection', in Rock Joints, edited by N. Barton and O. Stephansson, Balkema, 557-564.

Rutqvist, J., 1993, ' DECOVALEX, Test Case 6, Borehole Injection Test', Doc 93/139, DECOVALEX Secretariat, Engineering Geology, Royal Institute of Technology, Stockholm.

Roberds W.J. and H.H. Einstein, 1978, ' Comprehensive model for rock discontinuities', J. Geotech. Eng., Proc. ASCE,**104**, 553-569.

Sandhu R.S. and E.L. Wilson, 1969, ' Finite element analysis of flow in saturated porous media', J. Eng. Mech. Div., ASCE, 95 (EM3), 641-652.

Schiffman R.L., 1984, ' A bibliography of consolidation', in Fundamentals of transport phenomena in porous media, ed. by J. Bear and M.Y. Corapcioglu, 617-669.

Schiffman R.L. and A. Fungaroli , 1965, ' Consolidation due to tangential loads', Proc. 6th Int. Conf. Soil Found. Eng., Montreal, Canada, 1, 188-192.

Schiffman R.L., A.T.F. Chen and J.C. Jordan, 1969, ' An analysis of consolidation theories', J. Soil Mech. Found. Div., ASCE, 95 (SM1), 285-312.

Schneefuss J., H. Kull and T. Brasser, 1988, ' Stress and temperature effects on the permeability in granitic rock around a gallery excavated by continuous mining', in Excavation response in geological repositories for radioactive waste, proc. of an NEA workshop, OECD, Paris.

Schweiger H.F., W. Haas and E. Handle, 1990, ' A thin-layer element for modelling joints and faults', Proc. Int. Conf. on Jointed and Faulted Rocks, ed. by H.P. Rossmanith, Vienna, 559-564.

Selvadurai, A.P.S. (ed.), 1979, 'Elastic analysis of soil-foundation interaction', Developments in Geotechnical Engineering vol.17, Elsevier.

Selvadurai A.P.S., 1994, ' Experimental modelling of thermal consolidation around a high level waste repository', AECB INFO doc., Atomic Energy Control Board, Ottawa,

Canada.

Selvadurai A.P.S. (ed.), 1995-a, ' Recent development in poroelasticity', Kluwers (in press).

Selvadurai A.P.S. (ed.), 1995-b, ' Thermal consolidation effects around a NFW repository - phase 2', a research proposal to the Atomic Energy Control Board.

Selvadurai A.P.S and R. Karpurapu, 1989, 'Composite infinite element for modelling unbounded saturated soil media', Journ. Geotechn. Eng., ASCE, **115**, 1633-1646.

Selvadurai A.P.S and Yue Z.Q., 1994, ' On the indentation of a poroelastic layer', Int. J. Num. and Analytical Methods in Geomechanics, **18**, 161-175.

Selvadurai A.P.S. and M. Boulon (eds.), 1995, ' Mechanics of geomaterial interfaces ', Elsevier, Amsterdam, The Netherlands.

Selvadurai A.P.S. and P. Carnaffan, 1995, 'Pulse tests for the determination of permeability of granite: laboratory simulations and theoretical models', International workshop on hydro-thermo-mechanics of engineered clay barriers and geological barriers, Montreal, Dept. civil. eng. and appl. mech., McGill Univ. (in press).

Selvadurai A.P.S. and T.S. Nguyen, 1995, 'Computational modelling of isothermal consolidation of fractured porous media', Computers and Geotechnics, **17**, 39-73.

Seneviratne H.N., J.P.Carter and J.R. Booker, 1994, ' Analysis of fully coupled

thermomechanical behaviour around a rigid cylindrical heat source buried in clay', Int. J. Num. Analyt. Meth. Geomechanics, **18**, 177-203.

SKI (Swedish Nuclear Power Inspectorate), 1993, ' DECOVALEX - Mathematical Models of coupled T-H-M Processes for Nuclear Waste Repositories, Report of Phase I', Report SKI TR 93:31, Stockholm, Sweden.

Skinas C. A . , S. Bandis and C.A. Demiris, 1990, ' Experimental investigations and modelling of rock joint behaviour under constant stiffness', Proc. of the Int. Symp. on Rock Joints, Loen, Norway, Balkema.

Small J. C., J.R. Booker and E.H. Davis, 1976, ' Elastoplastic consolidation of soil', Int. J. Solids and Struct., **12**, 431-448.

Smith I.M. and Griffiths D.V., 1988, 'Programming the finite element method', John Wiley & Sons.

Stesky R.M., W.F. Brace, D.K. Riley and P.Y.F. Robin, 1974, ' Friction in faulted rock at high temperature and pressure', Tectonophysics, **23**, 177-203.

Tardieu B. and P. Pouyet, 1974, 'Proposition d'un modèle de joint tridimensionnel courbe', Proc. 3rd Int. Soc. Rock Mech. Congress, Denver, **2B**, 833-836.

Terzaghi K., 1923, ' Die Berechnung der Durchlassigkeitsziffer des Tones aus dem Verlauf der hydrodynamischen Spannungserscheinungen', Ak. der Wissenschaften in Wien, Sitzungsberichte mathematisch-naturwissenschaftliche Klasse, part IIa, 132(3/4),

125-38.

Tsang C.F., 1987, ' Introduction to coupled processes', in Coupled Processes Associated with Nuclear Waste Repositories, edited by C.F. Tsang, 1-8, Academic Press Inc (1987).

Vaziri H., Christian H.A. and Pitman T., 1992, ' Generalized Form of Terzaghi's Consolidation Solution', Proc. of the 1992 Canadian Geotechnical Conference, paper 65.

Verruijt A., 1965, ' Discussion', Sixth int. conf. soil mech. and found. eng., 3, 401-402.

Vincent J.S. and V.K. Prest, 1987, 'The Early Wisconsinian History of the Laurentide Ice Sheet', Géographie physique et Quaternaire, **41**(2),199-213.

Walcott, R.I., 1970a, 'Flexural rigidity, thickness, and viscosity of the lithosphere', J. Geophys. Res., **75**, 281-294.

Walcott, R.I., 1970b, ' Isostatic response to loading of the crust in Canada', Can. J. Earth Sci., 7, 716-721.

Wilson, E.L., 1977, 'Finite element for foundations, joints and fluids', in Finite elements in geomechanics, ed. by G. Gudehus, John Wiley & Sons.

Witherspoon P. A., C.H. Amick, J.E. Gale and K. Iwai, 1979, ' Observations of a potential size effect in experimental determination of the hydraulic properties of fractures', Water Resources Research, **15**, no.5.

Witherspoon P.A., 1987, ' The need for field research in coupled processes', in Coupled Processes Associated with Nuclear Waste Repositories, edited by C.F. Tsang, 775-780, Academic Press Inc.

Wolfram Research Inc., 1993, MATHEMATICA, version 2.2, Champaign, Illinois, USA.

Yue Z.Q., and A.P.S. Selvadurai, 1994, ' On the asymmetric indentation of a consolidating poroelastic half space', Appl. Math. modelling, **18**, 170-185.

Yue Z.Q., and A.P.S. Selvadurai, 1995 ' Contact problems for saturated poroelastic solids', J. Eng. Mech., **121**, 502-512.

Zienkiewicz O.C., B. Best, C. Dullage and K. Stagg, 1970, ' Analysis of non-linear problems in rock mechanics with particular reference to jointed rock systems', Proc. 2nd Congress Int. Soc. Rock Mech., Belgrade, Yugoslavia, **3**, 501-509 (1970) .

Zienkiewicz O.C., C. Humpheson and R.W. Lewis, 1977, ' A unified approach to soil mechanics problems (including plasticity and viscoplasticity) ', in ' Finite Element in Geomechanics', edited by G. Gudehus, 151-178, John Wiley & Sons Ltd .

APPENDIX A

RELATIVE IMPORTANCE OF THE HEAT CONVECTION COMPONENT

In the governing equations solved by the FRACON code, the convective heat transfer component is neglected. This allows a decoupling of the temperature field from the displacement and the pore pressure fields that substantially simplifies the development of the computer code. In this Appendix, we shall discuss the relative importance of the convective and conductive heat transfer components based on an analytical solution for the one-dimensional heat transfer equation and using typical properties of sparsely fractured granitic rock mass of the Canadian Shield.

As mentioned in chapter 2, the component of the heat flux due to conduction is:

$$q_i^c = - \kappa_{ij} \frac{\partial T}{\partial x_j} \qquad \text{(A-1)}$$

The heat flux due to convection is given by:

$$q_i^{conv} = \rho_f C_f n V_{if} T \qquad \text{(A-2)}$$

where ρ_f and C_f are the density and the specific heat (per unit mass) of the pore fluid; V_{if} is

the fluid velocity as defined in equation (2.1) and n is the porosity of the geological medium.

Taking into account both the convective and conductive heat components, the equation of heat transfer in a porous medium becomes:

$$\frac{\partial}{\partial x_i}\left(\kappa_{ij}\frac{\partial T}{\partial x_j}\right) + nV_{if}\rho_f C_f \frac{\partial T}{\partial x_i} = \rho C\frac{\partial T}{\partial t} \qquad \text{(A-3)}$$

where κ_{ij} is the heat conductivity tensor; ρ and C are the density and the specific heat of the bulk medium.

Ogata (1970) obtained the one-dimensional solution to equation (A-3) for a homogeneous half-space with a constant fluid velocity field V_f in the x-direction and the following boundary conditions (figure A.1):

$$T(x,0) = 0 \quad x \geq 0 \qquad \text{(A-4)}$$

$$T(0,t) = T_0 H(t) \qquad \text{(A-5)}$$

$$T(\infty,t) = 0 \quad t \geq 0 \qquad \text{(A-6)}$$

where H(t) is the Heaviside step function.

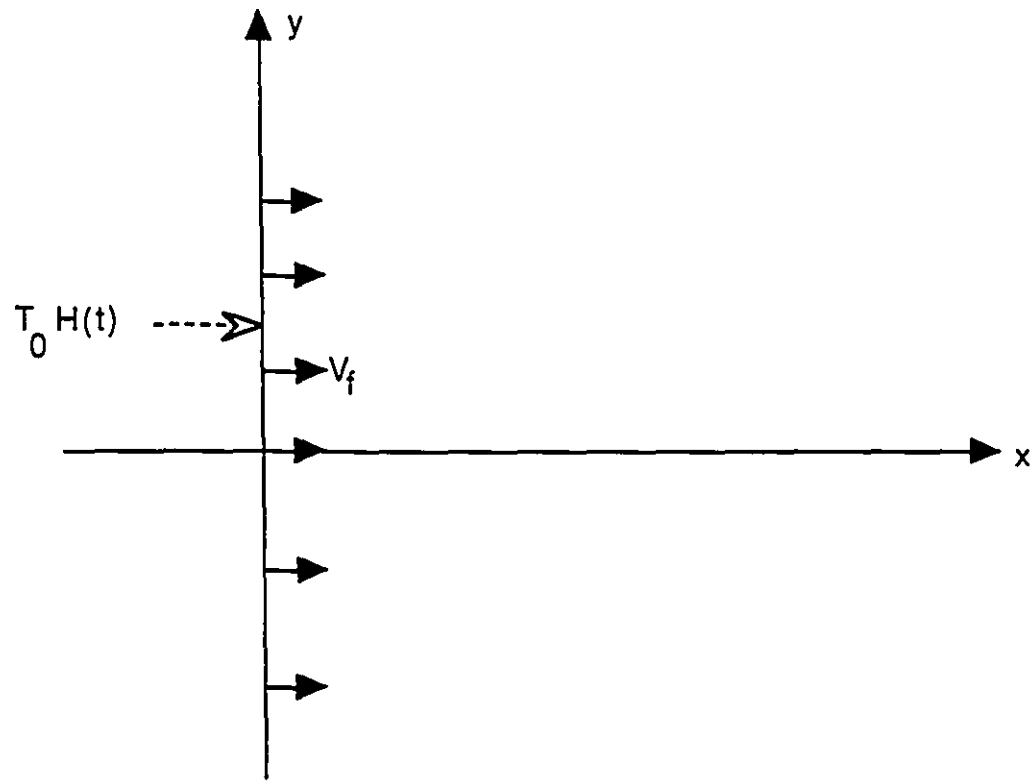

Figure A.1 Geometry for Ogata's (1970) one-dimensional solution to the convection-diffusion equation

That solution is:

$$\frac{T}{T_0} = \frac{1}{2}\left[\operatorname{erfc}\left(\frac{x-\bar{v}t}{2\sqrt{Dt}}\right) + \exp\left(\frac{\bar{v}x}{D}\right)\operatorname{erfc}\left(\frac{x+\bar{v}t}{2\sqrt{Dt}}\right)\right] \tag{A-7}$$

where :

$$D = \frac{\kappa}{\rho C} \tag{A-8}$$

$$\bar{v} = nV_f\frac{\rho_f C_f}{\rho C} \tag{A-9}$$

κ is the thermal conductivity of the medium.

The solution given in (A-7) becomes the solution to a purely heat conduction problem when V_f is zero. The value of V_f is given by the simplified Darcy's equation:

$$nV_f = K\,i \qquad \text{(A-10)}$$

where K is the hydraulic conductivity of the geological medium and i is the hydraulic gradient. For relatively unfractured granitic rock of the Canadian Shield, K varies between 10^{-10} to 10^{-12} m/s.

For fracture zones, K varies between 10^{-6} to 10^{-10} m/s (AECL, 1994-c). The thermally induced hydraulic gradient, as shown in chapter 8, could attain values close to one, in the first 100 years, at distances less than 100 m around the vault. For distances greater than 100 m, the hydraulic gradient decreases rapidly to existing regional gradients (or the order of 0.001 to 0.01).

A.1 Assessment of the importance of heat convection for competent rock

Let us consider a plausible situation when the convective heat component might become important, e.g. for:

$K=10^{-10}$ m/s

$i=1$

The comparison between temperature profiles for the cases with and without heat convection, using equation (A-7) is shown in figure A-2. It could be seen that the two

curves are undistinguishable and the omission of heat convection is justified for competent rock.

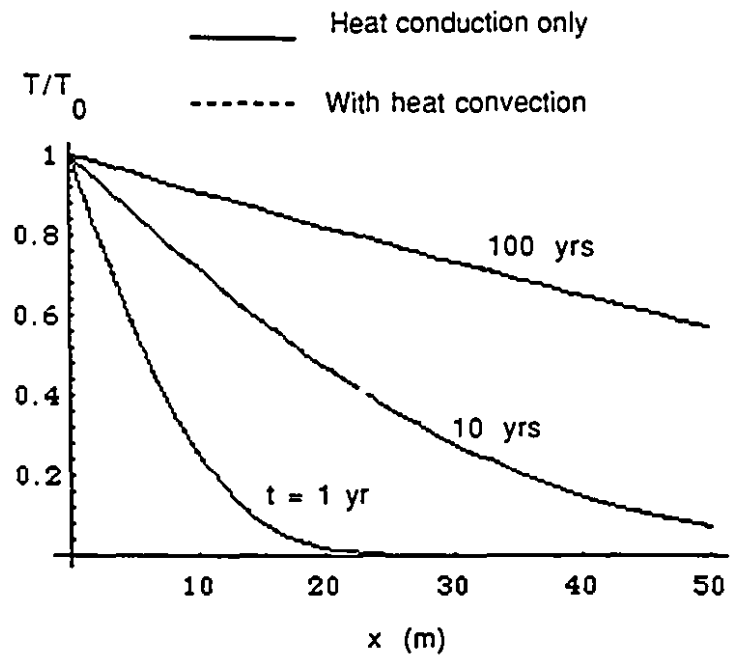

Figure A-2 Relative importance of heat convection in competent rock

A.2 Assessment of the importance of heat convection for fracture zones

Let us consider a value of the hydraulic conductivity in the higher range for a fracture zone:

$K = 10^{-7}$ m/s

Consider two cases for the hydraulic gradient:

i=1 for fracture zone within 100 m of the repository and i=0.1 beyond 100 m of the repository.

For the first case, figure A-3 shows that neglecting heat convection can result in an underestimate of the temperature field by approximately 20% at larger times (100 years). For the case when the fracture zone is 100 m away from the repository , figure A-4 shows that neglecting heat convection results in only negligible underestimate of the temperature field.

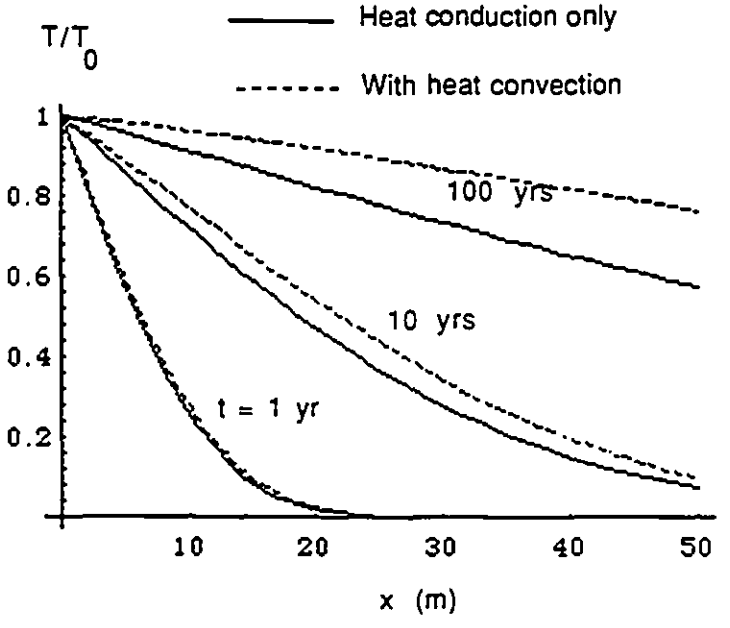

Figure A-3 Importance of heat convection for fracture zone near the heat source

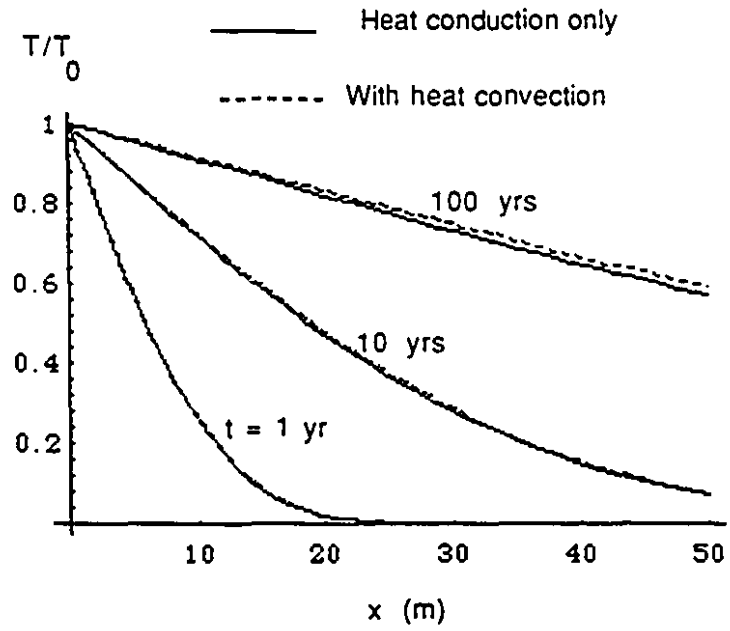

Figure A-4 Importance of heat convection for a fracture zone located far from the heat source

A.3 Conclusion

For typical hydraulic properties of sparsely fractured rock masses of the Canadian Shield, the convective component of heat transfer could be neglected for most situations. The convective heat transfer component becomes important only for fracture zones with extremely high permeability that intersect the heat source.